Photoinduced Cobalt-Hydride Hydrogen Atom Transfer Catalyzed Cross Coupling and Rearrangement Reactions

Von der Fakultät für Mathematik, Informatik und Naturwissenschaften der RWTH Aachen University zur Erlangung des akademischen Grades eines Doktors der Naturwissenschaften genehmigte Dissertation

vorgelegt von

M.Sc. Jingyang Qin

aus

Henan, China

Berichter: *Prof. Dr. Franziska Schoenebeck*
Prof. Dr. Christopher J. Teskey

Tag der mündlichen Prüfung: 19/09/2025

Acknowledgements

The sun beyond the mountain glows,
The Yellow River seawards flows.
You can enjoy a grander sight,
By climbing to a greater height.

This poem by Zhihuan Wang, a poet of the Tang Dynasty, is widely known across China. It has long been my favorite verse to practice in calligraphy. The spirit of striving embedded in these words has always inspired me to keep reaching higher, even in the face of uncertainty, challenges, pain, and hardship, from completing my master's to pursuing my PhD. Now, as my doctoral journey nears its end, the belief in 'climbing to a greater height' continues to guide me forward.

I would like to take this opportunity to express my deepest gratitude to all those who have contributed to this important stage of my academic and personal life.

First and foremost, I would like to express my sincere appreciation to my supervisor, Prof. Dr. Christopher J. Teskey, for his unwavering guidance, insightful feedback, and continuous encouragement throughout my doctoral studies. Your academic rigor, clarity of thought, and dedication to research have profoundly shaped my own approach to scholarship. Thank you for your patience, your mentorship, and for always pushing me to reach higher standards.

I am also grateful to Prof. Dr. Franziska Schoenebeck and her staff (Dr. Bettray, Theresa, Kristina, and Desiree) for their technical and logistical support since the beginning of my PhD journey.

I would also like to thank the current members of our group: Martina, Lucas, Nikita, Samikshan, Victor, Hanqi, Maria, Chen, Moritz, and Matthias, as well as the former members: Enrico, Danijela, Manuel, and Daniel. It has been a great honor to work alongside all of you from different parts of the world and to experience the richness of diverse cultures. My sincere thanks also go to the group's administrative and support staff—Alina, Mandkhai, and Miriem for their kind assistance. I am also grateful to the Chinese PhD students I met at RWTH—Peng Wu, Xingben Wang, Fang Li, and others—for their companionship and help.

Most importantly, I am deeply grateful to my family. To my wife, I owe you so much. While you needed me the most, I was studying thousands of miles away in Germany. I am truly thankful for your patience, understanding, and the encouragement you gave me during my most difficult moments. To my son, Luming, your birth gave my life a new sense of purpose and reminded me why perseverance matters. To my parents, thank you for your unconditional love, understanding, and lifelong support. Your unwavering belief in me has been a constant source of strength throughout this journey.

Jingyang Qin

Abstract

The first chapter of the thesis serves as a preamble to introduce the concept of Metal-Hydride Hydrogen Atom Transfer (MHAT) catalysis, highlighting its merger with photocatalysis and its applications in alkene hydrofunctionalization.

Chapter 2 describes a cross-coupling reaction between pyridines and dienes, enabled by photoredox/cobalt hydride dual catalysis. This approach generates a transient allylic radical from dienes and a persistent radical from pyridyl phosphonium salts. The combination of these two radical species provides rapid and selective access to C4-functionalized pyridine derivatives bearing C=C bonds. Mechanistic studies reveal that the distinctive selectivity for dienes, even in the presence of other alkenes, arises from a significantly higher barrier associated with hydrogen atom transfer (HAT) to alkenes.

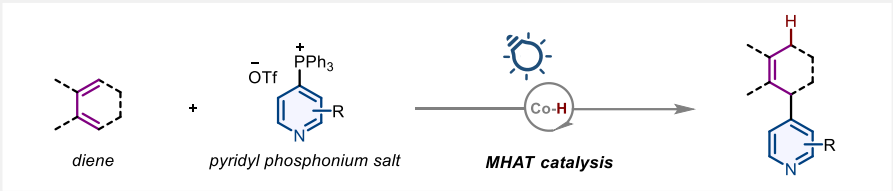

Chapter 3 presents another photoinduced Co-HAT catalyzed cross-coupling reaction, in which a styrene and a Michael acceptor serve as the reactants. A Truce-Smiles rearrangement would be triggered by the initial radical addition when *N*-arylsulfonyl acrylamide was used as the Michael acceptor, leading to the alkene carboarylation products. The occupation of the 2-position in the migrating group significantly impacts the rearrangement process; without this substitution pattern, no rearrangement follows the initial olefin coupling.

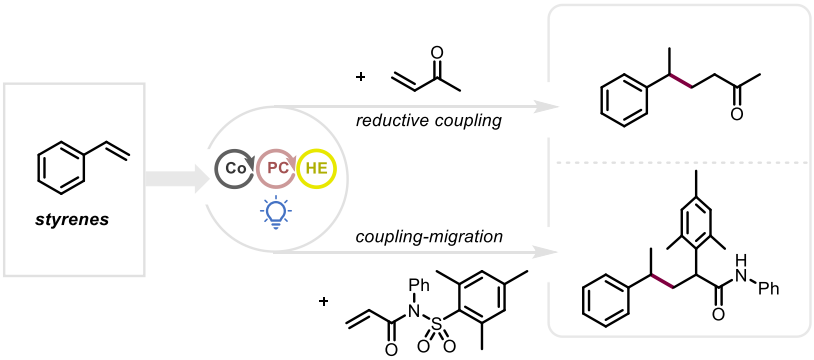

In chapter 4, a dual-catalytic semipinacol rearrangement is described. This method provides a platform for synthesizing α-aryl ketones from allylic alcohols via a radical pathway.

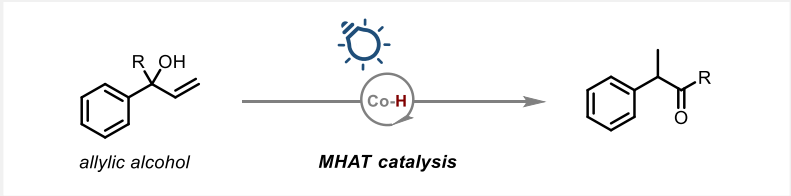

Zusammenfassung

Das erste Kapitel der Dissertation dient als Einführung in das Konzept der Metall-Hydrid-vermittelten Wasserstoffatomübertragung (MHAT)-Katalyse. Dabei werden insbesondere die Verbindung mit der Photokatalyse und deren Anwendungen in der Hydrofunktionalisierung von Alkenen hervorgehoben.

Kapitel 2 behandelt eine Kreuzkupplungsreaktion zwischen Pyridinen und Dienen, die durch eine photoredox- und kobalthydrid-duale Katalyse ermöglicht wird. In diesem Ansatz wird ein nicht langlebiges allylisches Radikal aus Dienen sowie ein persistentes Radikal aus Pyridylphosphoniumsalzen generiert. Die Kombination dieser beiden Radikalspezies ermöglicht einen schnellen und selektiven Zugang zu C4-funktionalisierten Pyridinderivaten mit C=C-Doppelbindungen. Mechanistische Untersuchungen zeigen, dass die ausgeprägte Selektivität gegenüber Dienen auch in Anwesenheit anderer Alkene erhalten bleibt, da die Wasserstoffatomübertragung (HAT) auf Alkene mit einer deutlich höheren Energiebarriere verbunden ist.

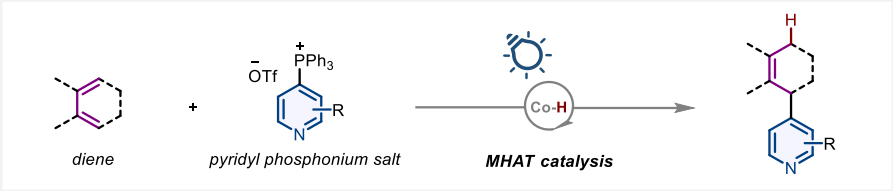

Kapitel 3 behandelt eine weitere photochemisch induzierte, durch Co-HAT katalysierte Kreuzkupplungsreaktion, bei der Styrol und ein Michael-Akzeptor als Reaktanten eingesetzt werden. Bei Verwendung von *N*-Arylsulfonylacrylamid als Michael-Akzeptor wird durch die initiale radikalische Addition eine Truce-Smiles-Umlagerung ausgelöst, die zur Bildung von Alken-Carboarylierungsprodukten führt. Die Substitution an der 2-Position der migrierenden Gruppe hat dabei einen entscheidenden Einfluss auf den Umlagerungsprozess. Ohne dieses Substitutionsmuster erfolgt nach der initialen Olefinkupplung keine Umlagerung.

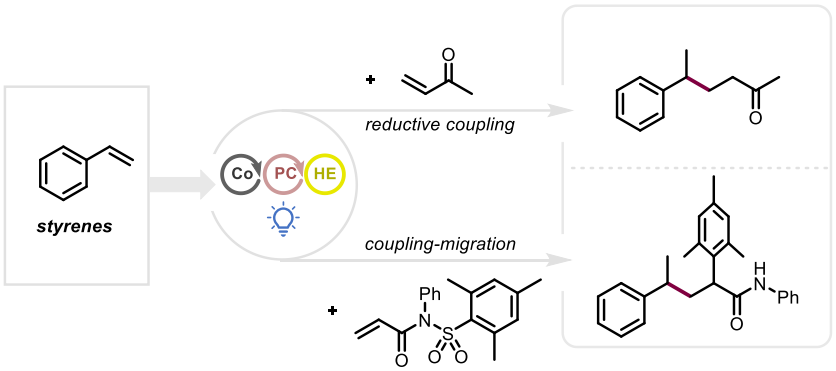

Kapitel 4 beschreibt eine dualkatalysierte Semipinakol-Umlagerung. Diese Methode bietet eine Plattform zur Synthese von α-Arylketonen aus allylischen Alkoholen über einen radikalischen Reaktionsweg.

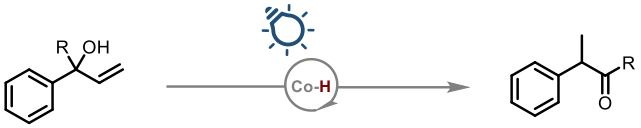

allylic alcohol ***MHAT catalysis***

Publications and Copyright Permissions

Parts of the work described in this thesis have already been published in the following publications.[1-2]

(1) **Qin, L.**; Barday, M.; Jana, S.; Sanosa, N.; Funes-Ardoiz, I.; Teskey, C. J.* Photoinduced cobalt catalysis for the reductive coupling of pyridines and dienes enabled by paired single-electron transfer. *Angew. Chem. Int. Ed.* **2023**, *62*, e202310639.

(2) Lunic, D.; Vystavkin, N.; **Qin, L.**; Teskey, C. J.* Dual-Catalytic Structural Isomerisation as a Route to α-Arylated Ketones. *Angew. Chem. Int. Ed.* **2024**, *63*, e202409388.

Abbreviations

Ac	Acetyl
acac	Acetylacetonate
Ar	Aryl
BDE	Bond dissociation enthalpy
BDFE	Bond dissociation free energy
Bn	Benzyl
Boc	*tert*-Butyloxycarbonyl
BOX	Bis(oxazoline)
bpy	2,2′-Bipyridyl
brsm	Based on recovered starting material
Cbz	Carboxybenzyl
cod	Cyclooctadiene
Cp	Cyclopentadienyl ligand
Cy	Cyclohexyl
4CzIPN	1,2,3,5-Tetrakis(carbazol-9-yl)-4,6-dicyanobenzene
DABCO	1,4-Diazabicyclo[2.2.2]octane
DBU	1,8-Diazabicyclo[5.4.0]undec-7-ene
DCE	1,2-Dichloroethane
DCM	Dichloromethane
DEMS	Diethoxymethylsilane
DFT	Density functional theory
dibm	Diisobutyrylmethane
DIPEA	Di-*iso*-propylethylamine
DMA	*N,N*-Dimethylacetamide
DMAP	4-Dimethylaminopyridine
DME	Dimethoxyethane
DMF	*N,N*-Dimethylformamide
dmg	Dimethylglyoxime
dpm	Dipivaloyl methanato
DMPU	*N,N'*-Dimethylpropylurea
DMSO	Dimethylsulfoxide
DPA	9,10-Diphenylanthracene
dppb	1,4-Bis(diphenylphosphino)butane
dppe	1,2-Bis(diphenylphosphino)ethane
dppf	1,1′-Bis(diphenylphosphino)ferrocene
d.r.	Diastereomeric ratio
dtbbpy	4,4′-Di-*tert*-butyl-2,2′-dipyridyl
EDA	Electron donor-acceptor
ee	Enantiomeric excess
ET	Electron transfer
EtOAc	Ethyl acetate
EWG	Electron-withdrawing group

FDA	Food and drug administration
FLPs	Frustrated Lewis pairs
HAA	Hydrogen atom abstraction
HAT	Hydrogen atom transfer
HE	Hantzsch ester
HFIP	Hexafluoro-2-propanol
IBX	2-Iodoxybenzoic acid
IF	Intermediate field
^{i}Pr	*iso*-Propyl (2-propyl)
IPr	1,3-(2,6-Diisopropylphenyl)imidazol-2-ylidene
LED	Light-emitting diode
LMCT	Ligand-to-metal charge transfer
MAD	(2,6-*t*-Bu_2-4-Me-$C_6H_2O)_2$AlMe
Me	Methyl
MeCN	Acetonitrile
Mes	Mesityl (2,4,6-trimethylphenyl)
MHAT	Metal-hydride hydrogen atom transfer
MTBE	Methyl *tert*-butyl ether
*n*Bu	*n*-Butyl
NFSI	*N*-Fluorobenzenesulfonimide
NHC	*N*-Heterocyclic carbene
NMR	Nuclear magnetic resonance spectroscopy
Nu	Nucleophile
OAc	Acetate
OTf	Triflate (trifluoromethanesulfonate)
PC	Phthalocyanine or photocatalyst
PET	Photoinduced electron transfer
Ph	Phenyl
phen	Phenanthroline
PivOH	Pivalic acid
ppy	2-Phenylpyridine
psi	Pound per square inch
PT	Proton transfer
PTH	*N*-Phenyl benzo[b]phenothiazine
Py	Pyridine
salen	Bis(salicyliden)ethylendiamine
SCE	Standard calomel electrode
SET	Single electron transfer
SF	Strong field
S_NAr	Nucleophilic aromatic substitution
TBA	Tetrabutylammonium
TBAF	Tetra-*n*-butylammonium fluoride
TBHP	*tert*-Butylhydroperoxide
^{t}Bu	*tert*-Butyl

TBS	*tert*-Butyldimethylsilyl
TEA	Triethylamine
Tf	Trifluoromethanesulfonyl
TFA	Trifluroacetic acid
THF	Tetrahydrofuran
TM	Transition metal
TMOPP	Tetramethoxyphenylporphyrin
TMS	Trimethylsilyl
TPP	Tetraphenylporphyrin
TS	Transition state
Ts	Tosyl
TSR	Truce-Smiles rearrangement
UV	Ultraviolet
Vis	Visible
WF	Weak field
XAT	Halogen atom transfer

Table of Contents

1 Metal-hydride hydrogen atom transfer (MHAT) catalysis 14

1.1 Introduction to MHAT catalysis 14

1.1.1 Overview of MHAT catalysis 14

1.1.2 Transition metal hydrides 15

1.1.3 Strong-field (SF) and weak-field (WF) ligands in metal hydrides 16

1.1.4 Cage effect and divergent MHAT reactions 17

1.1.5 Comparison with other activation modes 18

1.2 MHAT catalyzed alkene hydrofunctionalization 22

1.2.1 MHAT catalyzed alkene hydrofunctionalization based on first row transition metals 22

1.2.2 MHAT in asymmetric catalysis 33

1.2.3 Applications of MHAT in total synthesis 35

1.3 Merger of MHAT catalysis with photocatalysis 36

1.3.1 General mechanism of photoinduced MHAT catalysis 37

1.3.2 Visible-light photocatalytic MHAT reactions 37

1.3.3 Hydrofunctionalization of other electrophilic π-systems 43

1.4 Summary and outlook 44

2 Photoinduced Co-HAT catalyzed reductive cross coupling of pyridines and dienes 46

2.1 Pyridyl phosphonium salts 46

2.1.1 Overview of pyridine and pyridyl phosphonium salts 46

2.1.2 Synthesis of pyridyl phosphonium salts 48

2.2 Co-HAT catalysis for the coupling of pyridyl phosphonium salts and dienes 49

2.2.1 Introduction 49

2.2.2 Reaction development 52

2.2.3 Substrate scope 54

2.2.4 Mechanistic studies 60

2.2.5 Summary and outlook 66

3 Co-HAT catalyzed cross-coupling and rearrangement reactions of styrenes and Michael acceptors 68

3.1 Giese reaction 68

3.1.1 Introduction of Giese reaction 68

3.1.2 Photoredox-mediated Giese reaction 69

3.2 Reaction development 76
3.2.1 Reaction design 76
3.2.2 Reaction optimization 77
3.2.3 Reaction scope 78
3.2.4 Preliminary investigation of the Giese addition/Truce-Smiles rearrangement cascade 80
3.2.5 Summary and outlook 84
4 Co-HAT catalyzed semipinacol rearrangement 86
4.1 Photocatalytic semipinacol rearrangement 86
4.2 Summary and outlook 89
5. Supporting information 91
5.1 General materials and methods 91
5.2 Supporting information for chapter 2 92
5.2.1 Synthesis of starting materials 92
5.2.2 General procedure and characterization data of products 102
5.2.3 Mechanistic experiments 116
5.2.4. Computational details 137
5.3 Supporting information for chapter 3 142
5.3.1 Selected optimization reactions 142
5.3.2 Synthesis of starting materials 144
5.3.3 General procedure and characterization data of products 145
6. Literature 151

1

Metal-Hydride Hydrogen Atom Transfer (MHAT) Catalysis

1 Metal-hydride hydrogen atom transfer (MHAT) catalysis

1.1 Introduction to MHAT catalysis

1.1.1 Overview of MHAT catalysis

The concept of Metal-hydride hydrogen atom transfer, also referred to as Metal-catalyzed hydrogen atom transfer (abbreviated as MH HAT or MHAT), emerged in the early 1970s. At the time, Halpern first proposed a catalytic pathway involving a hydrogen atom transfer from a cobalt hydride to anthracene (Scheme 1.1 a).[1] Two years later, the same group established the MHAT mechanism during their investigation of the manganese (Mn)-catalyzed hydrogenation of styrenes (Scheme 1.1 b).[2]

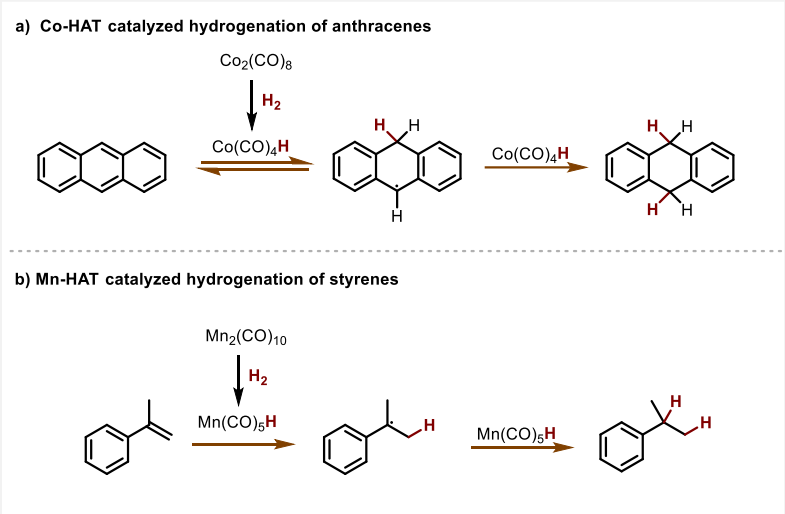

Scheme 1.1 Halpern's early work on MHAT catalysis

With the rapid advances in this field, the scope of MHAT chemistry has expanded significantly, and a unified mechanistic outline has gradually emerged.[3,4] For example, in a typical MHAT catalytic cycle with cobalt as the metal center (Scheme 1.2), first the Co(II) undergoes oxidation to form the high-valent Co(III)–X (X = OH, F) species. This step often requires a stoichiometric oxidant, such as O_2 or *N*-fluoro compounds. Then Co(III)–X reacts with a hydride equivalent (commonly using silanes or borohydrides) to facilitate the formation of Co(III)–H. At this point, MHAT takes place and a hydrogen atom from the cobalt hydride (Co–H) is transferred to an alkene, giving rise to a carbon-centered radical. The open-shell radical intermediate can be trapped by a radicalophile or electrophile to afford Markovnikov-selectivity product.

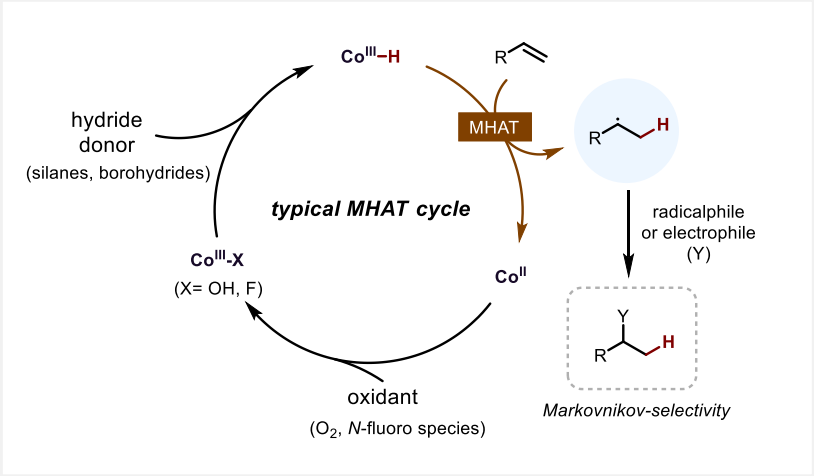

Scheme 1.2 Typical MHAT catalytic cycle

Nowadays, MHAT catalysis has emerged as a powerful tool for functionalization of compounds with electrophilic π-systems, particularly alkenes, generally having high chemo- and regioselectivity.

1.1.2 Transition metal hydrides

Transition metal hydrides are not only widely used in organometallic catalysis, but also play a significant role in energy conversion and hydrogen storage.[5-7] For example, metal hydrides are commonly involved in C–H activation reactions[8] and serve as key intermediates in the formation of many carbon-based fuels[9] as well as in achieving reversible H_2 storage.[10] The reactivity of metal hydrides results from how the M–H bond is cleaved. Since metal hydride species generally have a small dipole moment, there are different pathways including homolytic and heterolytic dissociation, leading to three possible active species: proton (H^+), hydrogen atom ($H^\bullet$) and hydride (H^-) (Figure 1.1).[11,12] Three parameters are used to describe the corresponding thermodynamic properties: acidity (pK_a) for H^+, bond dissociation free energy (BDFE) for $H^\bullet$ and hydricity ($\Delta G°_{H^-}$) for H^-.[13] Notably, in actual reactions, the M–H bond does not always undergo complete cleavage prior to interaction with the substrates. As a result, it is inappropriate to rigidly classify a reaction into a single cleavage mode. For example, the insertion of an alkene into an M–H bond typically involves a concerted process that does not fall strictly into any one category. Moreover, certain metal hydrides, such as $HW(CO)_3Cp$, $HMo(CO)_3Cp$, $HMn(CO)_5$, and $HRe(CO)_5$, can engage in all three pathways, depending on the nature of the substrates.[14]

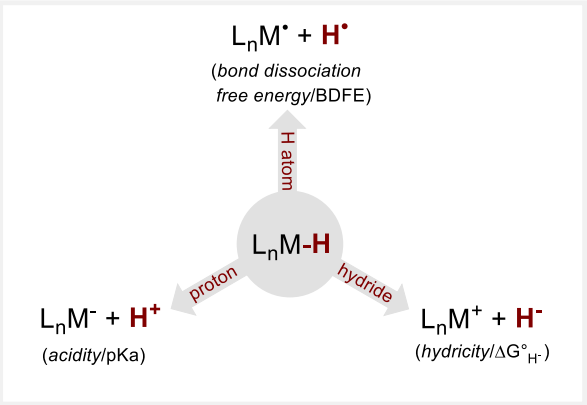

Figure 1.1 Different modes of M–H bond cleavage

The field of MHAT catalysis focuses on the study of metal hydrides undergoing HAT process via homolysis. In this case, BDFE (or BDE, bond dissociation enthalpy, is also widely seen in the literature) is an important parameter in MHAT reactions and must have a value typically lower than 60 kcal/mol.[15]

1.1.3 Strong-field (SF) and weak-field (WF) ligands in metal hydrides

The properties of metal hydrides vary depending on the types of ligands coordinated to the metal center, which influences the reactivity and selectivity in many reactions. According to ligand field theory, metal hydrides in MHAT reactions can be broadly classified based on the type of their ligands: those possessing strong-field (SF) ligands, such as carbonyl, phosphine and pyridine, as well as those with weak-field (WF) ligands, such as salen, acetylacetonate and oxalate.[15] In SF systems, metal hydrides have higher BDFE, generally ranging from 50 to 60 kcal/mol, leading to lower catalytic rates. Due to their stability, metal hydride complexes are often isolable and typically exist in the +1 and +2 oxidation states. However, the reaction types in SF systems are relatively limited, primarily including isomerizations, cyclizations, and hydrogenations. Mechanistically, MHAT is the rate-determining step, and it is thermodynamically endothermic (Figure 1.2 a).[15,16] In contrast, WF systems feature weaker M–H bonds with lower BDFE (generally < 35 kcal/mol), resulting in higher reaction rates and milder conditions, although metal hydrides in these systems are often not isolable. The corresponding metals exhibit an oxidation state of +3. Compared to SF systems, WF systems have a broader range of reaction types. In terms of mechanism, metal hydride formation is the rate-determining step, while the MHAT step is thermodynamically exothermic (Figure 1.2 b).[15,17]

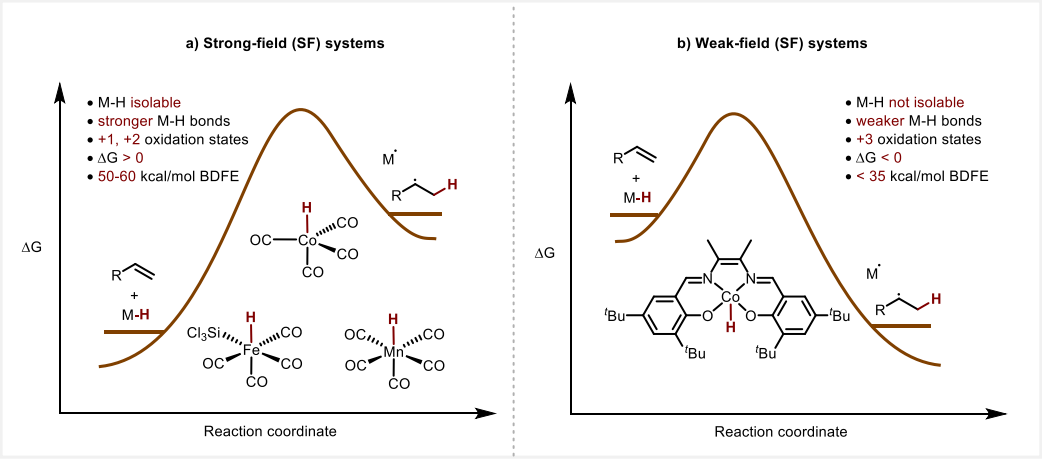

Figure 1.2 Difference between SF and WF ligands in MHAT catalysis

1.1.4 Cage effect and divergent MHAT reactions

Cage effect, a concept first proposed by Franck and Rabinowitsch, was used to describe the relationship between molecular properties and their surrounding environment, particularly the solvent.[18] Similar to the formation of carbocation/anion pair in acid catalyzed reactions via proton transfer, the MHAT process can generate radical pairs, whose behavior is influenced by factors such as solvent viscosity and spin state.[15] The radical pairs become surrounded by solvent molecules, leading to the formation of a solvent cage. In MHAT reactions, the solvent-caged metallo/alkyl radical pair (exemplified here by cobalt) can either undergo cage escape or cage collapse (Figure 1.3). In the path of cage escape, the nucleophilic carbon-centered radical intermediate **A** could be intercepted by an electrophilic radicalophile to furnish the hydrofunctionalization products or react with a second metal-hydride equivalent to yield hydrogenation products. In contrast, cage collapse results in the formation of an organometallic complex **B**. At this point, several pathways are possible: reforming the starting material or undergoing isomerization via β-hydride elimination. The intermediate **B** could also be applied in the cross-coupling reactions through transmetallation with another metal species (exemplified here by nickel). In some reactions, an alkylcobalt(IV) complex, **C**, can be generated from the collapsed alkylcobalt(III) through single electron transfer (SET). The species **C** would go through a S_N2-like substitution reaction, which can be made asymmetric by using a metal catalyst with asymmetric ligands. In some reports, a carbocation **D** is proposed, which can be formed either from oxidation of the escaped alkyl radical [19] or from the heterolysis of alkylcobalt(IV). [20]

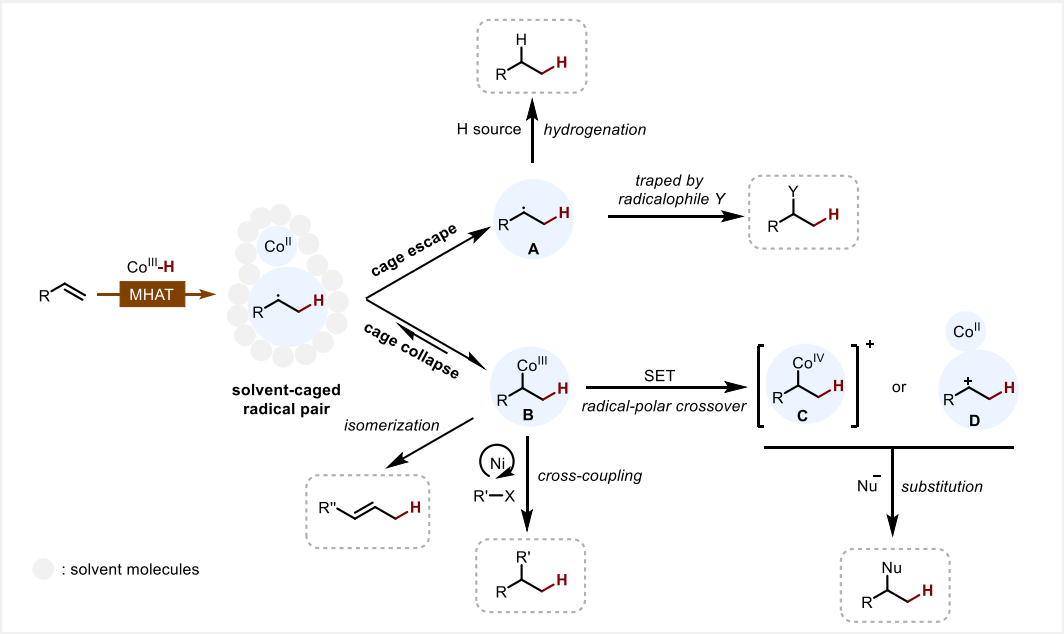

Figure 1.3 Cage effect and divergent MHAT reactions

1.1.5 Comparison with other activation modes

MHAT catalysis exhibit distinctive chemo-, regioselectivity under mild conditions for the functionalization of carbon-carbon double bonds, making it stand out from other activation modes including metal hydrometallation, Brønsted acid catalysis and directed functionalization.[21] The chemoselectivity originates from the rapid kinetics and favorable thermodynamics of HAT step especially for the metal hydrides with weak M–H bonds.[17,22] On the other hand, the key intermediates in MHAT reactions, metal hydrides, are sensitive to steric hindrance, which drives the HAT process to preferentially occur at less hindered positions. Moreover, compared to their carbocation counterparts, the carbon-centered radical generated via MHAT exhibit lower energy and longer lifetimes.[23] These features collectively result in MHAT reactions typically displaying near exclusive Markovnikov regioselectivity.

1) Comparison with Brønsted acid catalysis

Although both MHAT and Brønsted acid catalysis in alkene hydrofunctionalization both exhibit Markovnikov-selectivity, the generated intermediates and functional group tolerance differ significantly. In Brønsted acid catalysis, the carbocation intermediate is highly electrophilic, leading to reactivity with nucleophiles (Scheme 1.3 a). Additionally, the adjacent C–H bonds of the carbocation are highly acidic, with a *p*Ka of approximately –17. As a result, acid-sensitive groups may undergo undesired reactions, ultimately leading to overall poor chemoselectivity.[24] Similar reactivity has also been observed in Lewis acid catalysis. In contrast, the carbon-based radical intermediates generated by MHAT tend to be nucleophilic (Scheme 1.3 b).[25] It also allows the presence of acid or base-labile functional groups. As a result, MHAT catalysis offers higher functional group tolerance, in the substrate and coupling partner, while ensuring excellent chemo- and regioselectivity. Furthermore, these general features provide more possibilities for retrosynthetic analysis. For example, in the following retrosynthetic analysis (Scheme 1.3 c), to synthesize the substituted cyclohexane, the carbon atom attached to the R^1 and R^2 group is

supposed to be nucleophilic to match the polarity. A radical makes it feasible, however, a carbocation, being electrophilic, cannot achieve this transformation.

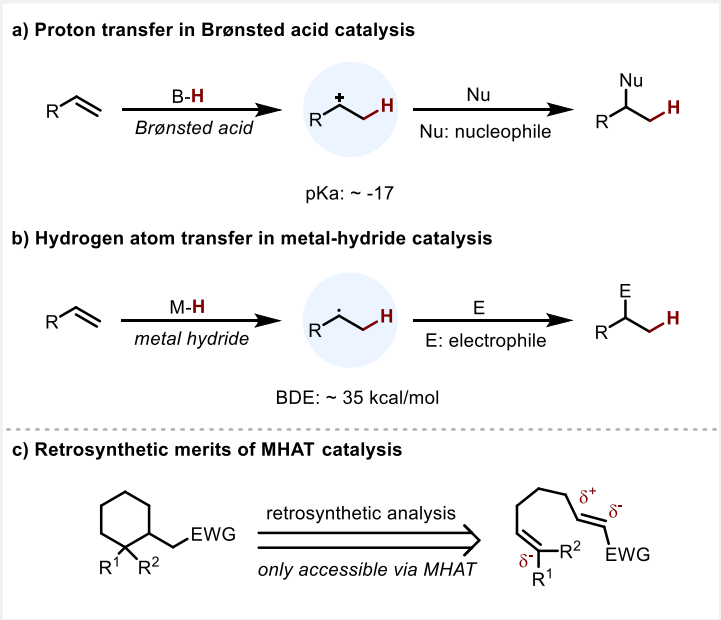

Scheme 1.3 Proton transfer versus hydrogen atom transfer and retrosynthetic merits of MHAT catalysis

2) Comparison with coordinative hydrometallation

In addition to HAT process, metal hydrides can also undergo coordinative hydrometallation. However, the selectivity of such reactions can vary significantly depending on the type of substrate. For electronically unbiased double bonds, steric effects typically lead to linear selectivity (Scheme 1.4). In contrast, for electronically biased substrates such as styrenes, allenes, and enones, the reaction often exhibits branched (i.e., Markovnikov) selectivity. Moreover, since hydrometallation relies on the coordination between the C=C bond and the metal complex, these reactions are generally limited to terminal, sterically unhindered alkenes and are often inhibited by strong Lewis bases.[26]

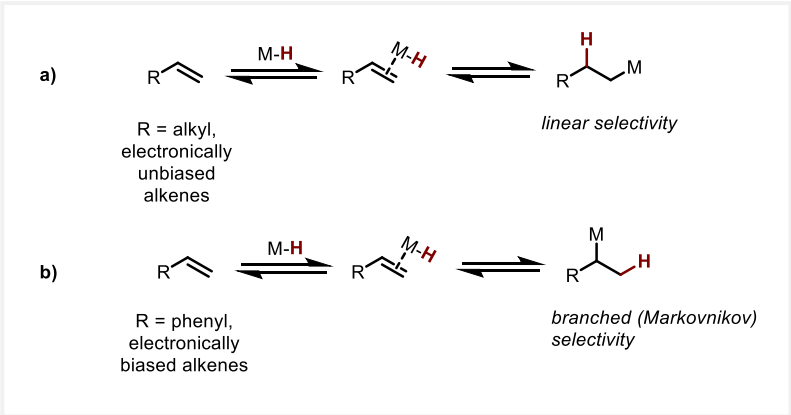

Scheme 1.4 Linear *vs.* branched selectivity based on different substrates

The inherent complexity of selectivity in hydrometallation has led to early examples in the literature occasionally being misidentifed as metalation, despite an MHAT mechanism being more likely. Recently, Shenvi critically examined the mechanistic divergence between MHAT and coordinative hydrometallation in Drago-Mukaiyama reactions (Scheme 1.5).[27] They concluded that an MHAT elementary step was more feasible, as it could reasonably account for the exclusive Markovnikov selectivity observed in the reaction, as well as the carbon-centered radical behavior observed experimentally. Moreover, the reaction's low sensitivity to Lewis basic functional groups and various alkene substitution patterns could also be rationalized under this mechanism. In contrast, if the reaction proceeded via a hydrometallation pathway, alkene insertion into the M–H bond would typically be governed by steric factors and favor anti-Markovnikov selectivity, which is inconsistent with the experimental results. Additional discrepancies include the observation that certain metal complexes can still react efficiently even without a vacant coordination site cis to the M–H bond—required for a traditional hydrometallation mechanism. Furthermore, this mechanism cannot explain the observed tolerance toward Lewis basic groups.

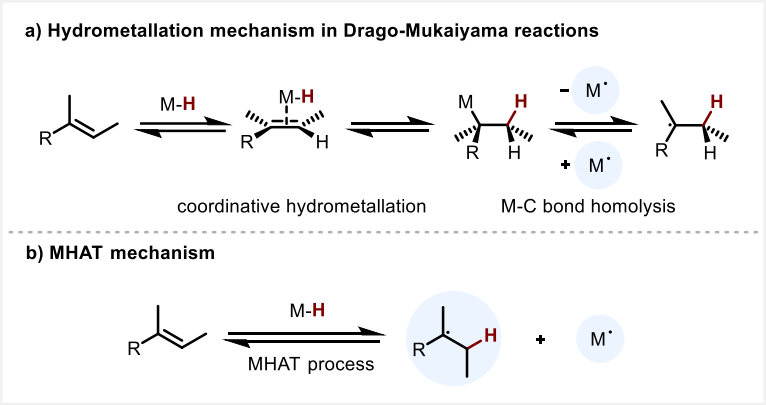

Scheme 1.5 Comparison of coordinative hydrometallation and MHAT processes

3) Comparison with directed functionalization

The strategy of using substrate-directing groups can also facilitate the hydrofunctionalization of alkenes, allowing for precise selectivity control and overcoming steric and electronic limitations.[28] However, employing directing groups has some disadvantages, such as the need for specific spatial proximity to the double bond, as well as difficulties in their preinstallation and subsequent removal. For instance, the Baidya group recently achieved a selective hydroamination of allyl amines under palladium (Pd) catalysis using picolinamide as a directing group (Scheme 1.6).[29] Coordination of the directing group with Pd enhances the electrophilic activation of the alkene, enabling the nucleophilic sulfoximine to preferentially attack the β-position. This process facilitates the formation of a more stable 5,5-palladacycle intermediate, leading to exclusive Markovnikov selectivity as observed in MHAT reactions.

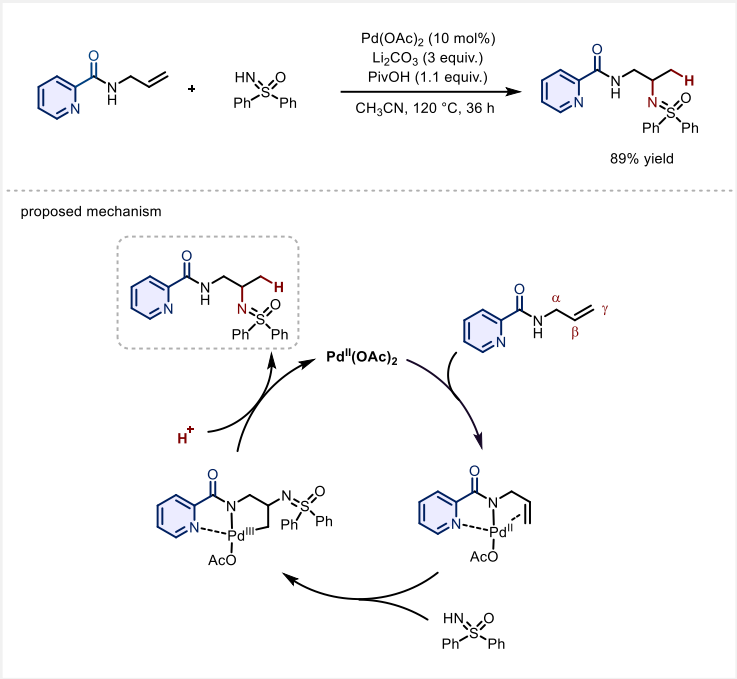

Scheme 1.6 Directing-group-assisted Markovnikov-selective hydroamination of allylamines

1.2 MHAT catalyzed alkene hydrofunctionalization

1.2.1 MHAT catalyzed alkene hydrofunctionalization based on first row transition metals

Most of the MHAT reactions employ first-row transition metals, primarily based on manganese (Mn), iron (Fe) and cobalt (Co), although other metals such as vanadium (V), chromium (Cr), nickel (Ni), and copper (Cu) have also been reported (Figure 1.4). [3,21] They encompasses various transformations including C–C, C–X (X = O, N, S, halogens) bond formation, hydrogenation, isomerization and cross-coupling, while also enabling applications in total synthesis[30] and asymmetric catalysis.[31]

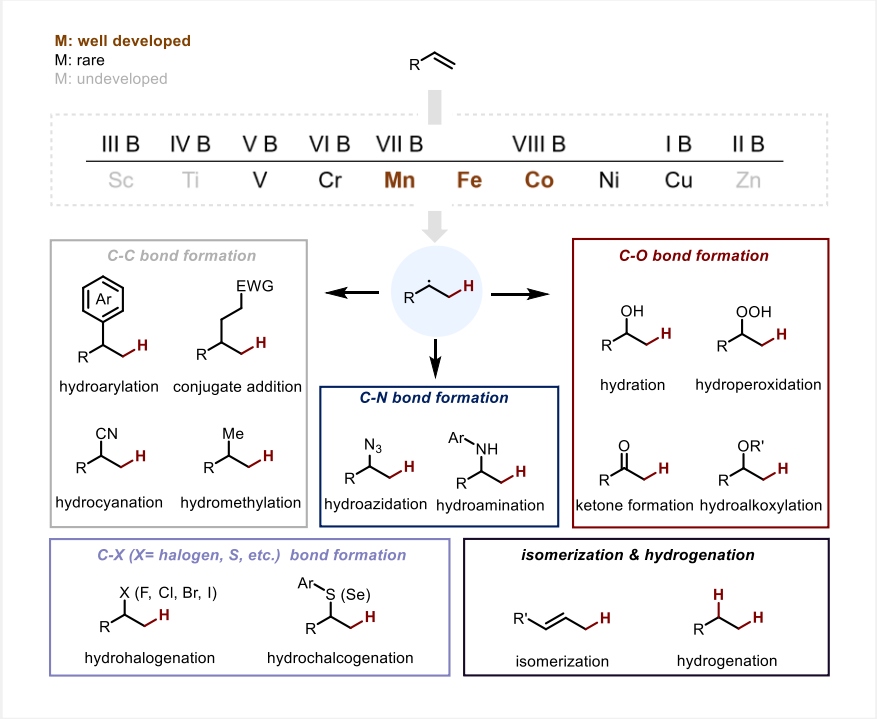

Figure 1.4 First-row transition metals used in MHAT and representative reaction types

In these reactions, particularly in recent studies, metal catalysts are often coordinated with well-defined WF or intermediate field (IF) ligands. Representative frameworks commonly used in cobalt catalysis—along with Fe and Mn—include acetylacetonate, salen, and porphyrin ligands (Figure 1.5).

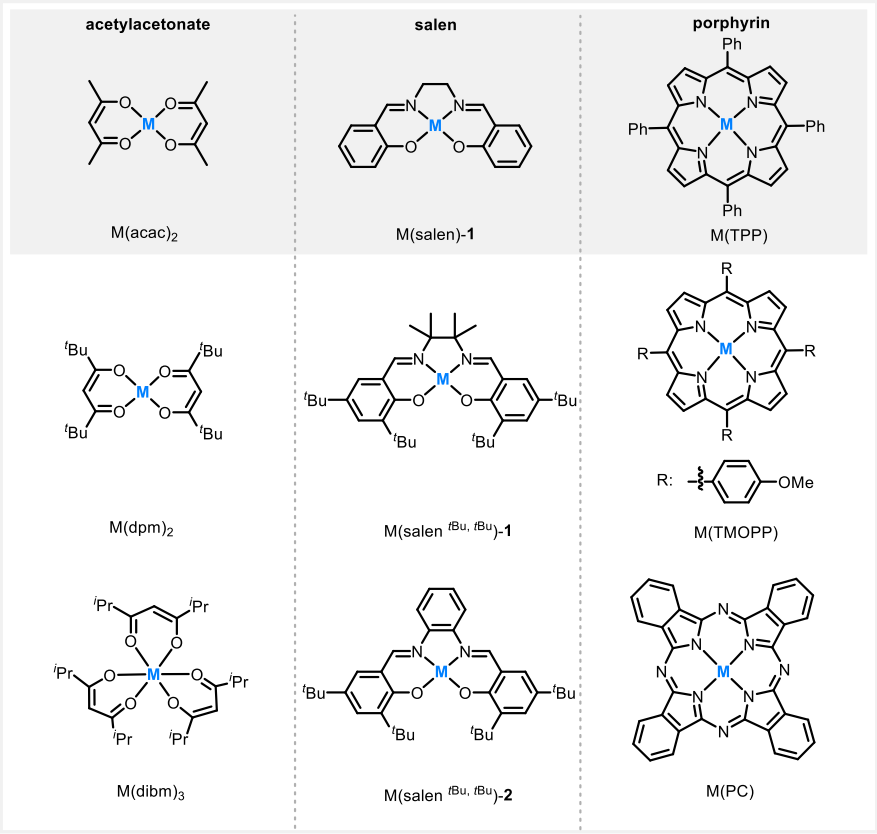

Figure 1.5 Frequently used ligand scaffolds in modern MHAT reactions. acac, acetylacetonate; salen, bis(salicyliden)ethylendiamine; TPP, tetraphenylporphyrin; dpm, dipivaloyl methanato; TMOPP, tetramethoxyphenylporphyrin; dibm, diisobutyrylmethane; PC, phthalocyanine

1) Mn-, Fe-, Co-HAT catalyzed alkene hydrofunctionalization

Manganese, iron, and cobalt were the first metals successfully employed in MHAT-catalyzed hydrofunctionalization of alkenes and remain the most extensively utilized metals. Although the concept and mechanism of MHAT were only explicitly proposed in 1975 and experimentally validated in 1977, the history of MHAT chemistry traces back further, originating from the study of metalloenzyme cofactor ligands by bioinorganic chemists in the 1960s. The structural elucidation of heme protein cytochrome P450 later prompted organic chemists to mimic its iron porphyrin core for catalytic aerobic oxidations.[32,33] Subsequently, Okamoto and Oka, inspired by the central structure of coenzyme B12, employed $Co(dmgH)_2(py)Cl$ for alkene hydration, albeit with low yields (Scheme 1.7).[34] They further discovered that Co(TPP) could facilitate a similar transformation using Et_4NBH_4 as a reductant, achieving yields of up to 87%.[35]

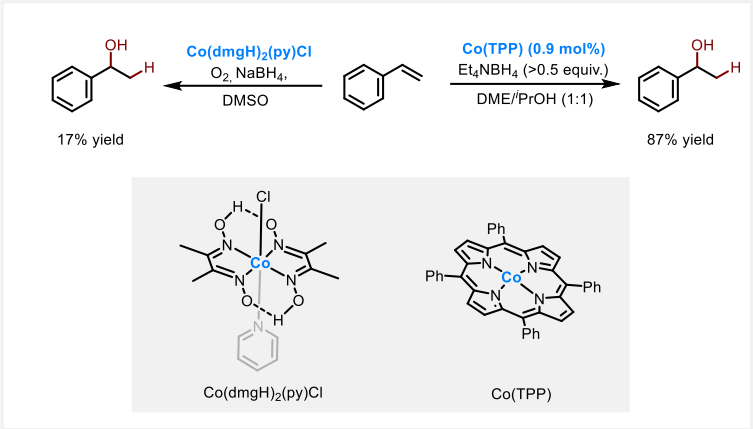

Scheme 1.7 Early work of MHAT catalyzed reactions

Building on these foundational studies, Mukaiyama, Carreira, Baran and other groups significantly expanded the scope of MHAT chemistry. For example, Mukaiyama reported a $Co(acac)_2$ catalyzed hydration of unactivated alkenes using molecular oxygen as the oxidant, with ^{i}PrOH serving as both solvent and reductant (Scheme 1.8 a).[36] The systematic investigation of various reaction parameters, including catalysts and reductants, ultimately led to the well-established Mukaiyama hydration. Inspired by Mukaiyama's work, the Carreira group developed numerous MHAT-catalyzed hydrofunctionalization reactions of alkenes around the early 2000s. Notably, in 2004, they reported $Mn(dmp)_3$-catalyzed hydrohydrazination of diverse alkenes, including highly challenging tetrasubstituted alkenes (Scheme 1.8 b).[37] They compared Co and Mn catalysts and found that Mn exhibited higher catalytic activity than Co. In subsequent studies of hydrocyanation of unactivated alkenes, cobalt catalysts bearing salen ligands showed excellent reactivity, enabling C–C bond formation under mild conditions. Investigations revealed that both Co(II) and Co(III) could catalyze the reaction but Co(II) exhibited superior catalytic activity (Scheme 1.8 c).[38]

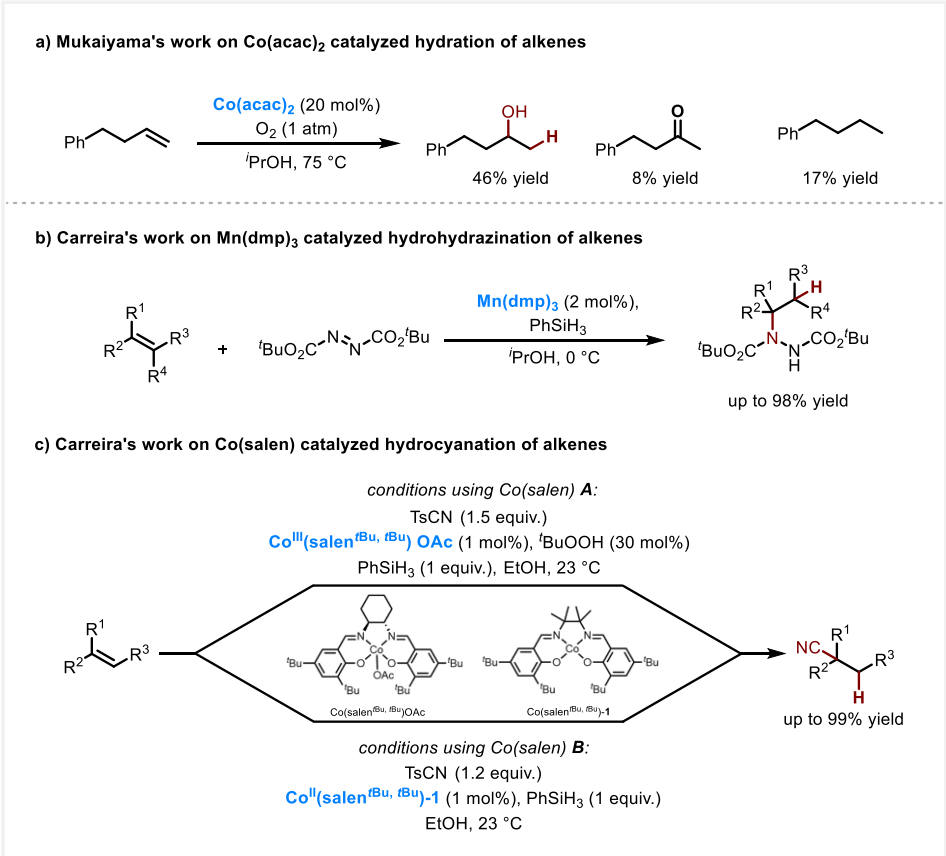

Scheme 1.8 Mukaiyama and Carreira's work of MHAT catalyzed reactions

The Baran group has also made significant contributions to MHAT reactions, particularly in Fe-catalyzed Giese-type transformations, which has been widely applied in the synthesis of complex molecules and natural products. In their first-generation reaction, $Fe(acac)_3$ served as the MHAT catalyst, phenylsilane as the hydride donor, and ethanol as the solvent (Scheme 1.9 a).[39] In the same year, they developed second-generation conditions, replacing the iron catalyst ligand with diisobutyrylmethane (dibm), which allowed catalyst loading to be reduced to 5% (Scheme 1.9 b).[40] Additionally, the inclusion of a base improved yields and expanded the substrate scope to include alkenes substituted with O, N, S, Si, and halogens.

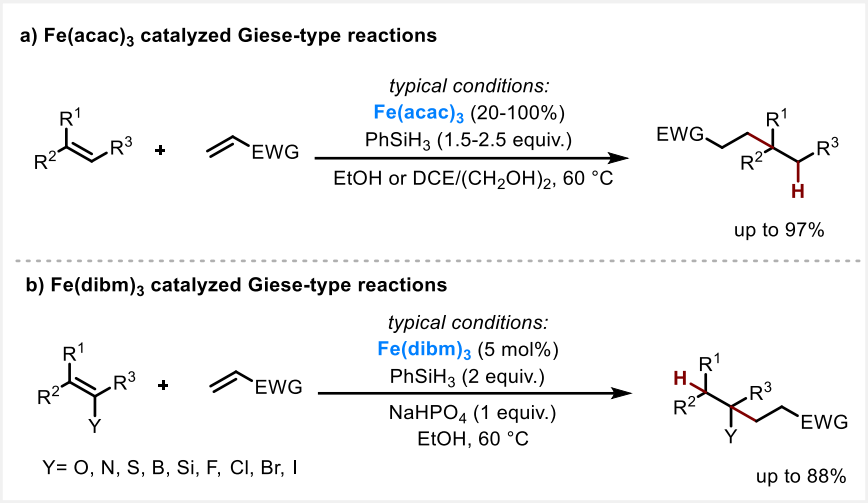

Scheme 1.9 Baran's work of Fe-HAT catalyzed Giese-type reactions

The Shenvi group has reported a variety of studies involving the merger of another transition metal catalytic cycle to facilitate coupling reactions. For instance, they were the first to achieve the cross-coupling of iodoarenes and alkenes through the cooperative catalysis of Co-HAT and Ni, leading to a series of branch-selective hydroarylation products (Scheme 1.10).[41] In the initially proposed mechanism, the authors suggested that the radical generated via the MHAT process undergoes cage escape and subsequently engages in the nickel catalytic cycle. However, through detailed mechanistic studies including reaction progress kinetic analysis, radical clock and stoichiometric experiments, they ruled out this mechanism. Alternatively, they proposed a pathway where reaction proceeds via direct transmetallation between an alkylcobalt species, formed through cage collapse, and a nickel complex.[42]

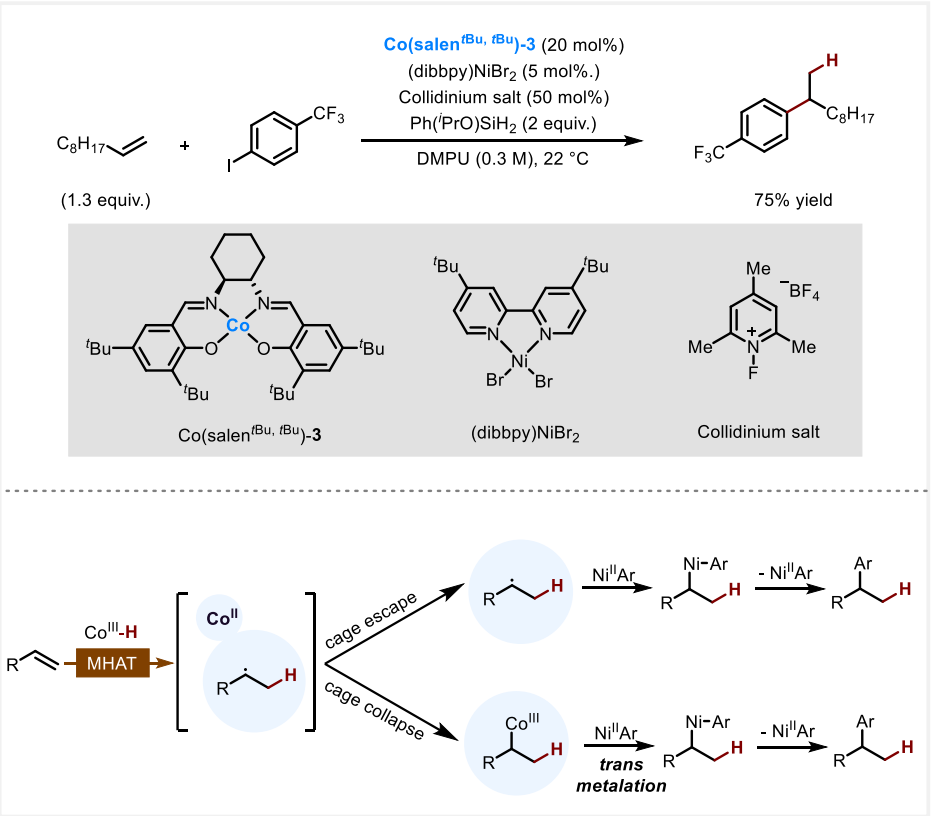

Scheme 1.10 Shenvi's work for Co-HAT catalyzed cross-coupling of iodoarenes and alkenes

In 2024, Morandi and coworkers reported a shuttle HAT strategy where the step of generating Co(III)–H species differs from the previous oxidative (Co(II)/Co(III)) or reductive (Co(II)/Co(I)) methods (see Chapter 1.3.1). In their work, *tert*-butyl iodide undergoes C–I bond cleavage by a metal catalyst to generate a *tert*-butyl radical (Scheme 1.11).[43] A hydrogen atom from adjacent C–H bond is then directly abstracted by Co(II), forming Co(III)–H via a HAA process. In the MHAT cycle, the generated alkyl radical enters the metal catalytic cycle, ultimately yielding the hydroiodination product. In this protocol, *tert*-butyl iodide serves not only as a functional group donor but also as a hydrogen atom donor.

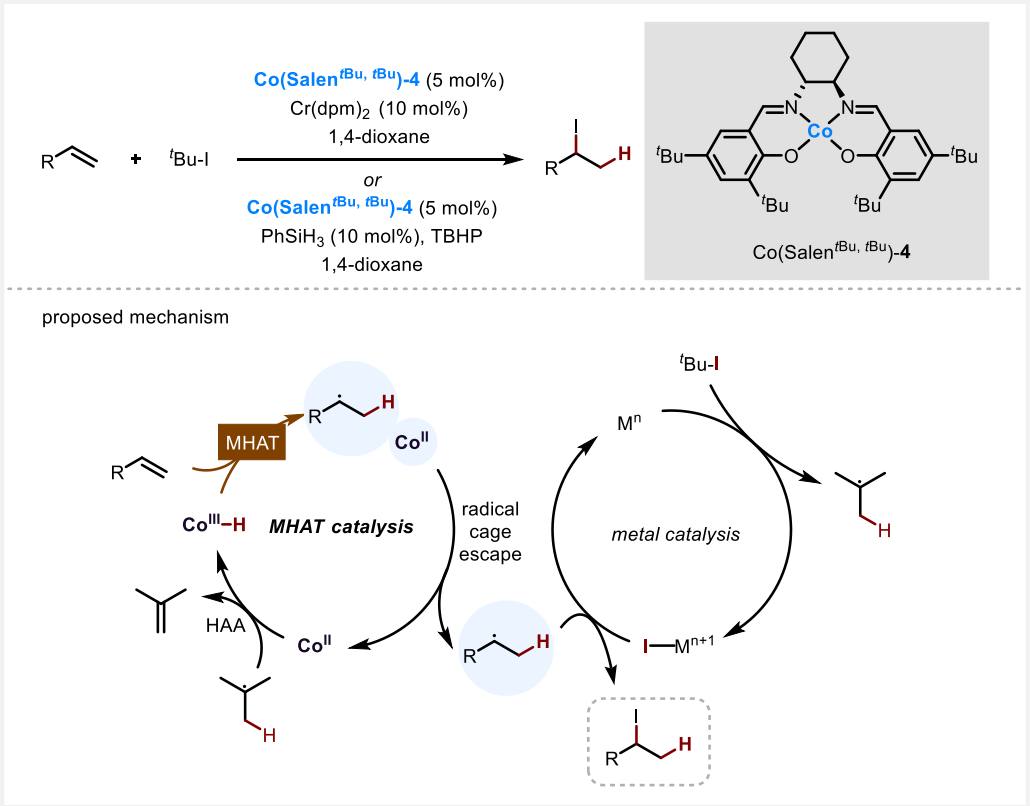

Scheme 1.11 Hydroiodination of alkenes enable by shuttle HAT catalysis

Various energy sources, such as light and electricity, have been increasingly applied in MHAT catalysis, which has expanded the scope of MHAT chemistry. These approaches often enable milder reaction conditions and enhanced functional group tolerance. For example, in 2022, the Zhu group developed an electrocatalytic MHAT process via a radical-polar crossover process (Scheme 1.12).[44] In this work, the alkylcobalt(IV) is generated electrochemically from the collapsed alkylcobalt(III) through anodic oxidation. This method yielded a range of hydrofunctionalization products, including hydroalkoxylation, hydroacyloxylation, hydroarylation, semipinacol rearrangement, and deallylation products, while avoiding the use of stoichiometric chemical oxidants.

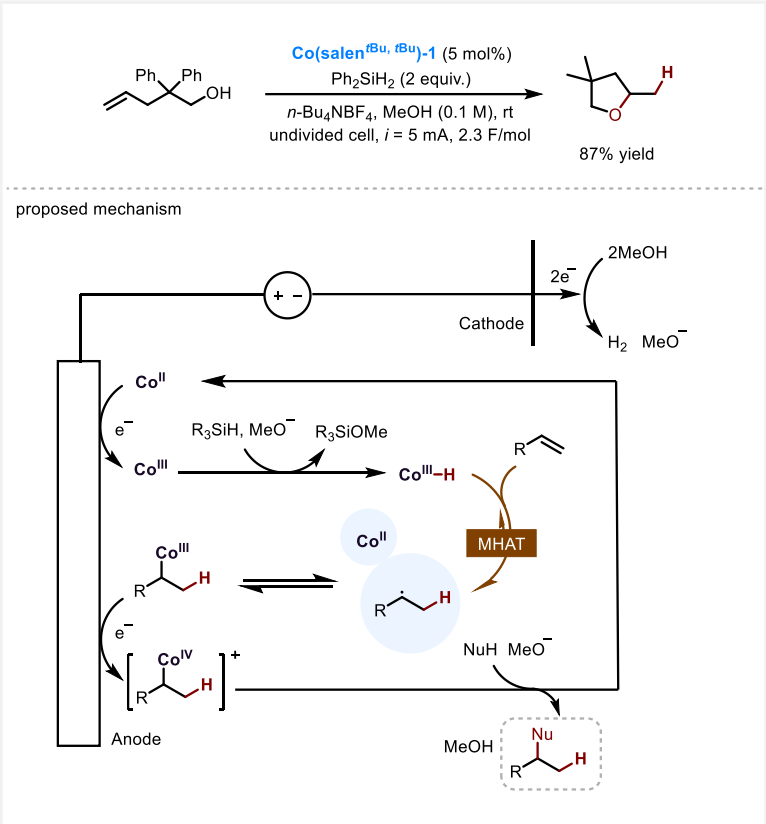

Scheme 1.12 Zhu's work of Co-HAT catalyzed hydrofunctionalization by electrochemistry

The combination of MHAT with visible light has also been extensively explored and will be discussed in detail in Chapter 1.3.

2) Cr- and V-HAT catalyzed alkene hydrofunctionalization

In contrast to other metals, chromium and vanadium are usually employed as stable metal hydrides in MHAT reactions, serving directly as catalyst. The Norton group has conducted extensive studies in this field, systematically investigating the properties and reactivity of Cr- and V-based metal hydrides. For instance, in 2007, Norton utilized $CpCr(CO)_3H$ as a catalyst to achieve the cyclization of dienes, affording substituted cyclopentanes with high yields (Scheme 1.13 a).[45] Subsequently, they explored the reactivity of different metal hydrides in cyclization reactions and found that only vanadium-hydride facilitated the formation of substituted tetrahydrofuran products (Scheme 1.13 b).[46] This outcome was attributed to the weaker V–H bond (57.5 kcal/mol), which favors the MHAT step to generate the α-ether radical. In contrast, $CpCr(CO)_3H$ leads to a reduction product due to the fast reverse reaction and slow HAT process from Cr–H to the styrenyl double bond.

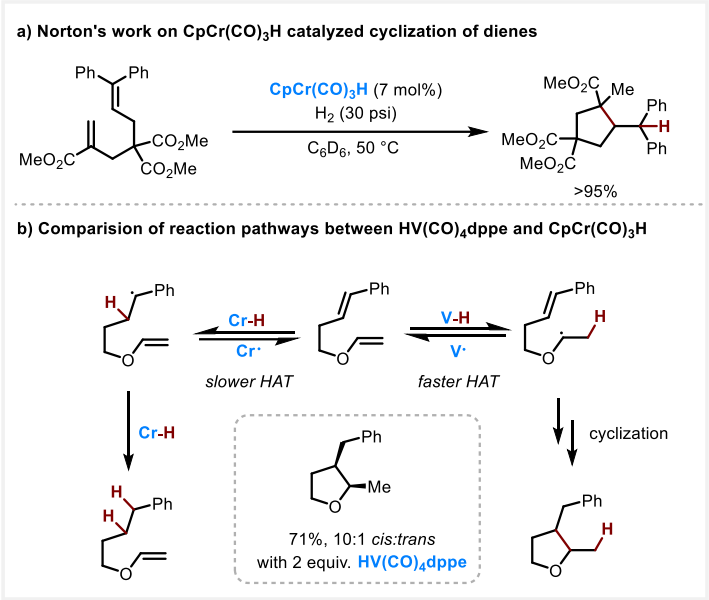

Scheme 1.13 Norton's work on Cr- and V-HAT reactions

In most reported cases of V-HAT reactions, stoichiometric amounts of vanadium hydride reagents are necessary. Moreover, despite a number of further studies, these reactions are yet to become synthetically practical methods. Continuing their work, however, Norton and coworkers reported a vanadium-catalyzed radical cyclization reaction in 2018 (Scheme 1.14).[47] Differing from the general MHAT mechanism, they proposed that an electron transfer (ET) rather than a HAT from $[CpV(CO)_3H]^-$ enables the initial radical formation. The generated 17e$^-$ species $CpV(CO)_3H$ would go through a HAT process to couple with the radial formed via ET, followed by radical anion fragmentation, ultimately affording the final product.

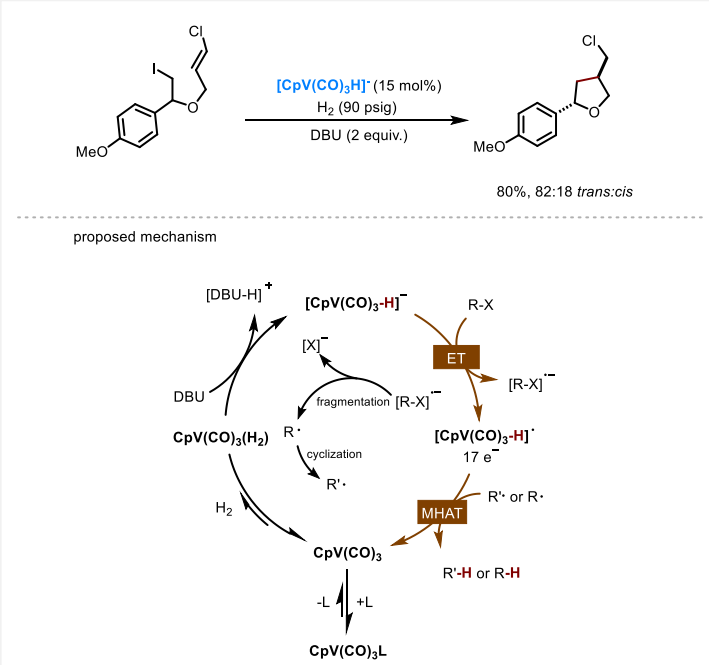

Scheme 1.14 Vanadium catalyzed radical cyclization

3) Ni- and Cu-HAT catalyzed alkene hydrofunctionalization

Nickel hydride (Ni–H) is rarely seen in MHAT reactions, as Ni–H (oxidation state of Ni is +1 or +2) species generally undergo hydrometallation, forming alkylnickel intermediates.[48] Organonickel species can then undergo chain-walking or related processes, enabling functionalization of alkenes at proximal or distal positions. Nonetheless, in 2020, the Norton group reported a hydrodefluorination of CF_3-substituted alkenes using a stable Ni(II)–H catalyst with a pincer ligand (Scheme 1.15).[49] However, two possible reaction pathways have been proposed: fluorine atom abstraction and HAT initiation. In the MHAT mechanism, the hydrogen atom from Ni(II)–H transfers to alkenes to generate a CF_3-substituted radical. This radical subsequently undergoes fluorine atom abstraction, giving the dehydrofluorination products.

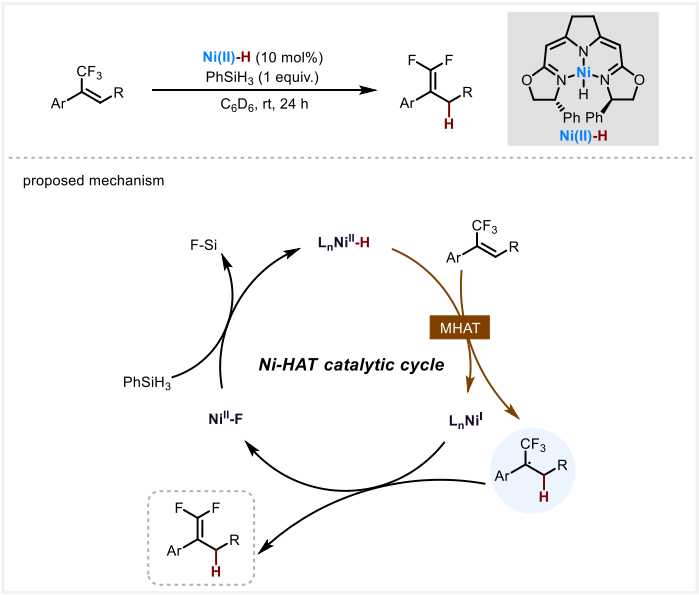

Scheme 1.15 Ni-HAT catalyzed hydrodefluorination of alkenes

Shortly thereafter, the Zhu group described a high-valent Ni(III)–H catalyzed hydrofluorination of unactivated alkenes using *N*-fluorobenzenesulfonimide (NFSI) as the fluorination reagent (Scheme 1.16).[50] The key intermediate nickel hydride species could be generated *in situ*, which underwent a HAT step with alkenes. The formation of an alkyl radical instead of an alkylnickel species could be observed by the cyclization experiment.

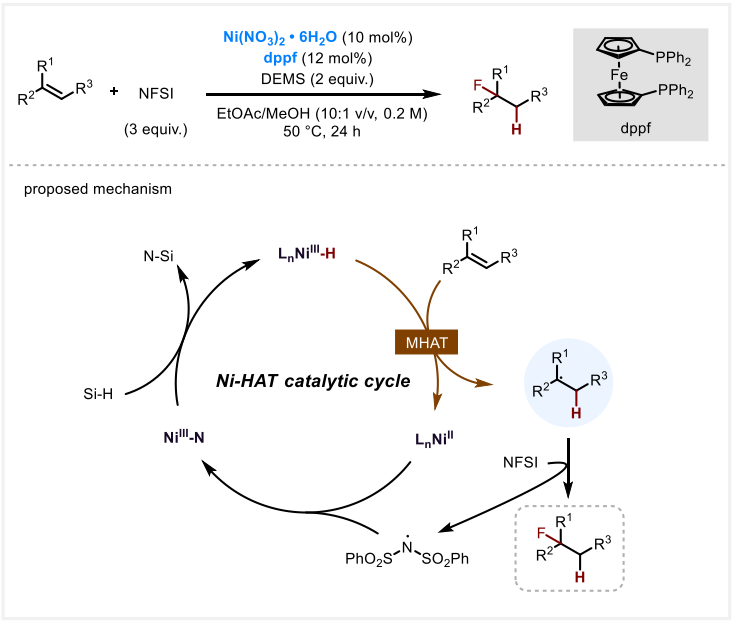

Scheme 1.16 Ni-HAT catalyzed hydrofluorination of alkenes

More recently, the copper hydride was also employed in the MHAT reactions. In contrast to the traditional Cu(I) hydride chemistry that exhibits polar reactivity in the alkene functionalization, the Zhu group proposed the formation of an oxidized copper hydride (Cu^{X}-H, x could be 1 or 2) or equivalent, which could undergo an MHAT process (Scheme 1.17).[51] The generated alkyl radical can react with various nucleophiles under the same catalytic system, forming C–O, C–N, C–X, and C–C coupling products. Similar to typical MHAT catalytic cycles, Cu^{x-1} was oxidized to form Cu^{X}–F, which abstracted H from silanes to generate the key intermediate Cu^{X}-H. DFT calculations suggested the HAT mechanism over hydride transfer. The BDE of Cu^{X}–H in this reaction was 16.5 kcal/mol, consistent with characteristic WF MHAT catalysis.

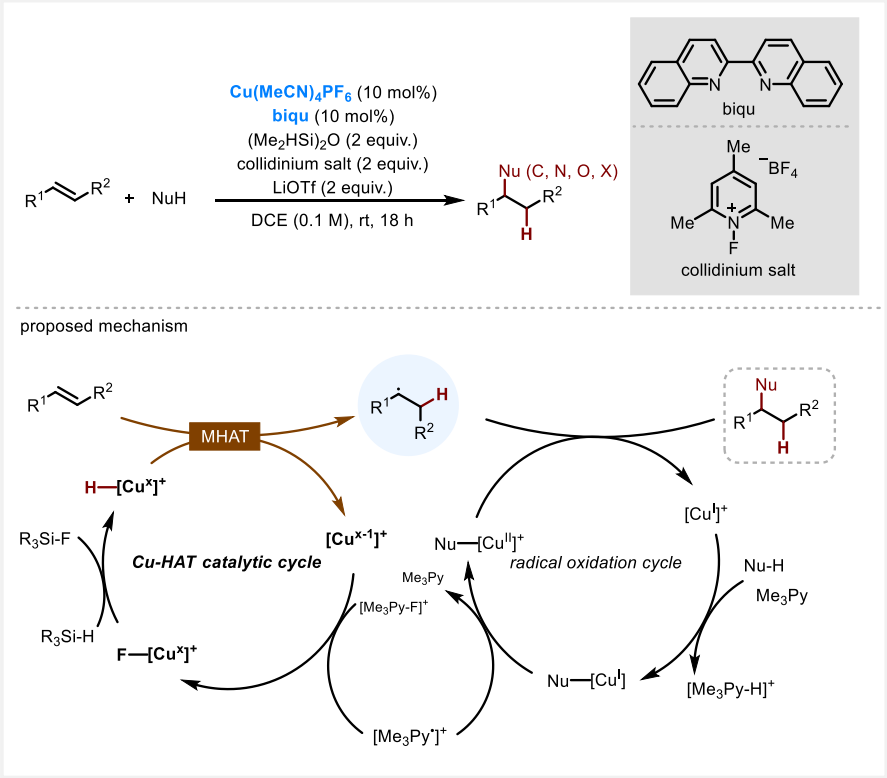

Scheme 1.17 Cu-HAT catalyzed hydrofunctionalization of alkenes

1.2.2 MHAT in asymmetric catalysis

As mentioned in Chapter 1.1.4, the alkylcobalt(IV) often behaves like a carbocation, which undergoes S_N2-like substitution with a nucleophile. This step can be stereochemically controlled by an appropriate chiral ligand, enabling asymmetric catalysis. An interesting observation is that cobalt-based catalysts have been most extensively employed in both non-asymmetric and asymmetric transformations, particularly in recent studies. Among ligand families, salen derivatives are the most widely used, whose structures can accommodate chiral frameworks to regulate stereoselectivity. As early as 2016, Shigehisa and coworkers discovered that chiral Co(salen) could enable asymmetric intramolecular hydroalkoxylation of unactivated alkenes. However, the stereoselectivity at the time was poor, with a maximum enantiomeric excess (*ee*) of only 28%.[52] It was not until 2019 that the Pronin group employed a sterically more congested chiral Co(salen) catalyst, using allylic alcohols as substrates, to afford a series of highly enantioenriched epoxide derivatives (Scheme 1.18).[53] This represented the first example of achieving high enantioselectivity via MHAT-based asymmetric catalysis. In the reaction mechanism, allylic alcohol goes through an MHAT process to generate a α-hydroxyl carbon-centered radical, followed by cage collapse to form an alkylcobalt(III) intermediate. The cobalt(III) species then undergoes radical-polar crossover, yielding a cationic Co(IV). The cation-π interaction within the catalyst stabilizes the radical cation, facilitating stereochemical induction. This step is the stereodetermining event.

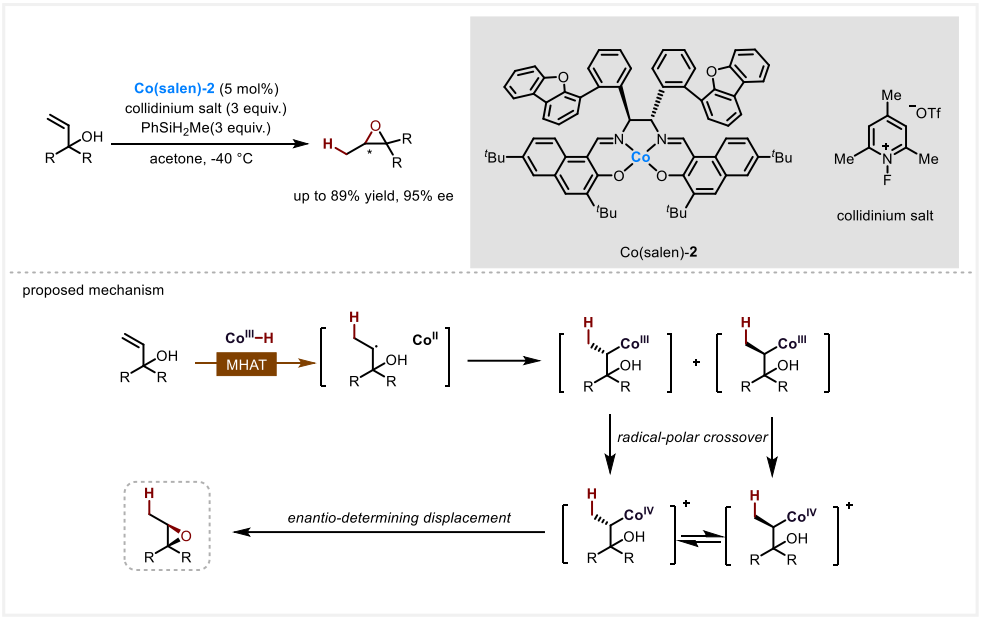

Scheme 1.18 Co-HAT catalyzed asymmetric epoxidation of allylic alcohols

On the other hand, the combination of MHAT catalysis with traditional transition-metal asymmetric catalytic systems can also achieve excellent enantioselectivity. For instance, in 2020, the Lin group developed a Co-HAT/Cu dual catalysis strategy for the asymmetric hydrocyanation of conjugated alkenes (Scheme 1.19).[54] Mechanistic studies suggest that under electrochemical conditions, styrenes undergo a Co-HAT catalytic cycle to generate benzyl radicals, which are then captured by a $Cu(OTf)_2$ complex coordinated with a chiral sBOX ligand. The resulting intermediate undergoes oxidative addition and reductive elimination to afford the final chiral product.

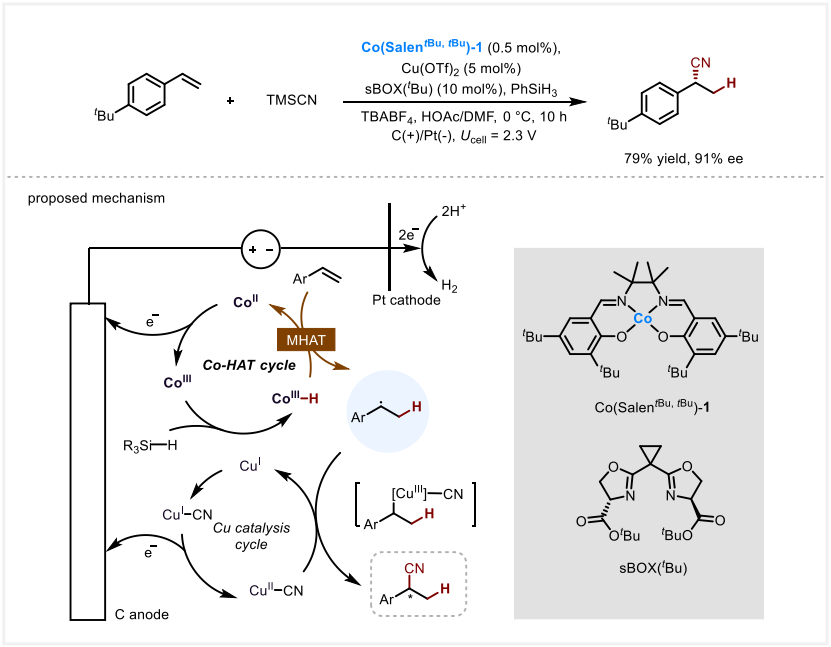

Scheme 1.19 Co/Cu dual catalytic asymmetric hydrocyanation of styrenes

1.2.3 Applications of MHAT in total synthesis

MHAT catalysis not only serves as a versatile and powerful tool in organic methodology but plays a crucial role in more practical area: total synthesis or synthesis of complex molecules.[30] In fact, MHAT catalysis have been employed in total synthesis since early on. In 1994, Matsushita *et al.* employed MHAT strategy in the total synthesis of (−)-pyrenophorin.[55] In the transformation from dienone **1.1** to 1,4-dicarbonyl compound **1.2**, a cobalt catalyst with a porphyrin ligand was used to generate a hydroperoxide firstly, followed by the treatment with acetic anhydride and 4-dimethylaminopyridine (DMAP) to afford the desired product **1.2** (Scheme 1.20).

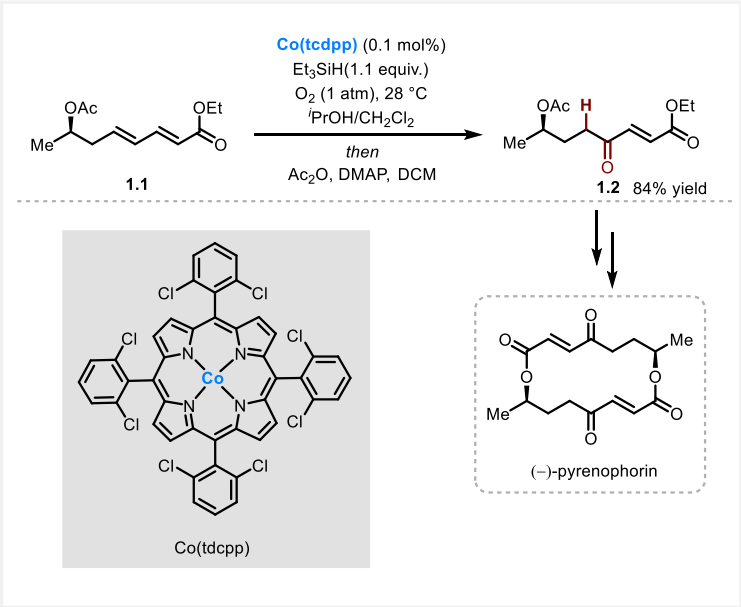

Scheme 1.20 Co-HAT catalysis in the total synthesis of (-)-pyrenophorin

Shortly after, the Wakamatsu group achieved the α-hydroxylation of α,β-unsaturated esters **1.3** under Mukaiyama conditions catalyzed by $Mn(acac)_2$ in the total synthesis of gomisin A, affording product **1.4** with a diastereoselectivity of 7:1 (Scheme 1.21).[56]

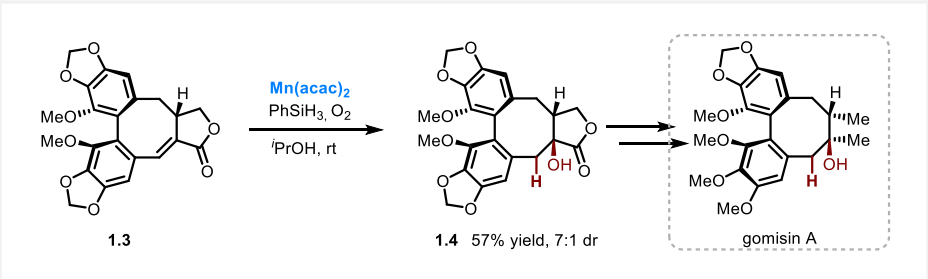

Scheme 1.21 Mn-HAT catalysis in the total synthesis of gomisin A

The Li group employed $Fe(acac)_3$-catalyzed MHAT reaction to construct the core frameworks of daphnezomine A and daphnezomine B, assembling compound **1.6** with a *trans*-fused ring junction as the sole cyclized product (Scheme 1.22).[57] In contrast, alternative strategies, such as Lewis acid-promoted ene cyclization and base-mediated anionic cyclization, failed to deliver the desired product, presumably due to the steric hindrance of the Michael acceptor. The success of the Fe-

catalyzed MHAT process is likely attributable to the radical intermediate's reduced sensitivity to steric constraints.

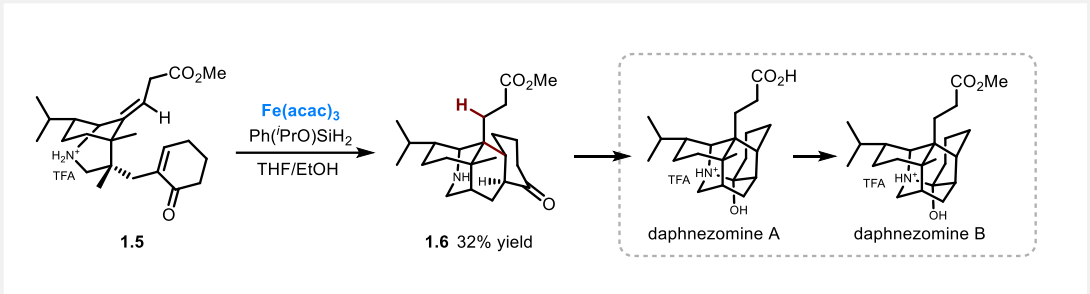

Scheme 1.22 Fe-HAT catalysis in the total synthesis of daphnezomine A and daphnezomine B

More recently, Gao and coworkers utilized MHAT catalysis twice as key steps in the synthesis of norzoanthamine to construct its congested carbocyclic core (Scheme 1.23).[58] In the Co-HAT catalysis, a quaternary carbon center in **1.8** was established through hydroarylation of double bond in **1.7**, while Mn-HAT catalysis enabled the stereoselective hydrogenation of a tetrasubstituted alkene in structure **1.9** to have access to compound **1.10**.

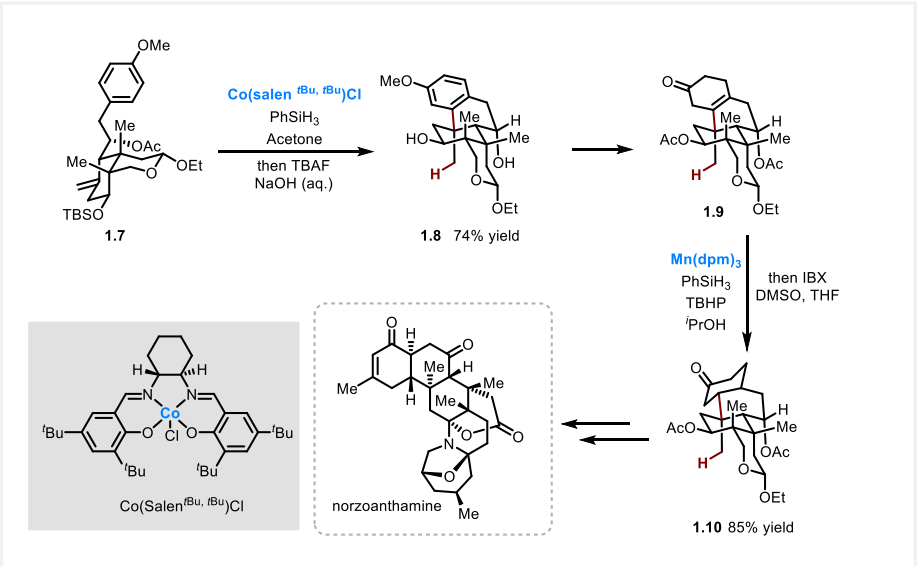

Scheme 1.23 Co- and Mn-HAT catalysis in the total synthesis of norzoanthamine

1.3 Merger of MHAT catalysis with photocatalysis

Over the past decades, photocatalysis has driven a renaissance in radical chemistry due to the ability to access open-shell species under mild conditions.[59-61] Its combination with other catalytic modes, such as transition-metal catalysis, is capable of the transformations that would otherwise be unattainable.[62-64] In traditional MHAT-catalyzed reactions, chemical oxidants or reductants are often required to generate the key metal hydride intermediate. The merger of photocatalysis enables the modulation of metal oxidation states via single electron transfer (SET) processes, thereby providing milder conditions to form metal hydrides and unlocking new possibilities in organic synthesis.

1.3.1 General mechanism of photoinduced MHAT catalysis

Based on the generation pathways of metal hydrides, the reaction mechanism can be classified into two types: oxidative and reductive generation (Scheme 1.24).[4] Since most of the current studies on photoinduced MHAT catalysis are based on cobalt, it is used as an example in the scheme below. The first follows an oxidative pathway, where the catalytic cycle begins with the oxidation of Co(II) to Co(III)–X via a SET process mediated by photocatalysis. The resulting Co(III)–X species then reacts with a hydride donor, such as silane, to generate the key Co(III)–H intermediate. The second follows a reductive pathway, in which the catalytic cycle starts with the photocatalytic reduction of Co(II) to Co(I). The Co(I) species subsequently reacts with a proton to afford the same Co(III)–H intermediate.

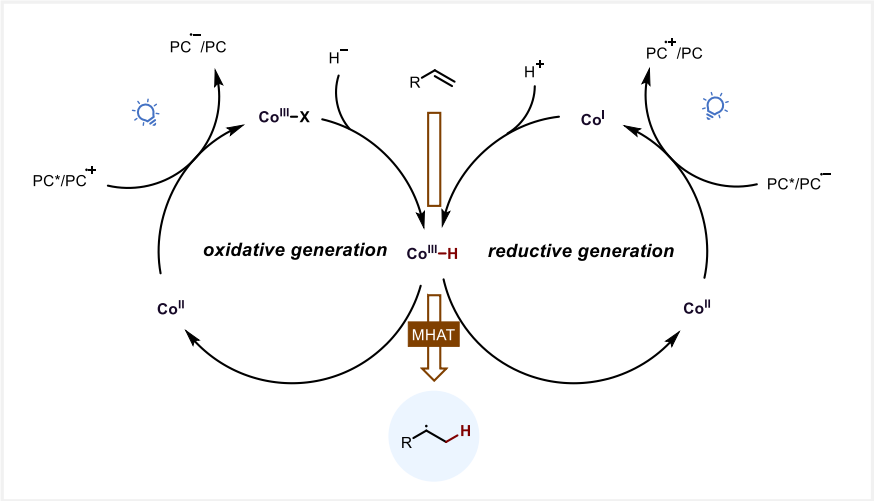

Scheme 1.24 General mechanism of photoinduced oxidative and reductive generation pathways

1.3.2 Visible-light photocatalytic MHAT reactions

In an oxidative pathway, radical coupling with species generated from another catalytic cycle, as well as radical-polar crossover processes, frequently occur. For example, Zhu and coworkers combined MHAT catalysis with ruthenium (Ru)-based photocatalysis to facilitate the reaction of alkenes with various nucleophiles, achieving a series of intermolecular hydrofunctionalization reactions (Scheme 1.25).[65] However, in the absence of both light and the photocatalyst, the reaction was significantly suppressed, with dimers of alkenes becoming the main products. Mechanistic investigations of the photoredox/MHAT dual catalysis demonstrated that the process involves a radical-polar crossover from a Co(III) to a Co(IV) species. The proposed mechanism is as follows: Co(III)–H reacts with the alkene via a HAT process, generating a radical pair that undergoes cage collapse to form an alkylcobalt(III) species. Subsequently, a radical-polar crossover occurs, yielding a Co(IV) species due to redox matching with the reductive quenching of the photocatalytic cycle. The Co(IV) intermediate is then intercepted by a nucleophile via S_N2-like substitution reaction, affording the final product while regenerating Co(II). In the presence of Ru(II) and an oxidant (hypervalent iodine reagent **1.11** or collidinium salt) , Co(II) is transformed to Co(III)–X (X = OH, F). Finally, Co(III)–H is regenerated, driven by the conversion from Si–H to Si–X bond.

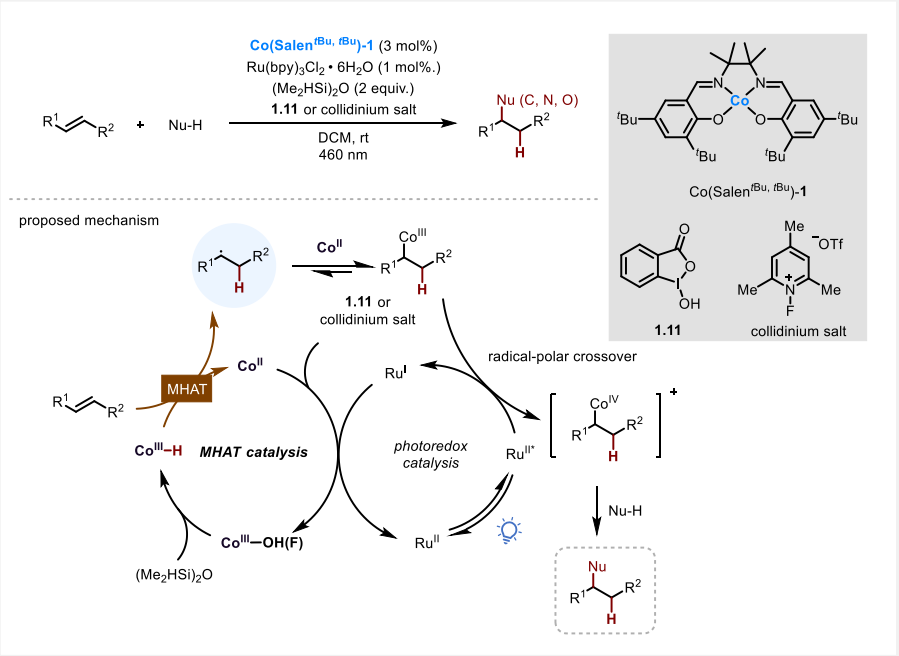

Scheme 1.25 Visible-light induced Co/Ru dual catalytic hydrofunctionalization of alkenes

In 2022, the Luo group developed a Co-HAT-catalyzed dehydrogenative reaction during the total synthesis of (−)-Triptonide (Scheme 1.26 a).[66] Initially, they aimed to achieve the Giese-type reaction from **1.12** to **1.13** using iron catalyzed method, but due to low yields, they instead employed a cobalt catalyst with a porphyrin ligand, ultimately achieving the transformation with a gram-scale yield of 68%. When extending this method to simpler substrates, such as dihydrofurans with Michael acceptors, the reaction outcome differed from that of traditional Giese reactions, yielding only the H-abstraction product without using external photocatalysts (Scheme 1.26 b).

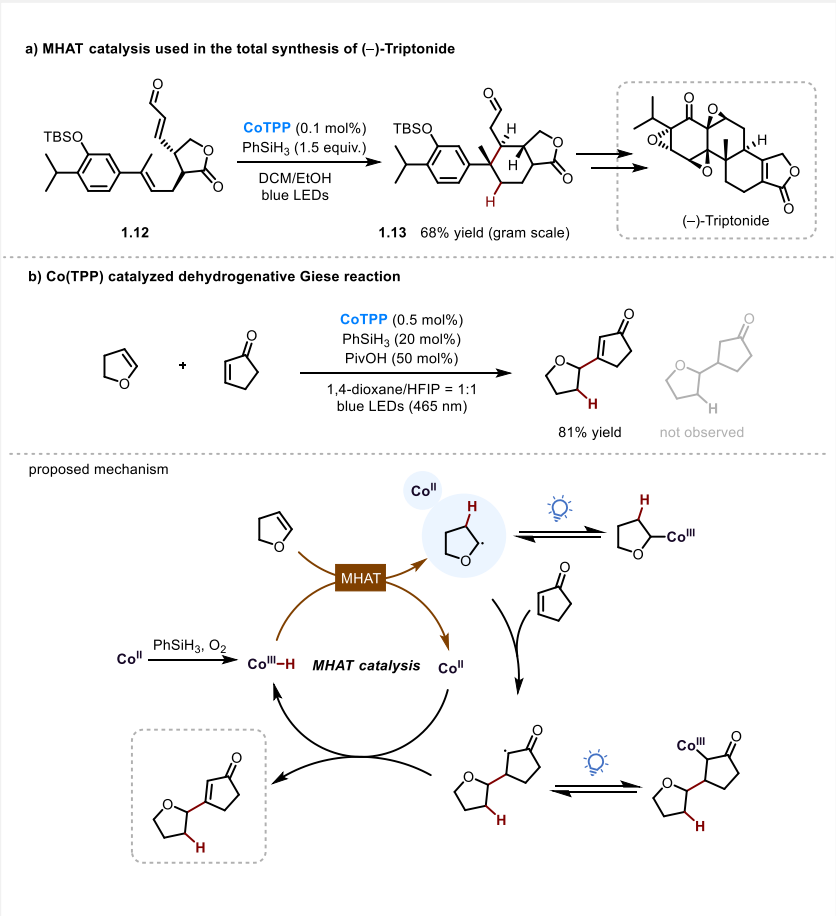

Scheme 1.26 Co(TPP) catalyzed Geise reaction in the synthesis of (–)-Triptonide and dehydrogenative Giese reaction

Previous MHAT reactions were mainly based on oxidative pathways. The Matsunaga group pioneered the use of ascorbic acid as both an electron and proton donor, enabling a series of reductive MHAT reactions. For instance, in 2021, they reported a Co-HAT catalyzed hydrogenation of alkenes.[67] Mechanistically, ascorbic acid donates a proton to generate the key intermediate Co(III)–H from Co(I), while the resulting anion supplies electrons to the photocatalytic cycle (Scheme 1.27). Additionally, it also facilitates the HAT process, converting alkyl radicals formed via MHAT process into the final hydrogenation products.

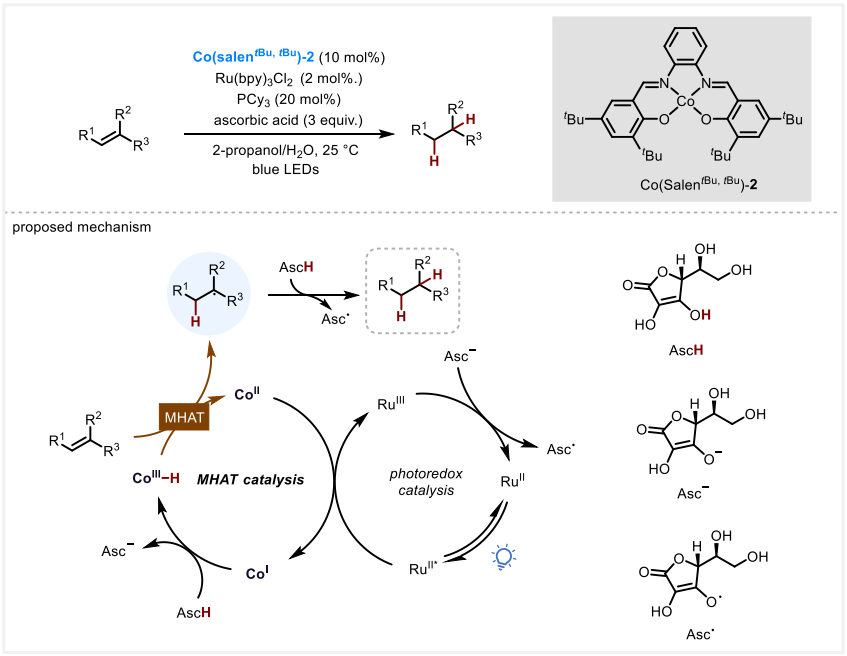

Scheme 1.27 Matsunaga's work of Co-HAT catalyzed hydrogenation of alkenes via reductive generation of Co–H

Our group is also interested in MHAT catalysis and has also developed numerous MHAT reactions via reductive pathways. In contrast to the Matsunaga group, we utilize Hantzsch ester (HE) as the proton and electron donor instead of ascorbic acid (Scheme 1.28).[68] HE can be directly photoexcited by visible light to its excited state, where it exhibits a high reducing ability (E_{red}* = −2.28 V vs SCE in DMF). This feature obviates the need for an additional photocatalyst in the reaction. Upon excitation, HE is capable of reducing both 4-cyanopyridine to generate a persistent radical and Co(II) to Co(I). Meanwhile, styrene undergoes an MHAT process to form a benzylic radical (a transient radical), which subsequently couples with the persistent radical to afford the final hydroarylation product.

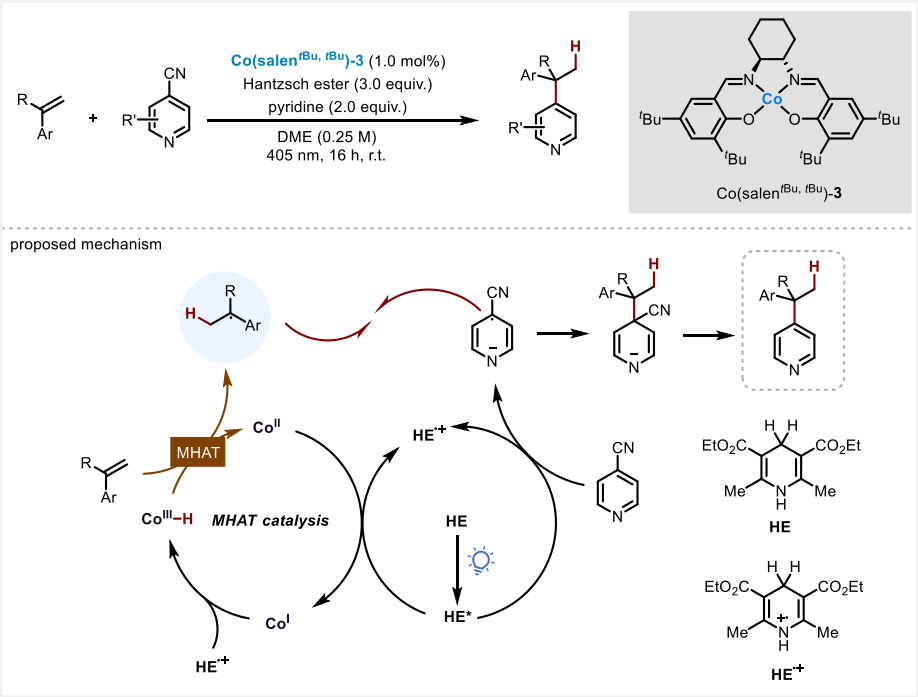

Scheme 1.28 Our group's work for Co-HAT catalyzed hydroarylation of styrenes

Recently, Ohmiya and colleagues combined photocatalyzed MHAT reactions with *N*-heterocyclic carbene (NHC) chemistry to achieve the carbonylation of styrenes (Scheme 1.29).[69] In this method, the aldehyde reaction partner serves not only as the carbonylation reagent but also as the proton source for the formation of the key intermediate Co(III)–H. In the NHC catalytic cycle, the *in situ* generated NHC species reacts with the aldehyde to form a Breslow intermediate, which undergoes single-electron oxidation and protonation to give a persistent ketyl radical. This radical then participates in a radical–radical coupling with a benzylic radical generated via the MHAT pathway, affording the final hydroacylation product. Meanwhile, the NHC is regenerated, completing the catalytic cycle.

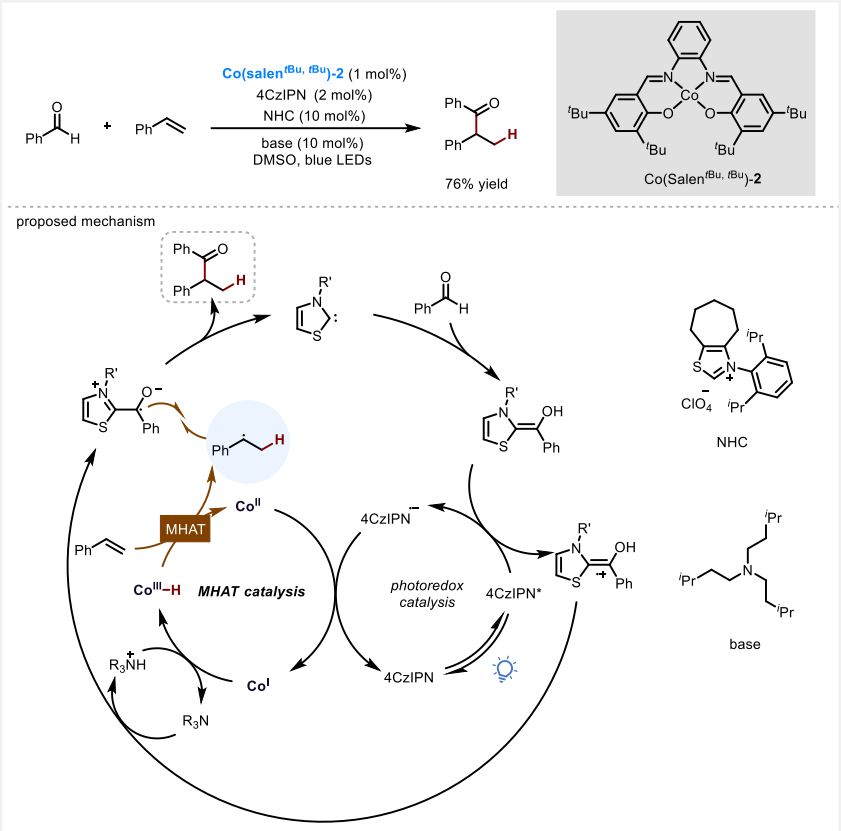

Scheme 1.29 Co-HAT catalyzed hydroacylation of styrenes with the combination of NHC catalysis

The above examples illustrate that these photoinitiated MHAT reactions typically require additional or no photocatalysts. However, some recent studies have adopted an alternative strategy. For example, the Wenger group developed an iridium (Ir)-based catalyst that serves as both a photocatalyst and an MHAT catalyst in alkene hydrogenation via HAT and isomerization reactions via hydrogen atom abstraction (HAA) (Scheme 1.30).[70] According to the proposed mechanism, the initially formed Ir(III)–H species has a BDFE too high for direct HAT and must first undergo reductive quenching by triethylamine (TEA), generating a weaker Ir(II)–H bond with a BDFE of approximately 44 kcal/mol. A substrate-catalyst encounter complex would be formed before the general MHAT process.

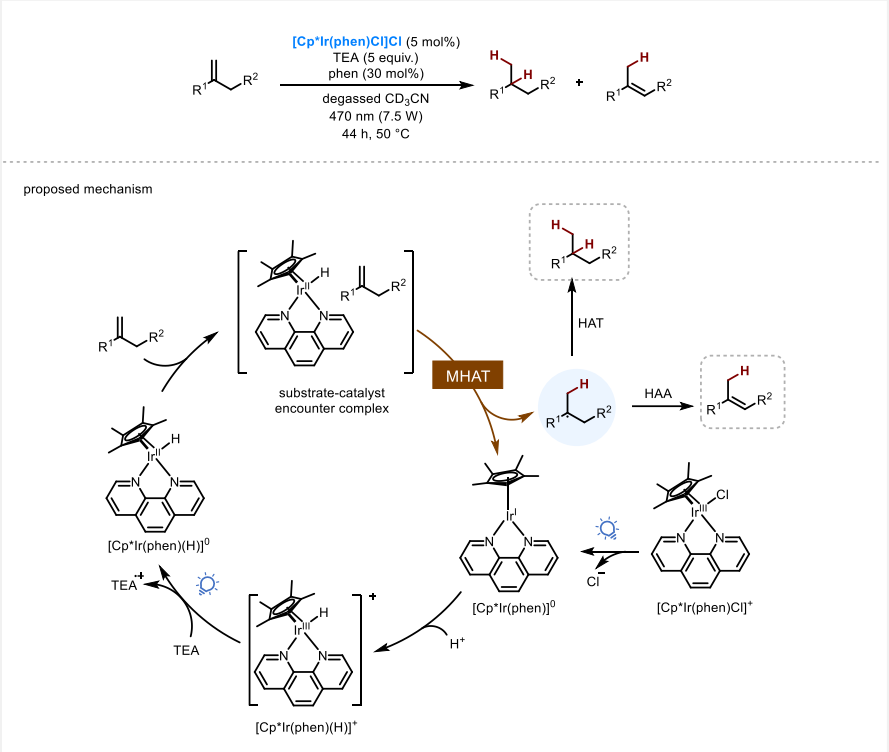

Scheme 1.30 Wenger's work of dual functional Ir-based catalyst in alkene functionalization

1.3.3 Hydrofunctionalization of other electrophilic π-systems

Most reactions utilizing the MHAT strategy use alkenes as starting materials, whereas crucial raw materials dienes and allenes, which also contain π-systems, have been rarely explored. This is primarily due to challenges in controlling chemoselectivity and regioselectivity. In recent years, the combination of visible light and MHAT catalysis has expanded the possibilities for the hydrofunctionalization of such type of compounds. Our group recently developed a dual catalytic system merging visible light and Co-HAT, enabling the selective hydropyridylation of dienes to construct a series of C4-pyridine derivatives. A detailed discussion of this work is provided in Chapter 2. Similarly, the Shi group employed a light-induced bimetallic catalytic strategy that combined a cobalt catalyst with titanium catalysis (Scheme 1.31 a).[71] Under this system, heteroatom (N, O, S)-substituted allenes undergo carbonyl allylation, affording β-functionalized homoallylic alcohols with high regio- and diastereoselectivity. The same strategy was subsequently applied to the transformation of dienes (Scheme 1.31 b).[72]

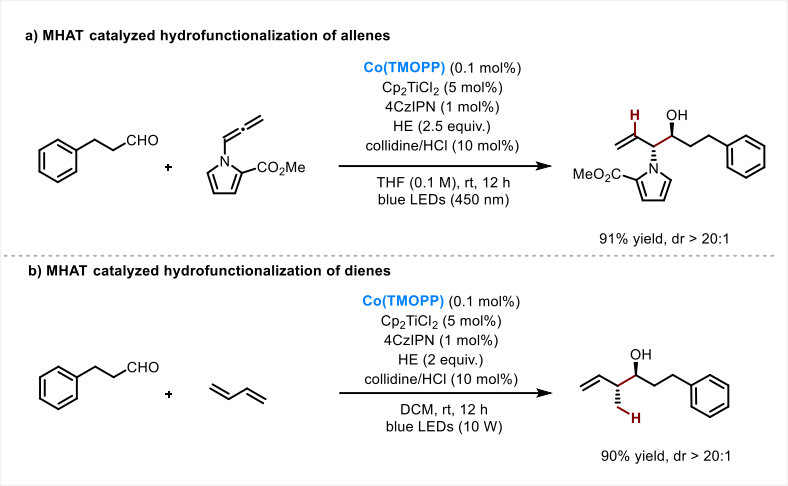

Scheme 1.31 MHAT catalyzed hydrofunctionalization of allenes and dienes

1.4 Summary and outlook

This chapter systematically introduces the concept, mechanism, and applications of MHAT catalysis, particularly its merger with photocatalysis and its role in alkene hydrofunctionalization. As a highly selective radical-mediated strategy, MHAT catalysis has demonstrated significant potential in various transformations, including alkene functionalization, cross-coupling, and total synthesis. The recent merger of MHAT with photocatalysis has further expanded its applicability, enabling precise modifications of complex molecules under mild conditions.

Despite the significant progress in MHAT catalysis, several challenges remain:

1. Current research on MHAT catalysis is primarily focused on Co, Fe, and Mn, while other first-row transition metals remain underexplored. Improving catalytic efficiency and selectivity for these metals remains an open question.

2. Most reported MHAT reactions are limited to alkene functionalization, with relatively few examples involving allenes, dienes, and other electrophilic π-systems. Broadening the substrate scope will be essential for future developments.

3. Although Co-HAT has been applied in asymmetric catalysis, achieving high enantioselectivity remains a challenge. Further advancements in chiral ligand design could improve the stereocontrol of MHAT reactions. In addition, asymmetric reactions of other transition metals frequently used in MHAT catalysis remain largely unexplored

Looking ahead, continued mechanistic studies and the merger of MHAT catalysis with other catalytic strategies—such as electrochemical catalysis and enzymatic catalysis—may overcome these limitations. Such advancements will provide more efficient and sustainable solutions for complex molecule synthesis.

2

Photoinduced Co-HAT Catalyzed Reductive Cross Coupling of Pyridines and Dienes

2 Photoinduced Co-HAT catalyzed reductive cross coupling of pyridines and dienes

2.1 Pyridyl phosphonium salts

2.1.1 Overview of pyridine and pyridyl phosphonium salts

Pyridine is an electron-deficient nitrogen-containing heteroarene that can be found in many agrochemicals,[73,74] functional materials,[75] and metal-catalyst ligands.[76] Of particular note, it is the most prevalent heteroarene in FDA approved small-molecule pharmaceuticals, underscoring its significance in medicinal chemistry (Scheme 2.1).[77] Given its widespread occurrence, the development of efficient methods for pyridine synthesis is of great importance.

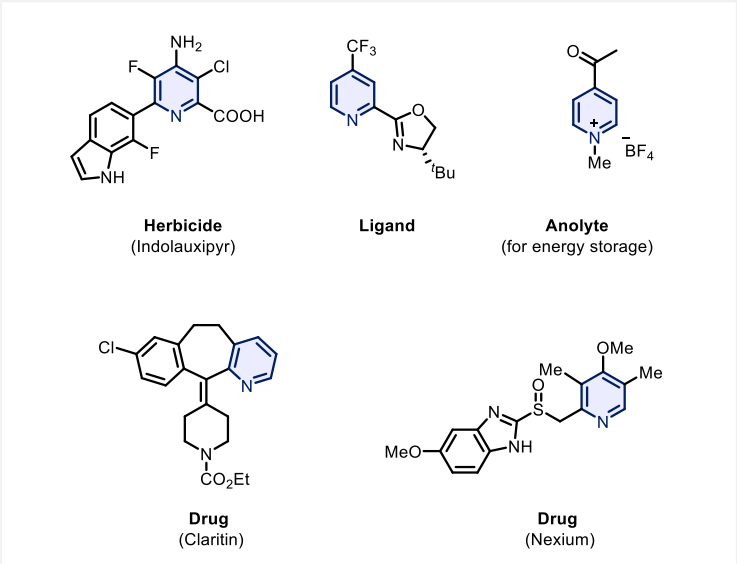

Scheme 2.1 Pyridine-core molecules in pharmaceuticals, ligands and materials

In contrast to traditional multi-step approaches that construct pyridine frameworks from acyclic precursors,[78,79] the direct and selective C–H functionalization of pyridine offers a more straightforward and efficient alternative.[80,81] However, this strategy is significantly challenged by the intrinsic electron-deficient aromatic nature of pyridine and its strong coordinating ability. Despite this, numerous regioselective C2-, C3-, and C4-functionalization methods have emerged over the past few decades. [82] For instance, nucleophilic aromatic substitution (S_NAr) and Minisci-type radical reactions enable C2-selective functionalization, while temporary dearomatization and non-directed metalation have been developed for C3 selectivity (Scheme 2.2). [83,84] Among them, efficient methods for C4-selective functionalization remain relatively scarce. The existing strategies mainly involve the use of *N*-functionalized pyridinium salts[85] and transition-metal-catalyzed C–H functionalization,[86] but they often suffer from selectivity issues.

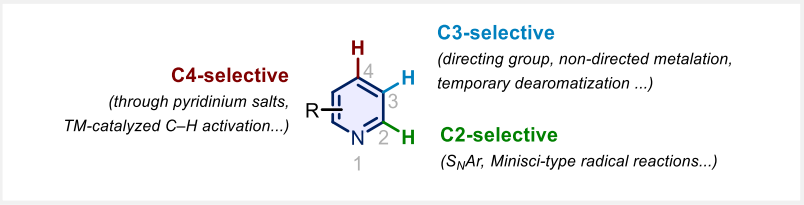

Scheme 2.2 Methods of direct C–H functionalization of pyridines

Recently, the development of pyridyl phosphonium salt reactivity has emerged as a powerful tool for C4-selective pyridine functionalization, providing a versatile platform for subsequent transformations. [87-89] The seminal work for the conversion of pyridine into pyridyl phosphonium salts was reported by the Anders group.[90] This pioneering work was followed by further investigations from Sugimoto and coworkers, although their approach was significantly limited with a narrow substrate scope.[91,92] Research in this area lay dormant until McNally improved the preparation method and synthesized a broad range of functionalized pyridyl phosphonium, giving renewed interest to this field.[93-95] For example, in 2016, McNally and co-workers developed a cross-coupling reaction based on pyridyl phosphonium salts. Under strongly reducing conditions with NaH, these salts reacted with a set of nucleophiles, including metallated heterocycles, alkoxides, alcohols, azides, and thiols, to form diverse C–C and C–heteroatom bonds (Scheme 2.3).[93] According to the proposed mechanism, the alkoxyl phosphorane intermediate undergoes either ligand coupling or direct S_NAr depending on the nature of the nucleophile, followed by loss of PPh_3. This method can also be extended to other nitrogen-containing heterocycles, such as pyrimidines and pyrazines.

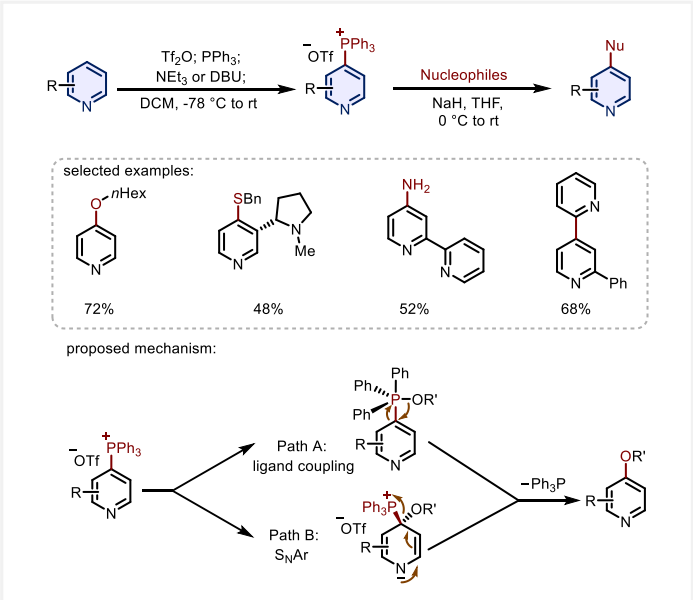

Scheme 2.3 McNally's work for synthesis of pyridyl phosphonium salts and subsequent coupling reactions

C4-Pyridylphosphonium salts exhibit superior functional group tolerance and enhanced reactivity toward diverse nucleophiles, enabling the formation of C–C, C–O, C–N, and C–X (X= S, halogens)

bonds.[89,96] Furthermore, their reactivity has been harnessed for late-stage functionalization of complex molecules, broadening their applicability in organic synthesis.[97,98]

2.1.2 Synthesis of pyridyl phosphonium salts

Pyridyl phosphonium salts can be synthesized through triflation with Tf_2O, followed by substitution with triphenylphosphine (PPh_3) and base-assisted rearomatization (Scheme 2.4). The selection of base (NEt_3 or DBU) and temperature control are crucial for this transformation.[93] This method exclusively yields C4-substituted pyridyl phosphonium salts in most cases. However, when the C4 position of pyridine is occupied, the reaction occurs at the C2 position. Consequently, the formation of pyridyl phosphonium salts provides an indirect yet effective approach for selective pyridine functionalization, particularly at the C4 position.

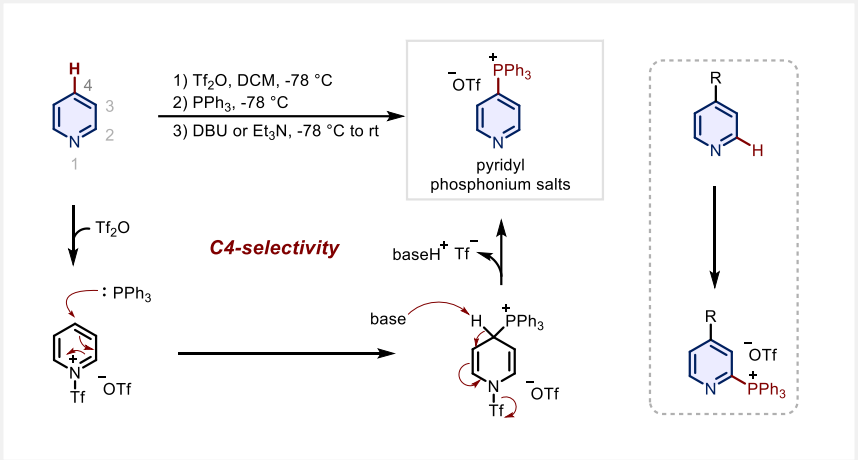

Scheme 2.4 Synthesis of pyridyl phosphonium salts from pyridines

2.2 Co-HAT catalysis for the coupling of pyridyl phosphonium salts and dienes

2.2.1 Introduction

The reactions described in this chapter were performed by Jingyang Qin, Manuel Barday and Samikshan Jana (PhD students and postdoc in the group) under the supervision of Prof. Dr. Christopher J. Teskey. The author contributions are as follow: C.J.T. and J.Q. designed the project. J.Q. and M.B. performed the optimization. Further synthetic work including scope and mechanistic investigations were performed by J.Q., M.B. and S.J.. Ignacio Funes-Ardoiz and Nil Sanosa performed all computational experiments. I.F.-A. and C.J.T. directed the work. This work is published in Angewandte Chemie International Edition.[99]

Due to their pronounced reactivity in double-bond transformations, allylic arenes serve as versatile intermediates for the derivatization into a broad range of functionalized structures. Dienes, as readily available and cost-effective feedstocks, enable the efficient construction of such structures via hydroarylation.[100] It offers advantages over alternative strategies such as allylic hydrogen atom abstraction (HAA) of alkenes that often encounters selectivity issues (Scheme 2.5).[101-104]

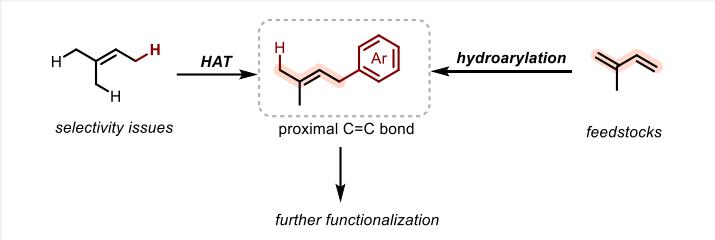

Scheme 2.5 Strategies for synthesis of allyl arenes

Extensive studies on the hydroarylation of 1,3-dienes have been reported using diverse methodologies. For example, Sigman and coworkers disclosed palladium (Pd)-catalyzed reductive coupling of 1,3-dienes and boronic esters through the generation of a π-allyl Pd species (Scheme 2.6 a).[105] Later, Meek and colleagues leveraged a hydrometallation strategy using Ni catalysis to achieve the hydroarylation of 1,3-dienes (Scheme 2.6 a).[106] However, these reactions primarily yield products from 1,2-hydroarylation of dienes and often require aryl substituents to stabilize the diene scaffold, limiting the scope of coupling partners, particularly for heteroarenes. An alternative approach involves the use of π-acidic metal species or Lewis acids to facilitate diene hydroarylation. The Meek group developed a carbodicarbene-Rh complex-catalyzed hydroarylation of dienes, wherein metal salts act as Lewis acid activators, mainly yielding 1,2-selectivity products under mild conditions (Scheme 2.6 b).[107] In 2021, Chatterjee employed boron as Lewis acid catalyst to couple dienes with arylamines, delivering 1,4-/4,1- and 1,2-adducts (the numbering is subject to this thesis). However, the selectivity remains substrate dependent and leads to one of the adducts or their mixtures (Scheme 2.6 b).[108] Notably, these studies primarily utilize electron-rich (hetero)arenes, whereas the hydroarylation with electron-deficient heterocycles remains largely underdeveloped.

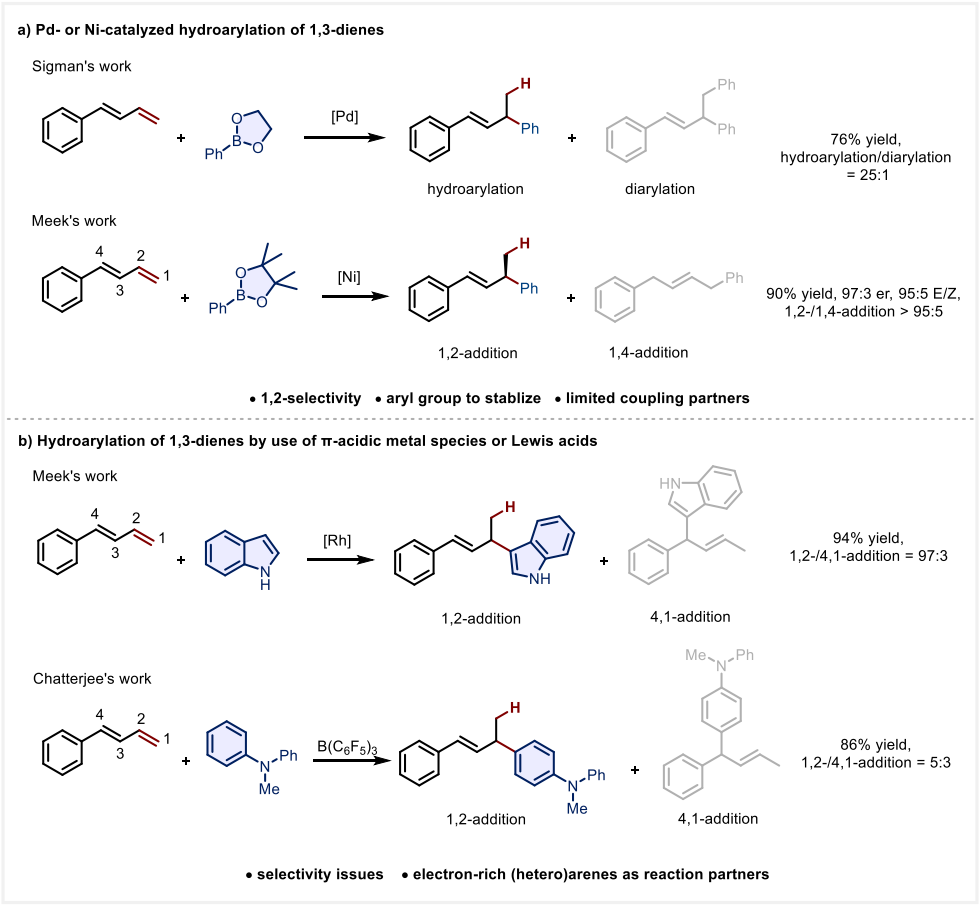

Scheme 2.6 Previous work for hydroarylation of 1,3-dienes

In recent years, numerous strategies have been developed for the C4-selective functionalization of pyridines.[109] For instance, the Hong group employed *N*-functionalized pyridinium salts as pyridine surrogates, enabling the synthesis of C4-alkylation products with alcohols and thiols (Scheme 2.7 a).[110] This transformation hinges on the frustrated Lewis pairs (FLPs) generated between the *N*-amidopyridinium salt and a phosphine reagent. On the other hand, Hiyama and colleagues achieved exclusively C4-selective alkylation via transition-metal-catalyzed C–H functionalization (Scheme 2.7 b).[111] In this strategy, a nickel catalyst and a very bulky Lewis acid, (2,6-*t*-Bu_2-4-Me-$C_6H_2O)_2AlMe$ (MAD), act as cooperative catalysts, while alkenes serve as the reaction partners. Very recently, Thomas introduced a metalation-capture tactic, in which a strong base, organosodium, directly deprotonates the pyridine C–H bond, generating a metalated pyridine intermediate that can undergo substitution or coupling reactions to achieve C4-selective functionalization (Scheme 2.7 c).[112]

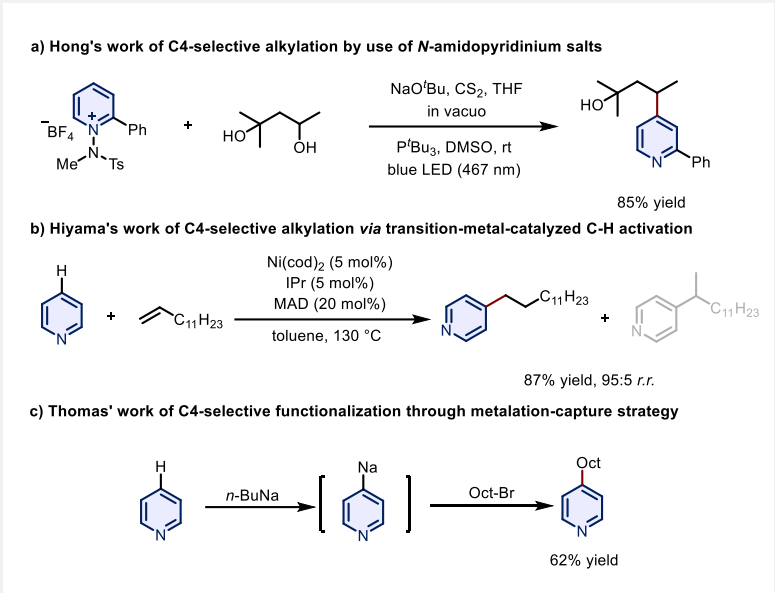

Scheme 2.7 Multiple strategies for C4-selective functionalization of pyridines

The allyl-substituted pyridine motifs obtained in our work bear similarities to the recent study by Melchiorre and coworkers (Scheme 2.8).[113] Their approach directly utilizes pyridines and alkenes as starting materials to afford a series of allyl-substituted pyridines. They discovered that the organocatalyst, dithiophosphoric acid, plays a multifaceted role under UV irradiation: (i) it protonates the pyridine substrate, (ii) facilitates the reduction of the generated pyridinium ion via an SET process, and (iii) enables abstraction of the allylic hydrogen from the reaction partner. Ultimately, the resulting pyridinyl radical and allyl radical undergo radical-radical coupling, furnishing the desired product. However, the necessity of UV light (instead of visible light) and the regioselectivity issues associated with both pyridine and alkene substrates impose certain limitations on this methodology.

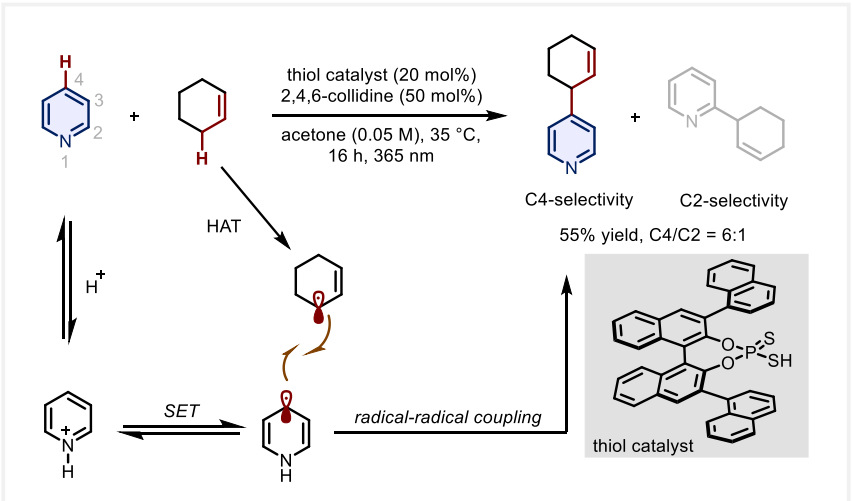

Scheme 2.8 Melchiorre's work for synthesis of allyl-substituted pyridines

Alternatively, we note that the McNally group has significantly expanded applications of pyridyl phosphonium salts in past years.[93] Recent studies have demonstrated that phosphonium salts can

serve as alternatives to cyanopyridines, undergoing single electron reduction to generate a radical zwitterion.[95] This species is a persistent radical capable of engaging in radical-radical coupling with benzylic radicals, according to the persistent radical effect.[114] Building on our group's ongoing exploration of MHAT catalysis, we hypothesized that dienes could undergo MHAT to generate a transient allylic radical, which might couple with the persistent radical derived from phosphonium salts (Scheme 2.9).[68] However, several challenges arise. First, regioselectivity is a key concern: in substituted dienes, it remains unclear which site of the diene would receive hydrogen atom transfer from the metal hydride. Second, there may be competition between the reactivity of alkenes and dienes.[115-117] Third, side reactions could occur, including the reductive cleavage of the C-P bond of the phosphonium salts, classical hydrogen evolution and isomerization.[22,118-120] Additionally, overreaction might lead to further hydrofunctionalization of the allylic pyridine. However, studies suggest that a stronger M–H bond could hinder the HAT process with alkenes due to the instability of the resulting carbon radical.[15] Therefore, selecting an appropriate MHAT catalyst is crucial for achieving selectivity in this transformation.

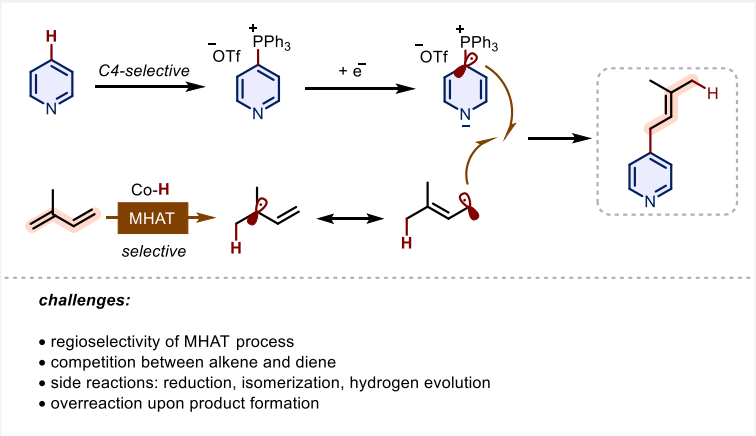

Scheme 2.9 Reaction design

2.2.2 Reaction development

We started our work by taking commercially available 1,3-cyclohexadiene **2.1** (0.1 mmol) and easily synthesized pyridyl phosphonium salt **2.2** (0.2 mmol) as the starting materials (Table 2.1). The reductive coupling product **2.3** bearing a cyclohexenyl group was smoothly formed under optimal conditions. In the early stage of condition screening, a range of cobalt catalysts were evaluated. To our surprise, **Co(salen^{tBu,tBu})** featuring a salen ligand, which we had frequently employed in previous studies, failed to yield any desired product (Table 2.1, entry 2).[68] We then turned our attention to cobalt catalysts with more extended conjugated ligands, phthalocyanine (PC) and porphyrin, they exhibited superior performance (Table 2.1, entries 3-5). Among them, tetraphenylporphyrin (TPP) with more electron-rich pendant aryl groups delivered the best outcome, with **Co(TMOTPP)** affording 80% isolated yield (Table 2.1, entry 1). Intriguingly, cobalt porphyrin catalysts have been widely applied in CO_2 reduction,[121] nitrene formation,[122] and alkane oxidation[123] but have rarely been utilized in MHAT chemistry.[71] Further investigations into solvents, concentration and bases revealed that 0.05 M of acetone and 1.0 equivalent 2.6-lutidine worked best (Table 2.1, entries 6-14). Modifying the catalyst loadings or reagent equivalents did not lead to improved results (Table 2.1, entries 15-17).

Control experiments showed that cobalt catalyst, Hantzsch ester (HE) and light were essential for the reaction, while the absence of a base still gave rise to good yields (Table 2.1, entries 18-21). This observation suggests that basic pyridine species may plausibly arise during the reaction, either from the oxidation of the HE or as a result of product formation. Replacing the phosphonium salt with 4-iodopyridine failed to yield the desired product (Table 2.1, entry 22), effectively ruling out a radical substitution pathway. Additionally, the introduction of additional caffeine did not give radical addition products (Table 2.1, entry 23), which underscored the high selectivity of the reaction toward phosphonium salt coupling. The practical utility of our protocol was also showcased when the model reaction was scaled up to 1.0 mmol, with a 67% isolated yield of product **2.3** obtained (Table 2.1, entry 24).

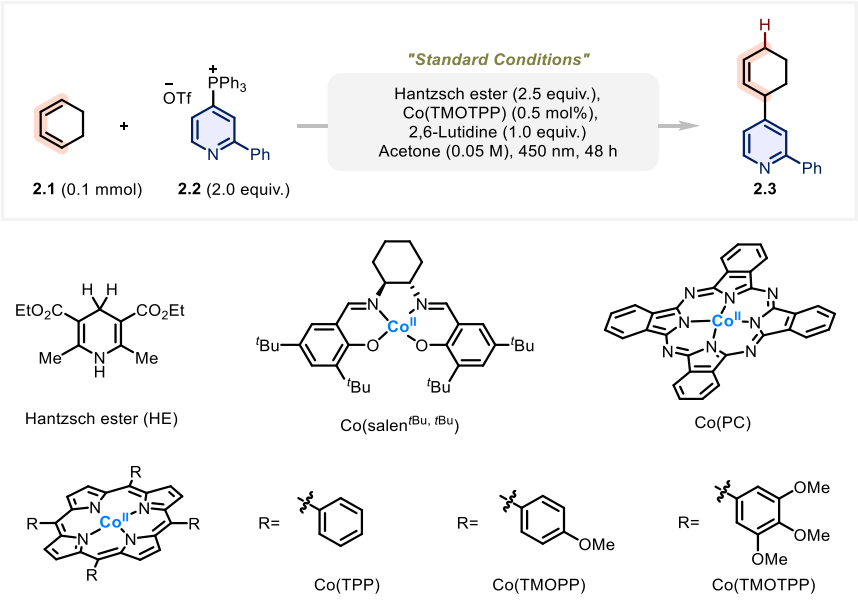

Entry	Variations	Product (%)[a]
1	none	86 (80)
2	**Co(salen^{tBu,tBu})** instead of **Co(TMOTPP)**	0
3	**Co(PC)** instead of **Co(TMOTPP)**	66
4	**Co(TPP)** instead of **Co(TMOTPP)**	73
5	**Co(TMOPP)** instead of **Co(TMOTPP)**	78
6	THF as solvent	54
7	Dioxane as solvent	38
8	DCM as solvent	54
9	Benzene as solvent	trace
10	EtOAc as solvent	24
11	Acetone (0.1 M) as solvent	73
12	Pyridine as base	55
13	Et_3N as base	45
14	DBU as base	52
15	**Co(TMOTPP)** (0.1 mol%)	57
16	1.5 equiv. **2.2**	64

17	2.0 equiv. HE	80
18	No [Co]	0
19	No HE	0
20	No light	0
21	No 2,6-lutidine	72
22	4-Iodopyridine instead of **2.2**	0
23	with additional 1.0 equiv. of caffeine	60
24	1.0 mmol of **2.1**, acetone (0.1M)	(67)

Table 2.1 Reaction optimization. Optimization reactions conducted with 0.1 mmol of **2.1** and 0.2 mmol of **2.2**. [a] Yields in **2.3** determined by ^{1}H-NMR analysis of crude reaction mixture with 1,3,5-trimethoxybenzene as an internal standard. Isolated yield in parentheses.

Finally, we attempted to apply the cobalt-catalyzed conditions reported by the Lin group for the coupling of olefins with cyanopyridines to the reaction between dienes and pyridyl phosphonium salts (Scheme 2.10).[124] In this reaction system, stoichiometric magnesium (Mg) powder served as the reductant, while acetic acid was used as the proton source. However, the reaction afforded only the reductive C–P bond cleavage product, 2-phenylpyridine, further highlighting the advantages of our approach.

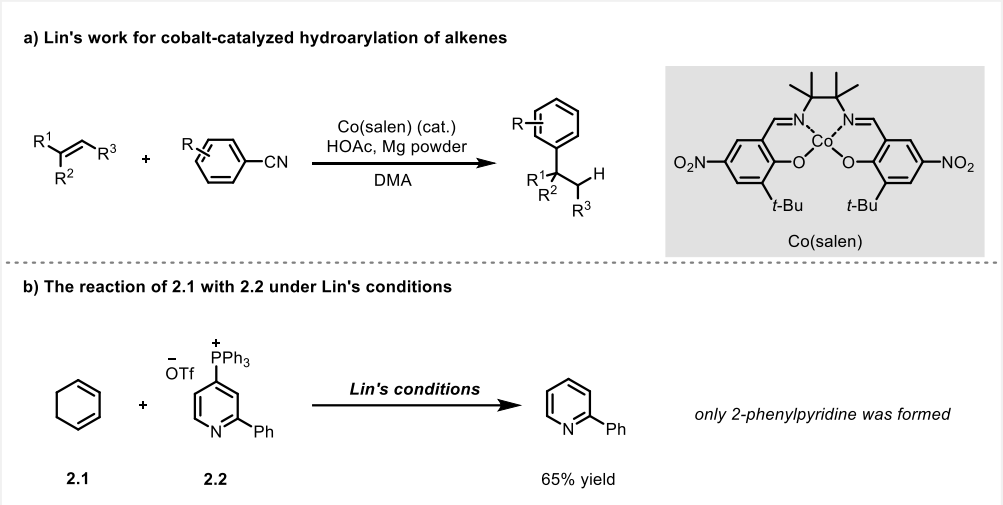

Scheme 2.10 The reaction of dienes and pyridyl phosphonium salts by employing Lin's conditions.

2.2.3 Substrate scope

After establishing the optimal reaction conditions, we proceeded to examine the generality and limitations of this photoinduced reductive coupling reaction (Scheme 2.11). 2-Aryl pyridyl phosphonium salts exhibited excellent compatibility with the reaction conditions, yielding good to excellent results regardless of whether electron-withdrawing halogen atoms or electron-donating methoxy groups were present (**2.3–2.8**). Notably, aryl halides remain intact under the reductive conditions, which highlights the selectivity of the single electron reduction process. Heteroaryl substituents at the C2 position, such as pyridine, thiophene and furan, were also found to be suitable (**2.9 – 2.11**). Of particular interest, bipyridine—a commonly used bidentate chelating

ligand—was selectively desymmetrized under our strategy to afford product **2.9**. When a benzyl group is present at the C2 position, the corresponding products **2.12** and **2.13** were obtained in 61% and 59% isolated yields, respectively. Next, we shifted our focus to non-cyclic dienes. Unlike conventional MHAT catalysis with alkenes, which typically results in branched selectivity, our approach predominantly produced the linear products via 1,4-hydropyridylation. In these reactions, the presence of an external photocatalyst $Ru(bpy)_3(PF_6)_2$ expanded the scope of the diene reaction partners beyond 2-aryl or 2-benzyl pyridyl phosphonium salts to include 2-methylpyridine and even unsubstituted pyridine, leading to the desired products **2.15** and **2.16**. In these cases, the reaction time was also lower at 16 hours.

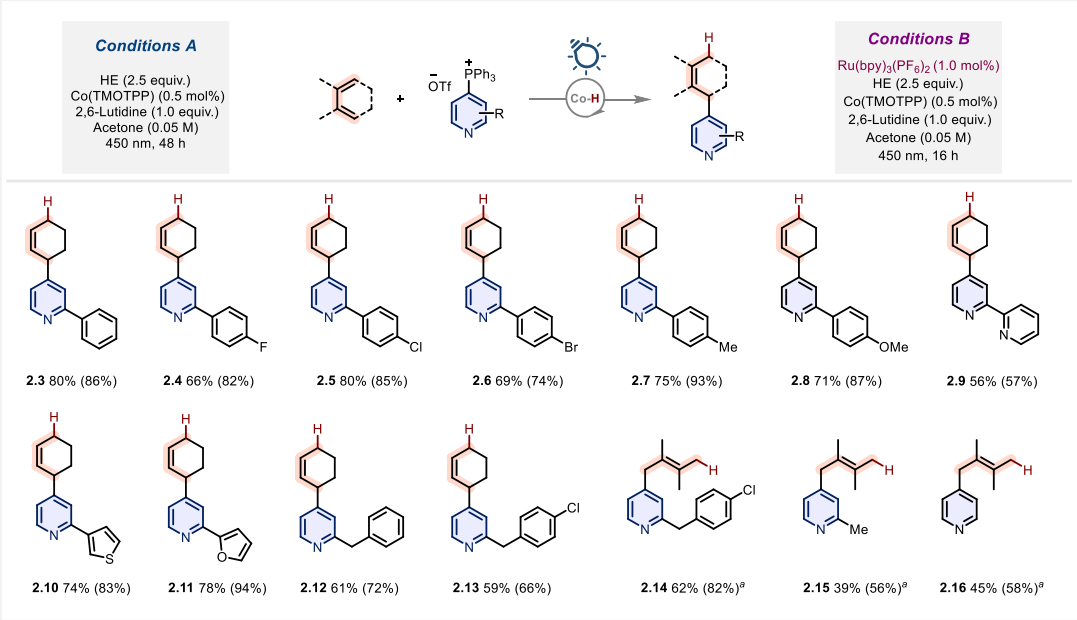

Scheme 2.11 Scope of pyridyl phosphonium salts. Notes: yield determined by ^{1}H NMR by comparison with 1,3,5-trimethoxybenzene as an internal standard is given in parentheses. Reactions were performed under conditions A unless otherwise indicated. [a]performed under condition B

We then further explored the substrate scope with respect to dienes (Scheme 2.12). When 2,3-dimethyl-1,3-butadiene was subjected to the standard conditions with 2-phenylpyridine phosphonium salt, the corresponding product **2.17** was obtained in very high yield. For unsymmetrical dienes, the experimental results indicated that the MHAT step preferentially occurred at the more electron-rich and less sterically hindered terminus of the diene. For instance, substrates 1,3-pentadiene and isoprene afforded **2.18** and **2.19**, respectively, with high regioselectivity. Additionally, this transformation demonstrated exceptional chemoselectivity toward 1,3-dienes, even in the presence of simple alkenes.

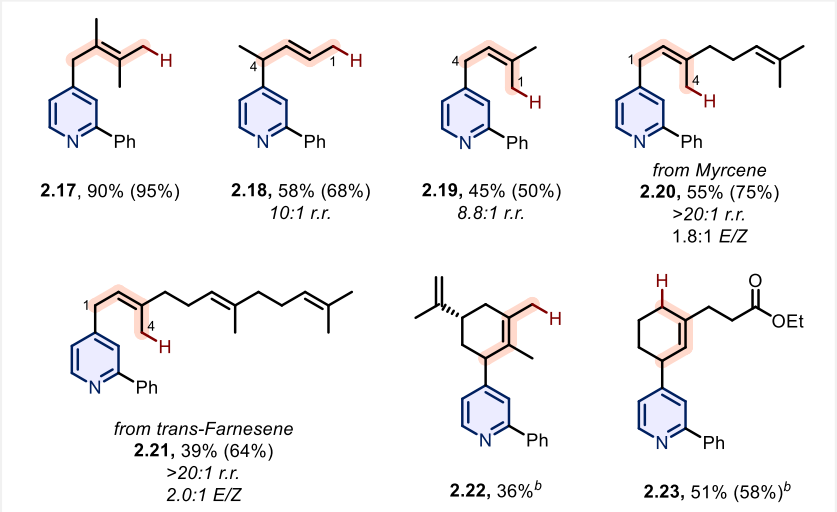

Scheme 2.12 Substrate scope of dienes. Notes: yield determined by ^{1}H NMR by comparison with 1,3,5-trimethoxybenzene as an internal standard is given in parentheses. *r.r* was determined by analysis of ^{1}H NMR of the reaction mixture. Reactions were performed under conditions A unless otherwise indicated. ^{b}performed under condition B with 48 h reaction time.

Terpene-derived polyenes, such as myrcene and trans-farnesene, both commonly used in the fragrance industry, underwent nearly complete conversion to the corresponding diene coupling products **2.20** and **2.21**. In stark contrast, when we applied the hydropyridylation conditions reported by the Herzon group to the two substrates, only complex mixtures were obtained (Scheme 2.13).[115]

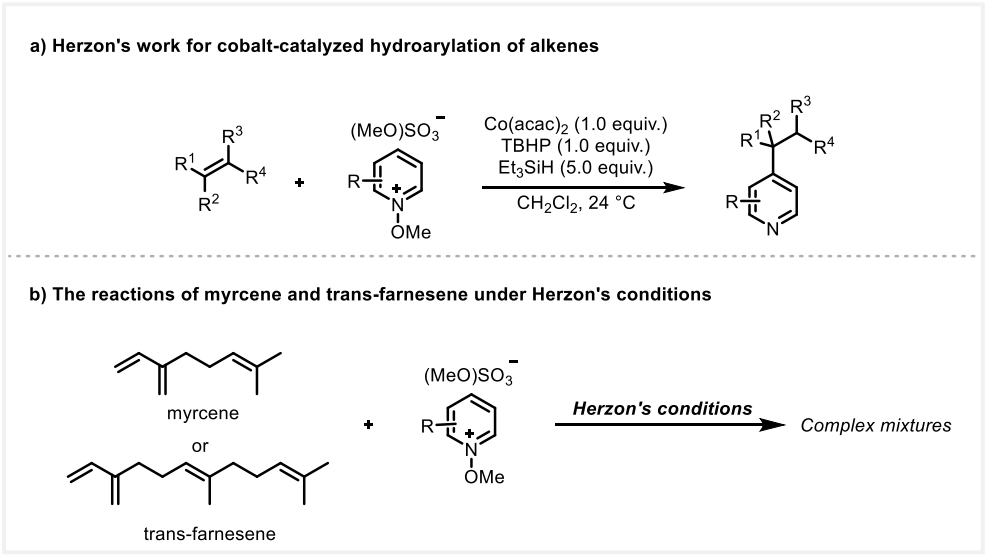

Scheme 2.13 Reactions of polyenes as substrates under Herzon's conditions

Another noteworthy example was a carvone-derived diene containing a double bond. Under our conditions, only the conjugated diene moiety reacted, following the same chemo- and regioselectivity trends observed for other unsymmetric dienes, to produce **2.22**. The pendant isopropenyl group, which typically has high reactivity in classical MHAT chemistry, remained completely unreacted. This not only underscores the unique selectivity of our methodology but

also underlines its orthogonality to the work of the Melchiorre group.[113] Functional groups such as esters were well tolerated under the optimized conditions, a moderate yield was recorded for the corresponding coupling product **2.23**.

We found that introducing substituents at different positions of 1,3-cyclohexadiene led to distinct selectivity in the MHAT step. 1-*n*-Butylcyclohexadiene showed a preference for 1,2-selectivity, whereas 2-*n*-butylcyclohexadiene favored 1,4-selectivity, yet both finally delivered a single regioisomer **2.24** (Scheme 2.14). These results are consistent with our earlier observations that Co–H preferentially undergoes HAT at the sterically less hindered and more electron-rich terminus of a diene and that the delocalized radical prefers C–C bond formation through the less hindered carbon.

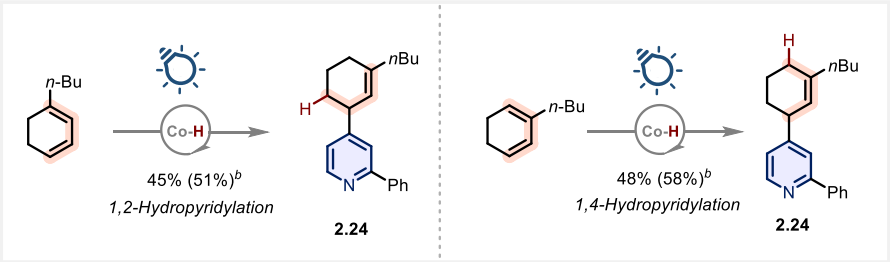

Scheme 2.14 Different selectivity of *n*-butylcyclohexadienes. Notes: yield determined by ^{1}H NMR by comparison with 1,3,5-trimethoxybenzene as an internal standard is given in parentheses. [b]performed under condition B with 48 h reaction time.

Beyond dienes, our protocol was also applicable to allenes, as shown by the hydropyridylation of cyclohexylallene, which provided product **2.25**, albeit with decreased reactivity (Scheme 2.15). Styrenes could also be used, electron-rich substrate 4-methoxystyrene and electron-deficient ethyl 4-vinylbenzoate successfully yielded **2.26** and **2.27**, respectively. Furthermore, β-substituted and heteroaromatic styrenes were employed in C4-functionalization of pyridine as well, delivering **2.29** and **2.30** with moderate yields. It should be noted that a photocatalyst was required for these transformations to achieve synthetically useful yields, which may be attributed to the fact that the additional photocatalyst enables more efficient utilization of light energy and accelerates the rate of radical generation.

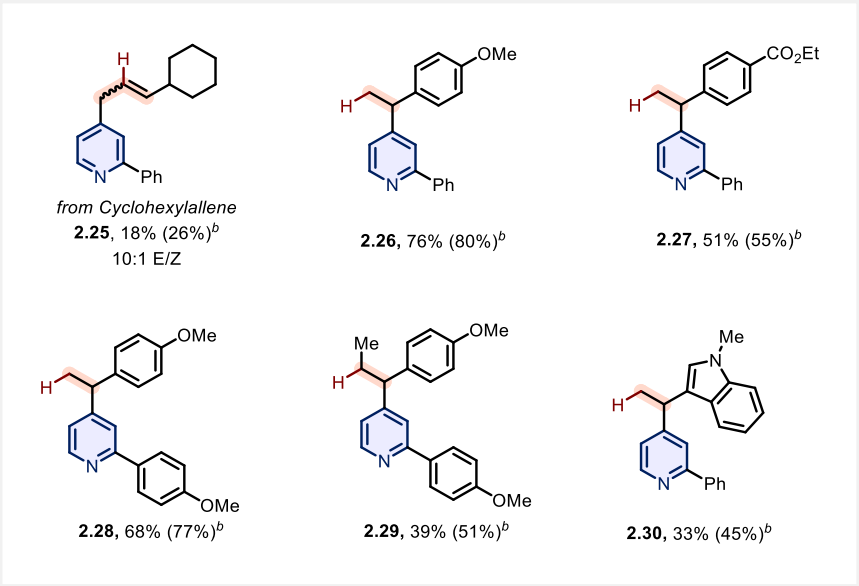

Scheme 2.15 Substrate scope of styrenes and allenes. Notes: yield determined by ^{1}H NMR by comparison with 1,3,5-trimethoxybenzene as an internal standard is given in parentheses. ^{b}performed under condition B with 48 h reaction time.

To assess the applicability of our strategy, we further explored the late-stage functionalization of drug-like molecules (Scheme 2.16). The phosphonium salt derived from Bisacodyl, coupled efficiently with structurally varied dienes and styrenes, affording a series of hydropyridylation products in moderate to good yields. For instance, reaction with cyclooctadiene furnished **2.32**, while coupling with a Simvastatin-derived molecule, generated **2.35** with high functionalization and as a single, predictable regio- and diastereoisomer. This highlights that our strategy enables highly selective late-stage functionalization of both dienes and pyridyl phosphonium salts. Additionally, benzofuran-pyridine-derived **2.36** and Boc-protected amine **2.37** were successfully obtained in 73% and 58% isolated yields, respectively. Moreover, the model substrate 2-phenylpyridyl phosphonium salt could be coupled with TBS protected-Simvastatin to afford **2.38**. Testosterone derivatives were also compatible, yielding the desired product **2.39**; however, the final outcome was a mixture of diastereomers and isomerized products.

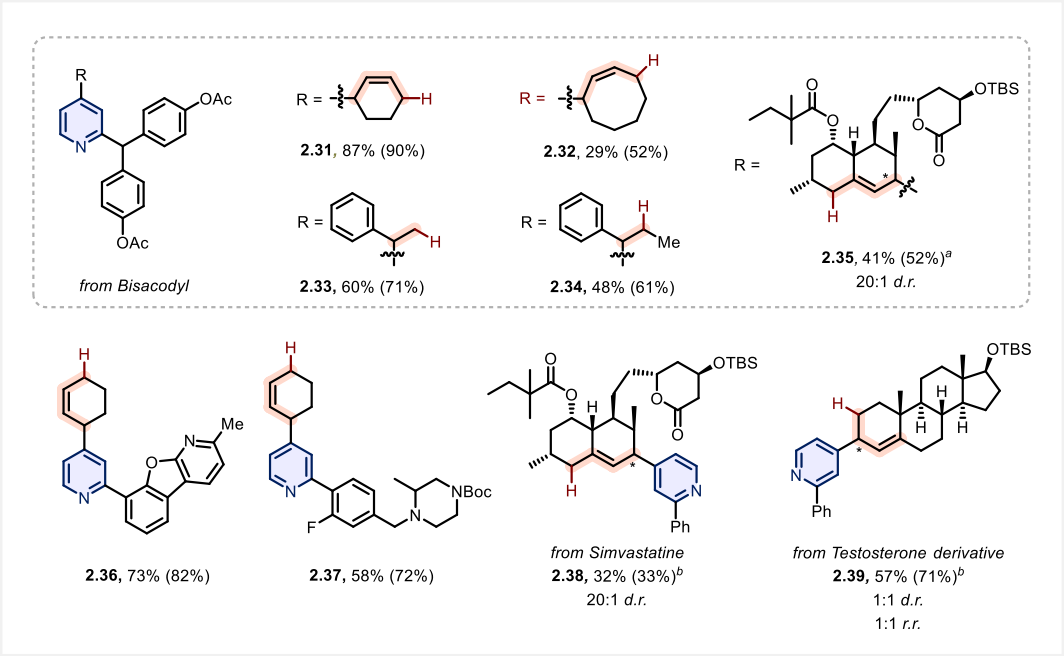

Scheme 2.16 Late-stage functionalization. Notes: yield determined by ^{1}H NMR by comparison with 1,3,5-trimethoxybenzene as an internal standard is given in parentheses. *r.r.* and *d.r.* was determined by analysis of ^{1}H NMR of the reaction mixture. Reactions were performed under conditions A unless otherwise indicated. [a]performed under condition B. [b]performed under condition B with 48 h reaction time.

Using our method, dienes can be transformed into pyridine derivatives bearing an allyl group, with the double bond positioned adjacent to the newly formed C–C bond. In this regard, the synthetic versatility of this ally group was explored using model product **2.3** as the starting material for a series of further derivatizations, including reduction and oxidation reactions, thereby affording a range of distinct structures, **2.40–2.43** (Scheme 2.17).

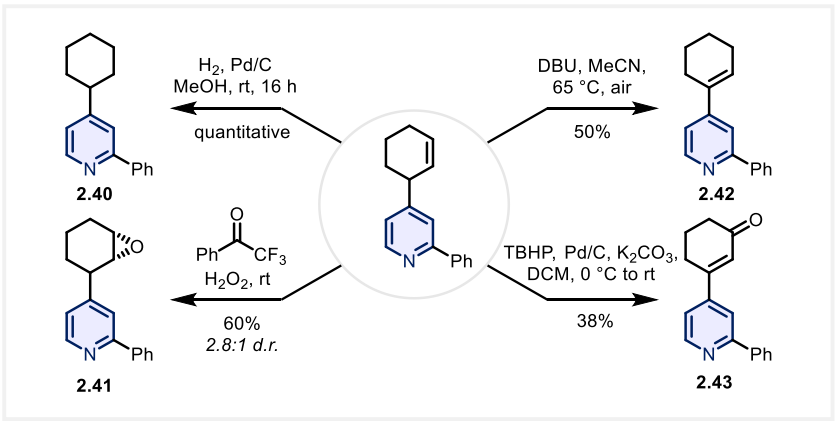

Scheme 2.17 Synthetic applications of model product

Although our protocol exhibits excellent chemo- and regioselectivity across a broad range of substrates, it is not without limitations. For instance, in the case of substituted cyclohexadienes, we also investigated phenyl, silyl enol ether, and α-amino alkyl substituents apart from alkyl groups. Despite the potential advantages of these substituents, their incorporation generally afforded

complex mixtures, failed to yield the corresponding target products, or resulted only in trace of products (Scheme 2.18). Moreover, terpenoid-like dienes bearing exocyclic terminal alkenes either does not take place or only traces of product are observed. Similarly, although the commonly employed *trans*-1-phenylbutadiene undergoes the reaction under our conditions, its yield remains modest (16% yield, determined by ^{1}H NMR analysis of the crude reaction mixture). Regarding the phosphonium salts, substitution at the 3-position of the pyridine ring, such as 3-phenylpyridine, quinoline, and the drug molecule Claritin, completely suppresses product formation under optimized conditions. C2-pyridylphosphonium salts also afford unsatisfactory outcomes, giving only trace amounts of the desired products. Additionally, when a halogen is present at the 2-position of pyridine, only 13% yield (as determined by 1H NMR analysis of the crude reaction mixture) is obtained in the reaction with 2,3-dimethyl-1,3-butadiene in the presence of additional photocatalyst (condition B).

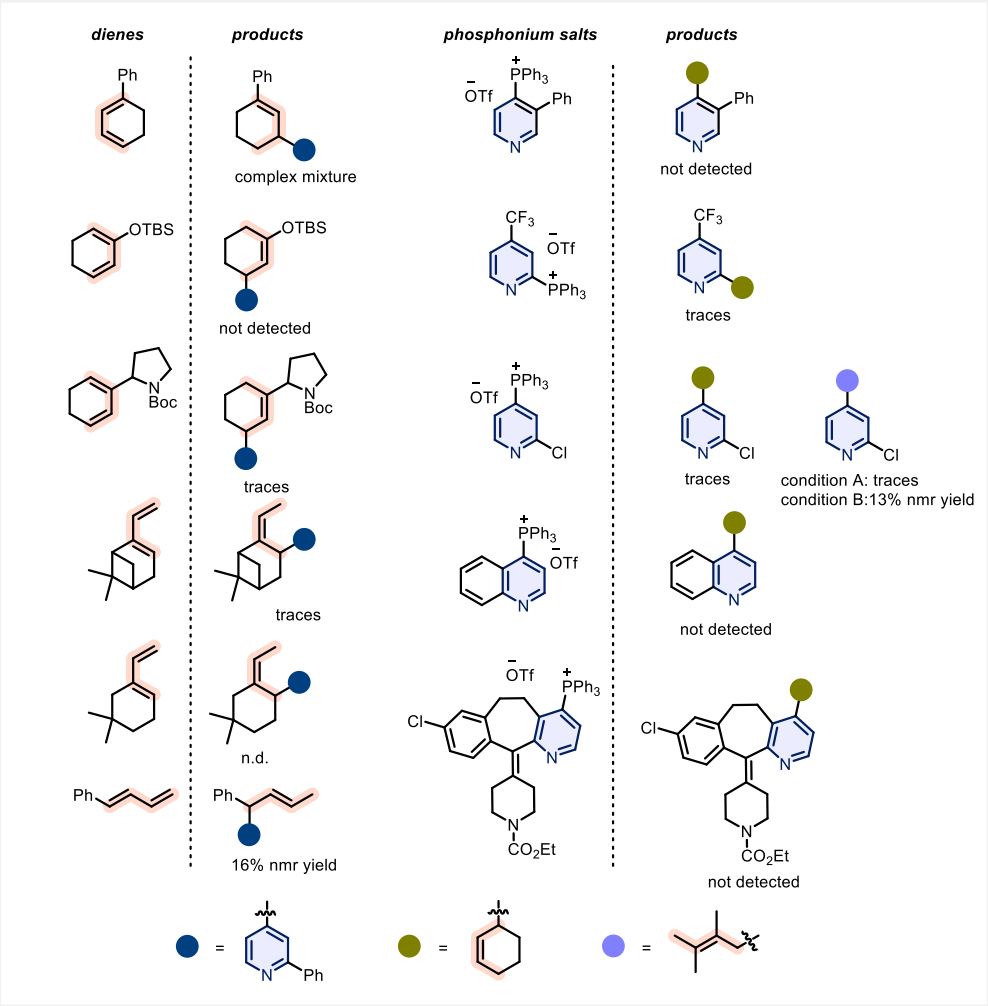

Scheme 2.18 Unsuccessful substrates

2.2.4 Mechanistic studies

Based on previous literature reports and experimental observations, we propose the following mechanistic cycle (Scheme 2.19).[68] At the beginning of the cycle, Co(II) can be reduced to Co(I) by the excited-state Hantzsch ester or through an SET process mediated by the Ru(II)/Ru(III) cycle in

where an additional photocatalyst is present. Meanwhile, 2-phenylpyridylphosphonium (E_{red} = −1.51 V vs. SCE)[95] can also be readily reduced by the excited state of Hantzsch ester (E_{ox}^* = −2.28 V vs SCE)[125], leading to the exergonic formation of the zwitterionic radical, as supported by experimental and computational redox potential data. Co(I), as a basic species, can undergo protonation to generate Co(III)–H, which then selectively transfers a hydrogen atom to the electron-rich terminus of the diene via an MHAT process, forming allylic radical **A**.[71,126] Its resonance structure **B** with less hindered carbon has a major contribution to the real structure of the delocalized system in the next step. Once formed, the persistent pyridyl radical, accumulated in the reaction medium, rapidly engages in a radical-radical coupling reaction, eventually affording a 1,4-selective product (in most cases).[114] In the step where **A** is formed, Co(II) is regenerated, thus completing the catalytic cycle.

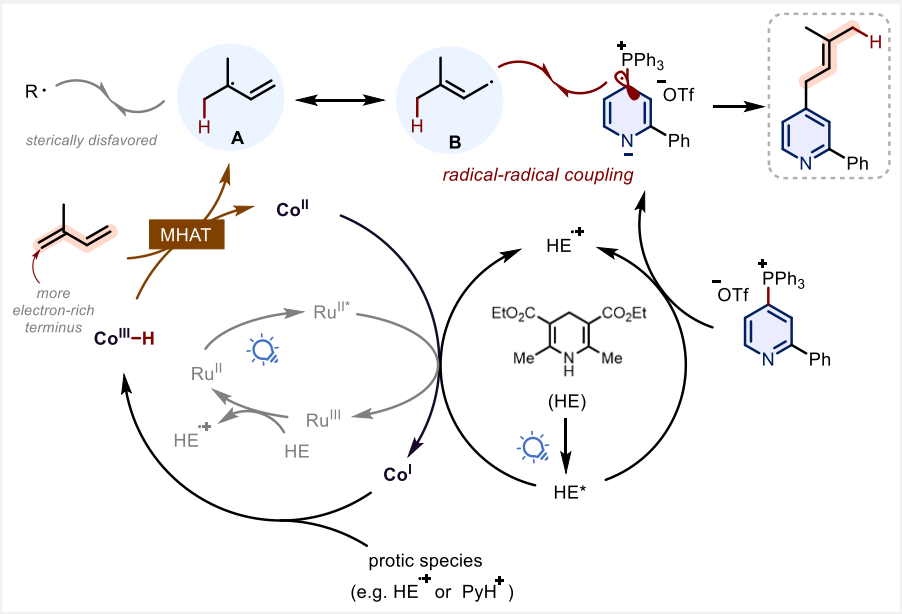

Scheme 2.19 Proposed reaction mechanism

To further elucidate the origin of selectivity and gain mechanistic insights, we performed density functional theory (DFT) calculations and several control experiments (Scheme 2.20, 2.21). Using 1,3-cyclohexadiene as the substrate, we investigated the regioselectivity of the MHAT process, which preferentially occurs at the terminal position of the diene. Calculations indicate that the free energy barrier for the Co(III)–H mediated HAT transition state at the external position (**$TS_{Ext.}$**) is 4.7 kcal/mol, whereas for the internal position (**$TS_{Int.}$**), it is 9.6 kcal/mol—comparable to that of cyclohexene. Distortion-interaction analysis revealed that the transition states for cyclohexene and the internal position of the diene exhibit significantly higher distortion energy than the external position due to the loss of conjugation. This explains why, in control experiments, when cyclohexene is used as the substrate, only dimeric and reduced products of pyridyl phosphonium salts are observed (Scheme 2.21 a). The insufficient concentration of cyclohexyl radicals prevents effective radical-radical coupling, thereby accounting for the high selectivity of our method for dienes.

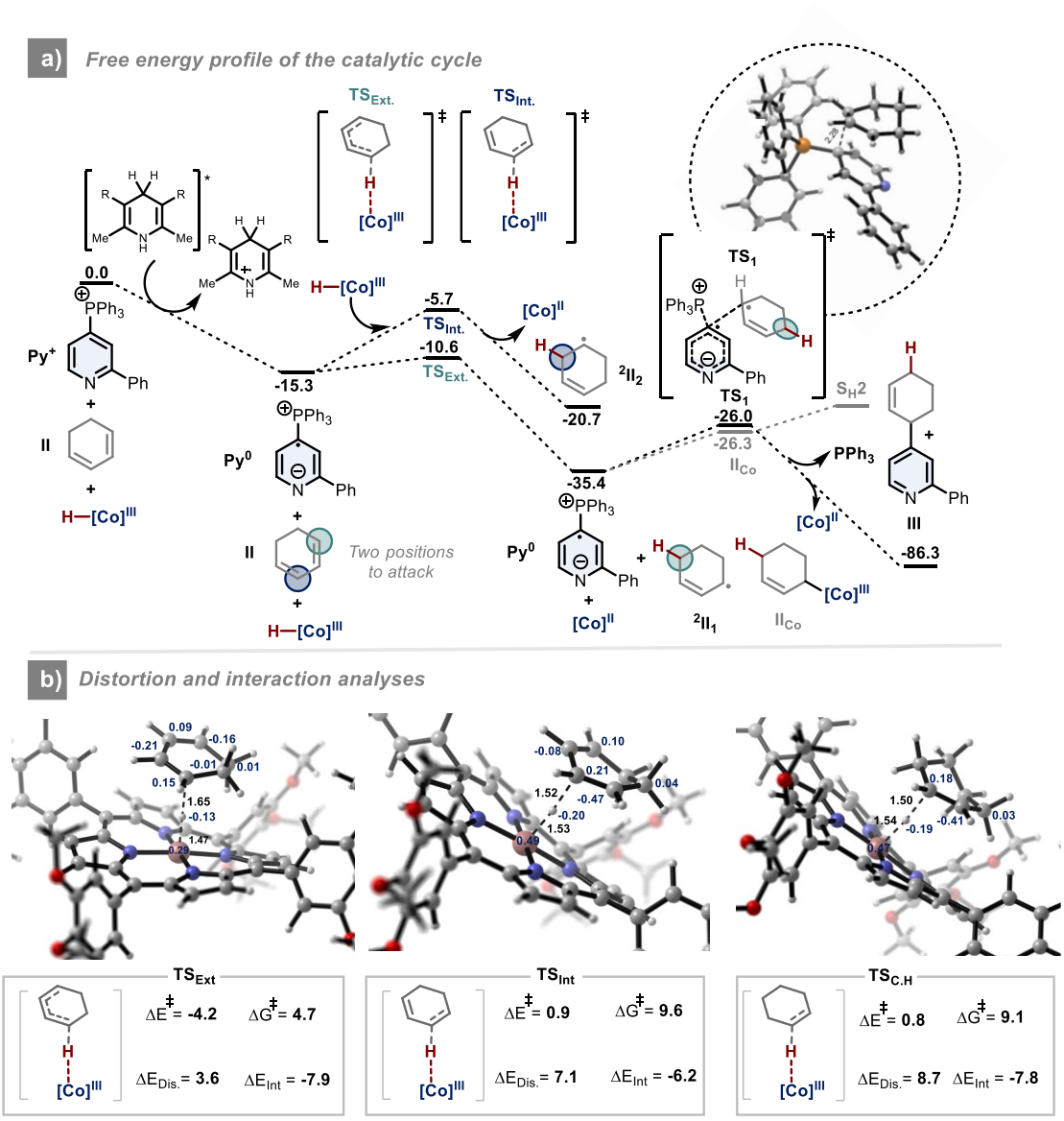

Scheme 2.20 a) Free energy profile of the proposed catalytic cycle (Energies in kcal/mol). b) 3D structures of Co(III)–H Hydrogen Atom Transfer to cyclohexadiene (black: bond distances in Å; blue: spin densities in a.u.) and cyclohexene.

Moreover, calculations indicate that the MHAT step is highly exergonic (−20.1 kcal/mol), suggesting its irreversibility. A control experiment (Scheme 2.21 b) supports this conclusion: when excess perdeuterated styrene-d_8 was reacted with the phosphonium salt **2.2**, the obtained product was fully incorporated with H at the terminal position, and no loss of deuterium or replacement with H was observed in the recovered styrene starting material, consistent with irreversible HAT process.

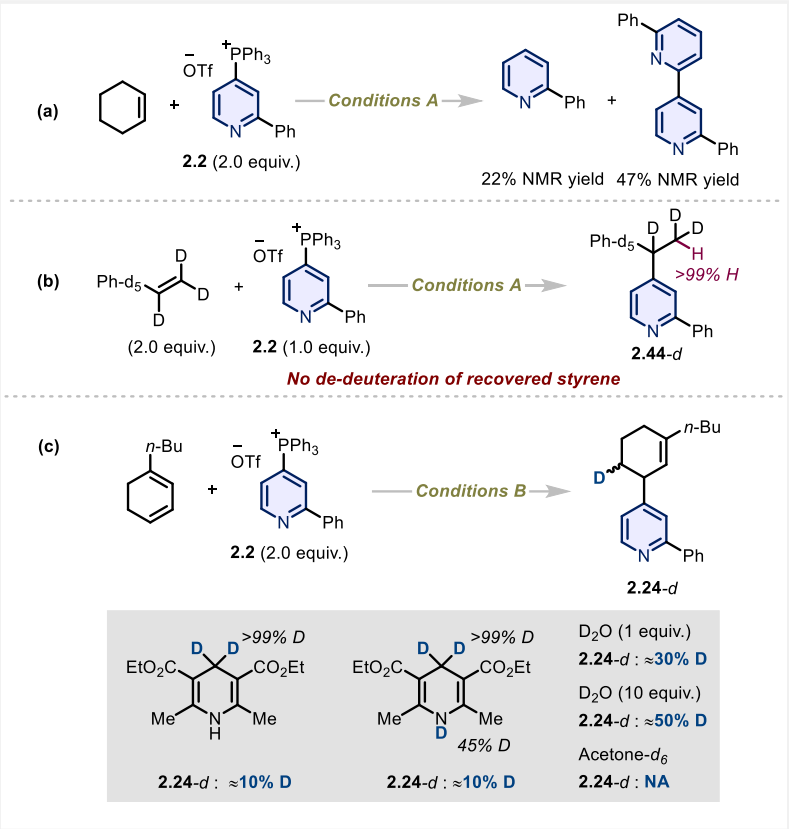

Scheme 2.21 Deuterium labelling mechanistic experiments

Additionally, deuterium labeling experiment (Scheme 2.21 c) suggested that HAT occurs specifically at the sterically less hindered terminal position. Computational results (Scheme 2.22) confirmed that HAT is favored at C4 position in 1-*n*-butylcyclohexadiene, but in 2-*n*-butylcyclohexadiene it preferentially occurs at the more electron-rich C1 position when the steric hindrance at terminus is equal.

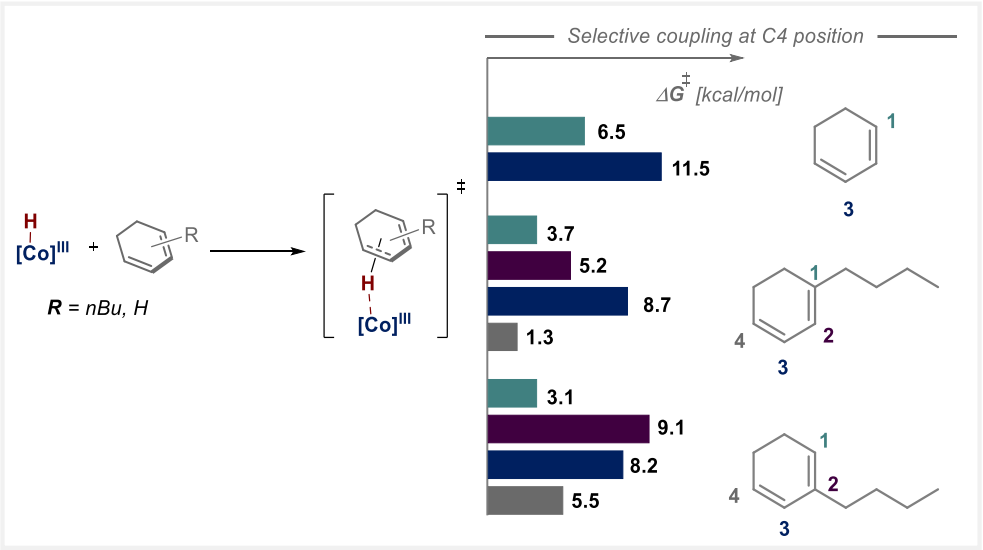

Scheme 2.22 Free energy values for HAT transition state barrier of the three distinct dienes

selected: cyclohexa-1,3-diene (top), 1-butylcyclohexa-1,3-diene (middle) and 2-butylcyclohexa-1,3-diene (bottom). Energy values provided from (SMD, acetone) PBE1PBE/Def2SVP// PBE1PBE/Def2TZVP are presented in kcal/mol

The highest deuterium incorporation (Scheme 2.21 c) was observed when excess D_2O was used, aligning with the hypothesis that Co–H is generated from the reaction of Co(I) with protic species.[71] The reaction of 3-phenyl-pyridylphosphonium was also calculated (Scheme 2.23). The results indicate that this process has a higher free energy barrier and transition state distortion, which explains the lack of reactivity observed for 3-substituted pyridine in our experiments.

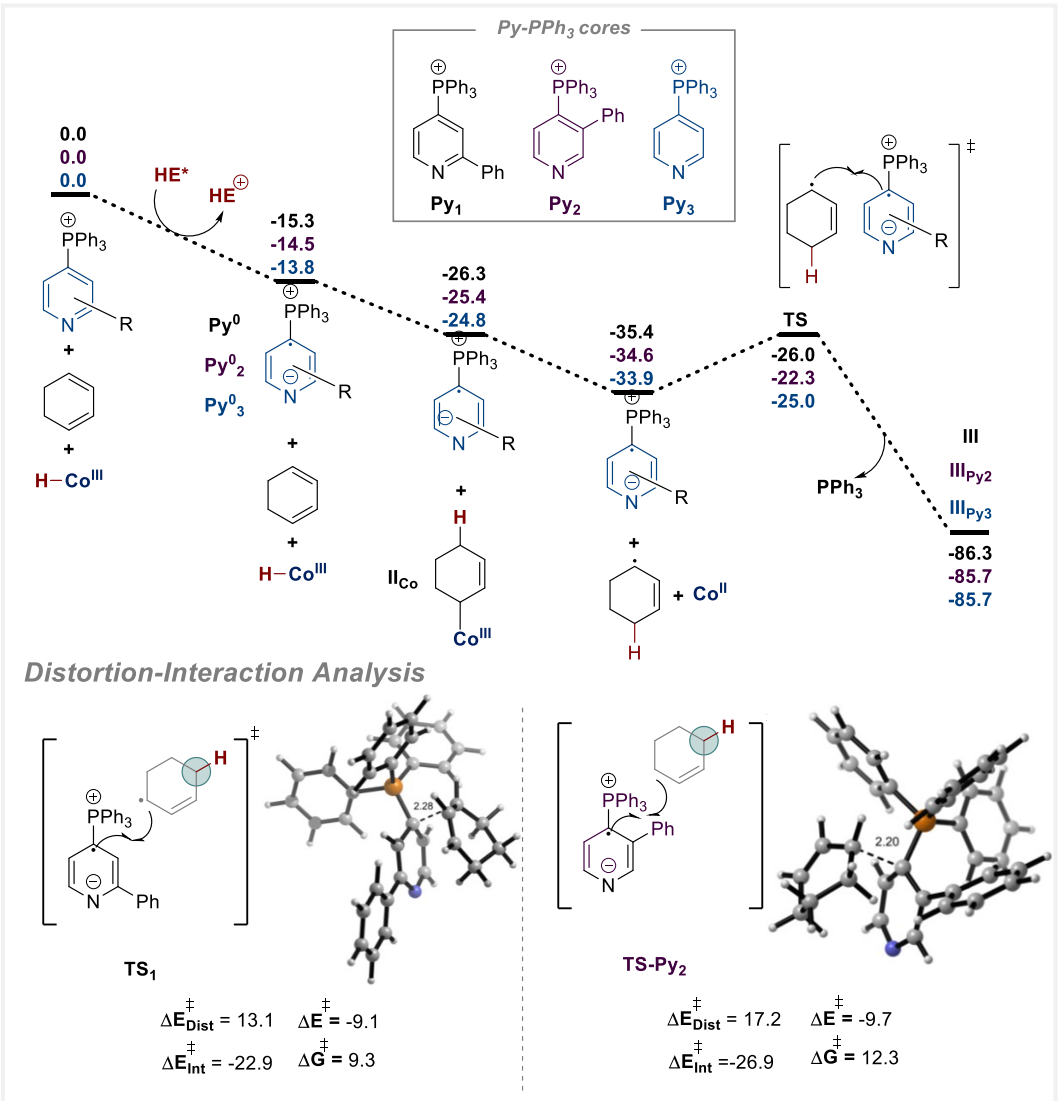

Scheme 2.23 A body of three different pyridines (Py_1, Py_2, Py_3) were employed in this computational study. Energy values provided from (SMD, acetone) PBE1PBE/Def2SVP// PBE1PBE/Def2TZVP are presented in kcal/mol. Bond distances (black) are in Angstroms

Furthermore, we also measured the UV-Vis absorption spectra of various reaction components as well as the reaction mixture of the model reaction (Scheme 2.24). In the visible region, Co(TMOTPP) exhibits pronounced absorption bands around 420 nm and 450 nm, whereas HE, **2.1**, **2,2** and 2,6-lutidine show no absorption. The absorption spectrum of the reaction mixture closely resembles

that of Co(TMOTPP) and HE. These observations suggest that under 450 nm blue light irradiation, Co(TMOTPP) is more likely to be the species that directly absorbs the light, rather than HE. Consequently, HE might reach its excited state indirectly through some interactions with Co(TMOTPP).

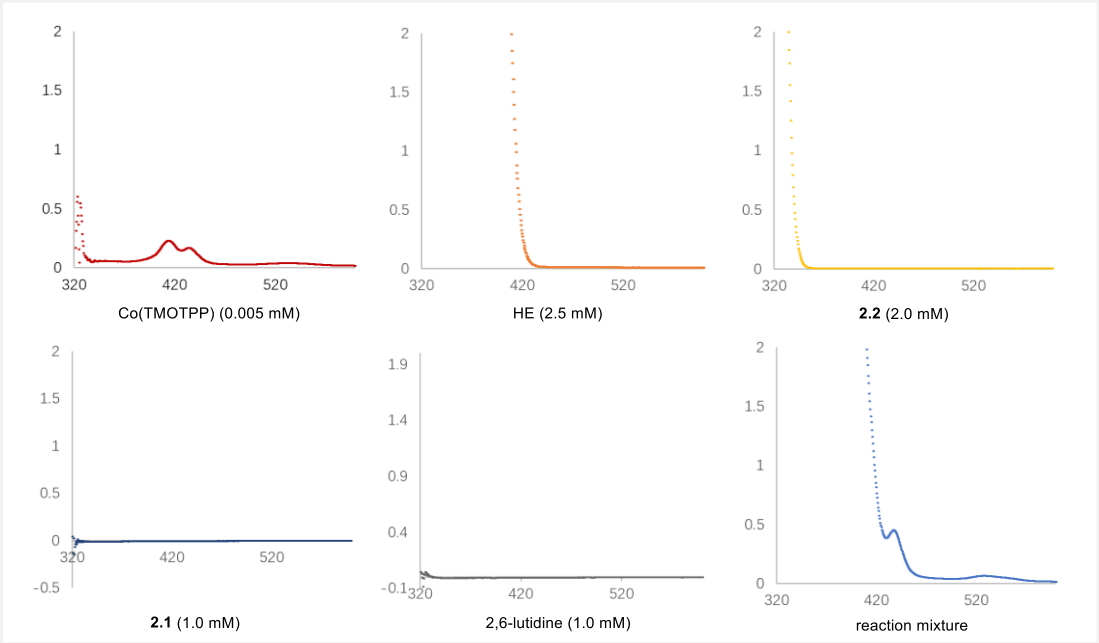

Scheme 2.24 UV-Vis absorption of reaction components and reaction mixture

UV-Vis absorption studies revealed that the combination of HE and phosphonium salt **2.2** did not generate any new absorption bands or have a redshift, thereby excluding the possibility of an EDA complex formation between these two species (Scheme 2.25).

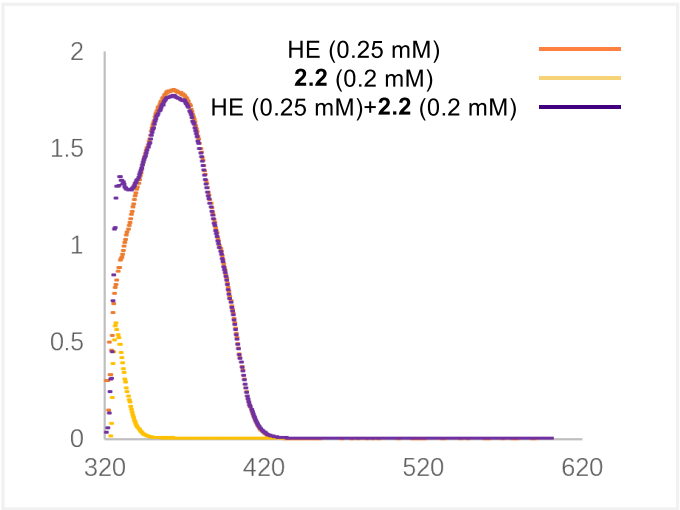

Scheme 2.25 UV-Vis absorption of reaction components and reaction mixture

Stern-Volmer fluorescence quenching experiments were conducted to investigate the interaction between HE and Co(TMOTPP) (Scheme 2.26). The results demonstrate efficient quenching of excited HE by Co (TMOTPP). While the quenching behavior between HE and **2.2** was more complex,

it exists the interaction of them.

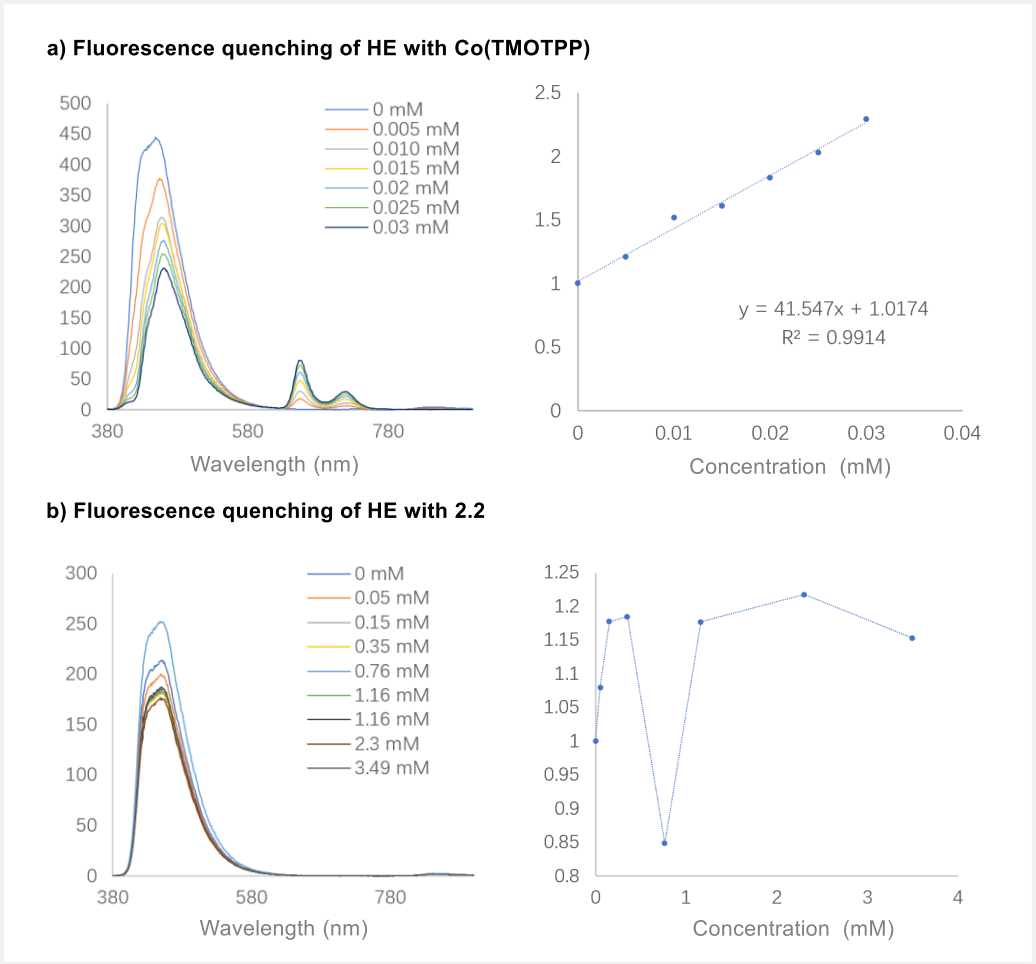

Scheme 2.26 Stern–Volmer fluorescence quenching experiments (excitation wavelength: 365nm)

Based on the aforementioned spectroscopic data, it can be concluded that a potential interaction between cobalt catalyst and the Hantzsch ester, though overall, they remain consistent with the proposed reaction pathway.[126]

2.2.5 Summary and outlook

In summary, we have developed a photochemically induced, Co-HAT catalyzed reductive coupling reaction between dienes and pyridyl phosphonium salts under mild conditions. Although this strategy is not amenable to some specific substrates, the unique selectivity and good functional group compatibility enable its successful application in the modification of complex molecules, including pharmaceutical compounds. In-depth mechanistic studies have elucidated the origins of the observed selectivity, thereby providing a powerful and predictable tool for transforming readily available starting materials into complex molecules. We anticipate the further development of radical traps for reductive coupling with dienes or olefins, for instance, employing electron-deficient alkenes as reaction partners in a Giese-type reaction to achieve the construction of C(sp^3)–C(sp^3) bonds.

3

Co-HAT Catalyzed Cross-Coupling and Rearrangement Reactions of Styrenes and Michael Acceptors

3 Co-HAT catalyzed cross-coupling and rearrangement reactions of styrenes and Michael acceptors

3.1 Giese reaction

3.1.1 Introduction of Giese reaction

As an essential class of highly reactive intermediates, radicals mediate reactions that are often performed under mild conditions and exhibit promising selectivity.[127-129] Most importantly, they enable transformations that polar counterparts cannot achieve.[128] Among the diverse radical-based reactions, the construction of C–C bonds remains a fundamental and continuously pursued research focus.[127]

Giese (or Giese-type) reactions, involve the trapping of a carbon-centered radical **A** by an electron-deficient alkene (Michael acceptors), providing a robust approach to construct a new C–C bond (Scheme 3.1).[130-132] The resulting radical intermediate **B** can subsequently undergo HAT or proceed through an SET process followed by protonation to afford an sp^3-enriched product (Scheme 3.1 above). Alternatively, the radical may bypass these pathways and be intercepted by other species, leading to structurally diverse frameworks (Scheme 3.1 below).[133,134]

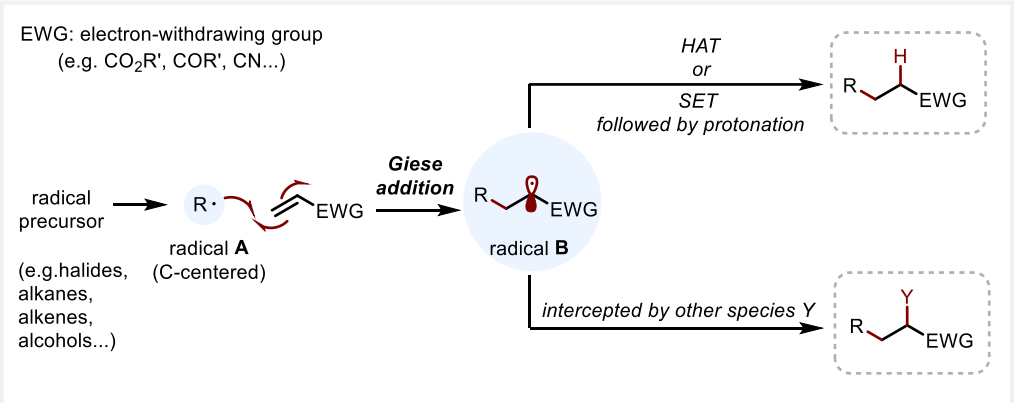

Scheme 3.1 General mechanism of Giese reaction

Traditional Giese reactions were principally centered around tin hydride (Sn–H, BDE = 78 kcal/mol) chemistry.[130-132] Under photochemical, thermal conditions or with the aid of a radical initiator (*e.g.,* AIBN), homolytic cleavage of the Sn–H bond yields a tin radical that initiates the reaction (Scheme 3.2). The tin radical can then abstract a halogen atom from the substrate via a halogen atom transfer (XAT) process to furnish an alkyl radical, which subsequently engages in further transformations. However, this approach is beset with several drawbacks, most notably the occurrence of competing side reactions. For example: (i) tin radicals can add to Michael acceptors, resulting in unproductive hydrostannylation reaction that competes with the desired XAT process. As a result, the X-atom needs to have high reactivity, typically as an iodide, which in turn limits the substrate scope; (ii) the initially generated alkyl radical **A** can abstract a hydrogen atom from the Sn–H bond, leading to undesired reduction; and (iii) the radical **B** may undergo successive

additions to multiple Michael acceptor molecules to form the corresponding oligomers. In addition, the inherent toxicity of tin reagents further impedes the development and application of this methodology.

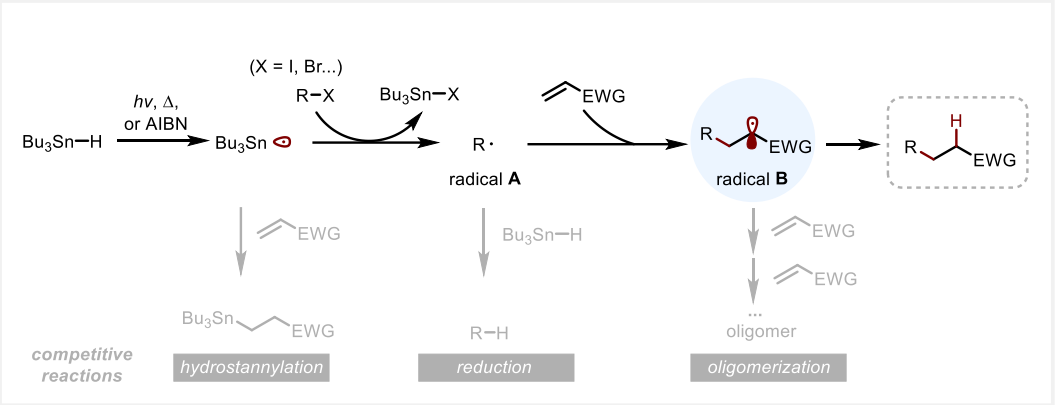

Scheme 3.2 Tin hydride-mediated Giese reactions and competitive reactions

3.1.2 Photoredox-mediated Giese reaction

With the resurgence and rapid development of photocatalysis in recent years, the combination of the Giese reaction with photoredox chemistry has proven increasingly advantageous.[135] This strategy obviates the need for tin reagents, while the use of light renders the process both milder and more environmentally benign. More importantly, photoredox facilitate the generation of a wider variety of radical species, which broaden the scope of the reaction. Photoinitiated Giese reactions have been also successfully applied in total synthesis,[128,136,137] bioconjugation,[138,139] and pharmaceutical chemistry.[140]

Chemists have now developed a diverse array of alkyl radical precursors that enable regioselective Giese additions to polarized alkenes. These precursors can be roughly categorized based on the substrate type or behavior of the radicals.

1) C-centered radical formation via formal defunctionalization process

Alkyl halides represent the most widely utilized class of substrates in tin hydride-mediated Giese reactions. However, their application is often restricted to iodides and bromides.[130-132] Benzylic radicals are resonance-stabilized and less nucleophilic than other alkyl radicals, resulting in slower addition to electron-deficient alkenes, with rates on the order of 4×10^2 to 2×10^3 M^{-1}/s.[141-143] As a result, benzylic radicals tend to undergo competitive reduction and hampers a productive Giese reaction in tin hydride chemistry. In contrast, photoredox-mediated reactions enable the effective engagement of alkyl chlorides and benzylic radicals. For example, in 2018, in contrast to the direct XAT pathway for generating alkyl radicals, Melchiorre and co-workers introduced an indirect dehalogenative strategy to produce benzylic radicals from benzylic halides, including benzylic chlorides (Scheme 3.3). In the proposed mechanism, the desired radical is generated via an S_N2 substitution of benzylic chloride with a thiocarbamate anion, followed by homolysis of the C–S bond.[144]

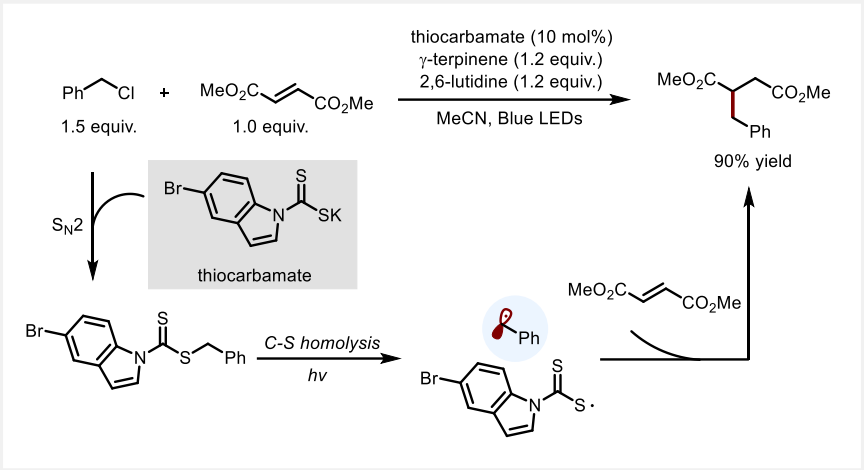

Scheme 3.3 Alkyl halides as radical precursors in Giese reaction

In the past decades, carboxylic acids have emerged as versatile radical precursors due to their non-toxicity, low cost, and structural diversity. Their extensive application in Giese reactions has led to the establishment of a new subdomain in organic synthesis—decarboxylative Giese reactions (DGRs).[145] For instance, the MacMillan group reported a direct decarboxylative Giese reaction under visible-light-mediated conditions (Scheme 3.4 a).[146] This method directly generates alkyl radicals through a photocatalytic single-electron oxidation process, which permits the release of CO_2 to generate Michael donors without the need for organometallic activation or propagation. Notably, it can be applied in the three-step synthesis of the commercialized drug molecule, pregabalin. Later, they expanded the scope by employing alcohols as radical precursors to achieve a deoxygenative Giese reaction. This strategy relies on an *N*-heterocyclic carbene (NHC) reagent that activates alcohols *in situ*, generating alkyl radicals via homolytic C–O bond cleavage (Scheme 3.4 b).[147]

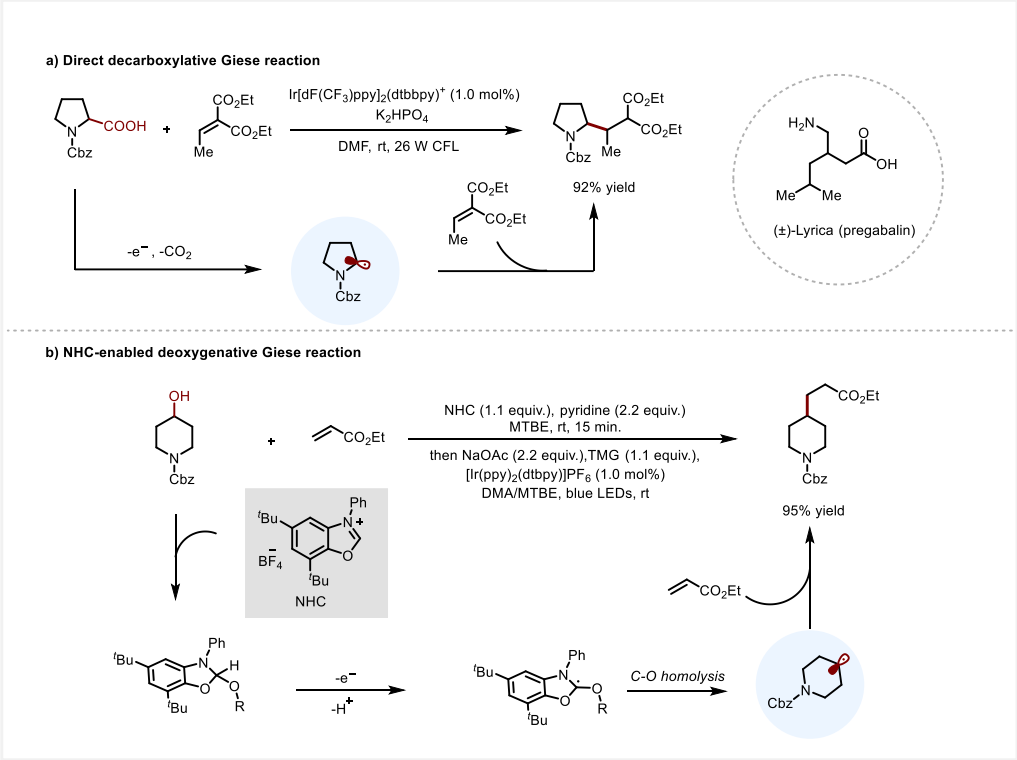

Scheme 3.4 MacMillan's work of decarboxylative and deoxygenative Giese reactions

In 2019, Aggarwal and co-workers developed a photocatalytic deaminative Giese reaction (Scheme 3.5).[148] This transformation is realized by the formation of an electron donor-acceptor (EDA) complex between the pyridinium-activated amine and Hantzsch ester (or triethylamine), which allows the production of alkyl radical via a photoinduced electron transfer (PET) process followed by fragmentation.

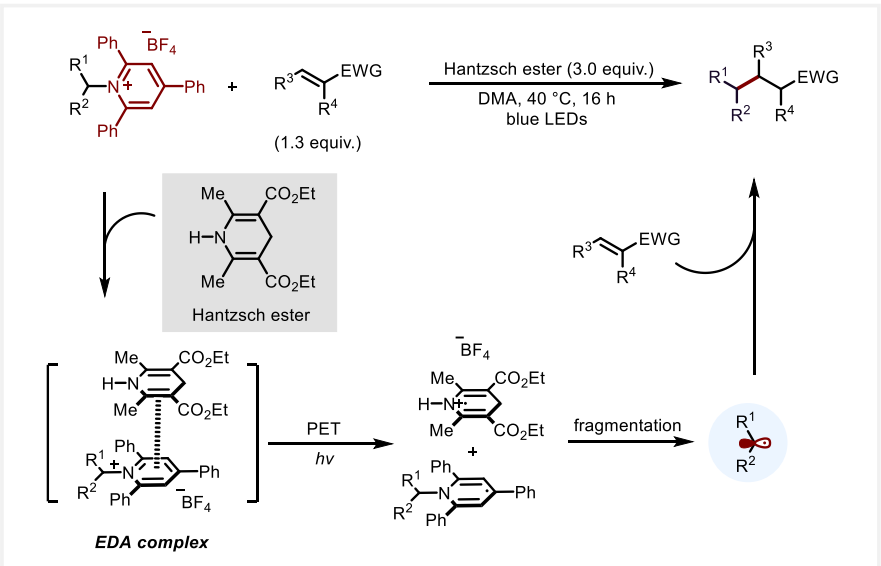

Scheme 3.5 Photocatalytic deaminative Giese reaction through EDA complex

Furthermore, by using photocatalysis, organotrifluoroborates,[149] α-organosilanes,[150] and other types of radical precursors[151] can also undergo single electron transfer to produce carbon-centered radicals, which subsequently participate in Giese addition reactions.

2) Dehydrogenative process to form alkyl radicals

Amines can undergo a SET process to generate radical cation intermediates that may be further deprotonated to form neutral α-amino carbon-centered radicals, thereby enabling the Giese reaction. Jui and co-workers reported such a transformation (Scheme 3.6).[152] Under photocatalytic conditions, structurally complex amines react with dehydroalanine (Dha) derivatives via Giese addition, capable of the synthesis of a diverse range of unnatural amino acids.

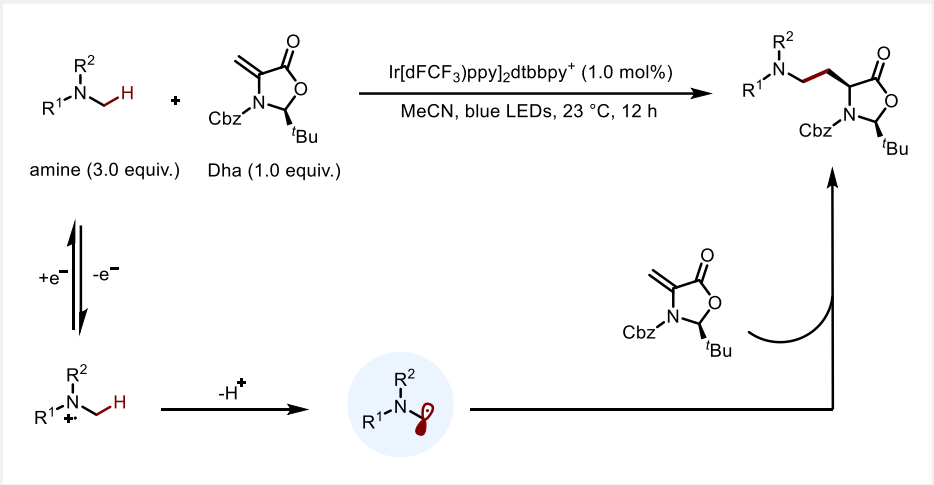

Scheme 3.6 The Giese reaction of amines and Dha through aminoalkyl radcials

Simple alkanes are able to participate in HAT pathways and form alkyl radicals. For instance, Zuo *et al.* developed an alcohol-directed Giese reaction using cerium trichloride as the photocatalyst (Scheme 3.7). In the proposed catalytic cycle, a methoxyl radical is generated from a Ce(IV)-methoxide complex by a photoinduced ligand-to-metal charge transfer (LMCT) process, facilitating the formation of carbon-centered radicals from unactivated alkanes through HAT.[153]

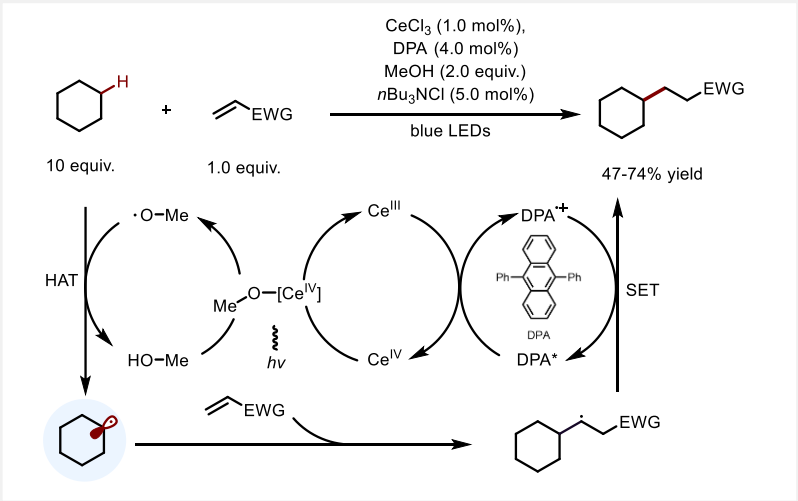

Scheme 3.7 The alcohol-directed Giese reaction with unactivated alkenes as radical precusors

In some reactions, HAT can be initiated by intramolecular alkoxyl radicals. In 2016, Chen and co-workers employed masked alcohols, specifically *N*-alkoxyphthalimides, as substrates in a visible-light-driven reaction in the presence of Hantzsch ester (Scheme 3.8).[154] The reaction proceeds via homolytic cleavage of the N–O bond to generate alkoxyl radicals, which undergo subsequent 1,5-HAT to form carbon-centered radicals. These radicals selectively add to electron-deficient alkenes with excellent regioselectivity.

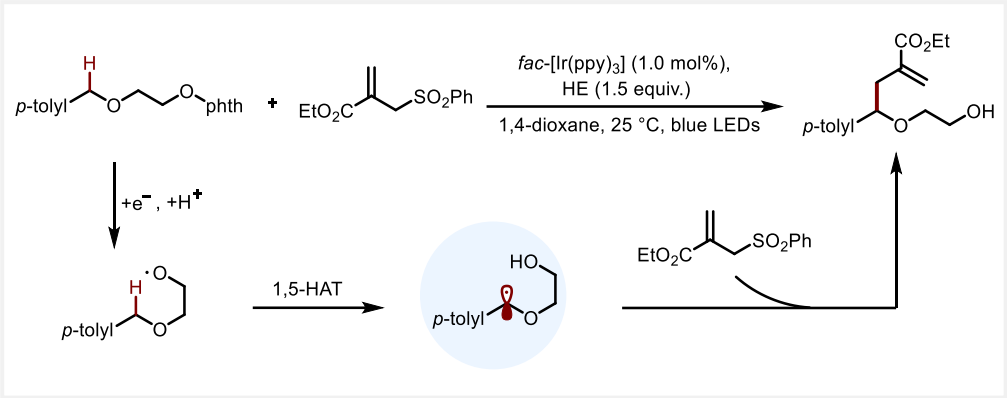

Scheme 3.8 Alkoxyl radicals-enabled the formation of alkyl radical via 1,5-HAT in Giese reactions

3) Alkenes as radical precursors

Studer and co-workers utilized an α-imino-oxy propionic acid bearing an alkene moiety as one of the starting materials, which was oxidized under photochemical conditions to generate an iminyl radical. Through a 5-exo cyclization process, an alkyl radical could be formed, followed by Giese addition to a Michael acceptor. (Scheme 3.9).[155]

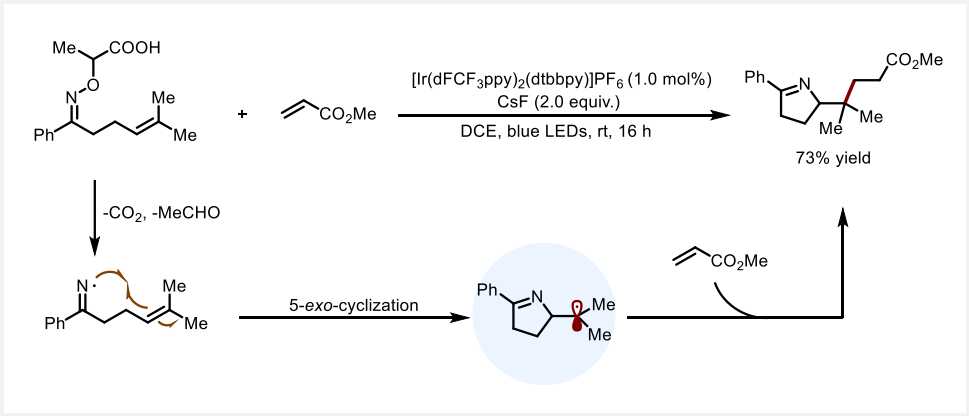

Scheme 3.9 Iminyl radical-initiated the formation of carbon-centered radical from alkenes

Later, the same group reported a three-component radical conjugate addition reaction (Scheme 3.10).[156] In this process, the initially generated amidyl radical first adds to an unactivated alkene, and the resulting alkyl radical undergoes a Giese-type addition to a Michael acceptor, affording a series of alkene carbonamination products.

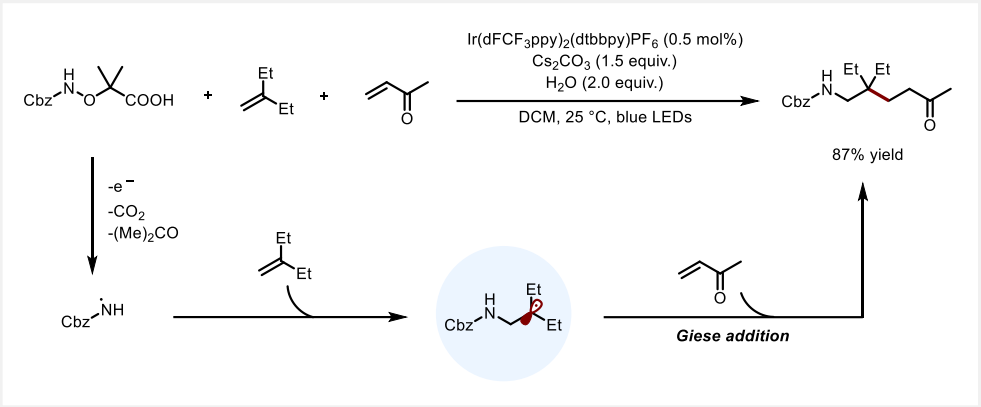

Scheme 3.10 Three-component radical conjugate additions of unactivated alkenes to Michael acceptors

4) Giese addition-initiated cascade reaction

In the aforementioned examples, alkyl radicals generated through radical addition typically undergo HAT or SET step to yield the final products. However, under appropriate conditions, radical **B** (Scheme 3.1) can be intercepted by another species as well, enabling subsequent transformations.[133,134] For example, Aggarwal and co-workers described a photocatalytic radical addition/cross-coupling cascade reaction, which allows for the highly selective synthesis of diverse alkyl boronic esters (Scheme 3.11).[157] Specifically, a carboxylic acid undergoes photocatalytic activation to generate an α-amino radical, which subsequently adds to alkenyl borate. The resulting carbon radical then participates in a nickel-catalyzed cross-coupling with aryl iodides. This method has been applied to the synthesis of complex structures, including sedum alkaloids.

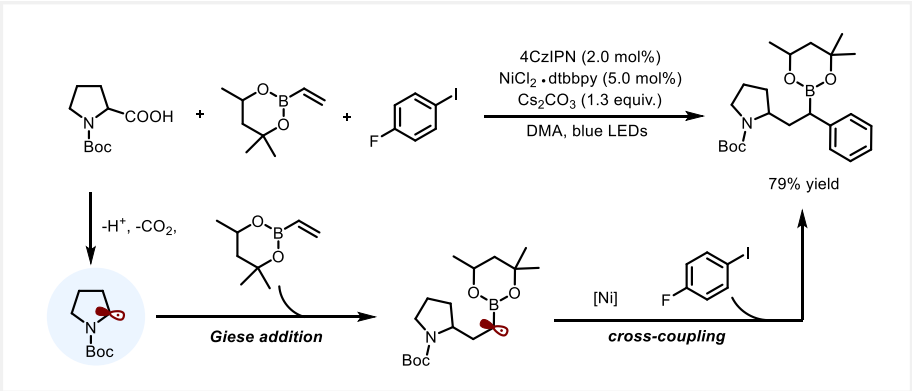

Scheme 3.11 Giese addition-initiated Ni-catalyzed cross-coupling reaction

The Truce-Smiles rearrangement (TSR) serves as an efficient strategy for introducing aryl groups.[158] This is particularly true for radical TSRs, which overcome the limitation of ionic rearrangements, which are typically restricted to electron-deficient aryl migrations.[159] By generating a spiro radical intermediate, this radical-based approach expands the scope of migrating groups to include neutral and electron-rich aryls, thereby enabling desulfonylative radical 1,4-aryl migrations.[160] Recently, the Guo group reported a photocatalytic Giese addition/Truce-Smiles rearrangement cascade (Scheme 3.12).[161] In this transformation, carbon-

centered radicals are generated via β-scission of alkoxy radicals, which originate from cycloalkyl hydroperoxides. Subsequent Giese addition to *N*-(phenylsulfonyl)acrylamide triggers the TSR process.

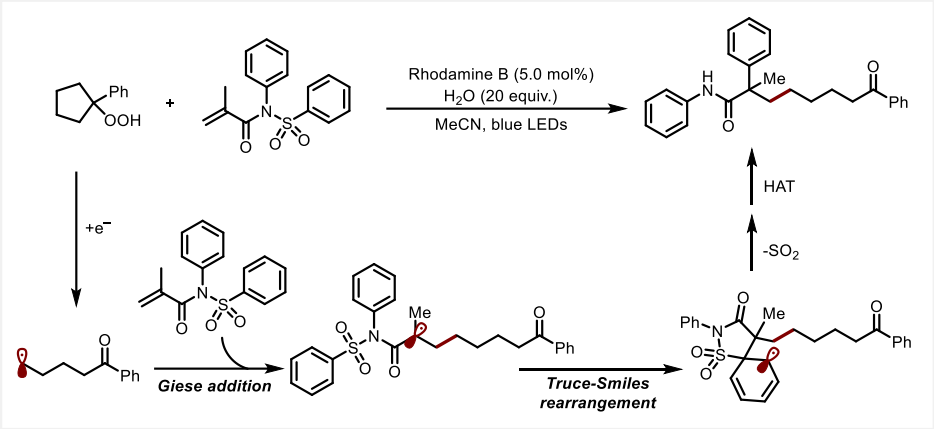

Scheme 3.12 Photocatalytic Giese addition/Truce-Smiles rearrangement cascade

3.2 Reaction development

3.2.1 Reaction design

Alkenes are common radical precursors but have rarely been utilized in Giese reactions, particularly in combination with photocatalysis.[155,156] Although the Baran group has reported several iron-catalyzed inter- and intramolecular Giese-type reactions of alkenes, these methods have notable limitations (Scheme 3.13 a).[39,40,117] For instance, they require relatively high catalyst loadings (typically exceeding 30%), elevated reaction temperatures, and pose purification challenges due to the use of silane. More recently, Luo and co-workers disclosed a visible-light-induced cobalt-catalyzed Giese reaction in the total synthesis of (–)-Triptnoide (Scheme 3.13 b).[66] However, when the reaction proceeded in an intermolecular fashion, only H- abstraction products were obtained, rather than the desired Giese-type adducts. More importantly, in both groups' work, styrene derivatives were not included or further explored, although they can generate benzylic radicals via an MHAT process—species that are often challenging to engage in Giese-type reactions.

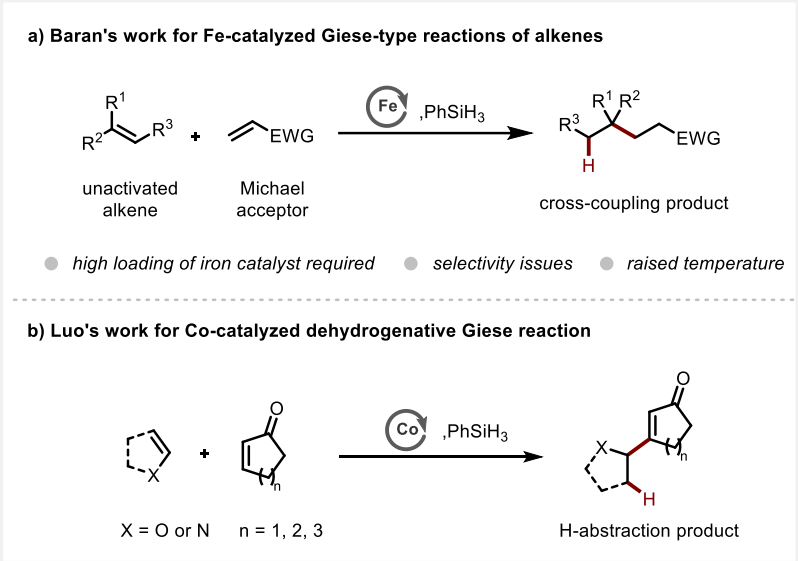

Scheme 3.13 Baran's work of Fe-catalyzed Giese-type reaction and Luo's work of Co-catalyzed dehydrogenative Giese reaction

Our group has a continuous interest in MHAT reactions, leading us to propose that the benzylic radical generated from styrene via cobalt-hydride catalysis could also undergo a 1,4-radical addition to a Michael acceptor to yield the reductive coupling product (Scheme 3.14 left). In contrast to Baran's work that is relied on an oxidative generation of key Fe^{III}–H species, the Co^{III}–H in our mechanism is generated in a reductive manner. The excited state of a photocatalyst reduces Co^{II} to Co^{I}, followed by a protonation to form the cobalt hydride. Furthermore, inspired by Nevado and other groups' work on the cascade aryl migration/ desulfonylation,[162-166] we envisioned that upon the Giese addition of the benzyl radical, a second cascade Smiles reaction could take place, thus enabling an overall alkene carboarylation reactlion (Scheme 3,14 right).

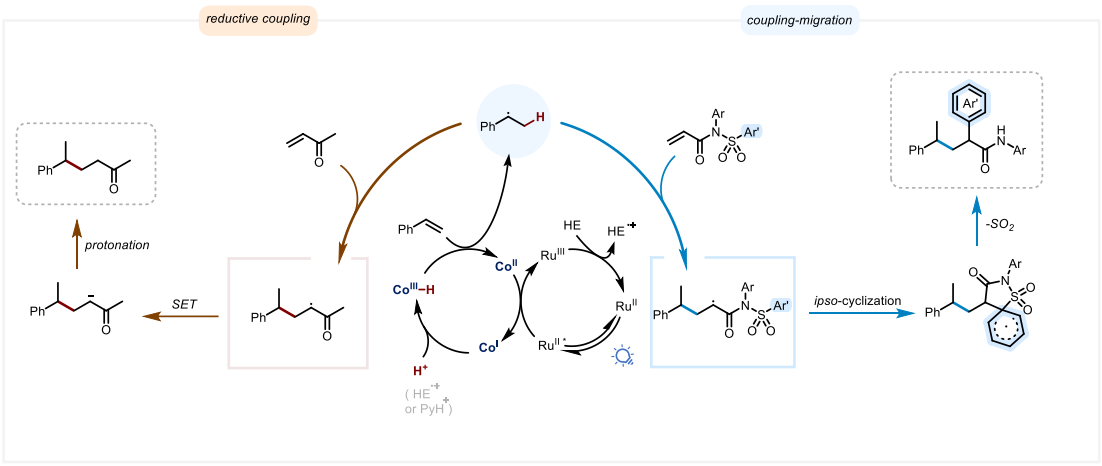

Scheme 3.14 Reaction design

3.2.2 Reaction optimization

We first focused on optimizing the reaction conditions of reductive coupling between styrenes and simple Michael acceptors (Table 3.1). Building on the optimal conditions established in Chapter 2 for the reaction between dienes and pyridyl phosphonium salts, we found that the model substrates styrene **3.1** and methyl vinyl ketone **3.2** could be efficiently converted to **3.3** in good yield using the commercially available **Co(TMOPP)** as MHAT catalyst (Table 3.1, entry 2). Encouraged by the preliminary result, we further screened a variety of solvents. Among them, DCM proved to be the most effective, affording an 81% yield (Table 3.1, entry 1). In contrast, using $CHCl_3$ led to a significant decrease in yield (Table 3.1, entry 3). DME resulted in only a 9% yield, while the dipolar aprotic solvent DMSO gave trace amounts of the product (Table 3.1, entries 4-5). The polar solvent EtOAc provided a moderate yield of 36% (Table 3.1, entry 6). Furthermore, we observed that a high reaction concentration was crucial for achieving optimal efficiency, suggesting that lower concentrations might hinder the reactivity. Indeed, during our optimization work, we found that decreasing the reaction concentration led to increased dimerization of styrene, which explains the slight drop in product yield under diluted conditions (Table 3.1, entry 7).

Next, we evaluated the catalytic performance of a range of cobalt complexes. Consistent with our previous work, cobalt catalysts bearing porphyrin ligands exhibited the highest activity. **Co(TMOTPP)**, which performed best in our previous reaction, gave a 78% yield in this case (Table 3.1, entry 11), whereas the commercially available **Co(TMOPP)** proved to be the most effective. In comparison, **Co(TPP)**, which lacks substituents on the benzene ring, showed the lowest activity among the three (Table 3.1, entry 10). Cobalt complexes with salen or PC ligands significantly impact the reaction efficiency, yielding the reductive coupling products in only 18% and 15% yield, respectively (Table 3.1, entries 8-9). We also tested other Ru-based photocatalysts, among which $Ru(phen)_3(PF_6)_2$ provided a 71% yield (Table 3.1, entry 13). Compared to 2,6-lutidine, organic bases, such as pyridine, triethylamine and 1,8-diazabicyclo[5.4.0]undec-7-ene (DBU), performed poorly (Table 3.1, entries 14-16). Control experiments confirmed that the photocatalyst, HE, and cobalt were all essential for the reaction, as the absence of a base led to a noticeable drop in yield (Table 3.1, entries 17-20). Finally, we found that adding water (as an additive) still resulted in a 75% yield, indicating that the reaction is not highly sensitive to moisture (Table 3.1, entry 21).

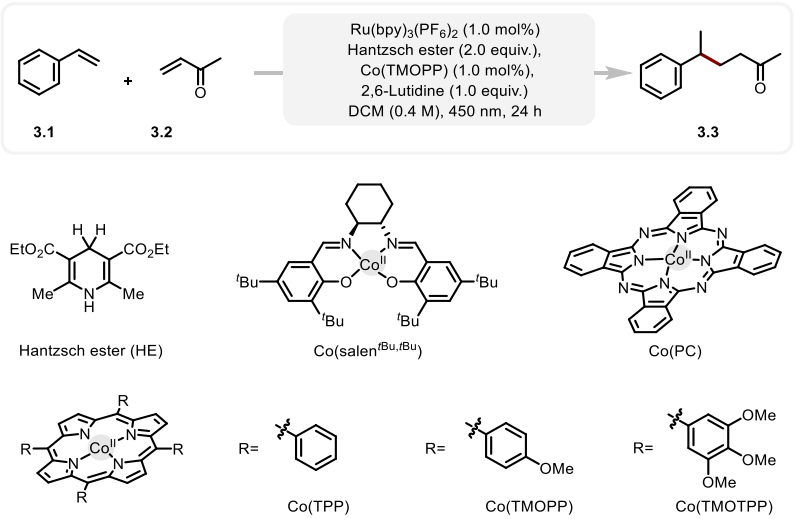

Entry	Variations	Product (%)[a]
1	None	81 (77)
2	Acetone	72
3	$CHCl_3$	54
4	DME	9
5	DMSO	<5
6	EtOAc	36
7	DCM (0.2 M)	74
8	**Co(salen^{tBu,tBu})**	18
9	**Co(PC)**	15
10	**Co(TPP)**	70
11	**Co(TMOTPP)**	78
12	$Ru(bpz)_3(PF_6)_2$	12
13	$Ru(phen)_3(PF_6)_2$	71
14	Pyridine	31
15	Et_3N	<5
16	DBU	9
17	w/o photocatalyst	Trace
18	w/o HE	0
19	w/o cobalt	0
20	w/o base	32
21	H_2O (1.0 equiv.) as additive	75

Table 3.1 Optimization reactions conducted with 0.2 mmol of **3.1** and 0.4 mmol of **3.2**. [a] Yields in **3.3** determined by ^{1}H-NMR analysis of crude reaction mixture with dibromomethane as an internal standard. Isolated yield in parentheses.

3.2.3 Reaction scope

With the optimal conditions in hand, we next explored the substrate scope for the coupling reaction between styrenes and Michael acceptors (Scheme 3.15). We first examined the range of styrene derivatives. Fortunately, styrenes bearing substituents with varying electronic properties on the

phenyl ring were well tolerated, affording moderate to excellent yields (**3.6**-**3.13**). As shown, electron-donating substituents generally led to higher yields compared to electron-withdrawing groups. Notably, α-methyl styrene also underwent coupling under the optimized conditions, furnishing the corresponding product with a quaternary center (**3.5**). *Ortho*-substituted derivatives, such as 2-bromostyrene and 2,4,6-trimethylstyrene, were also compatible, indicating that steric effects at the *ortho* position do not significantly hinder the reaction (**3.14** and **3.15**). Similarly, naphthyl- and heteroaryl-substituted alkenes exhibited comparable reactivity to styrene, yielding products **3.16** and **3.17** in moderate yields. Heteroatom-substituted alkenes represent a particularly intriguing class of substrates, as these alkenes typically exhibit electrophilic behavior at the position adjacent to the heteroatom when acting as donors. However, the radical intermediates generated via MHAT catalysis are nucleophilic, effectively reversing the intrinsic reactivity and enabling access to structural motifs that are challenging to obtain using conventional methods. To our delight, both vinyl thioethers and vinyl ethers successfully participated in the coupling reaction under our conditions, affording the desired products **3.18** and **3.19**.

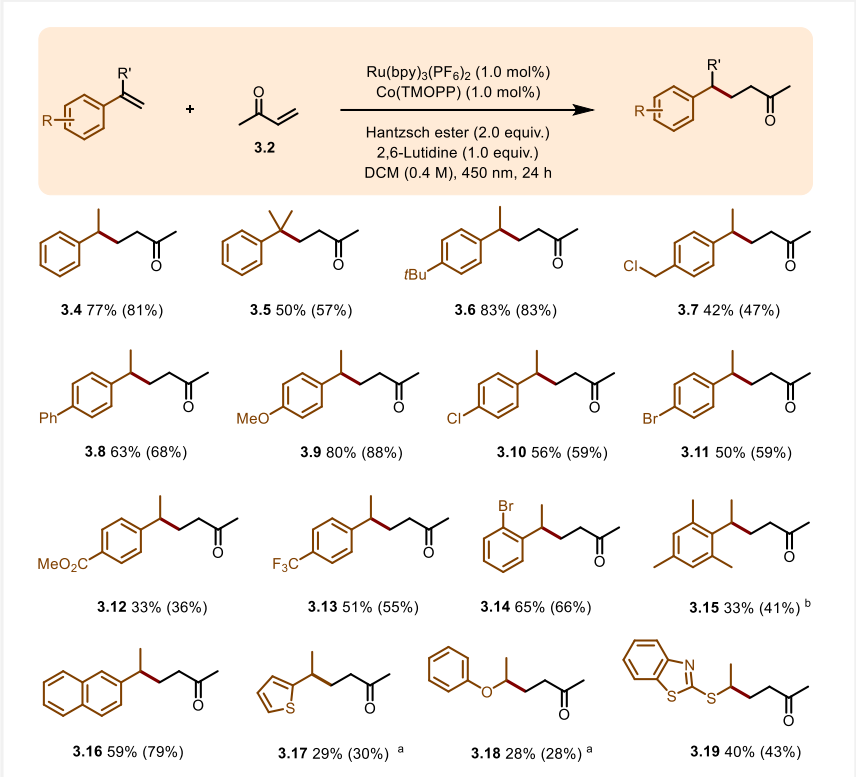

Scheme 3.15 Scope of styrenes. Note: yield determined by ^{1}H NMR by comparison with dibromomethane as an internal standard is given in parentheses. Reactions were performed under standard conditions unless otherwise indicated. [a] using 4 equiv. **3.2.** [b] reaction performed in acetone.

Extensive experimental investigations revealed that the scope of Michael acceptors in this reaction is relatively limited (Scheme 3.16). Under the optimal conditions, except when using acetone as the solvent, methyl and phenyl acrylates were well tolerated, affording the corresponding reductive coupling products in moderate yields (**3.20** and **3.21**). Similarly, unprotected sulfone was also identified as suitable coupling partner (**3.22**). Among all tested acceptors, acrylonitrile exhibited

the highest reactivity, delivering good yield under standard conditions (**3.23**). Unfortunately, other types of Michael acceptors either exhibited poor reactivity in the coupling or yielded only trace amounts of the desired product. In these reactions, significant amounts of styrene dimers, recovered starting materials, and unidentified byproducts were frequently observed. For instance, sterically hindered bicyclic and cyclic ketones failed to generate sufficient product. Acrylamide produced only trace amounts of the coupled product, while no product formation was detected for phosphonates. Michael acceptors bearing two electron-withdrawing groups and 3-phenyl acrylonitrile also failed to undergo coupling, likely due to steric hindrance.

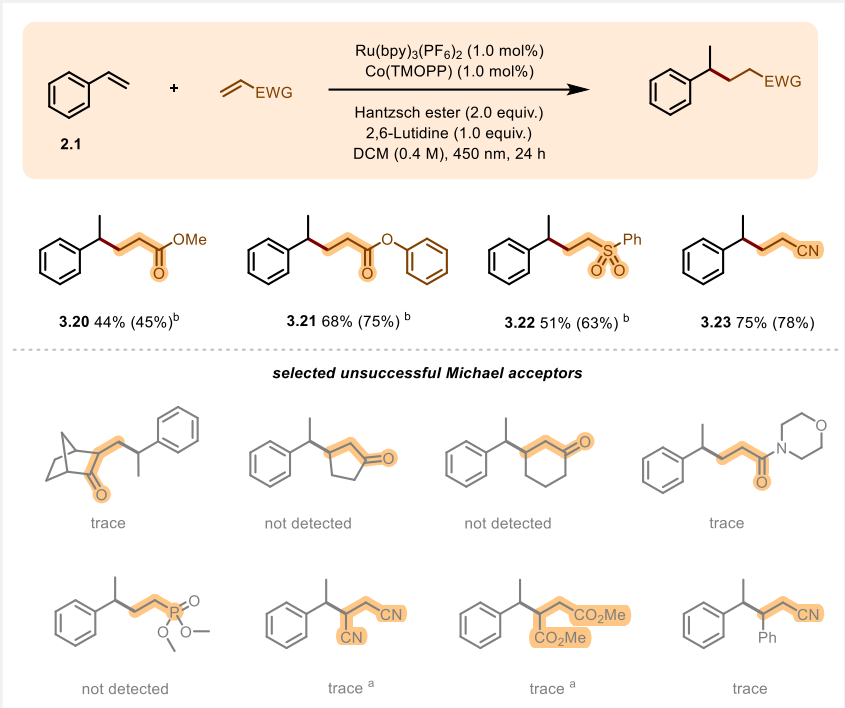

Scheme 3.16 Scope of Michael acceptors. Note: yield determined by ^{1}H NMR by comparison with dibromomethane as an internal standard is given in parentheses. Reactions were performed under standard conditions unless otherwise indicated. [a] using 4 equiv. Michael acceptor [b] reaction performed in acetone.

3.2.4 Preliminary investigation of the Giese addition/Truce-Smiles rearrangement cascade

After completing the substrate expansion, we proceeded to explore the optimal reaction conditions for the difunctionalization of activated alkenes.

Our investigation began with the reaction of unsubstituted styrene and *N*-phenyl-*N*-(phenylsulfonyl)acrylamide **3.24** (Scheme 3.17). When we directly applied the conditions used for the conjugate addition of styrene to a Michael acceptor, structural analysis revealed that the desired product was not obtained. Instead, the reaction primarily yielded a conventional reductive coupling product in 30% yield. The yield of **3.25** showed a slight increase when MeOH was used as the solvent. Furthermore, modifying the substituents on the nitrogen atom of sulfonyl acrylamide with different electronic properties still led to the formation of the same reductive coupling product. Notably, when *N*-methyl-*N*-(phenylsulfonyl)acrylamide was used as the reaction partner, a higher yield was achieved, with an isolated yield of 57%.

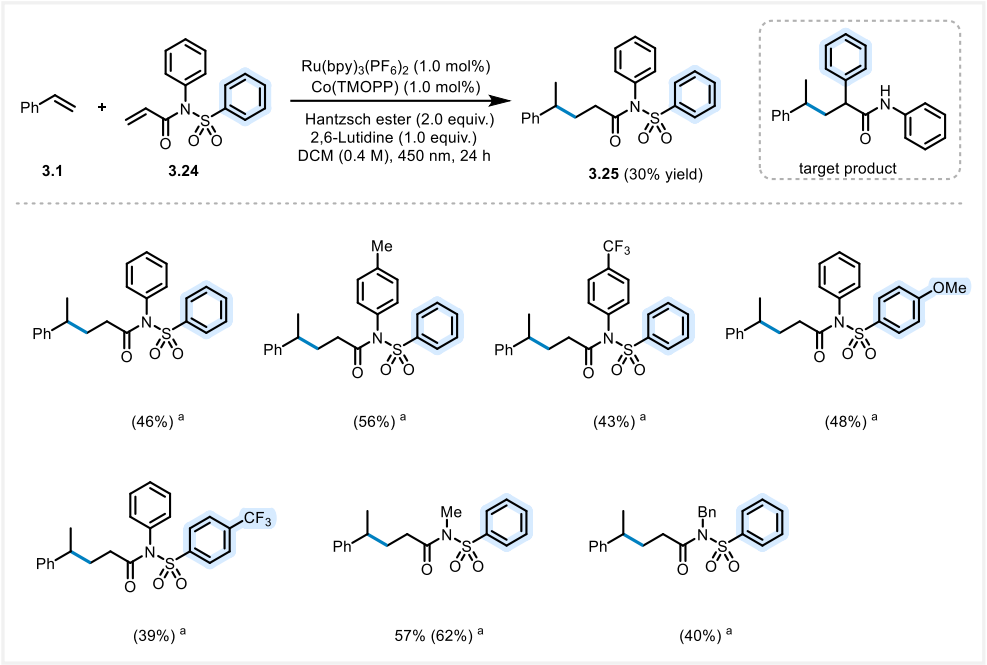

Scheme 3.17 The reaction between styrene and phenysulfonyl acrylamide. Note: yield determined by ^{1}H NMR by comparison with dibromomethane as an internal standard is given in parentheses. Reactions were performed under standard conditions unless otherwise indicated. [a] reaction performed in MeOH.

We sought to understand the reasons behind the generally low yields and aimed to obtain the desired coupling-migration products through appropriate substrate modifications. During reaction optimization, several side products were observed, including intramolecular Smiles rearrangement and reduction products of **3.24**, as well as dimerization and reduction products of styrene. In addition, based on the proposed mechanism, it is also possible that carbon radicals, formed through either intra- or intermolecular pathways, undergo *ortho*-addition to the aromatic ring, leading to the formation of six- and five-membered heterocyclic products (Scheme 3.18).

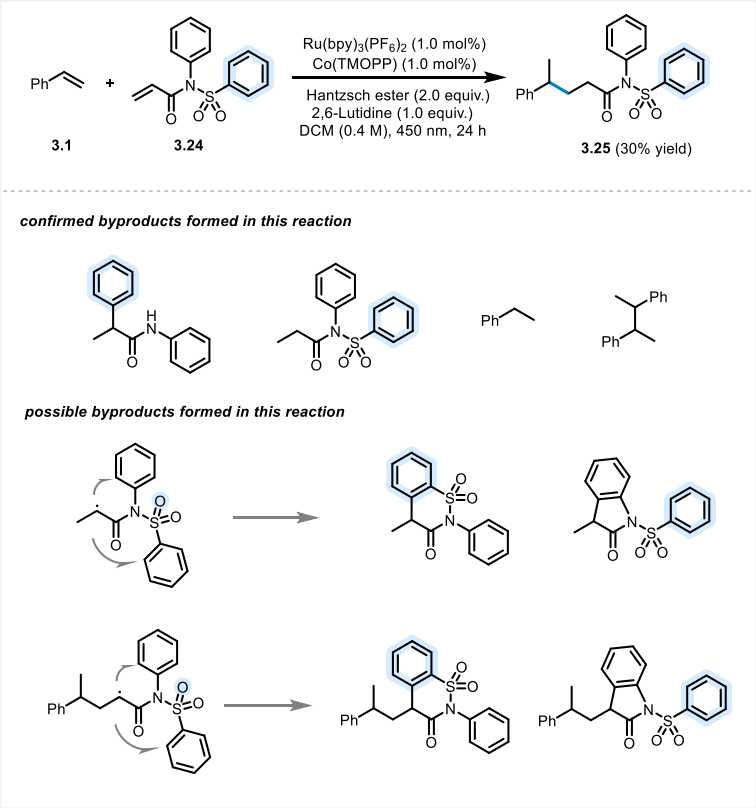

Scheme 3.18 Byproducts formed in the reaction of styrene **3.1** and *N*-phenyl-*N*-(phenylsulfonyl)acrylamide **3.24**

We therefore hypothesized that introducing a substituent at the *ortho* position of the sulfonyl phenyl ring could suppress the aforementioned *ortho*-cyclization side reaction. Additionally, the increased steric hindrance may twist the ring such that the *ipso*-carbon would be in closer proximity to the carbon-centered radical formed after the initial Giese addition, thereby facilitating the rearrangement reaction.[167] Based on this rationale, we selected *N*-phenyl-*N*-(mesitylsulfonyl)acrylamide **3.26** as a reaction partner. Encouragingly, the desired product was indeed obtained, albeit in a 22% yield with a 1.8:1 diastereomeric ratio (*d.r.*). However, we still observed the formation of some side products. To suppress these byproducts, we carried out extensive optimization of reaction conditions. The results indicated that chlorinated hydrocarbon solvents were more favorable for the formation of the target product, with chloroform affording a yield comparable to that of DCM (Table 3.2 entries 2-7). For the cobalt catalyst, porphyrin ligands still outperformed other ligand systems (Table 3.2, entries 8-11). Among several Ru-based and organic photocatalysts, $Ru(Phen)_3(PF_6)_2$ exhibited comparable efficiency to $Ru(bpy)_3(PF_6)_2$ (Table 3.2, entries 12-15). The addition of either base (*e.g.* pyridine, PhCOONa) or acid (*e.g.* $B(OMe)_3$, $AlCl_3$) did not inhibit the reaction, although both were less effective than lutidine under the standard conditions (Table 3.2, entries 16-19). Notably, when water was used as an additive, a yield of 20% was still obtained, suggesting that the reaction is tolerant to moisture (Table 3.2, entries 20).

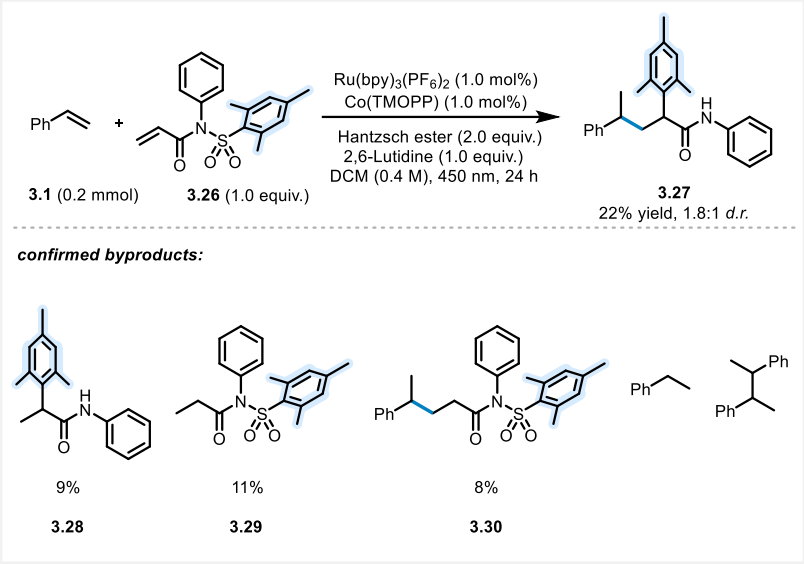

Entry	Variations	Yield (*d.r.*)[a]	Ratio of byproducts (3.28:3.29:3.30)
1	None	22 (1.8:1)	9:11:8
2	MeCN	9 (1.3:1)	1:6:18
3	Acetone	18 (1.3:1)	-:10:18
4	DMA	0	-:3:12
5	DCE	21 (1.3:1)	7:6:5
6	$CHCl_3$	23 (1.6:1)	-:3:8
7	DCM/HFIP=20:1	19 (1.7:1)	5:10:9
8	**Co(salen^{tBu,tBu})**	3 (2:1)	0:10:2
9	**Co(PC)**	<5	-
10	**Co(TPP)**	25 (1.3:1)	8:5:8
11	**Co(TMOTPP)**	21 (1.6:1)	-:12:7
12	$Ru(bpz)_3(PF_6)_2$	4 (3:1)	0:trace:2
13	$Ru(phen)_3(PF_6)_2$	23 (1.6:1)	7:8:9
14	$Ru(bpy)_3Cl_2$	9 (2:1)	trace:3:8
15	4CzIPN	14 (1.8:1)	-:12:6
16	Pyridine	11 (1.8:1)	8:7:4
17	PhCOONa	22 (1.8:1)	-:2:5
18	$B(OMe)_3$ instead of base	21 (1.6:1)	5:5:7
19	$AlCl_3$ instead of base	6 (2:1)	trace: 3:2
20	H_2O (5.0 equiv.) as additive	20 (1.9:1)	-:9:9

Table 3.2 The reaction between styrene **3.1** and *N*-phenyl-*N*-(mesitylsulfonyl)acrylamide **3.26** and observed byproducts

Simultaneously, we investigated variations in substrate structures (Scheme 3.19). However, the target product yield remained consistently low. Notably, when the *N*-substituents were mesitylsulfonyl and benzyl, the yield reached a maximum of 36%. Despite our optimization attempts, the yield has thus far remained unchanged at 36% or lower, and further efforts are ongoing.

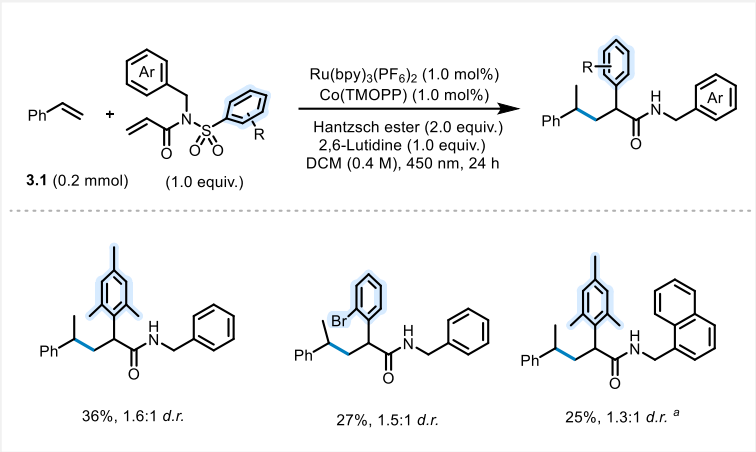

Scheme 3.19 The exploration of other substrates. Note: yield determined by ^{1}H NMR by comparison with dibromomethane as an internal standard is given in parentheses. Reactions were performed under standard conditions unless otherwise indicated. [a] using $Ru(phen)_3(PF_6)_2$ as photocatalyst

3.2.5 Summary and outlook

In summary, a photochemically induced Co-HAT catalytic system enables cross-coupling between styrenes and Michael acceptors. When *N*-arylsulfonyl acrylamides are used as the Michael acceptors, the Truce-Smiles reaction is triggered by the initial radical addition. We found that this rearrangement occurs only when the 2-position of the migrating aryl group is blocked. Without this substitution pattern, no rearrangement follows the initial olefin coupling. Despite these promising findings, several aspects of this work remain to be further developed. In the first part of olefin coupling, the scope of Michael acceptors is relatively narrow. However, *N*-arylsulfonyl acrylamides afford moderate yields, possibly due to their unique structural features. The results also suggest that alcoholic solvents may be more favorable for this coupling process. In the second part, coupling-rearrangement reaction, the yields remain unsatisfactory, typically below 30%. Future efforts may focus on substrate modification, such as introducing substituents at the 2-position of the *N*-aryl group to suppress undesired *ortho*-cyclization. Additionally, further solvent optimization, for instance using DCM/ethanol mixed solvents, could prove beneficial.

4

Co-HAT Catalyzed Semipinacol Rearrangement

4 Co-HAT catalyzed semipinacol rearrangement

4.1 Photocatalytic semipinacol rearrangement

The reactions described in this chapter were performed by Danijela Lunic, Nikita Vystavkin, Jingyang Qin (PhD students in the group) under the supervision of Prof. Dr. Christopher J. Teskey. The author contributions are as follow: C.J.T. and D.L. designed the project. D.L. and N.V. performed the optimization. Further synthetic work including scope and mechanistic investigations were performed by D.L., N.V. and J.Q.. This work is published in Angewandte Chemie International Edition.[168]

α-Arylated ketones represent a valuable class of structural motifs frequently found in bioactive and pharmaceutical compounds.[169] For instance, normethadone is a synthetic opioid analgesic and antitussive agent that contains such a framework (Scheme 4.1).[170]

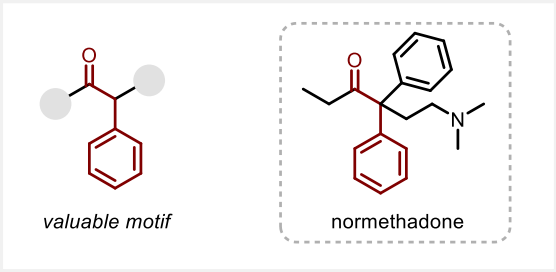

Scheme 4.1 The importance of α-arylated ketones

Traditional methods for the synthesis of such structural motifs primarily rely on the direct arylation of ketones.[171] However, these approaches often suffer from regioselectivity issues, particularly when applied to unsymmetrical dialkyl ketones.[172] To address this challenge, we envisioned an alternative strategy involving the use of tertiary allylic alcohols as substrates to construct α-arylated ketones via an MHAT-catalyzed semipinacol rearrangement (Scheme 4.2). Analogous to the previously proposed Co(II)/Co(I) catalytic cycle (see chapter 2 and 3), the starting material undergoes MHAT to generate a carbon-centered radical, which then attacks a proximal aryl group. The resulting aryl migration produces a new carbon radical, which subsequently rearranges into a ketyl radical. A sequence of SET and proton transfer (PT) steps finally affords the α-arylated ketone product.

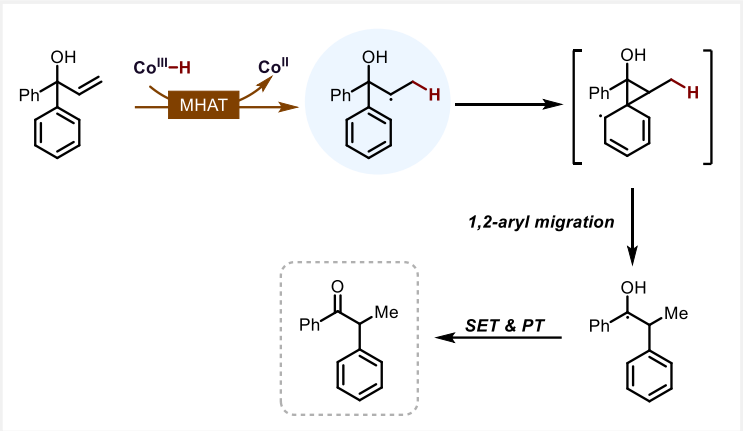

Scheme 4.2 Reaction design

Optimization of the reaction conditions identified the optimal system as follows: 3.0 mol% of **Co**-(*S*,*S*) as the MHAT catalyst, 1.0 mol% of *N*-phenyl benzo[*b*]phenothiazine (PTH) as the photocatalyst, 0.8 equiv of cyclohexyl Hantzsch ester (HE-Cy), 1.0 equiv of AcOH, and 9.5 equiv of HFIP, in benzene under irradiation with 405 nm blue light, affording the desired product in 75% yield (Scheme 4.3). Compound **4.3** was identified as the byproduct, which originates from the reduction of starting material **4.1**.

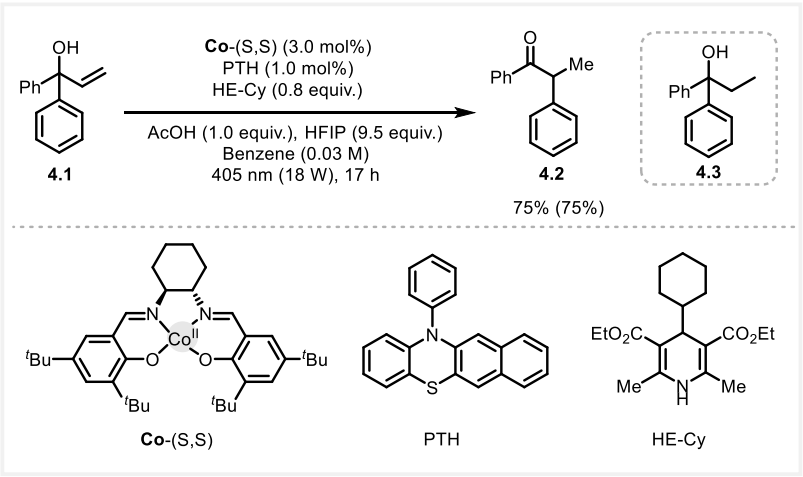

Scheme 4.3 Optimized reaction conditions. Reaction optimization was performed on 0.1 mmol scale. Yield determined by ^{1}H-NMR analysis of crude reaction mixture with $CHBr_3$ or CH_2Br_2 as the internal standard is given in parentheses.

Substrate scope studies revealed that for diaryl allylic alcohols, electron-deficient aryl groups are more prone to migration, consistent with the proposed radical pathway, wherein the nucleophilic carbon radical preferentially attacks electron-poor arenes (Scheme 4.4). But for few substrates with *ortho*-substitutions, the steric effects make *ipso* attack less favored, thus disfavoring the migration. For instance, in the formation of compound **4.7**, the migration of an electron-deficient *ortho*-chloro substituted aromatic is disfavored compared to the unsubstituted phenyl group, which suggests that steric effects override electronic factors in this case. Moreover, alkyl-aryl substituted allylic alcohols bearing a single aromatic ring were also compatible with the transformation.

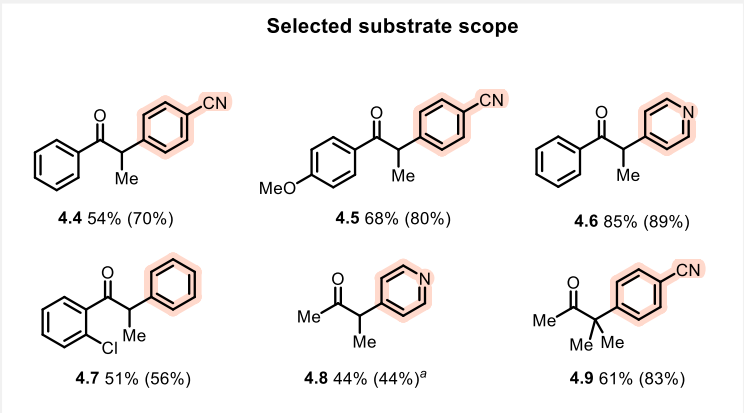

Scheme 4.4 Selected substrate scope. Yields determined by ^{1}H-NMR analysis of crude reaction mixture with $CHBr_3$ or CH_2Br_2 as the internal standard are given in parentheses. Reactions were performed under standard conditions on a 0.18 mmol scale unless otherwise indicated. [a] 0.1 mmol scale

Molecular editing refers to the precise modification of molecular structures at the atomic level and has been integral to the entire history of organic synthesis. It is generally classified into two categories. The first is the well-established peripheral editing, which targets modification on peripheral functional groups or non-core regions, such as C–H bond activation. The second, which has emerged as a growing area of research in recent years, aims to directly alter the skeleton of the molecular through atomic insertion, deletion, or swap.[173,174] Owing to its precision and efficiency, molecular editing has become a powerful tool across diverse domains including pharmaceuticals, materials science, and environmental chemistry. [175,176]

In light of recent advances, we sought to apply our semipinacol rearrangement protocol for the structural editing of aryl ketone-based drug molecules. This approach provides a distinct alternative to existing methods that rely on diazo reagents for similar skeletal modifications.[177] Specifically, we propose to prepare allylic alcohol precursors via Grignard addition firstly, followed by an MHAT-catalyzed rearrangement, ultimately affording homologated diaryl ketones with a carbon atom inserted into the core framework. For example, compound **4.10** (a known bioactive molecule) can be readily converted to the corresponding tertiary alcohol **4.11** via a Grignard addition, which subsequently undergoes semipinacol rearrangement, delivering **4.12** via pyridine ring migration (Scheme 4.5 a). Another example involves the derivatization of the *t*-butyl ester of ketoprofen, a well-known anti-inflammatory drug. Subjecting it to the same sequence—reaction with a vinyl magnesium Grignard reagent followed by rearrangement—ultimately afforded a mixture of compounds **4.15** and **4.16** (Scheme 4.5 b). Interestingly, this transformation introduces a CHMe unit into the molecular scaffold. While this differs slightly from the classic "magic methyl effect" where the installation of a single methyl group can lead to pronounced changes in drug potency, the subtle structural modification here might likewise modulate physicochemical and biological properties, such as drug half-life, selectivity, potency, and binding affinity.[178,179]

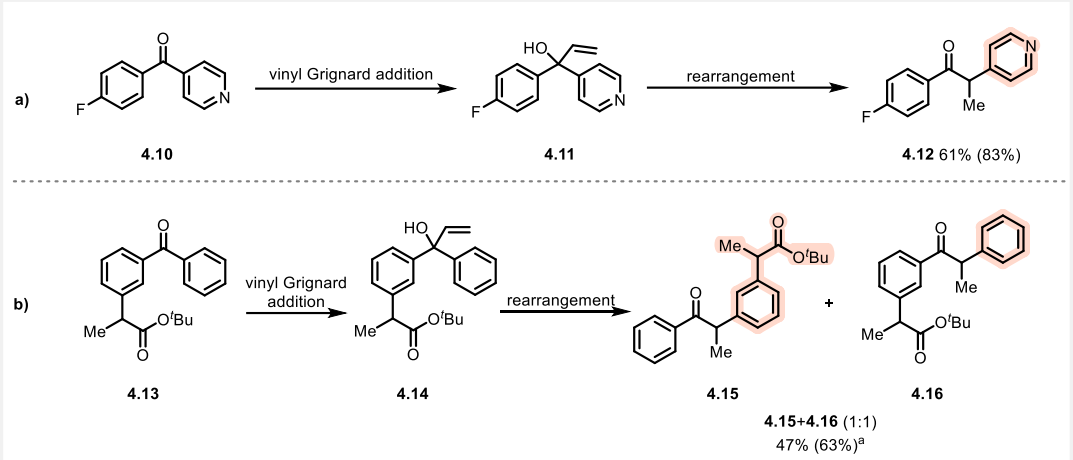

Scheme 4.5 Application of photocatalytic semipinacol rearrangement. Yields determined by ^{1}H-NMR analysis of crude reaction mixture with $CHBr_3$ or CH_2Br_2 as the internal standard are given in parentheses. Reactions were performed under standard conditions on a 0.18 mmol scale unless otherwise indicated. [a] 0.1 mmol scale

4.2 Summary and outlook

We have developed a dual-catalytic semipinacol rearrangement of allylic alcohols via a MHAT-based strategy to access α-arylated ketones through a radical pathway. The broad substrate scope and two-step structural editing demonstrate the synthetic versatility of this method. Looking ahead, the introduction of chiral cobalt catalysts for enantioinduction—particularly from racemic starting materials — holds significant promise for generating enantioenriched products and enhancing the practical applicability of this transformation.

5

Supporting Information

5. Supporting information

5.1 General materials and methods

Unless otherwise stated, all reactions were performed utilizing standard Schlenk techniques. All reagents and starting materials were purchased at reagent grade and used as received. Anhydrous solvents were dried using an Innovative Technology PS-MD-5 solvent purification system. Thin layer chromatography (TLC) was performed on Merck Kieselgel 60 F254 aluminum plates with unmodified silica and visualized either under UV light or stained with potassium permanganate or vanillin. Column chromatography was performed with Merck silica gel 60 (35–70 mesh).

All ^{1}H, ^{13}C, ^{19}F, and ^{31}P NMR spectra were recorded at ambient temperature on either Varian V-NMRS 600, Varian V-NMRS 400, Bruker AV-400, Bruker AV-600 or Varian Mercury 300 spectrometers. Chemical shifts (δ/ppm) were referenced to the residual solvent peak in ^{1}H (7.26 ppm for $CDCl_3$) and ^{13}C spectra (77.16 ppm for $CDCl_3$). Coupling constants (*J*) are given in Hz. Signals are described as br = broad, s = singlet, d = doublet, dd = doublet of doublets, t = triplet, q = quartet, p = quintet, h = sextet and m = multiplet. Where coincident coupling constants have been observed, the apparent (app) multiplicity of the proton resonance has been reported.

High-resolution mass spectrometry (HRMS) was performed using a Thermo Scientific LTQ Orbitrap XL spectrometer. Infrared (IR) spectra were recorded on a Perkin Elmer Spektrum 100 FT-IR spectrometer Spectrum 100 spectrometer with an UATR Diamond/KRS-5 crystal with attenuated total reflectance (ATR) and signals reported as wavenumbers in reciprocal centimeters. Gas chromatography coupled with mass spectrometry (GC-MS) was performed on an Agilent Technologies 5975 series MSD mass spectrometer under electrospray ionization (ESI) mode coupled with an Agilent Technologies 7820A gas chromatograph employing an Agilent 19091s-433 HP-5MS column (30 m x 0.250 µm x 0.250 µm). The UV-Vis measurements have been carried out on an Agilent Cary 60.

All the photochemical reactions were carried out in an EvoluChem™ PhotoRedOxBox Duo equipped with two EvoluChem 450PF LED lamps (λ_{max} = 450 nm, 18 W) or two EvoluChem 405PF LED lamps (λ_{max} = 405 nm, 18 W).

5.2 Supporting information for chapter 2

5.2.1 Synthesis of starting materials

Co(TMOTPP) was prepared according to the procedure reported by Org. Lett. 2022, 24, 4474–4478 and confirmed by HRMS (ESI, calculated for $C_{56}H_{53}CoN_4O_{12}$ $[M+H]^+$: 1031.2986, found: 1031.2993).

1) Synthesis of phosphonium salts

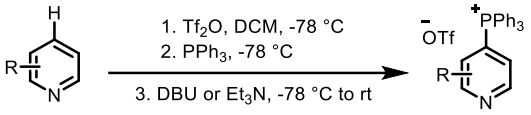

In an oven dried two-neck round bottom flask equipped with a stirring bar was added the substituted pyridine (1.0 equiv) and dry DCM (0.1 M) under an argon atmosphere. The reaction was cooled to −78 °C and Tf_2O (1.0 equiv) was then added dropwise over 5 minutes. After stirring for 30 minutes at this temperature, PPh_3 (1.1 equiv) was added in one portion. The reaction was subjected to three rapid cycles of vacuum/argon backfill and was stirred for a further 30 minutes at −78 °C. After that, DBU or Et_3N (1.0 equiv.) was added dropwise via syringe, the cooling bath was removed, and the reaction was allowed to warm to room temperature while stirring for about 20 minutes. When the reaction mixture reached room temperature, it was then quenched with H_2O and the mixture was transferred to a separatory funnel. The mixture was diluted with DCM and the resulting organic layer was washed three times with H_2O. The organic layer was dried by anhydrous $MgSO_4$, filtered and concentrated in vacuo to approximately 1 mL. An excess of chilled Et_2O (0 °C) was then added dropwise to the concentrated solution. The flask was then placed in a −20 °C refrigerator overnight. The resulting suspension was filtered on a Büchner funnel, washed with Et_2O, and dried in vacuo to provide the pure phosphonium salt.

Triphenyl(2-phenylpyridin-4-yl)phosphonium trifluoromethanesulfonate

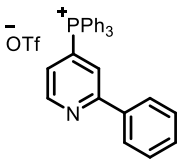

5.0 mmol scale, Et_3N was used as the base. After the purification procedure mentioned above, a white solid was obtained (2.15 g, 75% yield). **^{1}H NMR (400 MHz, $CDCl_3$)** δ 9.12 – 9.07 (app t, *J* = 5.1 Hz, 1H), 7.97 – 7.89 (m, 5H), 7.86 – 7.78 (m, 7H), 7.74 – 7.69 (m, 6H), 7.54 (ddd, *J* = 12.7, 5.0, 1.6 Hz, 1H), 7.56 – 7.47 (m, 3H). **^{13}C NMR (101 MHz, $CDCl_3$)** δ 159.5 (d, *J* = 9.8 Hz), 152.0 (d, *J* = 10.8 Hz), 137.0 (d, *J* = 1.5 Hz), 136.5 (d, *J* = 3.2 Hz, 3C), 134.7 (d, *J* = 10.4 Hz, 6C), 131.3 (d, *J* = 13.2 Hz, 6C), 130.8, 129.4 (d, *J* = 84.3 Hz), 129.1 (2C), 127.4 (2C), 125.5 (d, *J* = 7.8 Hz), 123.4 (d, *J* = 8.5 Hz), 120.2 (q, *J* = 322.1 Hz), 115.9 (d, *J* = 89.6 Hz, 3C).

These data are in agreement with those reported previously in the literature.[93]

(2-(4-Fluorophenyl)pyridin-4-yl)triphenylphosphonium trifluoromethanesulfonate

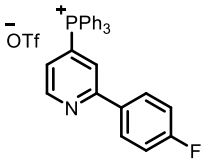

1.0 mmol scale, Et_3N was used as the base. After the purification procedure mentioned above, a white solid was obtained (0.37 g, 64% yield). **^{1}H NMR (600 MHz, $CDCl_3$)** δ 9.03 (app t, *J* = 5.1, 1H), 7.94 – 7.89 (m, 5H), 7.80 – 7.78 (m, 7H), 7.68 – 7.66 (m, 6H), 7.49 (ddd, *J* = 12.7, 5.0, 1.6 Hz, 1H), 7.14 – 7.09 (m, 2H). **^{13}C NMR (151 MHz, $CDCl_3$)** δ 164.4 (d, *J* = 251.2 Hz), 158.5 (d, *J* = 10.3

Hz), 151.8 (d, *J* = 10.8 Hz), 136.4 (d, *J* = 3.2 Hz, 3C), 134.7 (d, *J* = 10.6 Hz, 6C), 133.3 (d, *J* = 2.6 Hz), 131.2 (d, *J* = 13.2 Hz, 6C), 129.7 (d, *J* = 84.1 Hz), 129.5 (d, *J* = 8.8 Hz, 2C), 125.4 (d, *J* = 8.1 Hz), 123.2 (d, *J* = 8.8 Hz), 121.0 (q, *J* = 321.4 Hz), 116.3 (d, *J* = 21.8 Hz, 2C), 115.8 (d, *J* = 89.5 Hz, 3C). **^{19}F NMR (565 MHz, $CDCl_3$)** δ -78.1, -110.2. **^{31}P NMR (243 MHz, $CDCl_3$)** δ 22.8. **IR (neat):** ν 3064, 1596, 1439, 1276, 1251, 1108, 1026, 751, 687, 724 cm^{-1}. **HRMS (ESI)** calculated for $C_{29}H_{22}FNP$ $[M\text{-}OTf]^+$: 434.1468, found: 434.1459.

(2-(4-Chlorophenyl)pyridin-4-yl)triphenylphosphonium trifluoromethanesulfonate

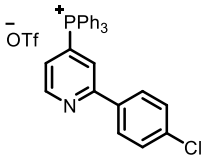

2.0 mmol scale, Et_3N was used as the base. After the purification procedure mentioned above, a white solid was obtained (0.71 g, 59% yield). **^{1}H NMR (400 MHz, $CDCl_3$)** δ 9.07 (app t, *J* = 5.1, 1H), 7.97 – 7.91 (m, 3H), 7.91 – 7.87 (m, 2H), 7.87 – 7.79 (m, 7H), 7.75 – 7.67 (m, 6H), 7.54 (ddd, *J* = 12.7, 5.0, 1.6 Hz, 1H), 7.46 – 7.41 (m, 2H). **^{13}C NMR (101 MHz, $CDCl_3$)** δ 159.1 (d, *J* = 10.7 Hz), 151.8 (d, *J* = 10.8 Hz), 137.1, 136.5 (d, *J* = 3.0 Hz, 3C), 135.5 (d, *J* = 1.5 Hz), 134.8 (d, *J* = 10.5 Hz, 6C), 131.2 (d, *J* = 13.2 Hz, 6C), 129.6 (d, *J* = 84.1 Hz), 129.3 (2C), 128.8 (2C), 125.7 (d, *J* = 8.3 Hz), 123.5 (d, *J* = 8.7 Hz), 122.9 (q, *J* = 327.5 Hz), 115.9 (d, *J* = 89.5 Hz, 3C).

These data are in agreement with those reported previously in the literature.[94]

(2-(4-Bromophenyl)pyridin-4-yl)triphenylphosphonium trifluoromethanesulfonate

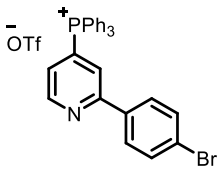

2.0 mmol scale, Et_3N was used as the base. After the purification procedure mentioned above, a white solid was obtained (0.75 g, 59% yield). **^{1}H NMR (600 MHz, $CDCl_3$)** δ 9.03 (app t, *J* = 5.1, 1H), 7.93 – 7.88 (m, 3H), 7.80 – 7.79 (m, 9H), 7.70 – 7.64 (m, 6H), 7.57 – 7.50 (m, 3H). **^{13}C NMR (151 MHz, $CDCl_3$)** δ 158.3 (d, *J* = 10.3 Hz), 151.9 (d, *J* = 10.8 Hz), 136.4 (d, *J* = 3.0 Hz, 3C)), 136.0 (d, *J* = 1.5 Hz) , 134.6 (d, *J* = 10.7 Hz, 6C), 132.4 (2C), 131.17 (d, *J* = 13.2 Hz, 6C), 129.8 (d, *J* = 84.0 Hz), 129.0 (2C), 125.8 (d, *J* = 7.9 Hz), 125.3, 123.3 (d, *J* = 8.6 Hz), 120.9 (q, *J* = 321.0 Hz), 115.8 (d, *J* = 89.5 Hz, 3C). **^{19}F NMR (565 MHz, $CDCl_3$)** δ -78.1. **^{31}P NMR (243 MHz, $CDCl_3$)** δ 22.8. **IR (neat):** ν 3060, 1583, 1438, 1256, 1107, 1028, 752, 723, 688 cm^{-1}. **HRMS (ESI)** calculated for $C_{29}H_{22}BrNP$ $[M\text{-}OTf]^+$: 494.0668, found: 494.0666.

Triphenyl(2-(p-tolyl)pyridin-4-yl)phosphonium trifluoromethanesulfonate

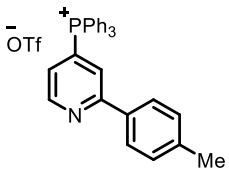

2.0 mmol scale, Et_3N was used as the base. After the purification procedure mentioned above, a white solid was obtained (0.85 g, 73% yield). **^{1}H NMR (600 MHz, $CDCl_3$)** δ 9.05 (app t, *J* = 5.1, 1H), 7.97 – 7.91 (m, 3H), 7.85 – 7.76 (m, 9H), 7.74 – 7.67 (m, 6H), 7.49 (ddd, *J* = 12.7, 5.0, 1.6 Hz, 1H), 7.28 (d, *J* = 8.0 Hz, 2H), 2.39 (s, 3H). **^{13}C NMR (151 MHz, $CDCl_3$)** δ 159.5 (d, *J* = 10.5 Hz), 151.9 (d, *J* = 10.6 Hz), 141.2, 136.5 (d, *J* = 3.0 Hz, 3C), 134.7 (d, *J* = 10.4 Hz, 6C), 134.3 (d, *J* = 1.5 Hz), 131.2 (d, *J* = 13.0 Hz, 6C), 130.1 (2C), 129.4 (d, *J* = 84.1 Hz), 127.2 (2C), 125.1 (d, *J* = 8.4 Hz), 123.1 (d, *J* = 8.5 Hz), 121.0 (q, *J* = 320.8 Hz), 115.9 (d, *J* = 89.1 Hz, 3C), 21.5.

These data are in agreement with those reported previously in the literature.[180]

(2-(4-Methoxyphenyl)pyridin-4-yl)triphenylphosphonium trifluoromethanesulfonate

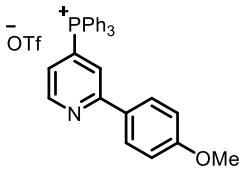

2.0 mmol scale, Et_3N was used as the base. After the purification procedure mentioned above, a white solid was obtained (0.66 g, 55% yield). **^{1}H NMR (400 MHz, $CDCl_3$)** δ 9.01 (app t, *J* = 5.3 Hz, 1H), 7.97 – 7.90 (m, 3H), 7.89 – 7.64 (m, 15H), 7.41 (dd, *J* = 12.8, 5.0 Hz, 1H), 7.01 – 6.95 (m, 2H), 3.84 (s, 3H). **^{13}C NMR (151 MHz, $CDCl_3$)** δ 162.0, 159.2 (d, *J* = 10.5 Hz), 151.7 (d, *J* = 10.7 Hz), 136.4 (d, *J* = 3.1 Hz, 3C), 134.7 (d, *J* = 10.6 Hz, 6C), 131.2 (d, *J* = 12.9 Hz, 6C), 129.2 (d, *J* = 1.4 Hz), 129.5 (d, *J* = 84.3 Hz), 128.9 (2C, 124.4 (d, *J* = 8.2 Hz), 122.7 (d, *J* = 8.7 Hz), 120.8 (q, *J* = 321.4 Hz), 116.0 (d, *J* = 89.5 Hz, 3C), 114.8 (2C), 55.6.

These data are in agreement with those reported previously in the literature.[94]

[2,2'-Bipyridin]-4-yltriphenylphosphonium trifluoromethanesulfonate

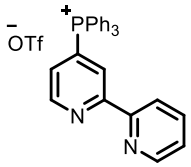

5.0 mmol scale, Et_3N was used as the base. After the purification procedure mentioned above, a white solid was obtained (2.69 g, 94% yield). **^{1}H NMR (400 MHz, $CDCl_3$)** δ 9.10 (app t, *J* = 5.0 Hz, 1H), 8.69 (dd, *J* = 14.0, 1.7 Hz, 1H), 8.63 – 8.57 (m, 1H), 8.53 (d, *J* = 8.0 Hz, 1H), 7.96 – 7.89 (m, 4H), 7.84 – 7.79 (m, 6H), 7.77 – 7.65 (m, 7H), 7.41 (ddd, *J* = 7.8, 4.8, 1.2 Hz, 1H). **^{13}C NMR (101 MHz, $CDCl_3$)** δ 157.4 (d, *J* = 10.1 Hz), 153.4 (d, *J* = 2.1 Hz), 151.7 (d, *J* = 10.5 Hz), 149.0, 138.2, 136.4 (d, *J* = 3.2 Hz, 3C), 134.8 (d, *J* = 10.6 Hz, 6C), 131.2 (d, *J* = 13.0 Hz, 6C), 130.0 (d, *J* = 84.21 Hz), 127.4 (d, *J* = 8.5 Hz), 125.4, 124.3 (d, *J* = 9.0 Hz), 122.4, 120.4 (q, *J* = 322.1 Hz), 116.0 (d, *J* = 89.5 Hz, 3C).

These data are in agreement with those reported previously in the literature.[93]

Triphenyl(2-(thiophen-3-yl)pyridin-4-yl)phosphonium trifluoromethanesulfonate

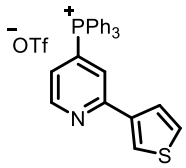

5.0 mmol scale, DBU was used as the base. After the purification procedure mentioned above, a white solid was obtained (2.03 g, 71% yield). **^{1}H NMR (600 MHz, $CDCl_3$)** δ 8.97 (app t, *J* = 5.1 Hz, 1H), 7.97 (dd, *J* = 3.0, 1.3 Hz, 1H), 7.95 – 7.91 (m, 3H), 7.80 (td, *J* = 7.9, 3.7 Hz, 6H), 7.72 – 7.65 (m, 7H), 7.53 (dd, *J* = 5.1, 1.3 Hz, 1H), 7.41 (dd, *J* = 5.0, 1.6 Hz, 1H), 7.38 – 7.37 (m, 1H). **^{13}C NMR (151 MHz, $CDCl_3$)** δ 155.4 (d, *J* = 10.8 Hz), 151.8 (d, *J* = 10.8 Hz), 139.9 (d, *J* = 1.6 Hz), 136.4 (d, *J* = 3.1 Hz, 3C), 134.6 (d, *J* = 10.4 Hz, 6C), 131.1 (d, *J* = 12.9 Hz, 6C), 129.3 (d, *J* = 83.8 Hz), 127.4, 126.6, 126.0, 124.8 (d, *J* = 8.0 Hz), 123.2 (d, *J* = 8.5 Hz), 121.2 (q, *J* = 321.8 Hz), 115.8 (d, *J* = 89.6 Hz, 3C).

These data are in agreement with those reported previously in the literature.[95]

(2-(Furan-2-yl)pyridin-4-yl)triphenylphosphonium trifluoromethanesulfonate

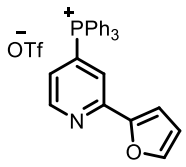

2.0 mmol scale, Et_3N was used as the base. After the purification procedure mentioned above, a light-yellow solid was obtained (0.45 g, 40% yield). **^{1}H NMR (600 MHz, $CDCl_3$)** δ 8.94 (app t, *J* = 5.0 Hz, 1H), 7.96 – 7.91 (m, 3H), 7.83– 7.80 (m, 6H), 7.76 – 7.71 (m, 1H), 7.75 – 7.65 (m, 6H), 7.51 (d, *J* = 1.7 Hz, 1H), 7.41 – 7.39 (m, 1H), 7.22 (d, *J* = 3.5 Hz, 1H), 6.55 (dd, *J* = 3.5, 1.8 Hz, 1H).**^{13}C NMR (151 MHz, $CDCl_3$)** δ 152.0 (d, *J* = 10.6 Hz), 151.6 (d, *J* = 1.6 Hz), 151.0 (d, *J* = 10.9 Hz), 145.2, 136.5 (d, *J* = 3.1 Hz, 3C), 134.6 (d, *J* = 10.4 Hz, 6C), 131.2 (d, *J* = 13.3 Hz, 6C), 129.5 (d, *J* = 84.4 Hz), 124.9 (d, *J* = 8.2 Hz), 121.1 (d, *J* = 9.2 Hz), 121.0 (q, *J* = 321.0 Hz), 115.8 (d, *J* = 89.6 Hz, 3C), 113.1, 112.3. **^{19}F NMR (565 MHz, $CDCl_3$)** δ -78.1. **^{31}P NMR (243 MHz, $CDCl_3$)** δ 22.7. **IR (neat):** ν 3068, 1597, 1487, 1438, 1259, 1153, 1106, 1026, 753, 690 cm^{-1}. **HRMS (ESI)** calculated for $C_{27}H_{21}NOP$ $[M\text{-}OTf]^+$: 406.1355,

found: 406.1353.

(2-Benzylpyridin-4-yl)triphenylphosphonium trifluoromethanesulfonate

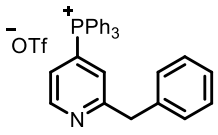

5.0 mmol scale, Et_3N was used as the base. After the purification procedure mentioned above, a white solid was obtained (2.12 g, 73% yield). **^{1}H NMR (600 MHz, $CDCl_3$)** δ 8.95 (app t, *J* = 5.1 Hz, 1H), 7.94 – 7.88 (m, 3H), 7.78 – 7.75 (m, 6H), 7.58 – 7.56 (m, 6H), 7.41 (ddd, *J* = 12.7, 5.1, 1.7 Hz, 1H), 7.30 – 7.16 (m, 6H), 4.29 (s, 2H). **^{13}C NMR (151 MHz, $CDCl_3$)** δ 164.2 (d, *J* = 9.7 Hz), 151.4 (d, *J* = 10.6 Hz), 137.9, 136.3 (d, *J* = 3.1 Hz, 3C), 134.5 (d, *J* = 10.5 Hz, 6C), 131.1 (d, *J* = 13.2 Hz, 6C), 129.3 (2C), 129.0 (2C), 128.9 (d, *J* = 83.5 Hz), 127.1, 126.5 (d, *J* = 8.5 Hz), 124.7 (d, *J* = 8.0 Hz), 121.0 (q, *J* = 320.7 Hz), 115.8 (d, *J* = 89.6 Hz, 3C), 44.6. **^{19}F NMR (565 MHz, $CDCl_3$)** δ -78.1. **^{31}P NMR (243 MHz, $CDCl_3$)** δ 22.4. **IR (neat):** ν 3088, 1580, 1438, 1261, 1106, 1026, 724, 692 cm^{-1}. **HRMS (ESI)** calculated for $C_{30}H_{25}NP$ $[M\text{-}OTf]^+$: 430.1719, found: 430.1720.

(2-(4-Chlorobenzyl)pyridin-4-yl)triphenylphosphonium trifluoromethanesulfonate

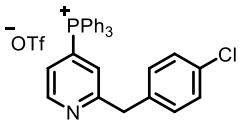

5.0 mmol scale, was used as the base. After the purification procedure mentioned above, a white solid was obtained (2.19 g, 72% yield). **^{1}H NMR (600 MHz, $CDCl_3$)** δ 8.90 (app t, *J* = 5.2 Hz, 1H), 7.91 – 7.85 (m, 3H), 7.76 – 7.72 (m, 6H), 7.60 – 7.54 (m, 6H), 7.39 (ddd, *J* = 12.8, 5.2, 1.7 Hz, 1H), 7.21 – 7.12 (m, 5H), 4.24 (s, 2H). **^{13}C NMR (151 MHz, $CDCl_3$)** δ 163.7 (d, *J* = 10.0 Hz), 151.3 (d, *J* = 10.6 Hz), 136.5, 136.2 (d, *J* = 3.1 Hz, 3C), 134.6 (d, *J* = 10.5 Hz, 6C), 132.8, 131.1 (d, *J* = 13.2 Hz, 6C), 130.9 (2C), 129.1 (d, *J* = 83.9 Hz), 129.0 (2C), 126.6 (d, *J* = 8.5 Hz), 124.8 (d, *J* = 8.0 Hz), 121.0 (d, *J* = 321.2 Hz), 115.8 (d, *J* = 89.2 Hz, 3C), 43.7. **^{19}F NMR (565 MHz, $CDCl_3$)** δ -78.1. **^{31}P NMR (243 MHz, $CDCl_3$)** δ 22.4. **IR (neat):** ν 3063, 1578, 1438, 1262, 1147, 1107, 1027, 753, 723, 688 cm^{-1}. **HRMS (ESI)** calculated for $C_{30}H_{24}ClNP$ $[M\text{-}OTf]^+$: 464.1329, found: 464.1327.

(2-Methylpyridin-4-yl)triphenylphosphonium trifluoromethanesulfonate

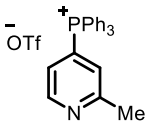

5.0 mmol scale, Et_3N was used as the base. After the purification procedure mentioned above, a white solid was obtained (1.72 g, 69% yield) **^{1}H NMR (400 MHz, $CDCl_3$)** δ 8.87 (app t, *J* = 5.3 Hz, 1H), 7.97 – 7.87 (m, 3H), 7.82 – 7.77 (m, 6H), 7.68 – 7.61 (m, 6H), 7.42 – 7.30 (m, 2H), 2.68 (s, 3H). **^{13}C NMR (151 MHz, $CDCl_3$)** δ 161.7 (d, *J* = 10.1 Hz), 151.2 (d, *J* = 10.8 Hz), 136.3 (d, *J* = 3.1 Hz, 3C), 134.6 (d, *J* = 10.4 Hz, 6C), 131.2 (d, *J* = 13.2 Hz, 6C), 128.7 (d, *J* = 83.6 Hz), 126.7 (d, *J* = 7.9 Hz), 124.3 (d, *J* = 8.0 Hz), 121.0 (q, *J* = 320.9 Hz), 116.0 (d, *J* = 89.4 Hz, 3C), 25.0.

These data are in agreement with those reported previously in the literature.[94]

Triphenyl(pyridin-4-yl)phosphonium trifluoromethanesulfonate

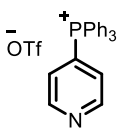

5.0 mmol scale, Et_3N was used as the base. After the purification procedure mentioned above, a white solid was obtained (1.69 g, 69% yield). **^{1}H NMR (600 MHz, $CDCl_3$)** δ 9.01 (app t, *J* = 5.5 Hz, 2H), 7.95 – 7.89 (m, 3H), 7.81 – 7.77 (m, 6H), 7.68 – 7.63 (m, 6H), 7.60 (ddd, *J* = 13.1, 4.4, 1.7 Hz, 2H). **^{13}C NMR (151 MHz, $CDCl_3$)** δ 151.9 (d, *J* = 9.8 Hz, 2C), 136.4 (d, *J* = 3.0 Hz, 3C), 134.7 (d, *J* = 10.4 Hz, 6C), 131.2 (d, *J* = 13.0 Hz, 6C), 128.6 (d, *J* = 84.2 Hz), 127.4 (d, *J* = 7.9 Hz, 2C), 120.7 (q, *J* = 320.12 Hz), 115.8 (d, *J* = 89.6 Hz, 3C).

These data are in agreement with those reported previously in the literature.[181]

(2-(2-Methylbenzofuro[2,3-b]pyridin-8-yl)pyridin-4-yl)triphenylphosphonium trifluoromethanesulfonate

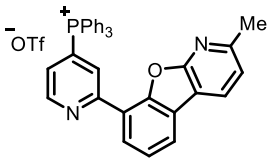

1.5 mmol scale, Et_3N was used as the base. After the purification procedure mentioned above, a white solid or light-yellow solid was obtained (0.55 g, 55% yield). **^{1}H NMR (600 MHz, $CDCl_3$)** δ 9.18 (app t, *J* = 5.2, 1H), 8.80 – 8.77 (m, 1H), 8.41 (dd, *J* = 7.8, 1.3 Hz, 1H), 8.17 (d, *J* = 7.7 Hz, 1H), 7.98 (dd, *J* = 7.6, 1.3 Hz, 1H), 7.97 – 7.93 (m, 3H), 7.90 – 7.87 (m, 6H), 7.81 – 7.74 (m, 6H), 7.68 (ddd, *J* = 12.4, 5.0, 1.7 Hz, 1H), 7.49 (t, *J* = 7.7 Hz, 1H), 7.25 (d, *J* = 7.5 Hz, 1H), 2.73 (s, 3H). **^{13}C NMR (151 MHz, $CDCl_3$)** δ 162.7, 157.1, 155.2 (d, *J* = 11.3 Hz), 152.0 (d, *J* = 10.8 Hz), 151.8, 136.4 (d, *J* = 3.0 Hz, 3C), 134.7 (d, *J* = 10.7 Hz, 6C), 131.4 (d, *J* = 13.2 Hz, 6C), 130.3, 129.5 (d, *J* = 84.1 Hz), 127.8, 127.19 (d, *J* = 9.2 Hz), 126.0 (d, *J* = 8.1 Hz), 124.2, 124.0, 123.4, 122.0, 120.9 (q, *J* = 319.5 Hz), 119.7, 116.0 (d, *J* = 89.5 Hz, 3C), 113.3, 24.8. **^{19}F NMR (565 MHz, $CDCl_3$)** δ -78.1. **^{31}P NMR (243 MHz, $CDCl_3$)** δ 22.6. **IR (neat):** ν 3062, 1576, 1484, 1439, 1386, 1263, 1149, 1109, 1209, 728, 689 cm^{-1}. **HRMS (ESI)** calculated for $C_{35}H_{26}N_2OP$ $[M\text{-}OTf]^+$: 521.1777, found: 521.1772.

(2-(4-((4-(tert-butoxycarbonyl)-2-methylpiperazin-1-yl)methyl)-2-fluorophenyl)pyridin-4-yl)triphenylphosphonium trifluoromethanesulfonate

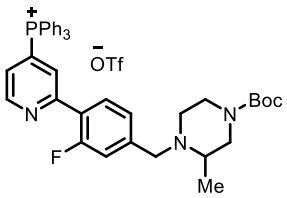

1.0 mmol scale, DBU was used as the base. After the purification procedure mentioned above, a white solid was obtained (0.60 g, 75% yield).**^{1}H NMR (600 MHz, $CDCl_3$)** δ 9.11 (app t, *J* = 5.2 Hz, 1H), 8.06 (t, *J* = 8.1 Hz, 1H), 7.94 – 7.89 (m, 4H), 7.81 – 7.78 (m, 6H), 7.70 – 7.64 (m, 6H), 7.58 (ddd, *J* = 12.7, 5.1, 1.6 Hz, 1H), 7.25 (d, *J* = 7.4 Hz, 1H), 7.14 (d, *J* = 12.5 Hz, 1H), 3.96 (d, *J* = 14.1 Hz, 1H), 3.61 (dd, *J* = 13.1, 4.0 Hz, 2H), 3.24 (d, *J* = 14.1 Hz, 1H), 3.08 (t, *J* = 11.3 Hz, 1H), 2.87 (s, 1H), 2.61 (dt, *J* = 12.2, 3.8 Hz, 1H), 2.45 (s, 1H), 2.16 – 2.05 (m, 1H), 1.43 (s, 9H), 1.07 (d, *J* = 6.2 Hz, 3H). **^{13}C NMR (151 MHz, $CDCl_3$)** δ 160.5 (d, *J* = 250.5 Hz), 154.8 (d, *J* = 10.8 Hz), 154.5, 151.8 (d, *J* = 10.8 Hz), 136.2 (d, *J* = 3.2 Hz, 3C), 134.5 (d, *J* = 10.2 Hz), 134.4 (d, *J* = 10.6 Hz, 6C), 131.0 (d, *J* = 13.0 Hz, 6C), 130.7, 130.5 (d, *J* = 12.8 Hz), 128.9 (d, *J* = 84.2 Hz), 126.9 (dd, *J* = 12.2, 9.2 Hz, 2C overlapped), 125.5 (d, *J* = 8.0 Hz), 125.2, 123.5 (d, *J* = 9.9 Hz), 120.7 (q, *J* = 321.1 Hz), 116.3 (d, *J* = 23.3 Hz), 115.6 (d, *J* = 89.6 Hz, 3C), 79.5, 57.0, 54.9, 50.2, 44.1, 28.2 (3C), 15.1. **^{19}F NMR (565 MHz, $CDCl_3$)** δ -78.1, -117.7. **^{31}P NMR (243 MHz, $CDCl_3$)** δ 22.7. **IR (neat):** 2973, 2929, 1684, 1578, 1426, 1371, 1262, 1146, 1109, 1029, 873, 725 cm^{-1}. **HRMS (ESI)** calculated for $C_{40}H_{42}FN_3O_2P$ $[M\text{-}OTf]^+$: 646.2993, found: 646.3005.

(2-(Bis(4-(methoxycarbonyl)phenyl)methyl)pyridin-4-yl)triphenylphosphonium trifluoromethanesulfonate

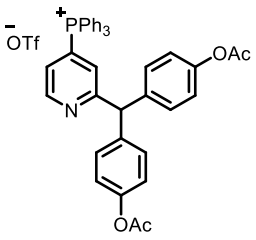

2.0 mmol scale, Et_3N was used as the base. After the purification procedure mentioned above, a white solid was obtained (0.57 g, 37% yield).**^{1}H NMR (400 MHz, $CDCl_3$)** δ 8.94 (app t, *J* = 5.1 Hz, 1H), 7.88 – 7.82 (m, 3H), 7.74 – 7.69 (m, 6H), 7.59 – 7.51 (m, 6H), 7.48 – 7.41 (m, 1H), 7.22 (d, *J* = 13.7 Hz, 1H), 7.13 – 7.11 (m, 4H), 6.99 – 6.92 (m, 4H), 5.72 (s, 1H), 2.25 (s, 6H). **^{13}C NMR (101 MHz, $CDCl_3$)** δ 169.5 (2C), 165.1 (d, *J* = 9.5 Hz),

152.3 (d, *J* = 10.4 Hz), 150.3 (2C), 138.7 (2C), 136.3 (d, *J* = 3.1 Hz, 3C), 134.6 (d, *J* = 10.5 Hz, 6C), 131.2 (d, *J* = 12.9 Hz, 6C), 130.4 (4C), 129.1 (d, *J* = 83.8 Hz), 127.6 (d, *J* = 8.8 Hz), 125.3 (d, *J* = 7.8 Hz), 122.0 (4C), 120.7 (q, *J* = 322.5 Hz), 112.1 (d, *J* = 89.7 Hz, 3C), 55.1, 21.3.

These data are in agreement with those reported previously in the literature. [182]

2) Synthesis of olefins

(*S*)-1-Methyl-6-methylene-4-(prop-1-en-2-yl)cyclohex-1-ene

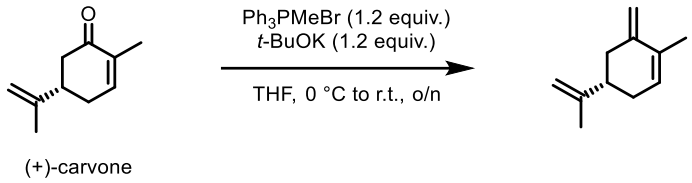

At 0 °C, a dry round-bottom flask under argon was charged with methyltriphenylphosphonium bromide (2.1 g, 6 mmol, 1.2 equiv.) followed by potassium *tert*-butoxide (6 mL, 6 mmol, 1.2 equiv., 1M in THF). The mixture was stirred for 1 hour before (+)-carvone (0.78 mL, 5 mmol, 1 equiv.) was added. The resulting mixture was stirred at room temperature overnight. Upon completion, the reaction was diluted with pentane and filtered over silica to remove the precipitate. Purification by flash column chromatography (100% pentane) afforded the corresponding diene as a colorless oil (0.54 g, 73% yield).

^{1}H NMR (600 MHz, $CDCl_3$) δ 5.70 (s, 1H), 4.90 (s, 1H), 4.79 (s, 1H), 4.74 (s, 1H), 4.73 (s, 1H), 2.53 – 2.42 (m, 1H), 2.35 – 2.18 (m, 3H), 2.13 – 2.03 (m, 1H), 1.82 (s, 3H), 1.74 (s, 3H). **^{13}C NMR (101 MHz, $CDCl_3$)** δ 149.3, 145.0, 132.6, 127.8, 109.1, 108.4, 42.3, 37.5, 31.9, 20.8, 19.4.

These data are in agreement with those reported previously in the literature.[183]

1-Butylcyclohexa-1,3-diene

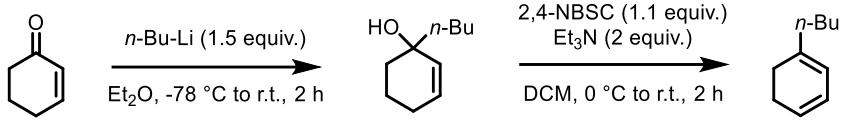

A dry round-bottom flask under argon was charged with cyclohex-2-en-1-one (0.97 mL, 10 mmol, 1 equiv.) and dry Et_2O (20 mL). The mixture was cooled to -78 °C before *n*-BuLi (6 mL, 15 mmol, 1.5 equiv., 2.5M) was added dropwise. The mixture was stirred for 10 minutes at -78 °C and 2 hours at room temperature. Then, the reaction was quenched at 0 °C with a saturated solution of ammonium chloride. The aqueous layer was extracted with Et_2O. The gathered organic layer was washed with brine, dried over MgSO4, filtered, evaporated and purified by flash column chromatography to afford the tertiary alcohol.

A dry round bottom flask under argon was charged with the intermediate (5 mmol, 1 equiv.) and DCM (20 mL), then cooled to 0 °C. Triethylamine (1.4 mL, 10 mmol, 2 equiv.) was added followed by 2,4-dinitrobenzenesulfonyl chloride (2,4-NBSC, 1.3 g, 5.5 mmol, 1.1 equiv.). The reaction was warmed to room temperature and allowed to stir for 2 hours. Upon completion, the mixture was diluted with pentane and filtered over celite. The organic layer was washed thoroughly with water

and brine, dried over $MgSO_4$, filtered, evaporated. Purification by flash column chromatography (100% pentane) afforded the corresponding diene as a colorless oil (0.34 g, 25% yield over the two steps).

^{1}H NMR (600 MHz, $CDCl_3$) δ 5.92 – 5.87 (m, 1H), 5.71 – 5.64 (m, 2H), 2.22 – 2.06 (m, 6H), 1.49 – 1.22 (m, 4H), 0.97 – 0.88 (m, 3H). **^{13}C NMR (101 MHz, $CDCl_3$)** δ 140.4, 124.9, 123.5, 118.5, 37.2, 29.9, 26.6, 23.1, 22.6, 14.1.

These data are in agreement with those reported previously in the literature.[184]

Cyclohexa-1,5-dien-1-yl trifluoromethanesulfonate

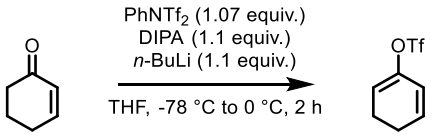

A dry round-bottom falsk equipped with a dropping funnel, under argon, was charged with diisopropylamine (1.5 mL, 11 mmol, 1.1 equiv.) and THF (23 mL). The mixture was cooled to 0 °C before addition of *n*-BuLi (4.4 mL, 11 mmol, 1.1 equiv. 2.5 M). The mixture was stirred for 5 minutes. Then, cyclohexanone (1.0 mL, 10 mmol, 1 equiv.) in THF (15 mL) was added dropwise at -78 °C. The mixture was stirred at this temperature for 30 minutes before the addition of N-Phenyl-bis(trifluoromethanesulfonimide) (3.9 g, 11 mmol, 1.07 equiv.) in THF (23 mL). The temperature was raised to 0 °C and the reaction was stirred for 2 h. Upon completion, all volatiles were removed *in vacuo*. The crude mixture was partitioned between Et_2O and H_2O. The aqueous layer was extracted with Et_2O (3 x 10 mL). The gathered organic layers were washed with brine, dried over $MgSO_4$, filtered and evaporated. Purification by flash column chromatography (100% pentane) afforded the corresponding diene as a colorless oil (1.20 g, 53% yield).

^{1}H NMR (600 MHz, $CDCl_3$) δ 6.01 (dt, *J* = 10.1, 4.3 Hz, 1H), 5.82 (dq, *J* = 10.1, 2.0 Hz, 1H), 5.68 (td, *J* = 4.7, 2.1 Hz, 1H), 2.42 – 2.36 (m, 2H), 2.28 – 2.22 (m, 2H). **^{13}C NMR (101 MHz, $CDCl_3$)** δ 146.1, 131.7, 121.0, 118.7 (q, *J* = 320.2 Hz), 114.8, 21.7, 21.5.

These data are in agreement with those reported previously in the literature.[185]

2-Butylcyclohexa-1,3-diene

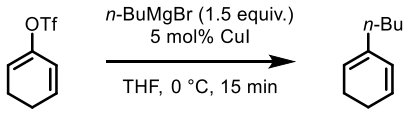

A dry Schlenk tube under argon was charged with CuI (10 mg, 0.05 mmol, 0.05 equiv.) and cyclohexa-1,5-dien-1-yl trifluoromethanesulfonate (0.2 g, 1.0 mmol, 1.0 equiv.) in THF (10 mL). *n*-Butylmagnesium chloride (0.8 mL, 1.5 mmol, 1.5 equiv., 2 M) was added at 0 °C and the mixture was stirred for 15 minutes. The reaction was quenched with the addition of a saturated solution of NH_4Cl (10 mL) and the aqueous layer was extracted with Et_2O (3 x 5 mL). The gathered organic layers were washed with brine, dried over $MgSO_4$, filtered and evaporated. Purification by flash column chromatography (100% pentane) afforded the corresponding diene as a colorless oil (58 mg, 43% yield).

^{1}H NMR (600 MHz, $CDCl_3$) δ 5.82 (s, 2H), 5.46 (s, 1H), 2.14 – 2.05 (m, 4H), 2.01 (t, *J* = 7.5 Hz, 2H), 1.41 – 1.35 (m, 2H), 1.33 – 1.28 (m, 2H), 0.90 (t, *J* = 7.3 Hz, 3H). **^{13}C NMR (101 MHz, $CDCl_3$)** δ 136.2, 127.5, 126.7, 120.0, 35.4, 30.8, 22.6, 22.5, 22.4, 14.1

These data are in agreement with those reported previously in the literature.[186]

Ethyl 3-(cyclohexa-1,5-dien-1-yl)propanoate

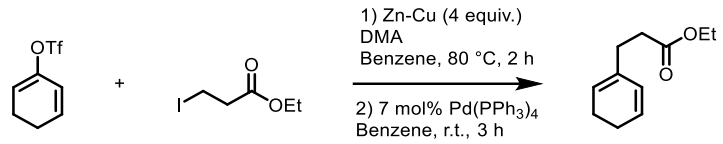

A dry Schlenk tube under argon was charged with Zn-Cu (0.4 g, 5.6 mmol, 4.0 equiv., prepared according to the procedure reported in *J. Org. Chem.* **1978**, *43*, 3255–3266), benzene (4 mL), DMA (0.5 mL) and ethyl 3-iodopropanoate (0.6 g, 2.8 mmol, 2.0 equiv.). The mixture was stirred for 2 h at 80 °C. Then, the mixture was cooled to room temperature and cyclohexa-1,5-dien-1-yl trifluoromethanesulfonate (0.3 g, 1.4 mmol, 1.0 equiv.) in benzene (10 mL) was added, followed by $Pd(PPh_3)_4$ (0.1 g, 0.1 mmol, 0.07 equiv.). The mixture was further stirred 3 h at room temperature. Upon completion, the reaction was quenched by addition of triethylamine (1 mL). The corresponding mixture was filtered over a short pad of celite, and all volatiles were removed *in vacuo*. Purification by flash column chromatography (pentane/EtOAc: 98/2) afforded the corresponding diene as a colorless oil (0.20 g, 79% yield).

^{1}H NMR (600 MHz, $CDCl_3$) δ 5.86 – 5.78 (m, 2H), 5.50 (s, 1H), 4.13 (q, *J* = 7.2 Hz, 2H), 2.42 – 2.38 (m, 2H), 2.36 – 2.32 (m, 2H), 2.14 – 2.06 (m, 4H), 1.25 (t, *J* = 7.1 Hz, 3H). **^{13}C NMR (101 MHz, $CDCl_3$)** δ 173.4, 134.4, 127.3, 126.8, 120.8, 60.4, 33.6, 30.8, 22.4 (2C).

These data are in agreement with those reported previously in the literature.[187]

(*S*)-1-Methyl-6-methylene-4-(prop-1-en-2-yl)cyclohex-1-ene

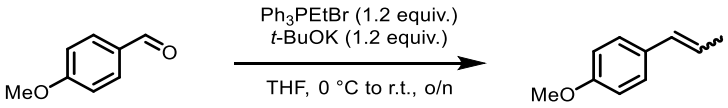

At 0 °C, a dry round-bottom flask under argon was charged with ethylltriphenylphosphonium bromide (0.9 g, 2.4 mmol, 1.2 equiv.) followed by potassium *tert*-butoxide (2.4 mL, 2.4 mmol, 1.2 equiv., 1 M in THF). The mixture was stirred for 1 hour before *para*-methoxybenzaldehyde (0.27 mL, 2.0 mmol, 1.0 equiv.) was added. The resulting mixture was stirred at room temperature overnight. Upon completion, the reaction was diluted with pentane and filtered over silica to remove the precipitate. Purification by flash column chromatography (100% pentane) afforded the corresponding styrene as a colorless oil (0.30 g, quantitative, 1.7:1 Z/E).

^{1}H NMR (600 MHz, $CDCl_3$) δ 7.28 – 7.23 (m, 2H, *maj + min*), 6.90 – 6.81 (m, 2H, *maj + min*), 6.40 – 6.32 (m, 1H, *maj + min*), 6.09 (dq, *J* = 15.8, 6.6 Hz, 0.3H, *min*), 5.70 (dq, *J* = 11.6, 7.2 Hz, 0.6H, *maj*), 3.81 (s, 1.9H, *maj*), 3.79 (s, 1.1H, *min*), 1.89 (dd, *J* = 7.3, 1.9 Hz, 1.9H, *maj*), 1.86 (dd, *J* = 6.7, 1.7 Hz, 1.1H, *min*). **^{13}C NMR (151 MHz, $CDCl_3$)** δ 158.7 (min), 158.2 (maj), 131.0 (min), 130.5 (maj), 130.1 (2C, maj + min), 129.4 (min), 127.0 (maj), 125.2 (maj), 123.6 (min), 114.0 (2C, min), 113.7 (2C,

maj), 55.4 (min), 55.4 (maj), 18.5 (min), 14.7 (maj).

These data are in agreement with those reported previously in the literature.[188]

(1S,3R,7S,8S,8aR)-8-(2-((2R,4R)-4-((*tert*-Butyldimethylsilyl)oxy)-6-oxotetrahydro-2H-pyran-2-yl)ethyl)-3,7-dimethyl-1,2,3,7,8,8a-hexahydronaphthalen-1-yl 2,2-dimethylbutanoate

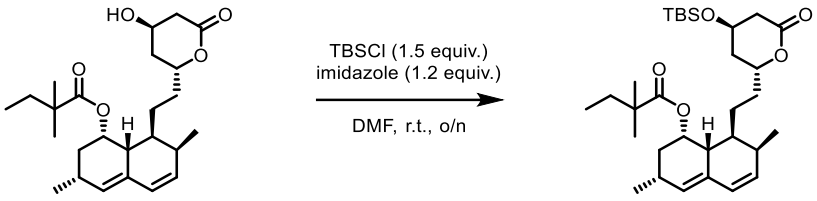

simvastatin

A dry round-bottom flask under argon was charged with simvastatin (0.4 g, 1.0 mmol, 1.0 equiv.), anhydrous DMF (10 mL), imidazole (0.082 g, 1.2 mmol, 1.2 equiv.) and TBSCl (0.2 g, 1.5 mmol, 1.5 equiv.). The mixture was stirred at room temperature overnight. The reaction was quenched with a saturated solution of $NaHCO_3$. The two layers were separated and the aqueous layer was extracted three times with DCM. The gathered organic layers were washed with brine, dried over $MgSO_4$, filtered and evaporated. Purification by flash column chromatography (pentane/EtOAc: 80/20) gave the corresponding diene as a colorless thick paste (0.41 g, 77% yield).

^{1}H NMR (600 MHz, $CDCl_3$) δ 5.99 (d, *J* = 9.5 Hz, 1H), 5.78 (dd, *J* = 9.5, 6.2 Hz, 1H), 5.51 (s, 1H), 5.33 (q, *J* = 3.3 Hz, 1H), 4.61 – 4.55 (m, 1H), 4.29 (quint., *J* = 3.6 Hz, 1H), 2.63 – 2.53 (m, 2H), 2.47 – 2.40 (m, 1H), 2.36 (sext. *J* = 6.5 Hz, 1H), 2.26 (dd, *J* = 12.2, 2.4 Hz, 1H), 2.00 (dd, *J* = 14.8, 3.2 Hz, 1H), 1.93 (ddd, *J* = 15.1, 8.2, 2.4 Hz, 1H), 1.88 – 1.79 (m, 2H), 1.69 (tt, *J* = 12.0, 4.2 Hz, 1H), 1.64 – 1.50 (m, 4H), 1.50 – 1.35 (m, 2H), 1.31 – 1.23 (m, 1H), 1.12 (d, *J* = 5.2 Hz, 6H), 1.08 (d, *J* = 7.3 Hz, 3H), 0.91 – 0.86 (m, 11H), 0.82 (t, *J* = 7.4 Hz, 3H), 0.07 (s, 3H), 0.06 (s, 3H). **^{13}C NMR (101 MHz, $CDCl_3$)** δ 177.7, 170.4, 133.0, 131.7, 129.8, 128.5, 76.6, 68.1, 63.7, 43.1, 39.4, 37.6, 37.0, 37.0, 33.4, 33.1, 32.9, 30.8, 27.4, 25.8 (3C), 25.8, 24.9, 24.8, 24.4, 23.1, 14.0, 9.4, -4.7, -4.8.

These data are in agreement with those reported previously in the literature.[189]

***tert*-Butyl(((8R,9S,10R,13S,14S,17S)-10,13-dimethyl-6,7,8,9,10,11,12,13,14,15,16,17-dodecahydro-1H-cyclopenta[a]phenanthren-17-yl)oxy)dimethylsilane**

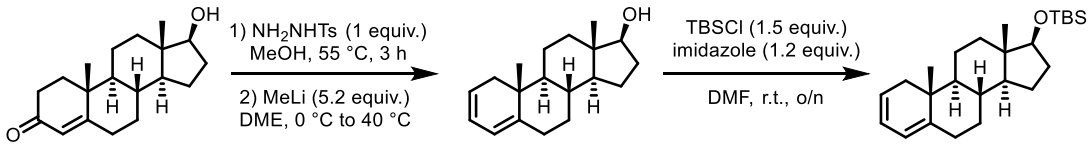

testosterone

A dry round-bottom flask under argon was charged with testosterone (0.7 g, 2.4 mmol, 1.0 equiv.) followed by tosylhydrazide (0.5 g, 2.4 mmol, 1.0 equiv.) in MeOH (3.6 mL), and the mixture was stirred at 55 °C for 3 h. Upon completion, the mixture was cooled to r.t. and quenched by addition of ice-water (10 mL). The aqueous layer was extracted with Et_2O (3 x 10 mL), and the gathered organic layers were washed with brine, dried over $MgSO_4$, filtered and evaporated. The crude product was transferred into a dry round bottom flask under argon with DME (39 mL). The mixture

was cooled to 0 °C before the dropwise addition of MeLi (7.5 mL, 12.4 mmol, 5.2 equiv., 1.6 M). Then, the reaction was stirred at 40 °C for 30 min. After full conversion of the hydrazone, the reaction was quenched at 0 °C with water. The aqueous layer was extracted with Et_2O (3 x 10 mL), and the gathered organic layers were washed with brine, dried over $MgSO_4$, filtered and evaporated. Purification by flash column chromatography afforded the corresponding diene as a colorless oil (0.34 g, 52% yield over the two steps).

A dry round-bottom flask under argon was charged with diene intermediate (0.34 g, 1.2 mmol, 1.0 equiv.), anhydrous DMF (34 mL), imidazole (0.1 g, 1.2 mmol, 1.2 equiv.) and TBSCl (0.3 g, 1.8 mmol, 1.5 equiv.). The mixture was stirred at room temperature overnight. The reaction was quenched with a saturated solution of $NaHCO_3$. The two layers were separated and the aqueous layer was extracted three times with DCM. The gathered organic layers were washed with brine, dried over $MgSO_4$, filtered and evaporated. Purification by flash column chromatography (Pentane 100%) gave the corresponding TBS-protected diene as a white solid (0.27 g, 59% yield).

^{1}H NMR (600 MHz, $CDCl_3$) δ 5.79 – 5.73 (m, 1H), 5.64 – 5.59 (m, 1H), 5.51 (dd, *J* = 5.2, 2.3 Hz, 1H), 3.55 (t, *J* = 8.4 Hz, 1H), 2.31 – 2.20 (m, 2H), 2.18 – 2.13 (m, 1H), 2.04 (d, *J* = 16.9 Hz, 1H), 1.91 – 1.83 (m, 1H), 1.75 (dt, *J* = 12.5, 3.6 Hz, 1H), 1.73 – 1.69 (m, 1H), 1.61 – 1.55 (m, 1H), 1.50 – 1.33 (m, 4H), 1.27 (qd, *J* = 12.3, 6.0 Hz, 1H), 1.02 – 0.86 (m, 16H), 0.73 (s, 3H), 0.01 (s, 3H), 0.00 (s, 3H). **^{13}C NMR (151 MHz, $CDCl_3$)** δ 146.4, 123.3, 123.1, 117.2, 82.0, 55.5, 50.5, 43.4, 38.4, 37.7, 37.4, 36.6, 31.5, 31.3, 31.1, 26.0 (3C), 23.8, 21.4, 18.3, 17.0, 11.4, -4.3, -4.6. **IR (neat):** ν 2927, 1464, 1364, 1249, 1137, 1089, 832, 777, 690 cm^{-1}. **HRMS (ESI)** calculated for $C_{25}H_{42}OSi$ $[M]^+$:386.3005, found: 386.2999.

1-Methyl-3-vinyl-1H-indole

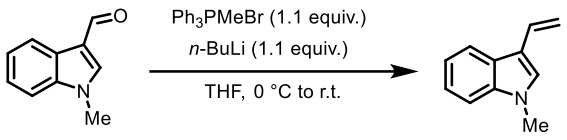

A suspension of methyl triphenylphosphonium bromide (3.21 g, 9.0 mmol, 1.1 equiv.) in 45 mL of anhydrous THF under an argon atmosphere was cooled to 0 °C on an ice bath. Then *n*-BuLi (3.6 mL, 9.0 mmol, 1.1 equiv.) was added dropwise. The reaction mixture was stirred for 20 minutes at 0 °C. Then, *N*-methyl-3-formylindole (1.34 g, 8.4 mmol, 1.0 equiv. in 10.5 mL of anhydrous THF) was added dropwise. The ice bath was removed, and the reaction mixture was stirred at room temperature overnight. After this time, the reaction was quenched with 10 mL saturated ammonium chloride solution and extracted with diethyl ether (3 x 8 mL). The collected organic phase was washed with brine and dried over $MgSO_4$. The mixture was concentrated *in vacuo.* Purification by flash column chromatography (pentane/EtOAc: 94/6) afforded 1-methyl-3-vinyl-1H-indole as a pale-yellow oil (1.09 g, 83% yield).

^{1}H NMR (400 MHz, $CDCl_3$) δ 7.87 (d, *J* = 7.9 Hz, 1H), 7.23 (m, 3H), 7.11 (s, 1H), 6.87 (dd, *J* = 17.8, 11.2 Hz, 1H), 5.66 (dd, *J* = 17.8, 1.5 Hz, 1H), 5.12 (dd, *J* = 11.2, 1.4 Hz, 1H), 3.75 (s, 3H). **^{13}C NMR (100 MHz, $CDCl_3$)** δ 129.3, 128.2, 126.1, 122.0, 120.2, 119.9, 114.3, 109.9, 109.4, 32.8.

These data are in agreement with those reported previously in the literature.[190]

5.2.2 General procedure and characterization data of products

1) General procedures for the coupling reactions

General procedure **A** (under condition A)

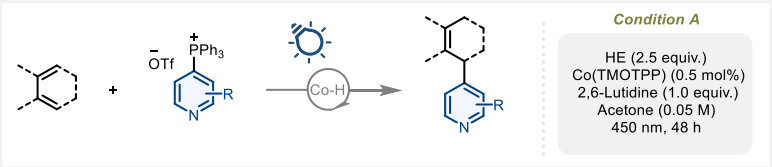

In an oven-dried 4 mL vial equipped with a magnetic stirring bar were added the phosphonium salt (0.20 mmol, 2.0 equiv.), Hantzsch ester (63.33 mg, 0.25 mmol, 2.5 equiv.), and Co(TMOTPP) (0.52 mg, 0.5 µmol, 0.5 mol%). A plastic cap with rubber septum was used to close the vial and the system was degassed with a stream of argon for 15 minutes. Acetone (2.0 mL, 0.05 M) was added followed by the diene or styrene (0.10 mmol, 1.0 equiv.) and 2,6-lutidine (11.6 µL, 0.10 mmol, 1.0 equiv.). The vial was then placed in the PhotoRedOx Box (see Materials and Methods for more details about the photochemical setup) and irradiated at 450 nm for 48 hours. The crude was then filtered on a plug of silica (EtOAc as eluent) and concentrated under reduced pressure.

General procedure **B** (under condition B)

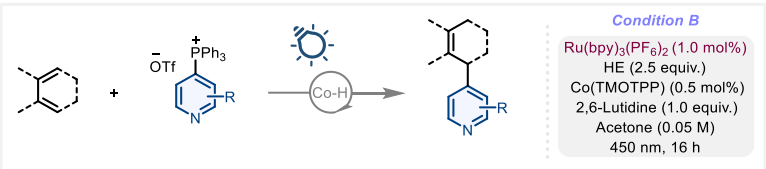

In an oven-dried 4 mL vial equipped with a magnetic stirring bar were added the phosphonium salt (0.20 mmol, 2.0 equiv.), Hantzsch ester (63.33 mg, 0.25 mmol, 2.5 equiv.), Co(TMOTPP) (0.52 mg, 0.5 µmol, 0.5 mol%) and $Ru(bpy)_3(PF_6)_2$ (0.86 mg, 1.0 µmol, 1.0 mol%,). A plastic cap with rubber septum was used to close the vial and system was degassed with a stream of argon for 15 minutes. Acetone (2.0 mL, 0.05 M) was added followed by the diene or styrene (0.10 mmol, 1.0 equiv.) and 2,6-lutidine (11.6 µL, 0.10 mmol, 1.0 equiv.). The vial was then placed in the PhotoRedOx Box (see Materials and Methods for more details about the photochemical setup) and irradiated at 450 nm for 16 hours (unless otherwise stated). The crude was then filtered on a plug of silica (EtOAc as eluent) and concentrated under reduced pressure.

4-(Cyclohex-2-en-1-yl)-2-phenylpyridine (2.3)

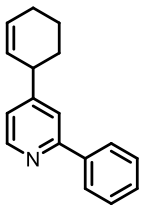

Prepared following general procedure **A**, **2.3** was obtained after purification by column chromatography (pentane/EtOAc: 50/1 to 20/1) as a colorless oil (18.8 mg, 80% yield). R_f = 0.49 (pentane: EtOAc= 10:1). **^{1}H NMR (600 MHz, $CDCl_3$)** δ 8.60 (d, *J* = 5.0 Hz, 1H), 7.98 (d, *J* = 8.0 Hz, 2H), 7.59 (s, 1H), 7.48 – 7.46 (m, 2H), 7.43 – 7.39 (m, 1H), 7.11 (d, *J* = 5.1 Hz, 1H), 6.01 – 5.97 (m, 1H), 5.75 – 5.68 (m, 1H), 3.48 – 3.45 (m, 1H), 2.15 – 2.11 (m, 2H), 2.10 – 2.04 (m, 1H), 1.79 – 1.74 (m, 1H), 1.69 – 1.64 (m, 1H), 1.63 – 1.56 (m, 1H).**^{13}C NMR (151 MHz, $CDCl_3$)** δ 157.6, 156.6, 149.5, 139.6, 130.0, 129.0, 128.9 (2C), 128.3, 127.2 (2C), 121.9, 120.3, 41.6, 32.0, 25.0, 21.0. **IR (neat):** ν 3023, 2928, 1597,

1550, 1472, 773, 742, 693 cm^{-1}. **HRMS (ESI)** calculated for $C_{17}H_{18}N$ $[M+H]^+$: 236.1434, found: 236.1430.

4-(Cyclohex-2-en-1-yl)-2-(4-fluorophenyl)pyridine (2.4)

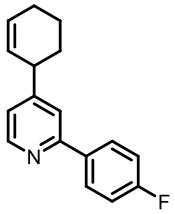

Prepared following general procedure **A**, **2.4** was obtained after purification by column chromatography (pentane/EtOAc: 100/1 to 50/1 to 30/1) as a colorless oil (16.7 mg, 66% yield). R_f = 0.69 (pentane: EtOAc= 10:1). **^{1}H NMR (600 MHz, $CDCl_3$)** δ 8.57 (d, *J* = 5.0 Hz, 1H), 7.99 – 7.94 (m, 2H), 7.53 (s, 1H), 7.16 – 7.13 (m, 2H), 7.10 (d, *J* = 5.0, 1H), 6.02 – 5.97 (m, 1H), 5.73 – 5.70 (m, 1H), 3.47 – 3.44 (m, 1H), 2.15 – 2.11 (m, 2H), 2.09 – 2.04 (m, 1H), 1.79 – 1.73 (m, 1H), 1.69 – 1.64 (m, 1H), 1.62 – 1.56 (m, 1H).**^{13}C NMR (151 MHz, $CDCl_3$)** δ 163.6 (d, *J* = 247.9 Hz), 156.7, 156.5, 149.7, 136.0 (d, *J* = 3.1 Hz), 130.0, 128.9 (d, *J* = 8.4 Hz, 2C), 128.3, 121.8, 119.8, 115.7 (d, *J* = 21.6 Hz, 2C), 41.6, 32.0, 25.1, 21.1. **^{19}F NMR (565 MHz, $CDCl_3$)** δ -113.5. **IR (neat):** ν 3022, 2929, 1601, 1510, 1470, 1420, 1224, 829, 724 cm^{-1}. **HRMS (ESI)** calculated for $C_{17}H_{17}FN$ $[M+H]^+$: 254.1340, found: 254.1345.

2-(4-Chlorophenyl)-4-(cyclohex-2-en-1-yl)pyridine (2.5)

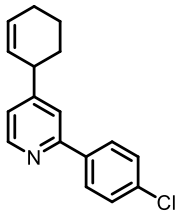

Prepared following general procedure **A**, **2.5** was obtained after purification by column chromatography (pentane/EtOAc: 50/1 to 20/1) as a colorless oil (21.6 mg, 80% yield). R_f = 0.47 (pentane: EtOAc= 10:1). **^{1}H NMR (600 MHz, $CDCl_3$)** δ 8.58 (d, *J* = 5.1 Hz, 1H), 7.95 – 7.91 (m, 2H), 7.55 (s, 1H), 7.45 – 7.41 (m, 2H), 7.12 (d, *J* = 5.1 Hz, 1H), 6.01 – 5.98 (m, 1H), 5.72 – 5,69 (m, 1H), 3.47 – 3.45 (m, 1H), 2.16 – 2.11 (m, 2H), 2.09 – 2.04 (m, 1H), 1.79 – 1.73 (m, 1H), 1.70 – 1.62 (m, 1H), 1.59 – 1.56 (m, 1H). **^{13}C NMR (151 MHz, $CDCl_3$)** δ 156.8, 156.3, 149.6, 138.1, 135.1, 130.1, 129.0 (2C), 128.4 (2C), 128.2, 122.2, 120.0, 41.6, 32.0, 25.0, 21.0. **IR (neat):** ν 3020, 2928, 1598, 1553, 1492, 1467, 826, 763, 722 cm^{-1}. **HRMS (ESI)** calculated for $C_{17}H_{17}ClN$ $[M+H]^+$: 270.1045, found: 270.1046.

2-(4-Bromophenyl)-4-(cyclohex-2-en-1-yl)pyridine (2.6)

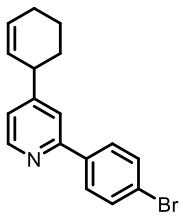

Prepared following general procedure **A**, **2.6** was obtained after purification by column chromatography (pentane/EtOAc: 100/1 to 50/1 to 30/1) as a colorless oil (21.8 mg, 69% yield). R_f = 0.65 (pentane: EtOAc= 10:1). **^{1}H NMR (600 MHz, $CDCl_3$)** δ 8.57 (d, *J* = 4.5 Hz, 1H), 7.91 – 7.83 (m, 2H), 7.60 – 7.58 (m, 2H), 7.54 (s, 1H), 7.12 (d, *J* = 4.9 Hz, 1H), 6.00 – 5.98 (m, 1H), 5.71 – 5.70 (m, 1H), 3.46 – 3.44 (m, 1H), 2.14 –2.11 (m, 2H), 2.10 – 2.02 (m, 1H), 1.77 – 1.72 (m, 1H), 1.70 – 1.62 (m, 1H), 1.62 – 1.53 (m, 1H).**^{13}C NMR (151 MHz, $CDCl_3$)** δ 156.6, 156.5, 149.8, 138.7, 132.0 (2C), 130.0, 128.7 (2C), 128.3, 123.4, 122.2, 119.9, 41.6, 32.0, 25.0, 21.1. **IR (neat):** ν 3021, 2927, 1671, 1598, 1551, 1467, 823, 719, 682 cm^{-1}. **HRMS (ESI)** calculated for $C_{17}H_{17}BrN$ $[M+H]^+$: 314.0539, found: 314.0537.

4-(Cyclohex-2-en-1-yl)-2-(p-tolyl)pyridine (2.7)

Prepared following general procedure **A**, **2.7** was obtained after purification by column chromatography (pentane/EtOAc: 100/1 to 50/1 to 30/1) as a colorless oil (18.6 mg, 75% yield).

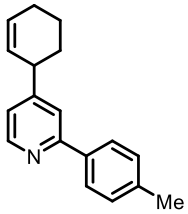

R_f = 0.50 (pentane: EtOAc= 10:1). **^{1}H NMR (600 MHz, $CDCl_3$)** δ 8.65 – 8.61 (m, 1H), 7.96 – 7.93 (m, 2H), 7.61 (s, 1H), 7.35 – 7.32 (m, 2H), 7.14 – 7.13 (m, 1H), 6.05 – 6.03 (m, 1H), 5.81 – 5.73 (m, 1H), 3.52 – 3.49 (m, 1H), 2.47 (s, 3H), 2.21 – 2.16 (m, 2H), 2.15 – 2.10 (m, 1H), 1.84 – 1.81 (m, 1H), 1.76 – 1.62 (m, 2H).**^{13}C NMR (151 MHz, $CDCl_3$)** δ 157.7, 156.2, 149.6, 138.9, 137.1, 129.8, 129.5 (2C), 128.5, 127.0 (2C), 121.6, 119.9, 41.6, 32.0, 25.1, 21.4, 21.1. **IR (neat):** ν 3020, 2926, 1651, 1597, 1552, 1466, 1345, 818, 728 cm^{-1}. **HRMS (ESI)** calculated for $C_{18}H_{20}N$ $[M+H]^+$: 250.1591, found: 250.1594

4-(Cyclohex-2-en-1-yl)-2-(4-methoxyphenyl)pyridine (2.8)

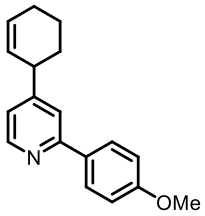

Prepared following general procedure **A**, **2.8** was obtained after purification by column chromatography (pentane/EtOAc: 10/1) as a colorless oil (18.9 mg, 71% yield). R_f = 0.71 (pentane: EtOAc= 5:1). **^{1}H NMR (600 MHz, $CDCl_3$)** δ 8.54 (d, *J* = 5.1 Hz, 1H), 7.97 – 7.92 (m, 2H), 7.52 (s, 1H), 7.04 (dd, *J* = 5.0, 1.6 Hz, 1H), 7.01 – 6.97 (m, 2H), 5.98 – 5.96 (m, 1H), 5.75 – 5.67 (m, 1H), 3.86 (s, 3H), 3.44 – 3.42 (m, 1H), 2.12 – 2.10 (m, 2H), 2.06 – 2.04 (m, 1H), 1.81 – 1.73 (m, 1H), 1.70 – 1.54 (m, 2H). **^{13}C NMR (151 MHz, $CDCl_3$)** δ 160.5, 157.3, 156.2, 149.6, 132.5, 129.8, 128.5, 128.4 (2C), 121.2, 119.4, 114.2 (2C), 55.5, 41.6, 32.0, 25.1, 21.1. **IR (neat):** 3018, 2927, 1724, 1601, 1514, 1465, 1398, 1247, 828, 729 cm^{-1}. **HRMS (ESI)** calculated for $C_{18}H_{20}NO$ $[M+H]^+$: 266.1539, found: 266.1542.

4-(Cyclohex-2-en-1-yl)-2,2'-bipyridine (2.9)

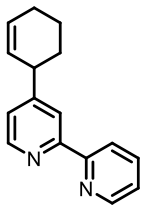

Prepared following general procedure **A**, **2.9** was obtained after purification by column chromatography (pentane/EtOAc: 20/1 to 10/1 to 5/1) as a colorless oil (13.1 mg, 56% yield). R_f = 0.63 (pentane: EtOAc= 2:1). **^{1}H NMR (600 MHz, $CDCl_3$)** δ 8.69 (d, *J* = 4.8 Hz, 1H), 8.59 (d, *J* = 5.0 Hz, 1H), 8.41 (d, *J* = 7.9 Hz, 1H), 8.28 (s, 1H), 7.86 – 7.78 (m, 1H), 7.32 – 7.30 (m, 1H), 7.20 (d, *J* = 5.1 Hz, 1H), 6.02 – 5.94 (m, 1H), 5.76 – 5.70 (m, 1H), 3.52 – 3.52 (m, 1H), 2.15 – 2.04 (m, 3H), 1.78 – 1.75 (m, 1H), 1.70 – 1.58 (m, 2H).**^{13}C NMR (151 MHz, $CDCl_3$)** δ 156.70, 156.56, 156.26, 149.30, 149.27, 137.03, 129.79, 128.47, 123.72, 123.34, 121.41, 120.62, 41.61, 31.88, 25.04, 21.20. **IR (neat):** ν 3053, 3019, 2927, 1583, 1555, 1456, 792, 744 cm^{-1}. **HRMS (ESI)** calculated for $C_{16}H_{16}N_2Na$ $[M+Na]^+$: 259.1206, found: 259.1205.

4-(Cyclohex-2-en-1-yl)-2-(thiophen-3-yl)pyridine (2.10)

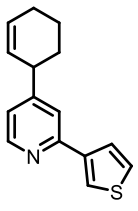

Prepared following general procedure **A**, **2.10** was obtained after purification by column chromatography (pentane/EtOAc: 30/1) as a colorless oil (17.8 mg, 74% yield). R_f = 0.72 (pentane: EtOAc= 10:1). **^{1}H NMR (600 MHz, $CDCl_3$)** δ 8.51 (d, *J* = 5.1 Hz, 1H), 7.89 (dd, *J* = 3.0, 1.3 Hz, 1H), 7.66 (dd, *J* = 5.0, 1.3 Hz, 1H), 7.48 – 7.46 (s, 1H), 7.39 (dd, *J* = 5.0, 3.0 Hz, 1H), 7.04 (dd, *J* = 5.1, 1.7 Hz, 1H), 6.01 – 5.95 (m, 1H), 5.72 – 5.69 (m, 1H), 3.45 – 3.41 (m, 1H), 2.14 – 2.10 (m, 2H), 2.08 – 2.03 (m, 1H), 1.76 – 1.73 (m, 1H), 1.70 – 1.64 (m, 1H), 1.61 – 1.56 (m, 1H). **^{13}C NMR (151 MHz, $CDCl_3$)** δ 156.3, 153.7, 149.7, 142.6, 129.9, 128.4, 126.5, 126.3, 123.5, 121.6, 119.9, 41.5, 31.9, 25.0, 21.1. **IR (neat):** 3105, 3019, 2927, 1648, 1597, 1551, 1470, 792, 725 cm^{-1}. **HRMS (ESI)** calculated for $C_{15}H_{16}NS$ $[M+H]^+$: 242.0998, found: 242.0990.

4-(Cyclohex-2-en-1-yl)-2-(furan-2-yl)pyridine (2.11)

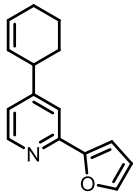

Prepared following general procedure **A**. **2.11** was obtained after purification by column chromatography (pentane/EtOAc: 50/1) as a yellowish oil (17.6 mg, 78% yield). R_f = 0.68 (pentane: EtOAc= 5:1). **^{1}H NMR (600 MHz, $CDCl_3$)** δ 8.49 (d, *J* = 5.0 Hz, 1H), 7.58 – 7.48 (m, 2H), 7.05 – 6.99 (m, 2H), 6.53 – 6.52 (m, 1H), 6.00 – 5.97 (m, 1H), 5.74 – 5.65 (m, 1H), 3.44 – 3.41 (m, 1H), 2.15 – 2.09 (m, 2H), 2.07 – 2.03 (m, 1H), 1.78 – 1.74 (m, 1H), 1.69 – 1.63 (m, 1H), 1.63 – 1.56 (m, 1H). **^{13}C NMR (151 MHz, $CDCl_3$)** δ 156.4, 154.0, 149.7, 149.5, 143.2, 129.9, 128.3, 121.7, 118.1, 112.2, 108.5, 41.5, 31.9, 25.0, 21.1. **IR (neat):** 3019, 2928, 1607, 1552, 1494, 1389, 1002, 817, 733 cm^{-1}. **HRMS (ESI)** calculated for $C_{15}H_{15}NNaO$ $[M+Na]^+$: 248.1046, found: 248.1051.

2-Benzyl-4-(cyclohex-2-en-1-yl)pyridine (2.12)

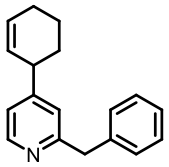

Prepared following general procedure **A**, **2.12** was obtained after purification by column chromatography (pentane/ EtOAc: 20/1 to 10/1) as a colorless oil (15.2 mg, 61% yield). R_f =0.43 (pentane: EtOAc=5:1). **^{1}H NMR (600 MHz, $CDCl_3$)** δ 8.47 (d, *J* = 5.0 Hz, 1H), 7.33 – 7.28 (m, 4H), 7.25 – 7.21 (m, 1H), 7.01 (dd, *J* = 5.0, 1.6 Hz, 1H), 7.00 (d, *J* =1.6 Hz, 1H), 5.96 – 5.92 (m, 1H), 5.66 – 5.63 (m, 1H), 4.15 (s, 2H), 3.36 – 3.33 (m, 1H), 2.12 – 2.08 (m, 2H), 2.03 – 1.96 (m, 1H), 1.75 – 1.70 (m, 1H), 1.66 – 1.58 (m, 1H), 1.55 – 1,49 (m, 1H). **^{13}C NMR (151 MHz, $CDCl_3$)** δ 160.9, 156.2, 149.4, 139.9, 129.6, 129.2 (2C), 128.7 (2C), 128.4, 126.4, 122.7, 120.9, 44.8, 41.3, 31.8, 25.0, 21.0. **IR (neat):** 3059, 3024, 2928, 1670, 1598, 1552, 1447, 734, 698 cm^{-1}. **HRMS (ESI)** calculated for$C_{18}H_{20}N$ $[M+H]^+$: 250.1590, found: 250.1582.

2-(4-Chlorobenzyl)-4-(cyclohex-2-en-1-yl)pyridine (2.13)

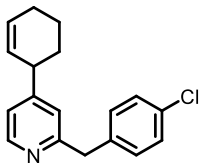

Prepared following general procedure **A**, **2.13** was obtained after purification by column chromatography (pentane/EtOAc: 50/1 to 20/1 to 10/1) as a colorless oil (16.7 mg, 59% yield). R_f = 0.42 (pentane: EtOAc= 5:1). **^{1}H NMR (600 MHz, $CDCl_3$)** δ 8.36 (d, *J* = 5.1 Hz, 1H), 7.21 – 7.17 (m, 2H), 7.15 – 7.10 (m, 2H), 6.92 (dd, *J* = 5.1, 1.7 Hz, 1H), 6.90 (d, *J* = 1.7 Hz, 1H), 5.86 – 5.84 (m, 1H), 5.58 – 5.51 (m, 1H), 4.01 (s, 2H), 3.26 – 3.24 (m, 1H), 2.03 – 1.99 (m, 2H), 1.93 – 1.88 (m, 1H), 1.68 – 1.61 (m, 1H), 1.58 – 1.49 (m, 1H), 1.45 – 1.39 (m, 1H). **^{13}C NMR (151 MHz, $CDCl_3$)** δ 160.3, 156.3, 149.6, 138.4, 132.3, 130.5 (2C), 129.8, 128.8 (2C), 128.3, 122.6, 121.1, 44.1, 41.3, 31.9, 25.0, 21.0. **IR (neat):** 3021, 2927, 1599, 1555, 1488, 798, 825, 720 cm^{-1}. **HRMS (ESI)** calculated for $C_{18}H_{19}ClN$ $[M+H]^+$: 284.1201, found: 284.1201.

2-(4-Chlorobenzyl)-4-(2,3-dimethylbut-2-en-1-yl)pyridine (2.14)

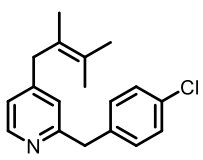

Prepared following general procedure **B**, **2.14** was obtained after purification by column chromatography (pentane/EtOAc: 50/1 to 20/1 to 10/1) as a colorless oil (17.6 mg, 62% yield). R_f = 0.45 (pentane: EtOAc= 5:1). **^{1}H NMR (600 MHz, $CDCl_3$)** δ 8.33 (d, *J* = 5.1 Hz, 1H), 7.21 – 7.16 (m, 2H), 7.14 – 7.11 (m, 2H), 6.83 (d, *J* = 5.1 Hz, 1H), 6.80 (s, 1H), 4.00 (s, 2H), 3.25 (s, 2H), 1.65 (s, 3H), 1.64 (s, 3H), 1.48 (s, 3H). **^{13}C NMR (151 MHz, $CDCl_3$)** δ 160.2, 151.1, 149.5, 138.4, 132.3, 130.5 (2C), 128.8 (2C), 127.5, 124.6, 123.4, 121.7, 44.0, 39.7, 20.9, 20.7, 18.7. **IR (neat):** 2988, 2918, 1598, 1556, 1488, 1375, 804, 778, 726 cm^{-1}. **HRMS (ESI)** calculated for $C_{18}H_{21}ClN$ $[M+H]^+$: 286.1357, found: 286.1357.

4-(2,3-Dimethylbut-2-en-1-yl)-2-methylpyridine (2.15)

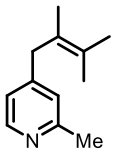

Prepared following general procedure **B**, **2.15** was obtained after purification by column chromatography (pentane/EtOAc: 20/1 to 10/1) as a colorless oil (6.9 mg, 39% yield). R_f =0.38 (pentane: EtOAc= 5:1). **^{1}H NMR (600 MHz, $CDCl_3$)** δ 8.29 (d, *J* = 5.2 Hz, 1H), 6.86 (s, 1H), 6.82 (d, *J* = 5.1 Hz, 1H), 3.27 (s, 2H), 2.45 (s, 3H), 1.69 (s, 3H), 1.67 (s, 3H), 1.52 (s, 3H). **^{13}C NMR (151 MHz, $CDCl_3$)** δ 158.2, 150.8, 148.9, 127.4, 124.8, 123.6, 121.2, 39.7, 24.4, 20.9, 20.8, 18.7. **IR (neat):** 2961, 1733, 1602, 1560, 1446, 1258, 794 cm^{-1}. **HRMS (ESI)** calculated for $C_{12}H_{18}N$ $[M+H]^+$:176.1434, found:176.1435.

4-(2,3-Dimethylbut-2-en-1-yl)pyridine (2.16)

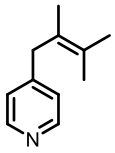

Prepared following general procedure **B**, **2.16** was obtained after purification by column chromatography (pentane/acetone: 20/1 to 10/1) as a colorless oil (7.3 mg, 45% yield). R_f =0.46 (pentane: acetone= 10:1). **^{1}H NMR (600 MHz, $CDCl_3$)** δ 8.49 – 8.45 (m, 2H), 7.07 (d, *J* = 5.4 Hz, 2H), 3.38 (s, 2H), 1.76 (s, 3H), 1.74 (s, 3H), 1.59 (s, 3H). **^{13}C NMR (151 MHz, $CDCl_3$)** δ 150.3, 149.8 (2C), 127.6, 124.7, 124.0 (2C), 39.7, 20.9, 20.7, 18.7. **IR (neat):** 2919, 1726, 1596, 1414, 1374, 794 cm^{-1}. **HRMS (ESI)** calculated for $C_{11}H_{16}N$ $[M+H]^+$:162.1277, found:162.1272.

4-(2,3-Dimethylbut-2-en-1-yl)-2-phenylpyridine (2.17)

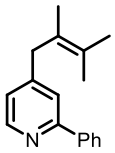

Prepared following general procedure **A**, **2.17** was obtained after purification by column chromatography (pentane/EtOAc: 50/1) as a colorless oil (21.4 mg, 90% yield). R_f = 0.65 (pentane: EtOAc= 10:1). **^{1}H NMR (600 MHz, $CDCl_3$)** δ 8.56 (d, *J* = 5.0 Hz, 1H), 7.98 – 7.93 (m, 2H), 7.50 (s, 1H), 7.48 – 7.46 (m, 2H), 7.42 – 7.39 (m, 1H), 7.03 (d, *J* = 5.0 Hz, 1H), 3.45 (s, 2H), 1.80 (s, 3H), 1.77 (s, 3H), 1.63 (s, 3H). **^{13}C NMR (151 MHz, $CDCl_3$)** δ 157.6, 151.1, 149.7, 139.9, 128.9, 128.8 (2C), 127.6, 127.1 (2C), 124.8, 122.6, 121.0, 40.0, 21.0, 20.8, 18.7. **IR (neat):** ν 2918, 2858, 1596, 1444, 1402, 1258, 1012, 790, 693 cm^{-1}. **HRMS (ESI)** calculated for $C_{17}H_{20}N$ $[M+H]^+$: 238.1590, found: 238.1580.

4-(3-Methylbut-2-en-1-yl)-2-phenylpyridine (2.18)

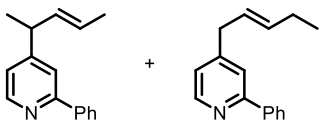

Prepared following general procedure **A**. **2.18** was obtained after purification by column chromatography (pentane/EtOAc: 19/1) as a colorless oil (12.9 mg, 58% yield, 10:1 r.r.). (NMRs reported for the major regioisomer) R_f = 0.30 (pentane: EtOAc= 19:1). **^{1}H NMR (600 MHz, $CDCl_3$)** δ 8.58 (d, *J* = 3.9 Hz, 1H), 7.98 (d, *J* = 7.2 Hz, 2H), 7.56 (s, 1H), 7.51 – 7.45 (m, 2H), 7.43 – 7.38 (m, 1H), 7.09 (s, 1H), 6.70 – 5.49 (m, 2H), 3.52 – 3.41 (m, 1H), 1.70 (d, *J* = 4.4 Hz, 3H), 1.38 (d, *J* = 1.4 Hz, 3H). **^{13}C NMR (151 MHz, $CDCl_3$)** δ 157.8, 156.1, 149.8, 139.9, 134.5, 128.9, 128.8 (2C), 127.1 (2C), 125.5, 121.3, 119.8, 42.2, 21.0, 18.1. **IR (neat):** 2966, 2925, 2874, 1597, 1553, 1445, 1402, 1072, 1025, 965, 890, 841, 774, 739, 693 cm^{-1}. **HRMS (ESI)** calculated for $C_{16}H_{18}N$ $[M+H]^+$: 224.1434, found: 224.1428.

4-(3-Methylbut-2-en-1-yl)-2-phenylpyridine (2.19)

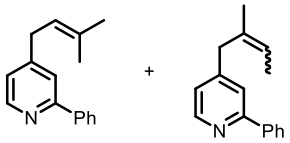

Prepared following general procedure **A**. **2.19** was obtained after purification by column chromatography (pentane/EtOAc: 19/1) as a colorless oil (10.0 mg, 45% yield, 8.8:1 r.r.). (NMRs reported for the major regioisomer). R_f = 0.30 (pentane: EtOAc= 19:1). **^{1}H NMR (600**

MHz, $CDCl_3$) δ 8.57 (d, *J* = 4.1 Hz, 1H), 7.97 (d, *J* = 7.3 Hz, 2H), 7.54 (s, 1H), 7.47 (t, *J* = 7.5 Hz, 2H), 7.40 (t, *J* = 7.3 Hz, 1H), 7.06 (s, 1H), 5.34 (t, *J* = 6.4 Hz, 1H), 3.40 (d, *J* = 7.5 Hz, 2H), 1.79 (s, 3H), 1, 74 (s, 3H). **^{13}C NMR (151 MHz, $CDCl_3$)** δ 157.7, 151.7, 149.7, 139.8, 134.6, 128.9, 128.8, (2C), 127.1 (2C), 122.4, 121.1, 120.8, 34.0, 25.9, 18.1. **IR (neat):** 2920, 1598, 1554, 1472, 1444, 1402, 1100, 1072, 1027, 830, 773, 736, 693 cm^{-1}. **HRMS (ESI)** calculated for $C_{16}H_{18}N$ $[M+H]^+$: 224.1434, found: 224.1428.

4-(3,7-Dimethylocta-2,6-dien-1-yl)-2-phenylpyridine (2.20)

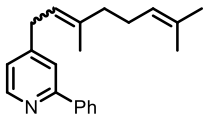

Prepared following general procedure **A**. **2.20** was obtained after purification by column chromatography (pentane/acetone: 19/1) as a colorless oil (16.0 mg, 55% yield, 1.8:1 mixture of geometric isomers). (^{1}H NMR reported for the E/Z mixture, ^{13}C NMR reported for the major isomer). R_f = 0.30 (pentane: EtOAc= 19:1). **^{1}H NMR (600 MHz, $CDCl_3$)** δ 8.57 (d, *J* = 4.2 Hz, 1H), 7.97 (d, *J* = 7.2 Hz, 2H), 7.54 (s, 1H), 7.47 (t, *J* = 7.3 Hz, 2H), 7.40 (t, *J* = 7.1 Hz, 1H), 7.07 (s, 1H), 5.40 – 5.30 (m, 1H), 5.18 – 5.07 (m, 1H), 3.41 (d, *J* = 7.0 Hz, 2H), 2.22 – 2.05 (m, 4H), 1.73 (s, 3H), 1.67 (s, 3H), 1.61 (s, 3H). **^{13}C NMR (151 MHz, $CDCl_3$)** δ 157.6, 151.7, 149.7, 139.8, 138.3, 131.8, 128.9, 128.8 (2C), 127.1 (2C), 124.1, 122.4, 121.0, 120.8, 39.8, 33.9, 26.7, 25.8, 17.9, 16.4. **IR (neat):** 2963, 2920, 2855, 1598, 1555, 1444, 1402, 1313, 1106, 1074, 1028, 831, 774, 736, 693 cm^{-1}. **HRMS (ESI)** calculated for $C_{21}H_{26}N$ $[M+H]^+$: 292.2060, found: 292.2052.

2-Phenyl-4-((6E)-3,7,11-trimethyldodeca-2,6,10-trien-1-yl)pyridine (2.21)

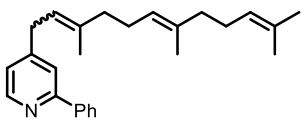

Prepared following general procedure **A**. **2.21** was obtained after purification by column chromatography (pentane/acetone: 19/1) as a colorless oil (14.2 mg, 39% yield, 2:1 mixture of geometric isomers). (^{1}H NMR reported for the E/Z mixture). R_f = 0.30 (pentane: EtOAc= 19:1). **^{1}H NMR (600 MHz, $CDCl_3$)** δ 8.56 (d, *J* = 5.0 Hz, 1H), 7.97 (d, *J* = 7.9 Hz, 2H), 7.54 (s, 1H), 7.46 (t, *J* = 7.4 Hz, 2H), 7.40 (t, *J* = 7.4 Hz, 1H), 7.07 (d, *J* = 4.8 Hz, 1H), 5.35 (q, *J* = 6.8 Hz, 1H), 5.14 (dt, *J* = 16.2, 6.8 Hz, 1H), 5.11 – 5.05 (m, 1H), 3.49 – 3.35 (m, 2H), 2.20 – 2.01 (m, 6H), 2.00 – 1.93 (m, 2H), 1.82 – 1.71 (m, 3H), 1.70 – 1.65 (m, 3H), 1.63 – 1.56 (m, 6H). **^{13}C NMR (151 MHz, $CDCl_3$)** δ 157.7 (min), 157.6 (maj), 151.7 (min), 151.7 (maj), 149.7 (maj+min), 139.8 (maj+min), 138.3 (min), 138.3 (maj), 135.8 (maj), 135.5 (min), 131.5 (min), 131.5 (maj), 128.9 (maj+min), 128.9 (2C, maj+min), 127.1 (2C, maj+min), 124.5 (maj), 124.4 (min), 124.0 (maj), 123.9 (min), 122.5 (min), 122.4 (maj), 121.7 (maj+min), 121.0 (min), 120.9 (maj), 39.9 (maj), 39.8 (min), 33.9 (maj), 33.8 (min), 32.2 (maj+min), 26.9 (maj), 26.8 (min), 26.6 (maj), 26.6 (min), 25.8 (2C, maj), 23.6 (2C, min), 17.8 (maj), 16.5 (min), 16.2 (maj), 16.2 (min). **IR (neat):** 2919, 2855, 1598, 1555, 1444, 1402, 1379, 1104, 1074, 1028, 986, 832, 774, 735, 693 cm^{-1}. **HRMS (ESI)** calculated for $C_{26}H_{34}N$ $[M+H]^+$: 360.2686, found: 360.2682.

4-((5S)-2,3-Dimethyl-5-(prop-1-en-2-yl)cyclohex-2-en-1-yl)-2-phenylpyridine (2.22)

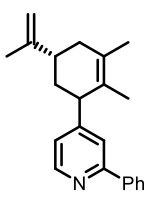

Prepared following general procedure **B** except that the reaction time was 48 hours. **2.22** was obtained after purification by column chromatography (pentane/EtOAc: 9/1) as a colorless oil (10.9 mg, 36% yield). R_f = 0.30 (pentane: EtOAc= 9:1). **^{1}H NMR (600 MHz, $CDCl_3$)** δ 8.58 (d, *J* = 3.6 Hz, 1H), 7.98 (d, *J* = 7.1 Hz, 2H), 7.56 (s, 1H), 7.49 – 7.45 (m, 2H), 7.43 – 7.38 (m, 1H), 7.03 (s, 1H), 4.72 (d, *J* = 5.8 Hz, 2H),

3.42 (s, 1H), 2.32 (t, *J* = 11.0 Hz, 1H), 2.15 (t, *J* = 13.5 Hz, 1H), 2.08 (d, *J* = 15.1 Hz, 2H), 1.74 (s, 6H), 1.41 (s, 4H). **^{13}C NMR (151 MHz, $CDCl_3$)** δ 157.8, 156.7, 149.8, 149.4, 139.8, 130.2, 129.0, 128.8 (2C), 127.2 (2C), 125.5, 122.3, 120.7, 109.1, 49.9, 41.7, 39.7, 37.8, 20.8, 20.0, 17.5. **IR (neat):** 2919, 1595, 1553, 1444, 1402, 1377, 1103, 1068, 1027, 887, 842, 743, 693 cm^{-1}. **HRMS (ESI)** calculated for $C_{22}H_{26}N$ $[M+H]^+$: 304.2060, found: 304.2061.

Ethyl 3-(3-(2-phenylpyridin-4-yl)cyclohex-1-en-1-yl)propanoate (2.23)

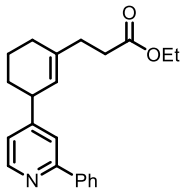

Prepared following general procedure **B** except that the reaction time was 48 hours. **2.23** was obtained after purification by column chromatography (pentane/EtOAc: 9/1) as a colorless oil (17.2 mg, 51% yield). R_f = 0.30 (pentane: EtOAc= 9:1). **^{1}H NMR (600 MHz, $CDCl_3$)** δ 8.57 (d, *J* = 5.2 Hz, 1H), 7.99 (d, *J* = 7.9 Hz, 2H), 7.54 (s, 1H), 7.47 (t, *J* = 7.5 Hz, 2H), 7.40 (t, *J* = 7.5 Hz, 1H), 7.06 (dd, *J* = 5.1, 1.4 Hz, 1H), 5.46 (s, 1H), 4.11 (q, *J* = 7.2 Hz, 2H), 3.43 (s, 1H), 2.54 – 2.45 (m, 2H), 2.41 – 2.37 (m, 2H), 2.15 – 2.06 (m, 1H), 2.06 – 1.98 (m, 2H), 1.83 – 1.73 (m, 1H), 1.69 – 1.60 (m, 1H), 1.51 (ddd, *J* = 12.9, 8.2, 2.9 Hz, 1H), 1.22 (t, *J* = 7.2 Hz, 3H). **^{13}C NMR (151 MHz, $CDCl_3$)** δ 173.2, 157.5, 156.4, 149.5, 139.6, 139.0, 128.7, 128.6 (2C), 127.0 (2C), 122.9, 121.6, 120.0, 60.3, 41.6, 32.8, 32.7, 31.7, 28.1, 21.3, 14.2. **IR (neat):** 2931, 1729, 1597, 1550, 1445, 1401, 1253, 1171, 1103, 1029, 912, 841, 775, 731, 695 cm^{-1}. **HRMS (ESI)** calculated for $C_{22}H_{26}NO_2$ $[M+H]^+$: 336.1958, found: 336.1953.

4-(3-Butylcyclohex-2-en-1-yl)-2-phenylpyridine (2.24)

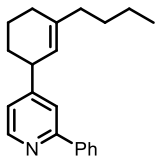

Prepared following general procedure **B** except that the reaction time was 48 hours. **2.24** was obtained after purification by column chromatography (pentane/EtOAc: 19/1) as a colorless oil (From 1-*n*-butylcyclohexadiene: 13.1 mg, 45% yield; From 2-*n*-butylcyclohexadiene: 13.8 mg, 48% yield). R_f = 0.30 (pentane: EtOAc= 9:1). **^{1}H NMR (600 MHz, $CDCl_3$)** δ 8.51 (s, 1H), 7.90 (d, *J* = 7.1 Hz, 2H), 7.50 (s, 1H), 7.43 – 7.36 (m, 2H), 7.36 – 7.29 (m, 1H), 7.02 (s, 1H), 5.36 (s, 1H), 3.37 (s, 1H), 2.04 – 1.87 (m, 5H), 1.76 – 1.65 (m, 1H), 1.60 – 1.52 (m, 1H), 1.49 – 1.35 (m, 2H), 1.33 – 1.16 (m, 3H), 0.87 (t, *J* = 7.2 Hz, 3H). **^{13}C NMR (151 MHz, $CDCl_3$)** δ 157.6, 157.1, 149.7, 141.0, 139.9, 128.9, 128.8 (2C), 127.1 (2C), 122.2, 121.9, 120.3, 41.9, 37.8, 32.1, 30.1, 28.3, 22.6, 21.6, 14.2. **IR (neat):** 2920, 1598, 1554, 1468, 1446, 1402, 1204, 1152, 1101, 1070, 887, 774, 735, 693 cm^{-1}. **HRMS (ESI)** calculated for $C_{21}H_{26}N$ $[M+H]^+$: 292.2060, found: 292.2057.

4-(3-Cyclohexylallyl)-2-phenylpyridine (2.25)

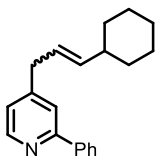

Prepared following general procedure **A**. **2.25** was obtained after purification by column chromatography (pentane/EtOAc: 19/1) as a colorless oil (5.1 mg, 18% yield). R_f = 0.30 (pentane: EtOAc= 19:1). **^{1}H NMR (600 MHz, $CDCl_3$)** δ 8.57 (d, *J* = 4.5 Hz, 1H), 7.98 (d, *J* = 7.6 Hz, 2H), 7.55 (s, 1H), 7.47 (t, *J* = 7.1 Hz, 2H), 7.41 (t, *J* = 7.3 Hz, 1H), 7.07 (d, *J* = 7.1 Hz, 1H), 5.60 – 5.48 (m, 2H), 3.37 (d, *J* = 3.4 Hz, 2H), 1.98 (s, 1H), 1.74 – 1.64 (m, 6H), 1.20 – 1.03 (m, 4H). **^{13}C NMR (151 MHz, $CDCl_3$)** δ 157.7, 151.1, 149.7, 139.9, 139.8, 129.0, 128.8 (2C), 127.1 (2C), 124.3, 122.6, 121.0, 40.8, 38.7, 33.2 (2C), 26.3, 26.2 (2C). **IR (neat):** 2922, 2851, 1727, 1598, 1555, 1445, 1260, 1073, 1016, 970, 778, 736, 693 cm^{-1}. **HRMS (ESI)** calculated for $C_{20}H_{24}N$ $[M+H]^+$: 278.1903, found: 278.1911.

4-(1-(4-Methoxyphenyl)ethyl)-2-phenylpyridine (2.26)

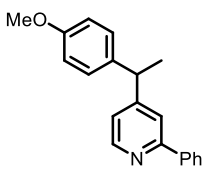

Prepared following general procedure **B** except that the reaction time was 48 hours. **2.26** was obtained after purification by column chromatography (pentane/acetone: 19/1) as a colorless oil (22.0 mg, 76% yield). R_f = 0.30 (pentane: acetone= 19:1). **^{1}H NMR (600 MHz, $CDCl_3$)** δ 8.57 (d, *J* = 5.1 Hz, 1H), 7.94 (dd, *J* = 7.4, 1.2 Hz, 2H), 7.56 (s, 1H), 7.46 (t, *J* = 7.4 Hz, 2H), 7.40 (tt, *J* = 6.6, 1.2 Hz, 1H), 7.16 (d, *J* = 8.7 Hz, 2H), 7.08 (dd, *J* = 5.0, 1.3 Hz, 1H), 6.86 (d, *J* = 8.8 Hz, 2H), 4.14 (q, *J* = 7.3 Hz, 1H), 3.79 (s, 3H), 1.67 (d, *J* = 7.3 Hz, 3H). **^{13}C NMR (151 MHz, $CDCl_3$)** δ 158.5, 157.8, 156.5, 149.8, 139.8, 136.8, 129.0, 128.8 (2C), 128.7 (2C), 127.2 (2C), 121.6, 120.0, 114.2 (2C), 55.4, 43.8, 21.5. **IR (neat):** 2963, 2928, 1722, 1597, 1552, 1509, 1447, 1401, 1245, 1178, 1111, 1032, 831, 775, 732, 695 cm^{-1}. **HRMS (ESI)** calculated for $C_{20}H_{20}NO$ $[M+H]^+$: 290.1539, found: 290.1546.

ethyl 4-(1-(2-phenylpyridin-4-yl)ethyl)benzoate (2.27)

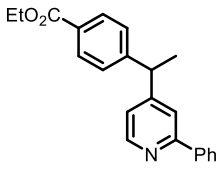

Prepared following general procedure **B** expect that the reaction time was 48 hours. **2.27** was obtained after purification by column chromatography (pentane/acetone: 19/1) as a colorless oil (16.8 mg, 51% yield). R_f = 0.30 (pentane: acetone= 19:1). **^{1}H NMR (600 MHz, $CDCl_3$)** δ 8.59 (d, *J* = 5.1 Hz, 1H), 8.00 (d, *J* = 8.4 Hz, 2H), 7.93 (d, *J* = 8.1 Hz, 2H), 7.54 (s, 1H), 7.45 (t, *J* = 7.6 Hz, 2H), 7.40 (t, *J* = 7.2, 1.0 Hz, 1H), 7.31 (d, *J* = 8.3 Hz, 2H), 7.07 (dd, *J* = 5.1, 1.4 Hz, 1H), 4.37 (q, *J* = 7.2 Hz, 2H), 4.24 (q, *J* = 7.2 Hz, 1H), 1.71 (d, *J* = 7.3 Hz, 3H), 1.38 (t, *J* = 7.2 Hz, 3H). **^{13}C NMR (151 MHz, $CDCl_3$)** δ 166.5, 158.0, 155.1, 150.0, 149.7, 139.6, 130.1 (2C), 129.2, 129.1, 128.8 (2C), 127.8 (2C), 127.1 (2C), 121.5, 120.0, 61.1, 44.6, 21.1, 14.5. **IR (neat):** 2975, 1713, 1597, 1273, 1179, 1105, 1020, 856, 698 cm^{-1}. **HRMS (ESI)** calculated for $C_{22}H_{22}NO_2$ $[M+H]^+$: 332.1645, found: 332.1651.

2-(4-Methoxyphenyl)-4-(1-(4-methoxyphenyl)ethyl)pyridine (2.28)

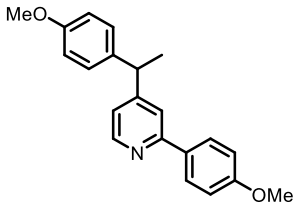

Prepared following general procedure **B** except that the reaction time was 48 hours. **2.28** was obtained after purification by column chromatography (pentane/acetone: 9/1) as a colorless oil (21.8 mg, 68% yield). R_f = 0.30 (pentane: acetone= 19:1). **^{1}H NMR (600 MHz, $CDCl_3$)** δ 8.53 (d, *J* = 5.0 Hz, 1H), 7.90 (d, *J* = 8.7 Hz, 2H), 7.49 (s, 1H), 7.15 (d, *J* = 8.7 Hz, 2H), 7.01 (dd, *J* = 5.2, 1.3 Hz, 1H), 6.98 (d, *J* = 8.9 Hz, 2H), 6.86 (d, *J* = 8.8 Hz, 2H), 4.12 (q, *J* = 7.2 Hz, 1H), 3.85 (s, 3H), 3.79 (s, 3H), 1.66 (d, *J* = 7.3 Hz, 3H). **^{13}C NMR (151 MHz, $CDCl_3$)** δ 160.3, 158.2, 157.2, 156.1, 149.5, 136.6, 132.2, 128.5 (2C), 128.2 (2C), 120.7, 119.1, 114.0 (2C), 114.0 (2C), 55.3, 55.2, 43.6, 21.3. **IR (neat):** 2963, 2932, 1602, 1510, 1463, 1422, 1244, 1175, 1030, 829, 731 cm^{-1}. **HRMS (ESI)** calculated for $C_{21}H_{22}NO_2$ $[M+H]^+$: 320.1645, found: 320.1643.

2-(4-Methoxyphenyl)-4-(1-(4-methoxyphenyl)propyl)pyridine (2.29)

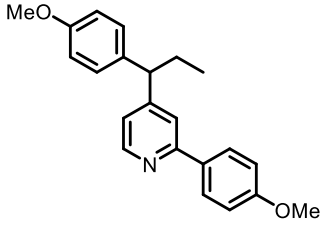

Prepared following general procedure **B** except that the reaction time was 48 hours. **2.29** was obtained after purification by column chromatography (pentane/EtOAc: 9/1) as a colorless oil (12.9 mg, 39% yield). R_f = 0.30 (pentane: acetone= 9:1). **^{1}H NMR (600 MHz, $CDCl_3$)** δ 8.52 (d, *J* = 4.8 Hz, 1H), 7.90 (d, *J* = 8.4 Hz, 2H), 7.50 (s, 1H), 7.16 (d, *J* = 8.1 Hz, 2H), 7.03 (d, *J* = 4.4 Hz, 1H), 6.98 (d, *J* = 8.7 Hz, 2H), 6.85 (d, *J* = 8.7 Hz, 2H), 3.85 (s, 3H), 3.80 – 3.38 (m, 4H), 2.13 –

2.05 (m, 2H), 0.93 (t, *J* = 7.0 Hz, 3H). **^{13}C NMR (151 MHz, $CDCl_3$)** δ 160.5, 158.4, 157.4, 155.2, 149.7, 135.6, 132.4, 129.0 (2C), 128.4 (2C), 121.2, 119.6, 114.2 (2C), 114.1 (2C), 55.5, 55.4, 52.2, 28.3, 12.8. **IR (neat):** 2959, 2078, 1602, 1511, 1463, 1303, 1246, 1176, 1031, 826 cm^{-1}. **HRMS (ESI)** calculated for $C_{22}H_{24}NO_2$ $[M+H]^+$: 334.1802, found: 334.1803.

1-Methyl-3-(1-(2-phenylpyridin-4-yl)ethyl)-1H-indole (2.30)

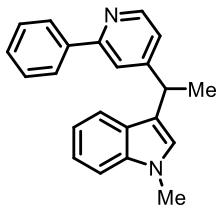

Prepared following general procedure **B** except that the reaction time was 48 hours, **2.30** was obtained after purification by column chromatography (pentane/EtOAc: 92/8) as a pale-yellow oil (10.4 mg, 33% yield). R_f = 0.46 (pentane: EtOAc= 9:1). **^{1}H NMR (400 MHz, $CDCl_3$)** δ 8.57 (d, *J* = 5.1 Hz, 1H), 7.95 (dq, *J* = 6.4, 1.3 Hz, 2H), 7.68 (s, 1H), 7.52 – 7.34 (m, 4H), 7.32 – 7.29 (m, 1H), 7.2 – 7.19 (m, 1H), 7.17 – 7.15 (m, 1H), 7.05 – 7.01 (m, 1H), 6.91 (s, 1H), 4.42 (q, *J* = 7.2 Hz, 1H), 3.79 (s, 3H), 1.75 (d, *J* = 7.2 Hz, 3H). **^{13}C NMR (100 MHz, $CDCl_3$)** δ 157.5, 156.6, 149.7, 139.7, 137.3, 128.7, 128.6 (2C), 127.0 (3C), 126.1, 121.8, 121.4, 119.8, 119.4, 118.9, 118.1, 109.3, 36.6, 32.7, 21.7. **IR (neat):** ν 3053, 2963, 2928, 2874, 1999, 1885, 1805, 1596, 1552, 1472, 1329, 811 cm^{-1}. **HRMS (ESI)** calculated for $C_{22}H_{21}N_2$ $[M+H]^+$: 313.1699, found: 313.1689.

((4-(Cyclohex-2-en-1-yl)pyridin-2-yl)methylene)bis(4,1-phenylene) diacetate (2.31)

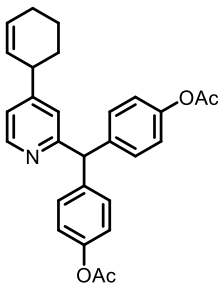

Prepared following general procedure **A**, **2.31** was obtained after purification by column chromatography (pentane/EtOAc: 20/1 to 10/1 to 5/1) as a colorless oil (38.5 mg, 87% yield). R_f = 0.40 (pentane: EtOAc= 2:1). **^{1}H NMR (600 MHz, $CDCl_3$)** δ 8.48 (d, *J* = 5.1 Hz, 1H), 7.19 (dd, *J* = 8.7, 3.0 Hz, 4H), 7.03 – 6.97 (m, 6H), 5.93 – 5.90 (m, 1H), 5.62 (s, 1H), 5.62 – 5.60 (m, 1H), 3.35 – 3.32 (m, 1H), 2.27 (s, 6H), 2.08 – 2.05 (m, 2H), 2.00 – 1.95 (m, 1H), 1.70 – 1.65 (m, 1H), 1.63 – 1.56 (m, 1H), 1.51 –1.45 (m, 1H).**^{13}C NMR (151 MHz, $CDCl_3$)** δ 169.6 (2C), 162.4, 156.5, 149.5, 149.4 (2C), 140.3 (2C), 130.4 (4C), 129.8, 128.2, 123.5, 121.5 (4C), 121.2, 58.1, 41.3, 31.9, 24.9, 21.3, 20.9. **IR (neat):** ν 3022, 2930, 1757, 1598, 1503, 1409, 1368, 1193, 729, 664 cm^{-1}. **HRMS (ESI)** calculated for $C_{28}H_{28}NO_4$ $[M+H]^+$: 442.2013, found: 442.2010.

(*Z*)-((4-(Cyclooct-2-en-1-yl)pyridin-2-yl)methylene)bis(4,1-phenylene) diacetate (2.32)

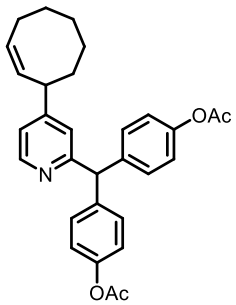

Prepared following general procedure **A**. **2.32** was obtained after purification by column chromatography (pentane/EtOAc: 20/1) as a colorless oil (13.6 mg, 29% yield). R_f = 0.59 (pentane: EtOAc= 3:1). **^{1}H NMR (600 MHz, $CDCl_3$)** δ 8.42 (d, *J* = 5.1 Hz, 1H), 7.19 (s, 1H), 7.12 (d, *J* = 8.3 Hz, 4H), 6.99 (dd, *J* = 5.1, 1.6 Hz, 1H), 6.94 (d, *J* = 8.3 Hz, 4H), 5.70 – 5.63 (m, 1H), 5.53 (s, 1H), 5.43 – 5.40 (m, 1H), 3.62 – 3.58 (m, 1H), 2.29 – 2.22 (m, 1H), 2.21 (s, 6H), 2.09 – 2.02 (m, 1H), 1.76 – 1.62 (m, 3H), 1.59 – 1.46 (m, 3H), 1.42 – 1.34 (m, 1H), 1.34 – 1.26 (m, 1H). **^{13}C NMR (151 MHz, $CDCl_3$)** δ 169.6 (2C), 162.6, 156.3, 149.8, 149.4 (2C), 140.4 (2C), 132.2, 130.6, 130.4 (4C), 123.1, 121.5 (4C), 120.9, 58.3, 42.0, 37.0, 29.5, 26.7, 26.7, 26.0, 21.3. **IR (neat):** ν 3014, 2925, 1758, 1598, 1503, 1445, 1368, 1194, 1013, 911, 749, 729 cm^{-1}. **HRMS (ESI)** calculated for $C_{30}H_{31}NNaO_4$ $[M+Na]^+$:492.2145, found: 492.2145

((4-(1-Phenylethyl)pyridin-2-yl)methylene)bis(4,1-phenylene) diacetate (2.33)

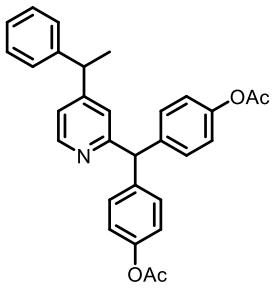

Prepared following general procedure **A**. **2.33** was obtained after purification by column chromatography (pentane/EtOAc: 20/1 to 10/1 to 5/1) as a colorless oil (27.8 mg, 60% yield). R_f = 0.44 (pentane: EtOAc= 5:1). **^{1}H NMR (600 MHz, $CDCl_3$)** δ 8.47 (d, *J* = 5.1 Hz, 1H), 7.29 (t, *J* = 7.6 Hz, 2H), 7.21 (t, *J* = 7.4 Hz, 1H), 7.16 – 7.14 (m, 6H), 7.02 – 6.96 (m, 6H), 5.57 (s, 1H), 4.06 (q, *J* = 7.2 Hz, 1H), 2.28 (s, 6H), 1.58 (d, *J* = 7.2 Hz, 3H). **^{13}C NMR (151 MHz, $CDCl_3$)** δ 169.6 (2C), 162.6, 156.0, 149.8, 149.4 (2C), 144.5, 140.3 (2C), 130.4 (4C), 128.7 (2C), 127.7 (2C), 126.7, 123.3, 121.5 (4C), 121.0, 58.2, 44.4, 21.3, 21.2. **IR (neat):** 2972, 2932, 1756, 1502, 1451, 1367, 1198, 1014, 911, 730, 702 cm^{-1}. **HRMS (ESI)** calculated for $C_{30}H_{27}NNaO_4$ $[M+Na]^+$: 488.1832, found: 488.1829.

((4-(1-Phenylpropyl)pyridin-2-yl)methylene)bis(4,1-phenylene) diacetate (2.34)

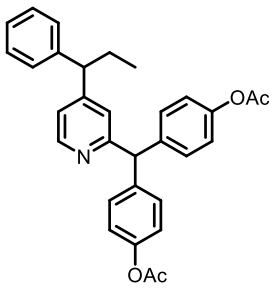

Prepared following general procedure **A**. **2.34** was obtained after purification by column chromatography (pentane/EtOAc: 20/1 to 10/1 to 5/1) as a colorless oil (23.1 mg, 48% yield). R_f = 0.40 (pentane: EtOAc= 5:1). **^{1}H NMR (600 MHz, $CDCl_3$)** δ 8.46 (d, *J* = 5.3 Hz, 1H), 7.28 (t, *J* = 7.6 Hz, 2H), 7.20 (t, *J* = 7.4 Hz, 1H), 7.16 – 7.14 (m, 6H), 7.00-6.99 (m, 6H), 5.59 (s, 1H), 3.72 (t, *J* = 7.7 Hz, 1H), 2.28 (s, 6H), 2.03 – 1.98 (m, 2H), 0.86 (t, *J* = 7.3 Hz, 3H). **^{13}C NMR (151 MHz, $CDCl_3$)** δ 169.6 (2C), 162.5, 155.2, 149.6, 149.4 (2C), 143.1, 140.2 (2C), 130.4 (4C), 128.8 (2C), 128.0 (2C), 126.8, 123.7, 121.5 (4C), 121.3, 58.0, 52.8, 28.1, 21.3, 12.7. **IR (neat):** 3030, 2932, 1756, 1596, 1502, 1454, 1368, 1194, 1014, 911, 731, 701 cm^{-1}. **HRMS (ESI)** calculated for $C_{31}H_{30}NO_4$ $[M+H]^+$: 480.2169, found: 480.2172.

((4-((3R,4S,4aR,5S,7S)-4-(2-((2R,4R)-4-((*tert*-Butyldimethylsilyl)oxy)-6-oxotetrahydro-2H-pyran-2-yl)ethyl)-5-((2,2-dimethylbutanoyl)oxy)-3,7-dimethyl-2,3,4,4a,5,6,7,8-octahydronaphthalen-2-yl)pyridin-2-yl)methylene)bis(4,1-phenylene) diacetate (2.35)

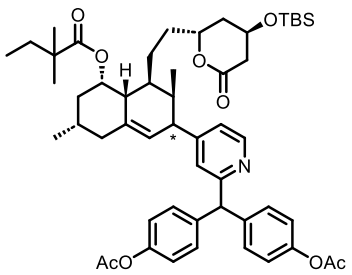

Prepared following general procedure **B**, **2.35** was obtained after purification by column chromatography (pentane/EtOAc: 10/1 to 5/1 to 2/1) as a colorless oil (36.7 mg, 41% yield). R_f = 0.38 (pentane: EtOAc= 2:1). **^{1}H NMR (600 MHz, $CDCl_3$)** δ 8.48 (d, *J* = 5.0 Hz, 1H), 7.20 – 7.13 (m, 4H), 7.10 (d, *J* = 5.0 Hz, 1H), 7.02 – 7.00 (m, 5H), 5.61 (s, 1H), 5.46 (d, *J* = 3.3 Hz, 1H), 5.27 – 5.23 (m, 1H), 4.61 – 4.52 (m, 1H), 4.28 – 4.26 (m, 1H), 3.01 – 3.00 (m, 1H), 2.62 – 2.51 (m, 2H), 2.37 – 2.32 (m, 1H), 2.27 (s, 3H), 2.27 (s, 3H), 2.17 (s, 1H), 2.14 (d, *J* = 13.9 Hz, 1H), 2.11 – 1.98 (m, 3H), 1.91 (dt, *J* = 15.1, 4.4 Hz, 1H), 1.85 – 1.76 (m, 2H), 1.66 – 1.54 (m, 3H), 1.49 – 1.36 (m, 4H), 1.07 (d, *J* = 7.2 Hz, 3H), 1.03 (s, 3H), 1.02 (s, 3H), 0.87 (s, 9H), 0.84 (d, *J* = 6.8 Hz, 3H), 0.70 (t, *J* = 7.4 Hz, 3H), 0.07 (s, 3H), 0.06 (s, 3H). **^{13}C NMR (151 MHz, $CDCl_3$)** δ 177.5, 170.4, 169.5 (2C), 162.5, 155.4 (2C), 149.6, 149.4 (2C), 140.3, 140.2 (2C), 130.4 (2C), 130.3 (2C) 124.0, 122.1, 121.6 (4C), 76.4, 63.7, 58.3, 46.5, 43.3, 42.9, 41.2, 39.4, 36.7, 36.1, 34.0, 33.3, 31.1, 27.9, 25.8 (3C), 25.0, 24.8, 21.3 (2C), 20.8, 18.1, 9.5, 1.2, -4.7 (2C). **IR (neat):** 2931, 1729, 1597, 1555, 1504, 1464, 1369, 1198, 1169, 836, 778, 732 cm^{-1}. **HRMS (ESI)** calculated for $C_{53}H_{71}NNaO_9Si$ $[M+Na]^+$:916.4790, found: 916.4790.

8-(4-(Cyclohex-2-en-1-yl)pyridin-2-yl)-2-methylbenzofuro[2,3-b]pyridine (2.36)

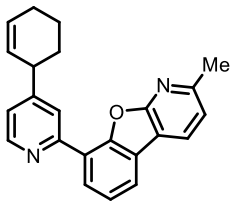

Prepared following general procedure **A**, **2.36** was obtained after purification by column chromatography (pentane/EtOAc: 20/1 to 10/1) as a colorless oil (24.8 mg, 73% yield). R_f =0.32 (pentane: EtOAc= 5:1). **^{1}H NMR (600 MHz, $CDCl_3$)** δ 8.67 (d, *J* = 5.0 Hz, 1H), 8.32 (dd, *J* = 7.7, 1.3 Hz, 1H), 8.29 (s, 1H), 8.18 (d, *J* = 7.7 Hz, 1H), 7.93 (dd, *J* = 7.6, 1.3 Hz, 1H), 7.49 (t, *J* = 7.6 Hz, 1H), 7.23 (d, *J* = 7.7 Hz, 1H), 7.18 (dd, *J* = 5.0, 1.6 Hz, 1H), 6.01 – 5.97 (m, 1H), 5.78 – 5.75 (m, 1H), 3.62 – 3.59 (m, 1H), 2.72 (s, 3H), 2.21 – 2.07 (m, 3H), 1.83 – 1.77 (m, 1H), 1.74 – 1.60 (m, 2H). **^{13}C NMR (151 MHz, $CDCl_3$)** δ 163.2, 156.6, 156.5, 153.3, 151.9, 149.8, 130.0, 129.7, 128.6, 128.3, 124.9, 124.4, 123.9, 123.6, 121.0, 121.3, 119.2, 113.9, 41.6, 32.0, 25.1, 24.7, 21.2. **IR (neat):** 3021, 2928, 1735, 1597, 1486, 1392, 1173, 910, 796, 730 cm^{-1}. **HRMS (ESI)** calculated for $C_{23}H_{21}N_2O$ $[M+H]^+$: 341.1648, found: 341.1644.

tert-Butyl 4-(4-(4-(cyclohex-2-en-1-yl)pyridin-2-yl)-3-fluorobenzyl)-3-methylpiperazine-1-carboxylate (2.37)

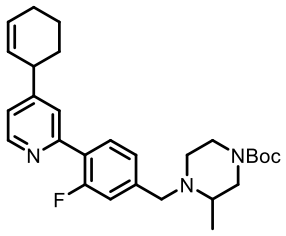

Prepared following general procedure **A**, **2.37** was obtained after purification by column chromatography (pentane/acetone: 20/1) as a yellowish oil (26.8 mg, 58% yield). R_f = 0.41 (pentane: acetone = 5:1). **^{1}H NMR (600 MHz, $CDCl_3$)** δ 8.60 (d, *J* = 5.1 Hz, 1H), 7.88 – 7.85 (m, 1H), 7.61 (s, 1H), 7.21 – 7.15 (m, 2H), 7.11 (dd, *J* = 5.1, 1.7 Hz, 1H), 5.99 – 5.95 (m, 1H), 5.74 – 5.68 (m, 1H), 4.00 (d, *J* = 13.8 Hz, 1H), 3.65 (d, *J* = 12.8 Hz, 2H), 3.50 – 3.42 (m, 1H), 3.24 (d, *J* = 13.6 Hz, 1H), 3.11 (s, 1H), 2.89 (s, 1H), 2.66 (d, *J* = 11.8 Hz, 1H), 2.47 (d, *J* = 9.1 Hz, 1H), 2.14 – 2.10 (m, 2H), 2.08 – 2.04 (m, 1H), 1.80 – 1.72 (m, 1H), 1.70 – 1.63 (m, 1H), 1.62 – 1.57 (m, 1H), 1.46 (s, 9H), 1.12 (d, *J* = 6.2 Hz, 3H). **^{13}C NMR (151 MHz, $CDCl_3$)** δ 160.6 (d, *J* = 249.5 Hz), 156.0, 154.9, 153.5, 149.8, 136.5, 131.0, 129.9, 128.3, 124.9, 124.1 (d, *J* = 8.2 Hz), 122.4, 122.0, 116.5 (d, *J* = 22.7 Hz), 79.7, 57.5, 41.4, 31.9, 31.1, 28.6 (3C), 25.0, 21.0. **^{19}F NMR (565 MHz, $CDCl_3$)** δ -117.7. **IR (neat):** 2971, 2929, 1692, 1597, 1457, 1423, 1366, 1244, 1167, 1128, 1049, 875, 731 cm^{-1}. **HRMS (ESI)** calculated for $C_{28}H_{36}FN_3NaO_2$ $[M+Na]^+$: 488.2684, found:488.2697.

(1S,3S,6S,7R,8S,8aR)-8-(2-((2R,4R)-4-((_tert_-Butyldimethylsilyl)oxy)-6-oxotetrahydro-2H-pyran-2-yl)ethyl)-3,7-dimethyl-6-(2-phenylpyridin-4-yl)-1,2,3,4,6,7,8,8a-octahydronaphthalen-1-yl 2,2-dimethylbutanoate (2.38)

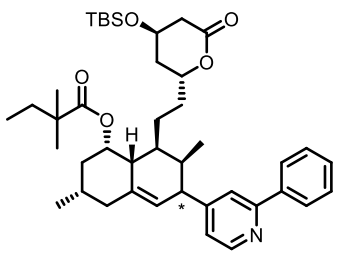

Prepared following general procedure **B** except that the reaction time was 48 hours. **2.38** was obtained after purification by column chromatography (pentane/acetone: 19/1) as a colorless oil (21.9 mg, 32% yield). R_f = 0.30 (pentane: acetone= 19:1). **^{1}H NMR (600 MHz, $CDCl_3$)** δ 8.59 (d, *J* = 5.2 Hz, 1H), 7.99 (dd, *J* = 8.4, 1.5 Hz, 2H), 7.65 (s, 1H), 7.46 (t, *J* = 7.3 Hz, 2H), 7.40 (tt, *J* = 7.3, 1.3 Hz, 1H), 7.18 (d, *J* = 4.9 Hz, 1H), 5.57 (s, 1H), 5.29 (s, 1H), 4.53 (s, 1H), 4.28-4.22 (m, 1H), 3.18 (s, 1H), 2.60-2.50 (m, 2H), 2.43-2.36 (m, 1H), 2.24 – 2.19 (m, 1H), 2.16 – 2.09 (m, 2H), 2.07 – 2.03 (m, 1H), 1.93 (dt, *J* = 15.5, 4.7 Hz, 1H), 1.85 (dq, *J* = 15.2, 2.3 Hz, 1), 1.78 (d, *J* = 14.0 Hz, 1H), 1.69 – 1.60 (m, 2H), 1.60 – 1.51 (m, 1H), 1.50 – 1.44 (m, 1H), 1.42 – 1.33 (m, 2H), 1.32 – 1.27 (m, 2H), 1.17 (d, *J* = 7.4 Hz, 3H), 1.00 – 0.91 (m, 9H), 0.86 (s, 9H), 0.65 (t, *J* = 7.4 Hz, 3H), 0.05 (d, *J* = 7.4 Hz, 6H). **^{13}C NMR (151 MHz, $CDCl_3$)** δ 177.5, 170.5, 157.5, 155.3, 149.6, 139.7, 129.0, 128.8

(3C), 127.1 (2C), 122.6, 120.9, 76.5, 63.6, 46.9, 42.9, 41.3, 39.4, 36.9, 36.3, 36.1, 34.0, 33.1, 32.1, 29.8, 29.4, 27.9, 25.8 (3C), 24.8, 24.7, 24.2, 20.8, 18.1, 14.3, 9.4, -4.8 (2C). **IR (neat):** 2928, 1721, 1597, 1464, 1387, 1358, 1247, 1147, 1080, 912, 835, 777, 730 cm^{-1}. **HRMS (ESI)** calculated for $C_{42}H_{62}NO_5Si$ $[M+H]^+$: 688.4392, found: 688.4369.

4-((8R,9S,10R,13S,14S,17S)-17-((*tert*-Butyldimethylsilyl)oxy)-10,13-dimethyl-2,3,6,7,8,9,10,11,12,13,14,15,16,17-tetradecahydro-1H-cyclopenta[a]phenanthren-3-yl)-2-phenylpyridine (2.39)

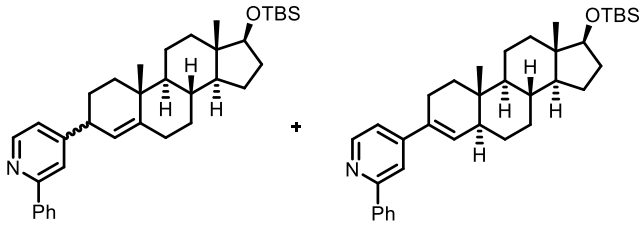

Prepared following general procedure **B**. **2.39** was obtained after purification by column chromatography (pentane/ EtOAc: 19/1) as a colorless oil (30.9 mg, 57% yield). R_f = 0.30 (pentane: EtOAc = 19:1). **^{1}H NMR (600 MHz, $CDCl_3$)** δ 8.61 – 8.55 (m, 1H), 8.01 – 7.95 (m, 2H), 7.62 – 7.38 (m, 4H), 7.19 – 7.02 (m, 1H), 5.62 – 5.27 (m, 1H), 3.63 – 3.29 (m, 2H), 2.39 – 2.24 (m, 1H), 2.21 – 1.97 (m, 2H), 1.95 – 1.69 (m, 4H), 1.62 – 1.35 (m, 5H), 1.15 – 1.06 (m, 3H), 1.04 – 0.79 (m, 16H), 0.78 – 0.68 (m, 3H), 0.04 – -0.03 (m, 6H). (^{13}C NMR reported for the main isomer) **^{13}C NMR (151 MHz, $CDCl_3$)** δ 157.2, 155.8, 149.3, 148.7, 139.8, 128.7, 128.7 (2C), 127.0, 127.0, 122.3, 120.7, 119.0, 81.8, 54.8, 50.5, 43.3, 40.1, 37.5, 37.2, 37.1, 36.2, 33.5, 32.6, 30.9, 29.1 27.1, 25.9 (3C), 23.6, 21.2, 19.5, 11.4, -4.5, -4.8 . **IR** (neat): 2931, 2855, 1598, 1553, 1467, 1447, 1399, 1251, 1205, 1143, 1084, 906, 885, 834, 773, 732, 693; **HRMS (ESI)** calculated for $C_{36}H_{52}NOSi$ $[M+H]^+$: 542.3813, found: 542.3789.

2) Synthetic transformations of 4-(Cyclohex-2-en-1-yl)-2-phenylpyridine 2.3

Synthesis of 4-Cyclohexyl-2-phenylpyridine (2.40)

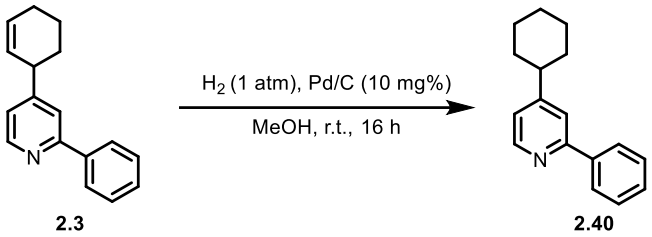

An oven-dried 10 mL round-bottom flask equipped with a magnetic stirring bar was added **2.3** (23.5 mg, 0.1 mmol, 1.0 equiv.), 10% Pd/C (2.4 mg, 10 mg%) and absolute methanol (2 mL). Then the flask was covered by a rubber stopper and sealed with sealing film. This system was degassed 3 times (vacuum/H_2) and filled with H_2 by a hydrogen balloon. The reaction was performed at room temperature for overnight (about 16 hours), after that, the mixture was filtered over Celite®. The filtrate was concentrated on rotary evaporator to provide the crude product. Purified by flash chromatography on silica gel eluted with pentane/EtOAc (50:1), **2.40** could be obtained as a colorless oil (23.7 mg, quantitative).

R_f = 0.50 (pentane: EtOAc= 10:1). **^{1}H NMR (600 MHz, $CDCl_3$)** δ 8.58 (d, *J* = 5.1 Hz, 1H), 8.00 – 7.95 (m, 2H), 7.56 (d, *J* = 1.7 Hz, 1H), 7.47 – 7.46 (m, 2H), 7.42 – 7.38 (m, 1H), 7.08 (dd, *J* = 5.1, 1.7 Hz, 1H), 2.57 – 2.54 (m, 1H), 1.97 – 1.85 (m, 4H), 1.80 – 1.77 (m, 1H), 1.53 – 1.37 (m, 4H), 1.29 – 1.25

(m, 1H). **^{13}C NMR (151 MHz, $CDCl_3$)** δ 157.7, 157.5, 149.7, 140.0, 128.8, 128.8 (2C), 127.1 (2C), 121.0, 119.5, 44.3, 33.7, 26.7, 26.1. **IR (neat):** 3053, 2924, 1732, 1597, 1552, 1445, 1405, 836, 773, 693 cm^{-1}. **HRMS (ESI)** calculated for $C_{17}H_{20}N$ $[M+H]^+$: 238.1590, found: 238.1588.

Synthesis of 4-(7-Oxabicyclo[4.1.0]heptan-2-yl)-2-phenylpyridine (2.41)

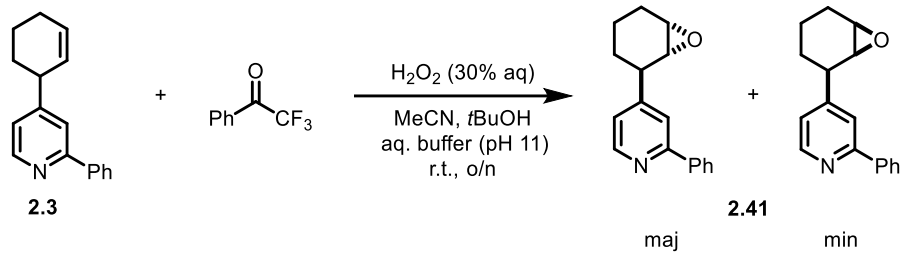

2.3 **2.41**

maj min

A dry 4 mL vial under argon was charged with **2.3** (23.5 mg, 0.1 mmol, 1.0 equiv.), MeCN (0.1 mL), *t*-BuOH (0.1 mL), a freshly prepared buffer solution (0.6 M K_2CO_3, 4 x 10^{-4} M EDTA disodium salt, 0.1 mL), H_2O_2 (30% aqueous solution, 0.2 mL) and 2, 2, 2-trifluoroacetophenone (3.0 µL, 0.02 mmol, 0.2 equiv.). The mixture was stirred at r.t. overnight. Upon completion of the reaction, the mixture was diluted with DCM (5 mL) and water (5 mL). The layers were separated and the aqueous layer was extracted with DCM (3 x 5 mL). The gathered organic layers were washed with brine, dried over $MgSO_4$, filtered and evaporated. Purification by flash column chromatography (pentane/EtOAc: 4/1) afforded **2.41** as a colorless oil (15.0 mg, 60% yield, 2.8/1 d.r.).

R_f = 0.30 (pentane: acetone= 4:1). **^{1}H NMR (600 MHz, $CDCl_3$)** 8.67 – 8.61 (m, 1H, maj+min), 8.02 – 7.96 (m, 2H, maj+min), 7.77 (s, 0.3H, min), 7.61 (s, 0.7H, maj), 7.52 – 7.38 (m, 3H, maj+min), 7.27 (d, *J* = 5.3 Hz, 0.3H, min), 7.14 (d, *J* = 4.9 Hz, 0.7H, maj), 3.35 (s, 0.7H, maj), 3.31 (d, *J* = 3.7 Hz, 0.3H, min), 3.26 (t, *J* = 4.5 Hz, 0.3H, min), 3.23 – 3.18 (m, 1.5H, maj), 3.05 (dd, *J* = 10.4, 5.7 Hz, 0.3H, min), 2.19 (dt, *J* = 15.2, 4.7 Hz, 0.7H, maj), 2.08 – 2.01 (m, 0.3H, min), 1.94 – 1.84 (m, 2H, maj+min), 1.72 – 1.58 (m, 1H, maj+min), 1.50 – 1.45 (m, 1H, maj+min), 1.36 – 1.28 (m, 1H, maj+min). **^{13}C NMR (151 MHz, $CDCl_3$)** 158.1 (maj), 157.9 (min), 153.9 (min), 153.7 (maj), 150.1 (maj), 149.9 (min), 139.7 (min), 139.5 (maj), 129.2 (maj), 129.0 (min), 128.9 (2C, maj), 128.8 (2C, min), 127.2 (2C, min), 127.1 (2C, maj), 121.9 (min), 121.7 (maj), 120.3 (maj), 55.3 (maj), 55.3 (min), 52.8 (maj), 52.1 (min), 42.6 (min), 41.2 (maj), 29.3 (maj), 27.0 (min), 24.5 (maj), 23.1 (min), 21.3 (min), 16.9 (maj) **IR (neat):** v 2929, 1724, 1599, 1553, 1445, 1406, 1260, 909, 831, 775, 734, 694 cm^{-1}. **HRMS (ESI)** calculated for $C_{17}H_{18}NO$ $[M+H]^+$: 252.1383, found: 252.1388.

Synthesis of 4-(Cyclohex-1-en-1-yl)-2-phenylpyridine (2.42)

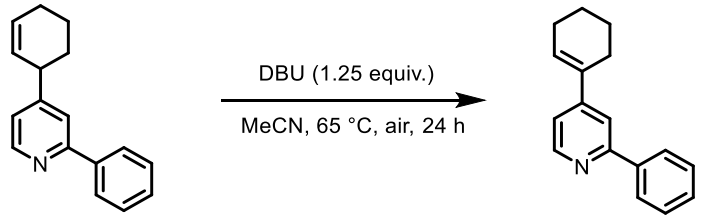

2.3 **2.42**

A 4 mL vial, under air, was charge with **2.3** (23.5 mg, 0.1 mmol, 1.0 equiv.), MeCN (0.5 mL) and DBU (15.0 µL, 0.1 mmol, 1 equiv.). The mixture was stirred for 24 h at 65 °C. Upon completion, the reaction was quenched by addition of a saturated solution of NH_4Cl (5 mL). The aqueous layer was

extracted with DCM (3 x 5 mL). The gathered organic layer were washed with brine, dried over $MgSO_4$, filtered and evaporated. Purification by flash column chromatography (pentane/EtOAc: 9/1) afforded **2.42** as a colorless oil (12.0 mg, 50% yield).

R_f = 0.35 (pentane: EtOAc= 9:1). **^{1}H NMR (600 MHz, $CDCl_3$)** δ 8.59 (d, *J* = 5.2 Hz, 1H), 7.98 (d, *J* = 7.5 Hz, 2H), 7.69 (s, 1H), 7.47 (t, *J* = 7.3 Hz, 2H), 7.41 (t, *J* = 7.3 Hz, 1H), 7.21 (dd, *J* = 2.0, 1.0 Hz, 1H), 6.42 (br s, 1H), 2.48 – 2.42 (m, 2H), 2.29 – 2.24 (m, 2H), 1.85 – 1.79 (m, 2H), 1.74 – 1.67 (m, 2H). **^{13}C NMR (151 MHz, $CDCl_3$)** δ 157.7, 150.6, 149.7, 140.0, 134.9, 128.9, 128.8 (2C), 128.6, 127.1 (2C), 118.3, 116.8, 26.8, 26.1, 22.9, 22.0. **IR (neat):** 3029, 2926, 1726, 1641, 1594, 1539, 1473, 828, 735, 693 cm^{-1}. **HRMS (ESI)** calculated for $C_{17}H_{18}N$ $[M+H]^+$: 236.1434, found: 236.1431.

Synthesis of 3-(2-Phenylpyridin-4-yl)cyclohex-2-en-1-one (2.43)

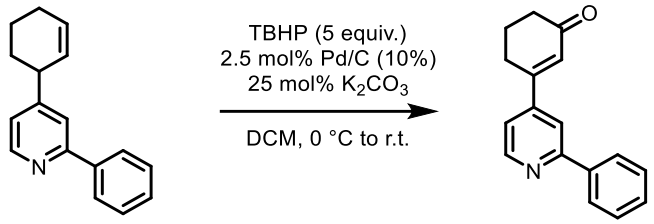

2.3 **2.43**

A 2 mL vial under argon was charged with **2.3** (23.5 mg, 0.1 mmol, 1.0 equiv.) in DCM (1 mL) at 0 °C, followed by Pd/C (2.8 mg, 2.5 x 10^{-6} mmol, 0.025 equiv.), K_2CO_3 (3.5 mg, 0.0025 mmol, 0.25 equiv.) and *tert*-butyl hydroperoxide (0.1 mL, 0.5 mmol, 5.0 equiv.). The mixture was stirred overnight letting the temperature raise to r.t. Then, the mixture was filtered over a short pad of Celite® and purified by flash column chromatography (pentane/EtOAc: 4/1) to afford **2.43** as a white solid (9.5 mg, 38% yield).

R_f = 0.28 (pentane: EtOAc= 5:1). **^{1}H NMR (600 MHz, $CDCl_3$)** δ 8.74 (dd, *J* = 5.1, 0.8 Hz, 1H), 8.04 – 7.97 (m, 2H), 7.79 (dd, *J* = 1.8, 0.8 Hz, 1H), 7.52 – 7.47 (m, 2H), 7.47 – 7.42 (m, 1H), 7.31 (dd, *J* = 5.2, 1.7 Hz, 1H), 6.54 – 6.53 (m, 1H), 2.81 (td, *J* = 6.0, 1.6 Hz, 2H), 2.54 (td, *J* = 7.5, 6.0 Hz, 2H), 2.23 – 2.19 (m, 2H). **^{13}C NMR (151 MHz, $CDCl_3$)** δ 199.5, 158.6, 157.3, 150.5, 147.3, 139.1, 129.5, 129.0 (2C), 127.6, 127.1 (2C), 118.8, 117.3, 37.4, 27.8, 22.8. **IR (neat):** ν 3047, 2930, 1661, 1594, 1540, 1445, 1403, 853, 774, 738, 694 cm^{-1}. **HRMS (ESI)** calculated for $C_{17}H_{15}NNaO$ $[M+Na]^+$: 272.1046, found: 272.1047.

5.2.3 Mechanistic experiments

1) Deuterium labelling experiments

Diethyl 2,6-dimethyl-1,4-dihydropyridine-3,5-dicarboxylate-4,4-*d*$_2$[191]

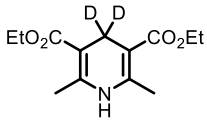

Ethyl acetoacetate (1.0 g, 8.0 mmol, 4.0 eq.), ammonium acetate (0.3 g, 4.0 mmol, 2.0 eq) and paraformaldehyde *d2* (0.06 g, 2.0 mmol, 1.0 eq) were dissolved in water (4.0 mL). The mixture was stirred at 86°C for 3 hours. The crude was then filtered and the solid residue washed with water and cold Et_2O. The resulting yellow solid was the dried under high vacuum (263 mg, 52%). **^{1}H NMR (600 MHz, $CDCl_3$)** δ 5.09 (s, 1H), 4.17 (q, *J* = 7.1 Hz, 4H), 2.29 (s, 6H), 1.28 (t, *J* = 7.1 Hz, 6H).

Diethyl 2,6-dimethyl-1,4-dihydropyridine-3,5-dicarboxylate-1,4,4-*d*$_3$[191]

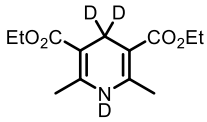

The C^4-D HEH (0.4 mmol) previously prepared was suspended in CD_3OD (1 mL) and the resulting mixture was stirred overnight under argon atmosphere. The solvent was then evaporated to afford the product as a yellow solid (0.1 g, quant.). **^{1}H NMR (600 MHz, $CDCl_3$)** δ 5.09 (s, 0.55H), 4.17 (q, *J* = 7.1 Hz, 4H), 2.19 (s, 6H), 1.28 (t, *J* = 7.1 Hz, 6H).

Reactions with deuterated Hantzsch esters

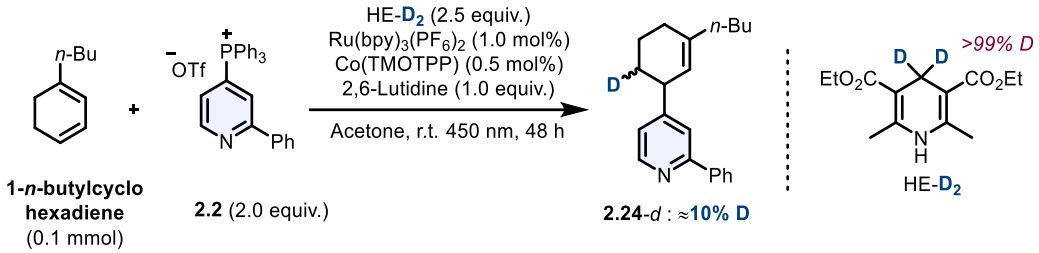

1-*n*-butylcyclo hexadiene (0.1 mmol)

2.2 (2.0 equiv.)

2.24-*d* : ≈**10% D**

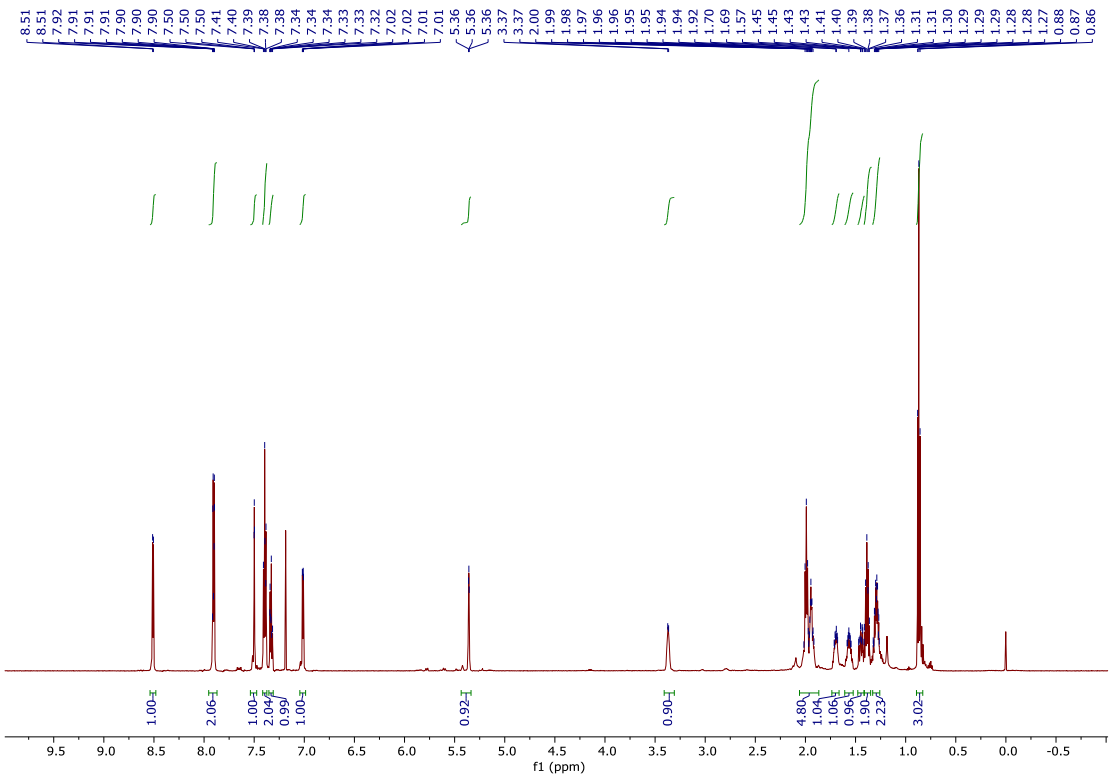
8.51 8.51 7.92 7.91 7.91 7.91 7.90 7.90 7.90 7.50 7.50 7.50 7.41 7.40 7.39 7.38 7.38 7.34 7.34 7.34 7.33 7.33 7.32 7.02 7.02 7.01 7.01 5.36 5.36 5.36 3.37 3.37 2.00 1.99 1.98 1.97 1.96 1.96 1.95 1.95 1.94 1.94 1.92 1.70 1.69 1.57 1.45 1.45 1.43 1.43 1.41 1.40 1.39 1.38 1.38 1.37 1.36 1.31 1.30 1.29 1.29 1.28 1.28 1.27 0.88 0.87 0.86
1.00 2.06 1.00 2.04 0.99 1.00 0.92 0.90 4.80 1.04 1.06 0.96 1.90 2.23 3.02
9.5 9.0 8.5 8.0 7.5 7.0 6.5 6.0 5.5 5.0 4.5 4.0 3.5 3.0 2.5 2.0 1.5 1.0 0.5 0.0 -0.5
f1 (ppm)

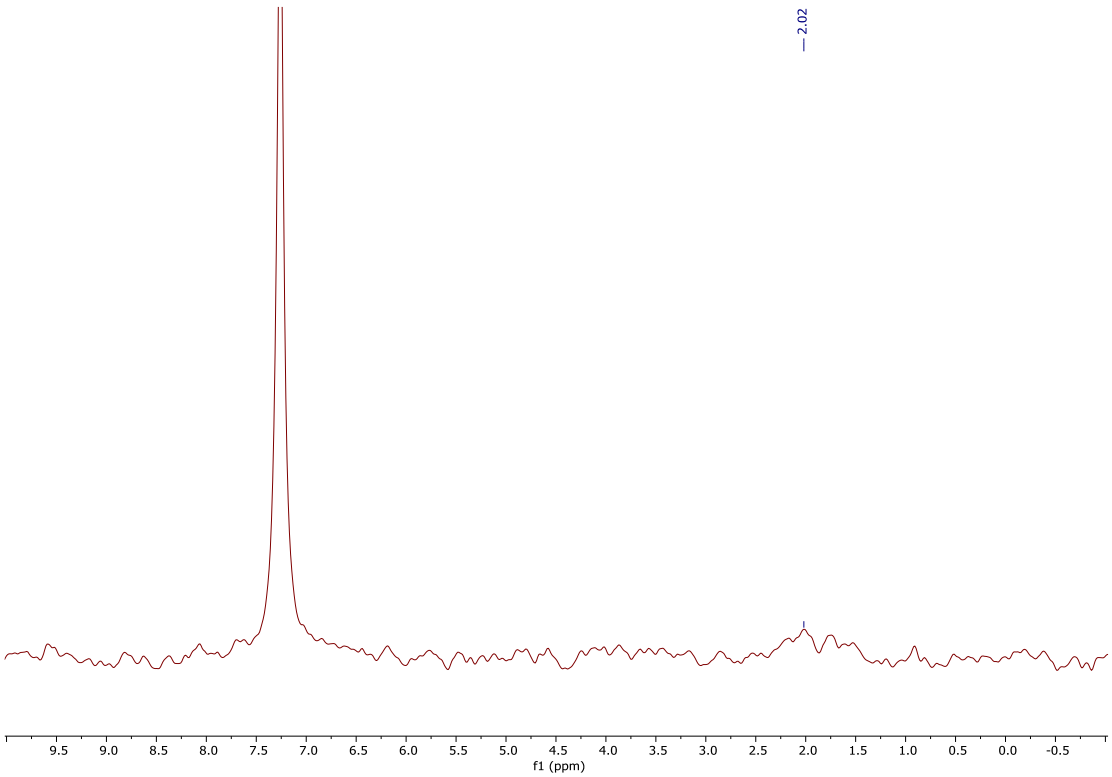
2.02
9.5 9.0 8.5 8.0 7.5 7.0 6.5 6.0 5.5 5.0 4.5 4.0 3.5 3.0 2.5 2.0 1.5 1.0 0.5 0.0 -0.5
f1 (ppm)

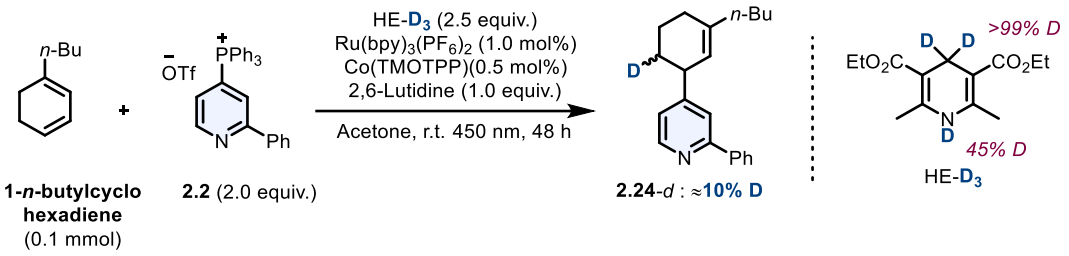

1-*n*-butylcyclo hexadiene (0.1 mmol)

2.2 (2.0 equiv.)

2.24-*d* : ≈**10% D**

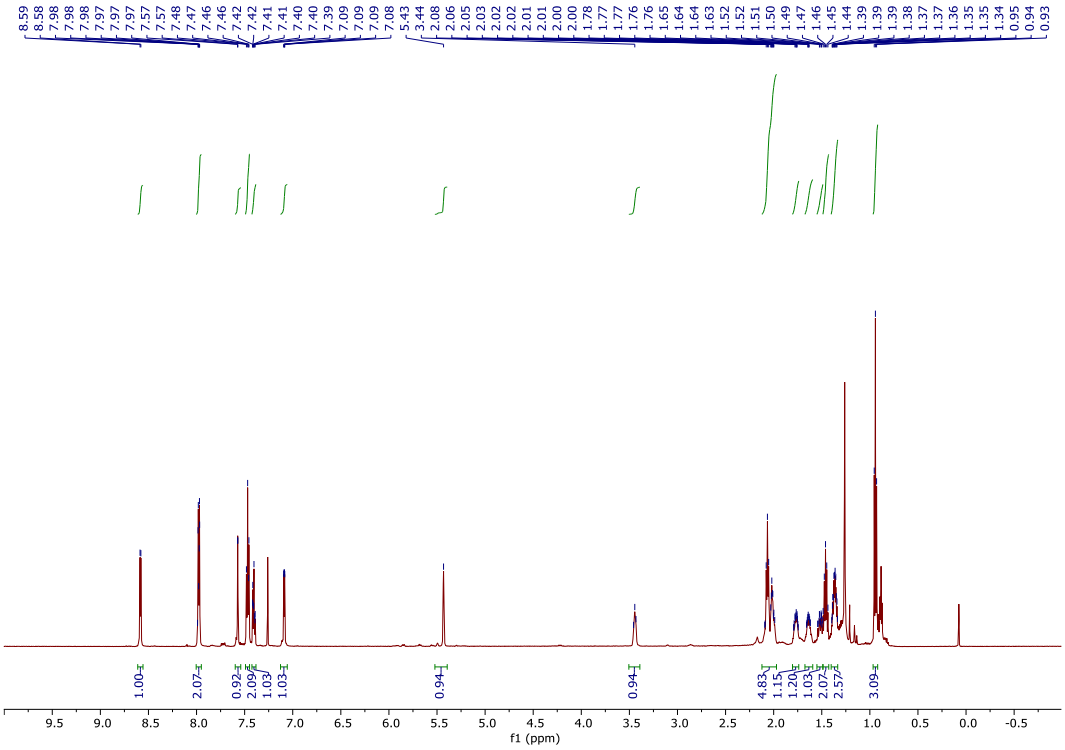

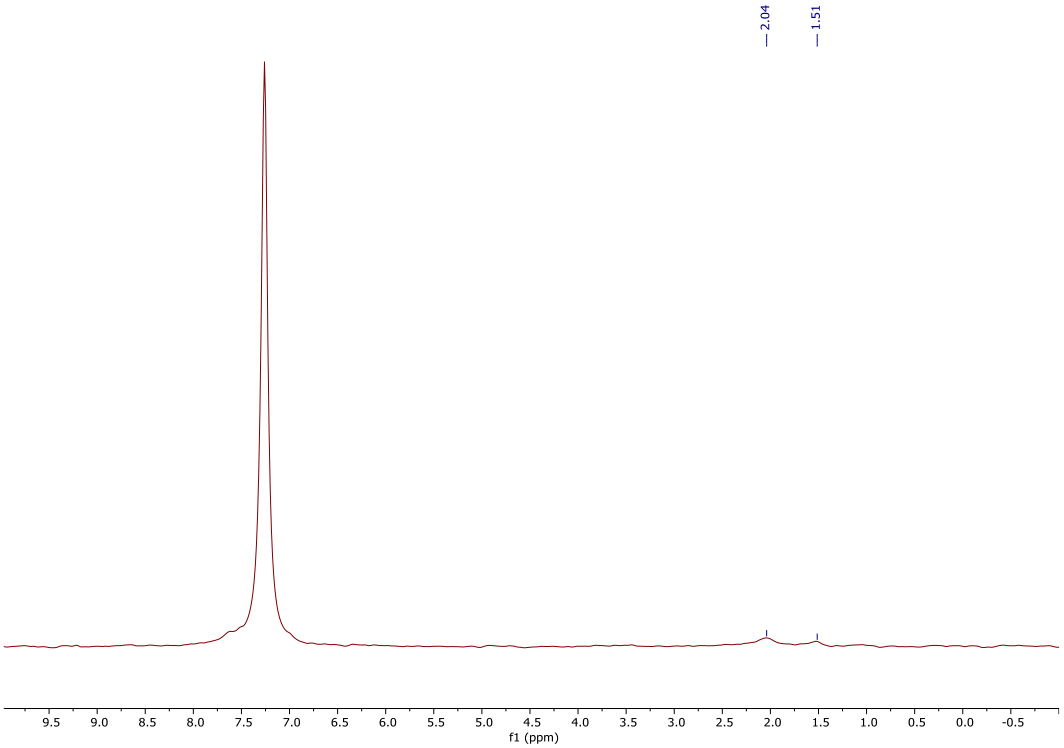

Reactions using deuterated water as additive

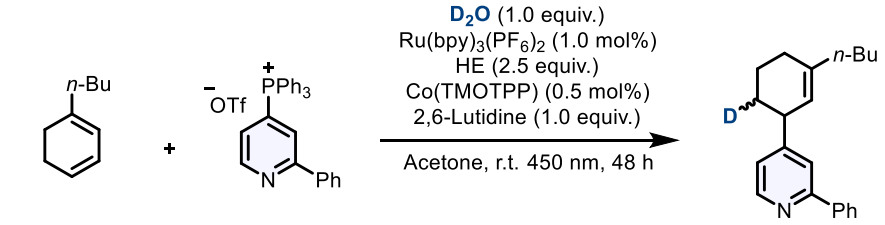

1-*n*-butylcyclo hexadiene (0.1 mmol)

2.2 (2.0 equiv.)

2.24-*d* : ≈**30% D**

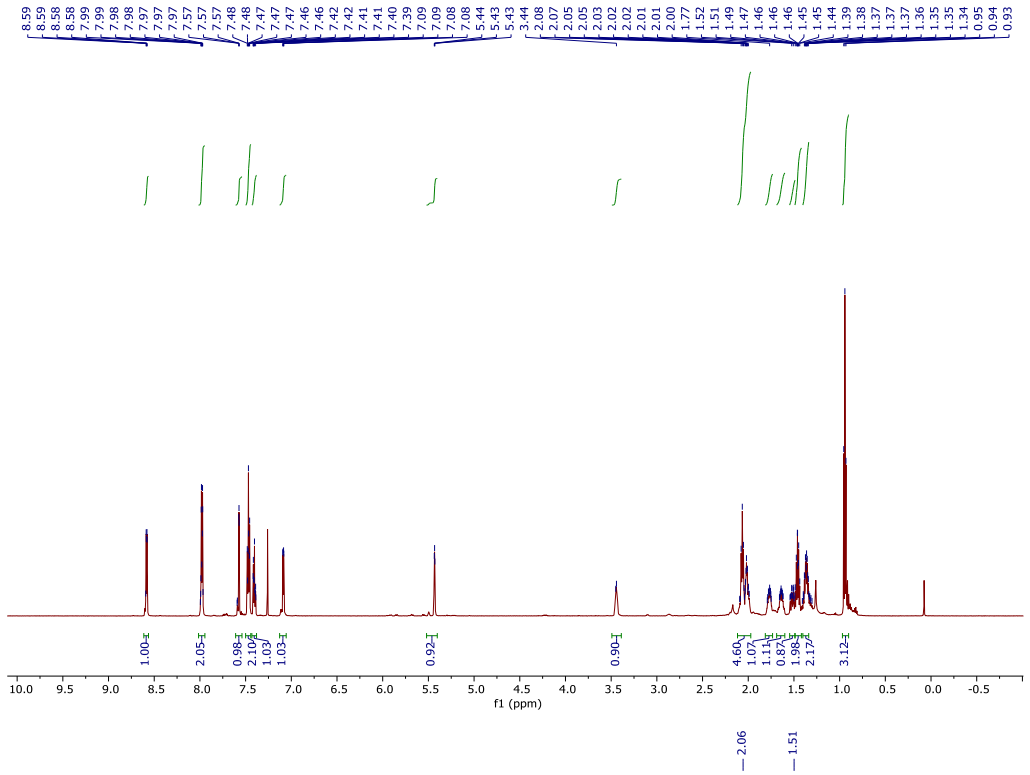

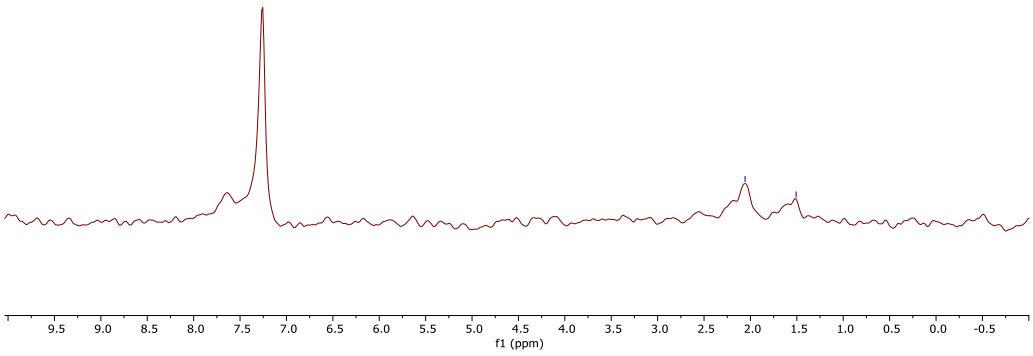

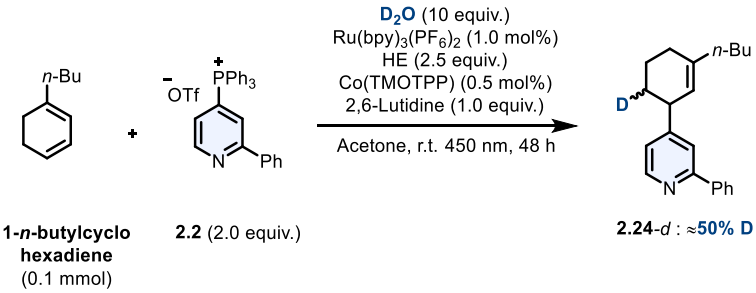

1-*n*-butylcyclo hexadiene (0.1 mmol)

2.2 (2.0 equiv.)

2.24-*d* : ≈**50% D**

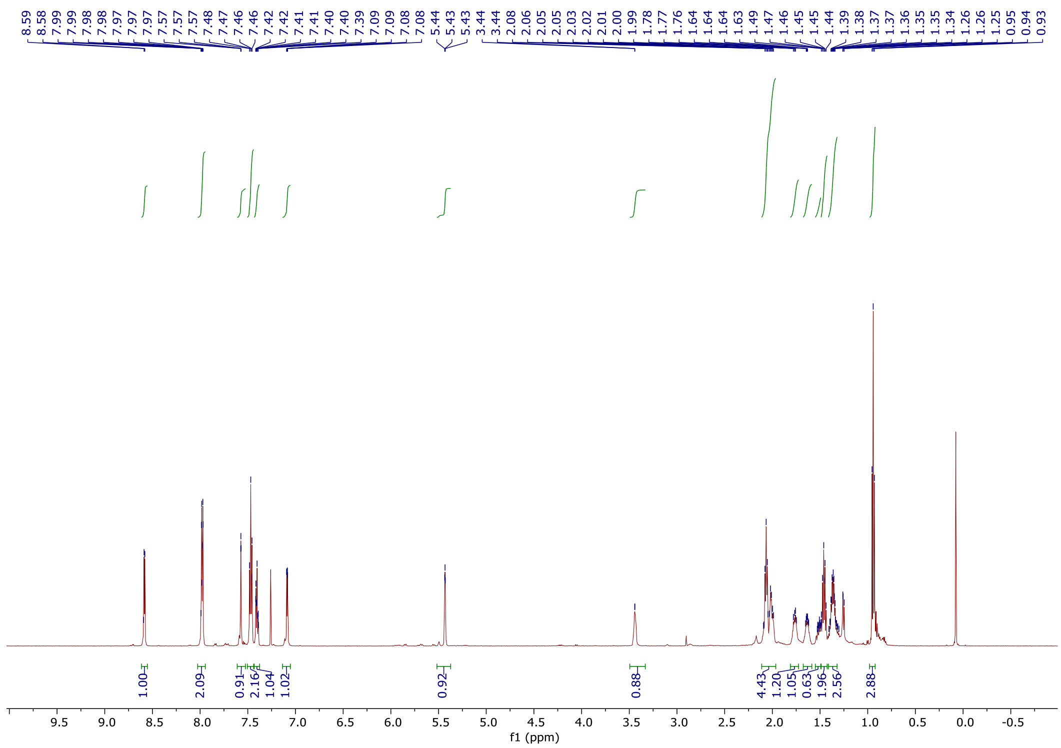
8.59 8.58 7.99 7.99 7.98 7.98 7.97 7.97 7.97 7.57 7.57 7.57 7.48 7.47 7.46 7.46 7.42 7.42 7.41 7.41 7.40 7.40 7.39 7.09 7.09 7.08 7.08 5.44 5.43 5.43 3.44 3.44 2.08 2.06 2.05 2.05 2.03 2.02 2.01 2.00 1.99 1.78 1.77 1.76 1.64 1.64 1.64 1.63 1.49 1.47 1.46 1.45 1.45 1.44 1.39 1.38 1.37 1.37 1.36 1.35 1.35 1.34 1.26 1.25 0.95 0.94 0.93
1.00
2.09
0.91
2.16
1.04
1.02
0.92
0.88
4.43
1.20
1.05
0.63
1.96
2.56
2.88
f1 (ppm)

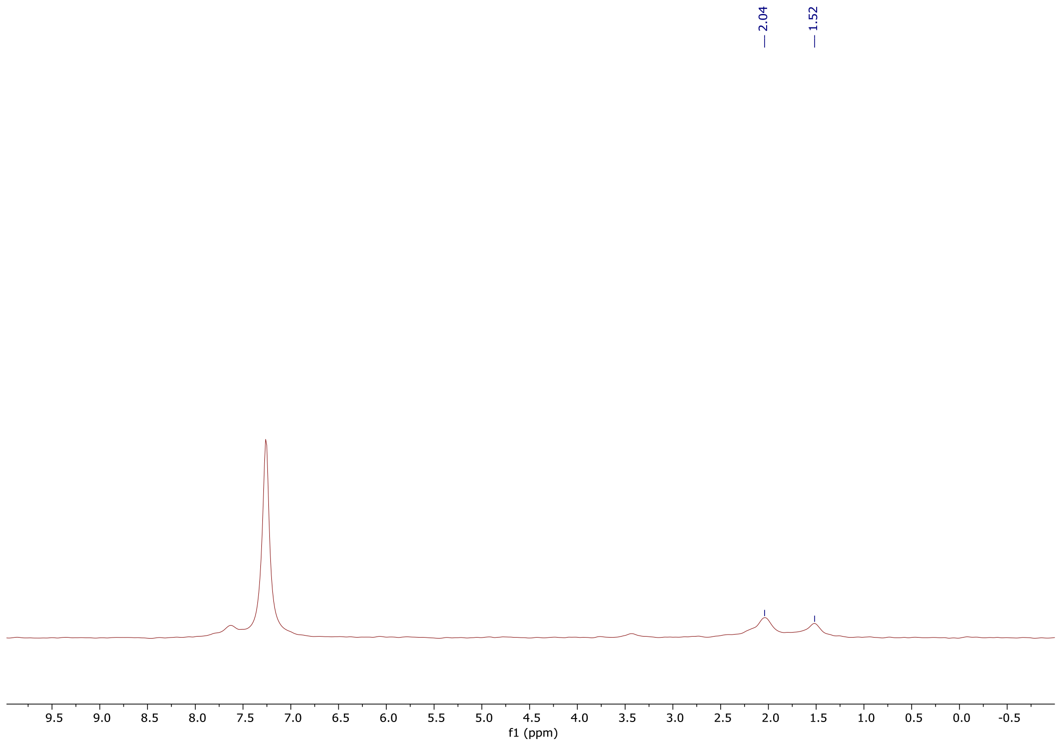
2.04
1.52
f1 (ppm)

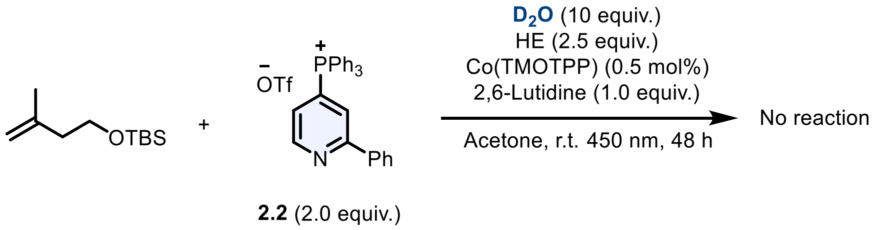
OTBS
+
OTf
PPh3
N
Ph
2.2 (2.0 equiv.)
D2O (10 equiv.)
HE (2.5 equiv.)
Co(TMOTPP) (0.5 mol%)
2,6-Lutidine (1.0 equiv.)
Acetone, r.t. 450 nm, 48 h
No reaction

No isomerization products and no deuterium incorporation in the recovered olefin was observed.

Reactions using deuterated acetone as solvent

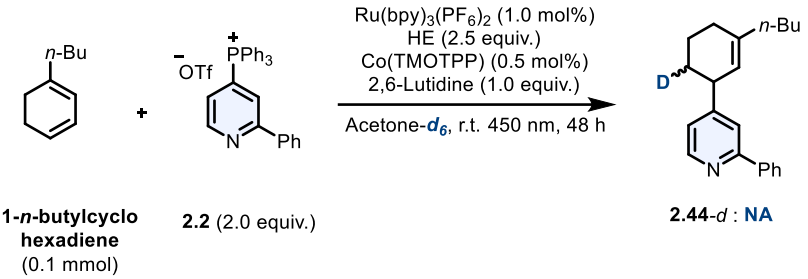

1-*n*-butylcyclo hexadiene (0.1 mmol)

2.2 (2.0 equiv.)

2.44-*d* : **NA**

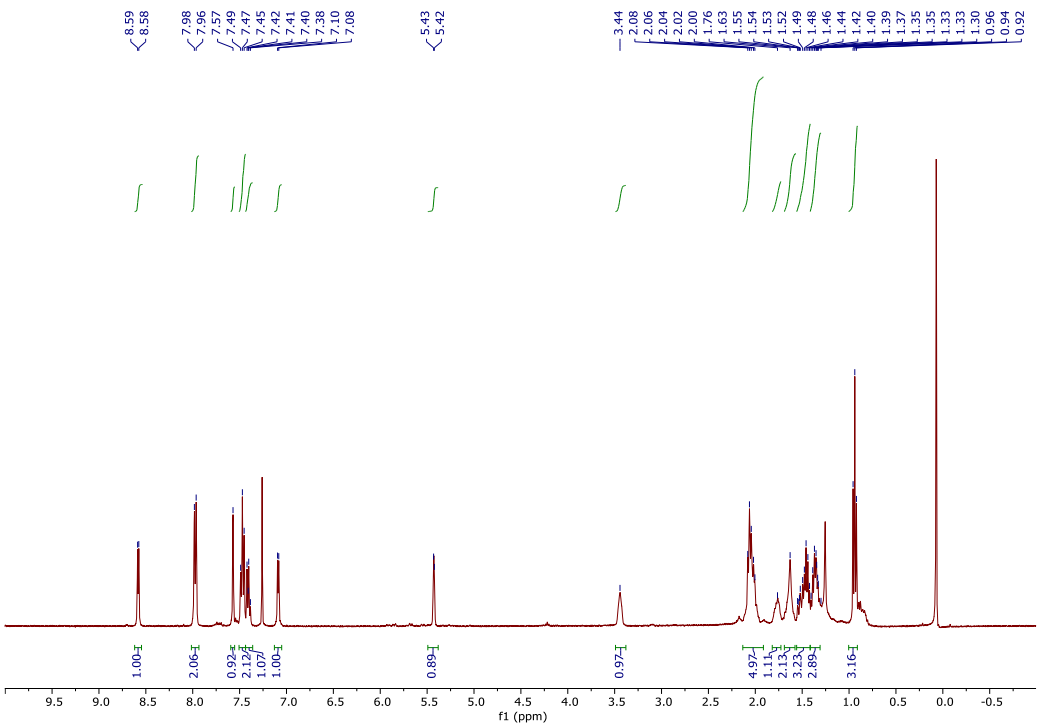

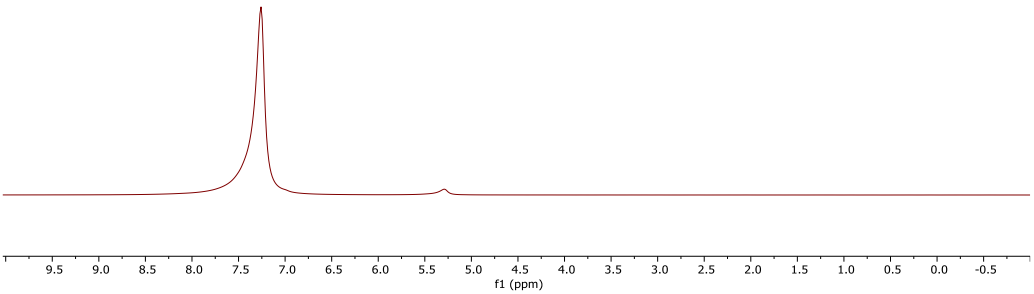
9.5
9.0
8.5
8.0
7.5
7.0
6.5
6.0
5.5
5.0
4.5
4.0
3.5
3.0
2.5
2.0
1.5
1.0
0.5
0.0
-0.5
f1 (ppm)

Reaction with styrene-d_8

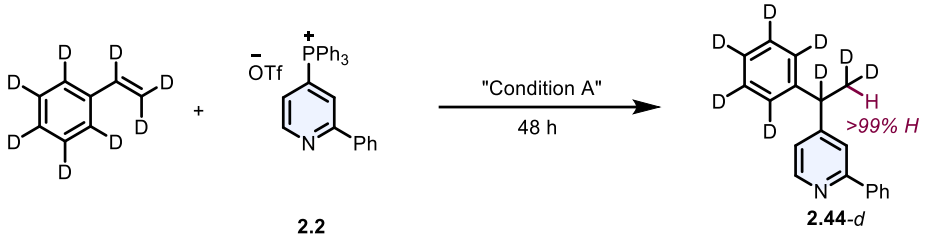

2.2 **2.44-*d***

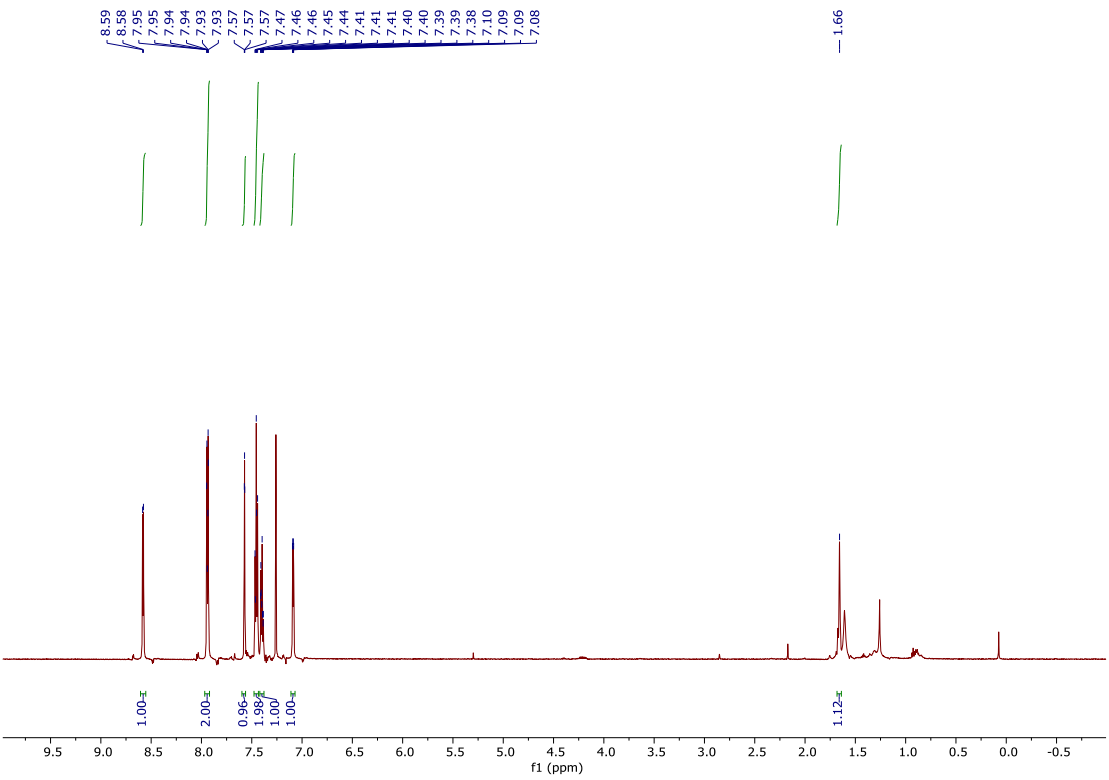

No deuterium / proton exchange was observed on the recovered styrene, consistent with irreversible HAT.

2) The reaction between cyclohexene and phosphonium salt 2.2

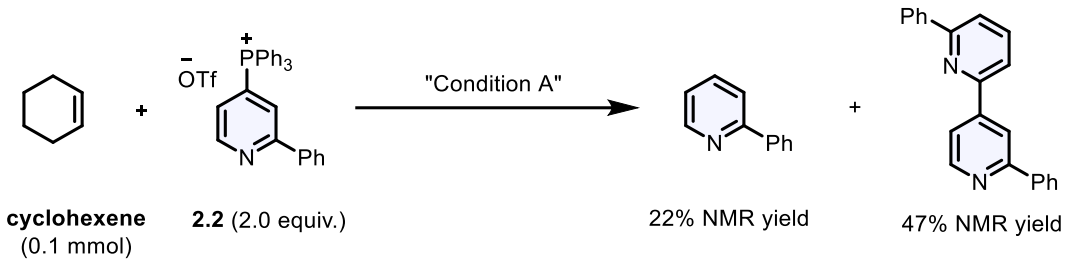

cyclohexene (0.1 mmol) **2.2** (2.0 equiv.) 22% NMR yield 47% NMR yield

2',6-diphenyl-2,4'-bipyridine

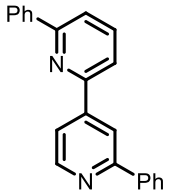

^{1}H NMR (600 MHz, $CDCl_3$) δ 8.83 (dd, *J* = 5.1, 0.6 Hz, 1H), 8.49 (dd, *J* = 1.4, 0.7 Hz, 1H), 8.18 – 8.15 (m, 2H), 8.13 – 8.10 (m, 2H), 7.96 (dd, *J* = 5.1, 1.6 Hz, 1H), 7.90 (dd, *J* – 8.0, 7.5 Hz, 1H), 7.83 – 7.81 (m, 2H), 7.55 – 7.51 (m, 4H), 7.49 – 7.43 (m, 2H).**^{13}C NMR (151 MHz, $CDCl_3$)** δ 158.4, 157.5, 154.6, 150.4, 147.6, 139.7, 139.1, 138.0, 129.5, 129.2, 129.0 (2C), 128.9 (2C), 127.3 (2C), 127.2 (2C), 120.5, 119.8, 119.3, 118.4. **IR (neat):** ν 2923, 1727, 1591, 1543, 1443, 1287, 1101, 764, 696 cm^{-1}. **HRMS (ESI)** calculated for $C_{22}H_{17}N_2$ $[M+H]^+$: 309.1386, found: 309.1386.

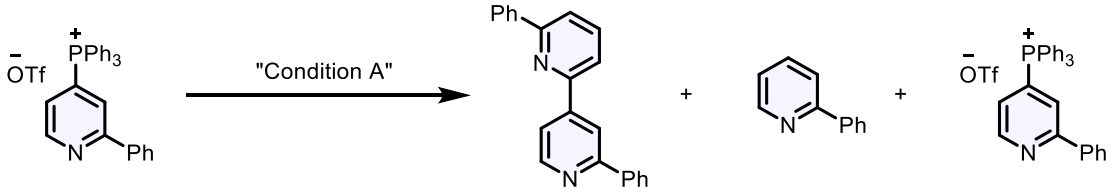

2.2 45% NMR yield 22% NMR yield 2%

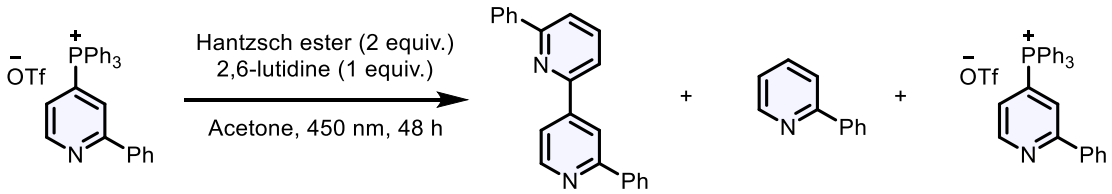

2.2 28% NMR yield 22% NMR yield 26%

The proposed mechanism as below (the OTf anion was omitted)

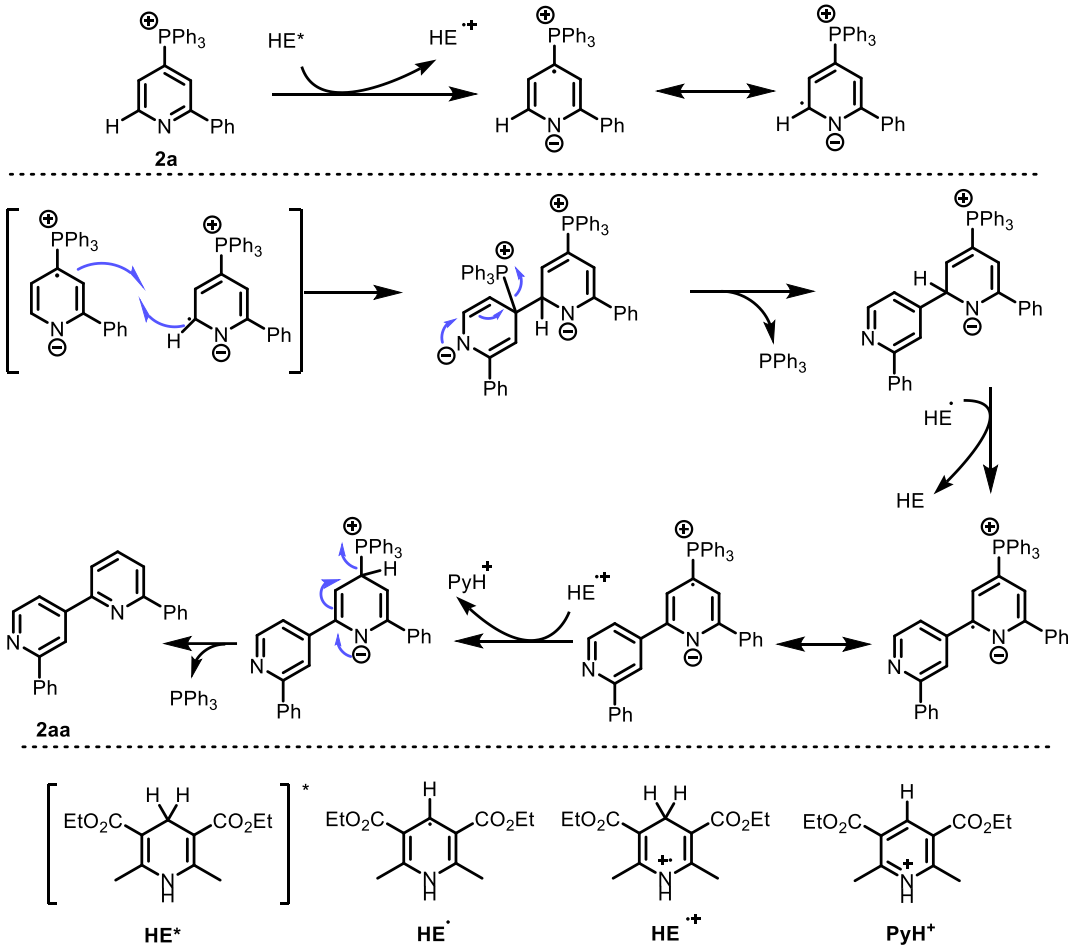
PPh3
HE*
HE
Ph
H
N
2a
Ph3P
PPh3
HE
PyH
2aa

EtO2C
CO2Et
H
N
HE*
HE
PyH+

3) UV-Vis absorption experiments

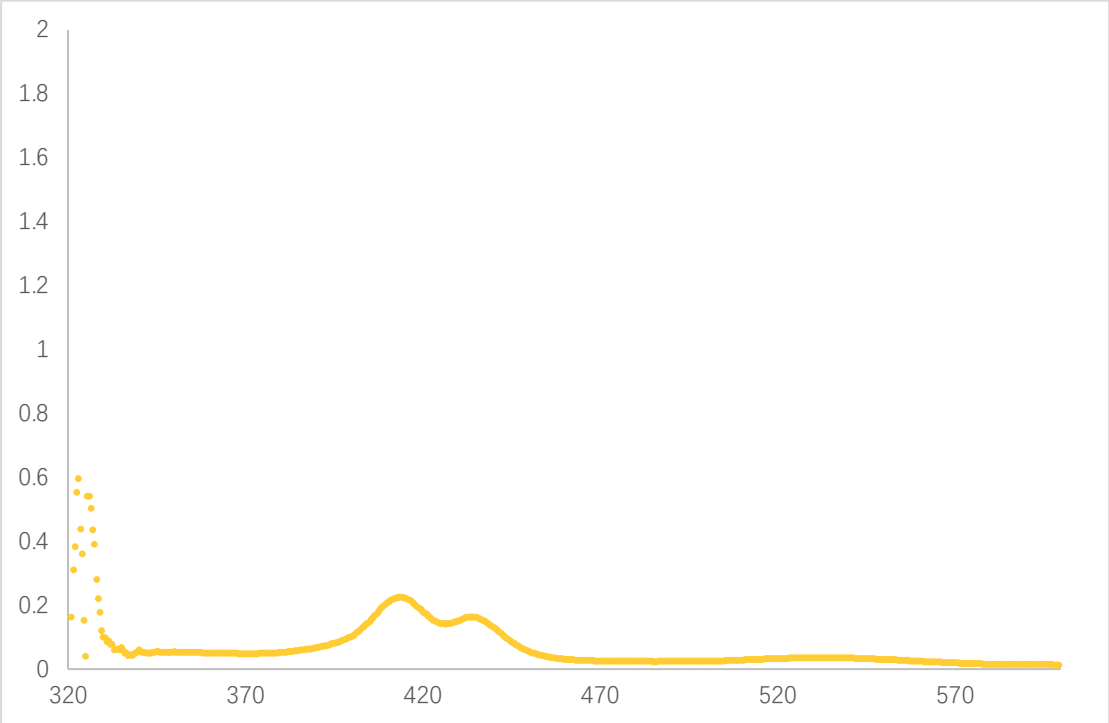

Figure 5.1 UV-Vis Absorption of Co(TMOTPP) (Concentration: 0.005 mM)

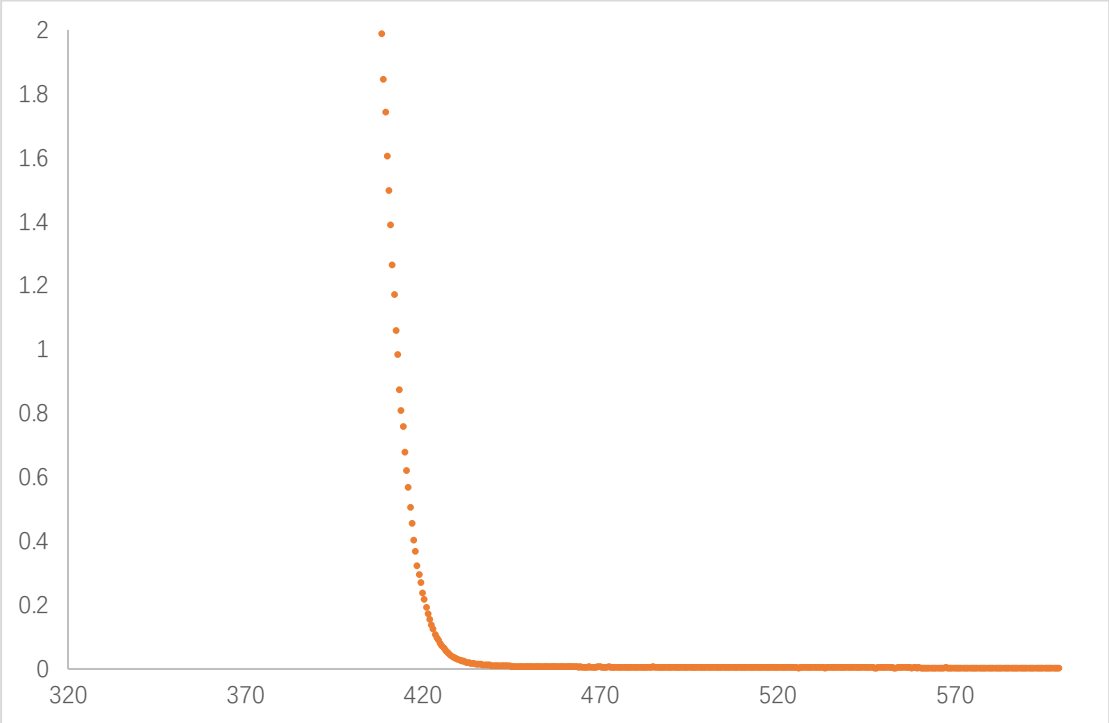

Figure 5.2 UV-Vis Absorption of Hantzsch ester (Concentration: 2.5 mM)

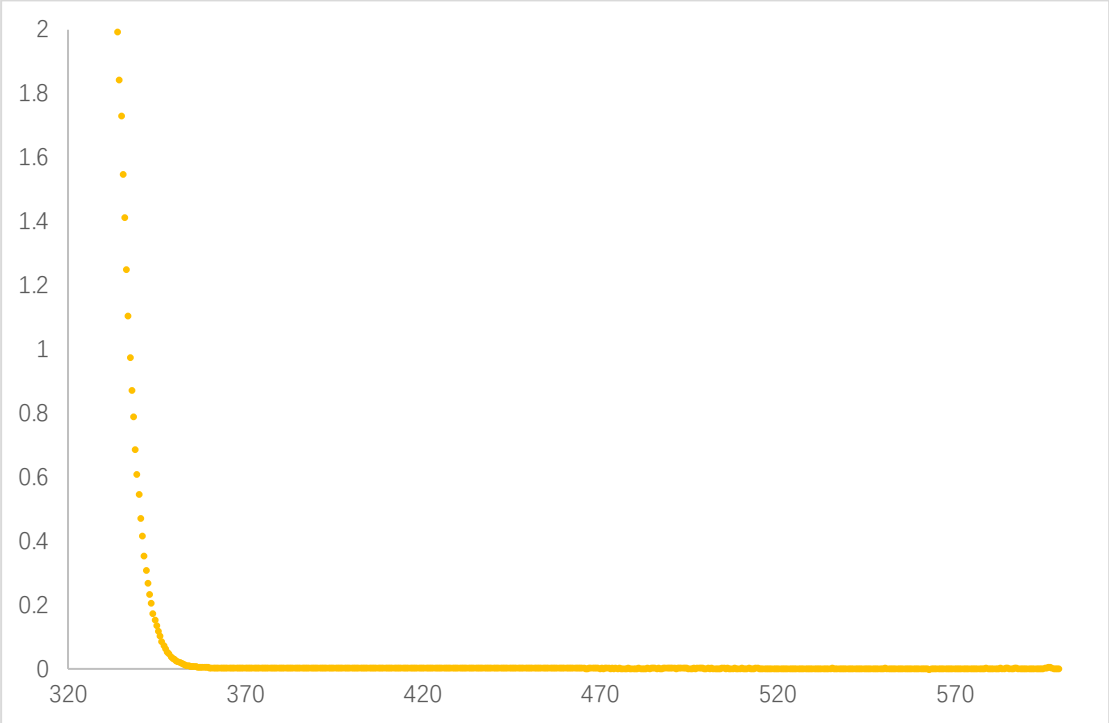

Figure 5.3 UV-Vis Absorption of **2.2** (Concentration: 2 mM)

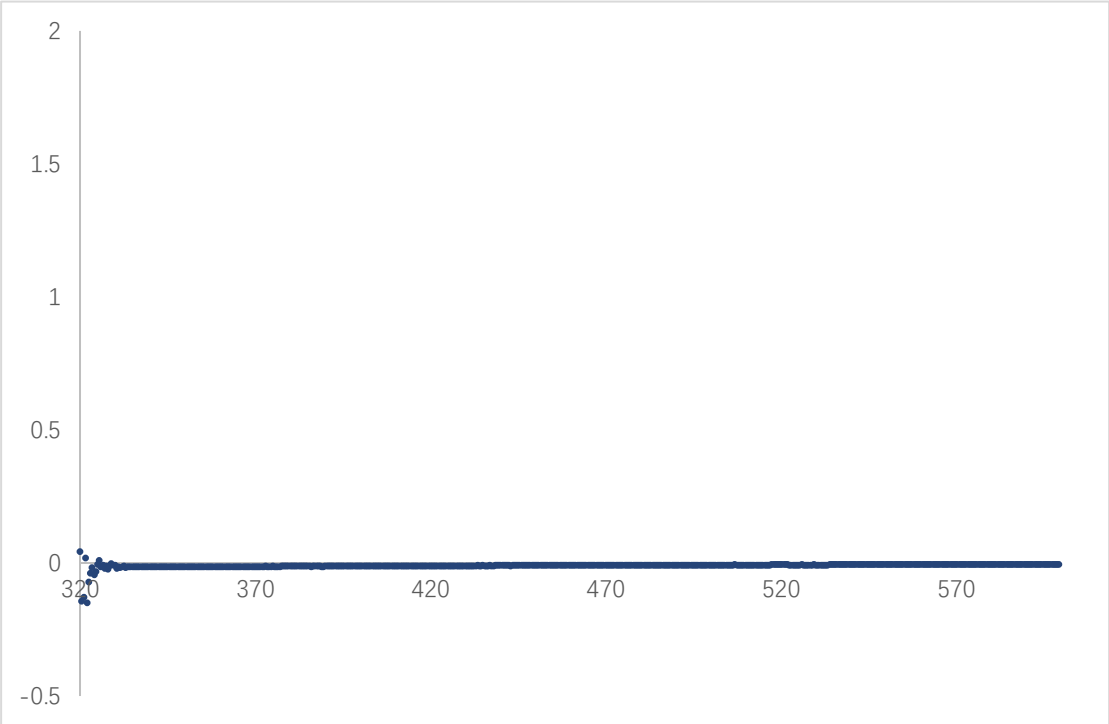

Figure 5.4 UV-Vis Absorption of **2.1** (Concentration: 1 mM)

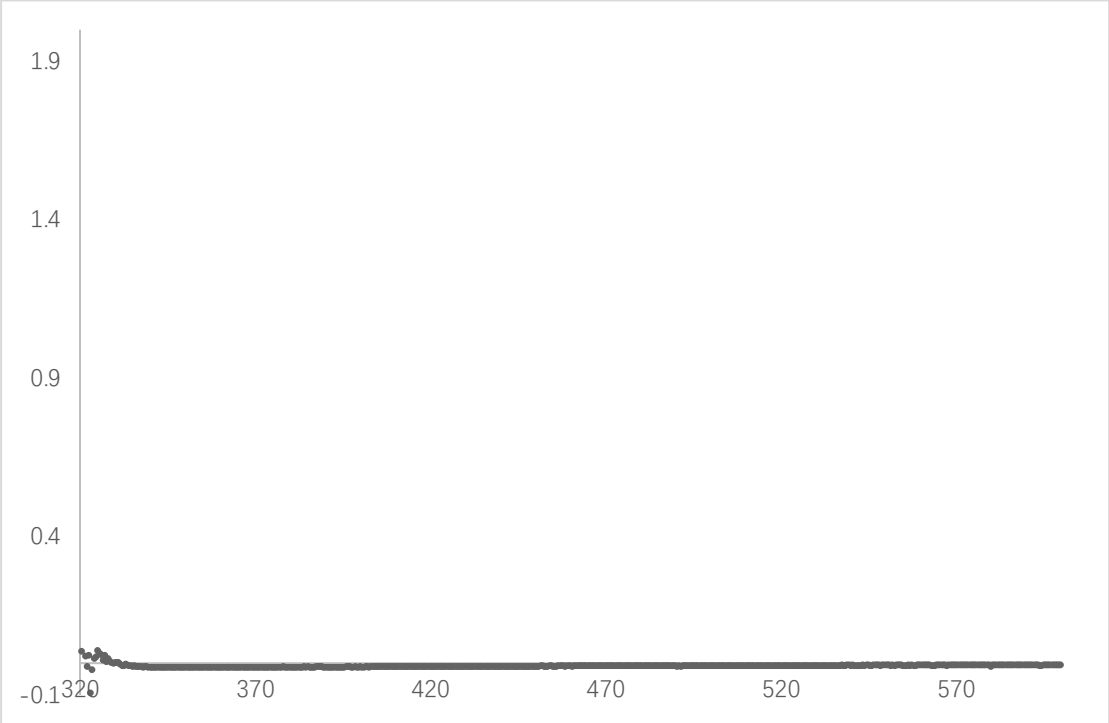

Figure 5.5 UV-Vis Absorption of 2,6-lutidine (Concentration: 1 mM)

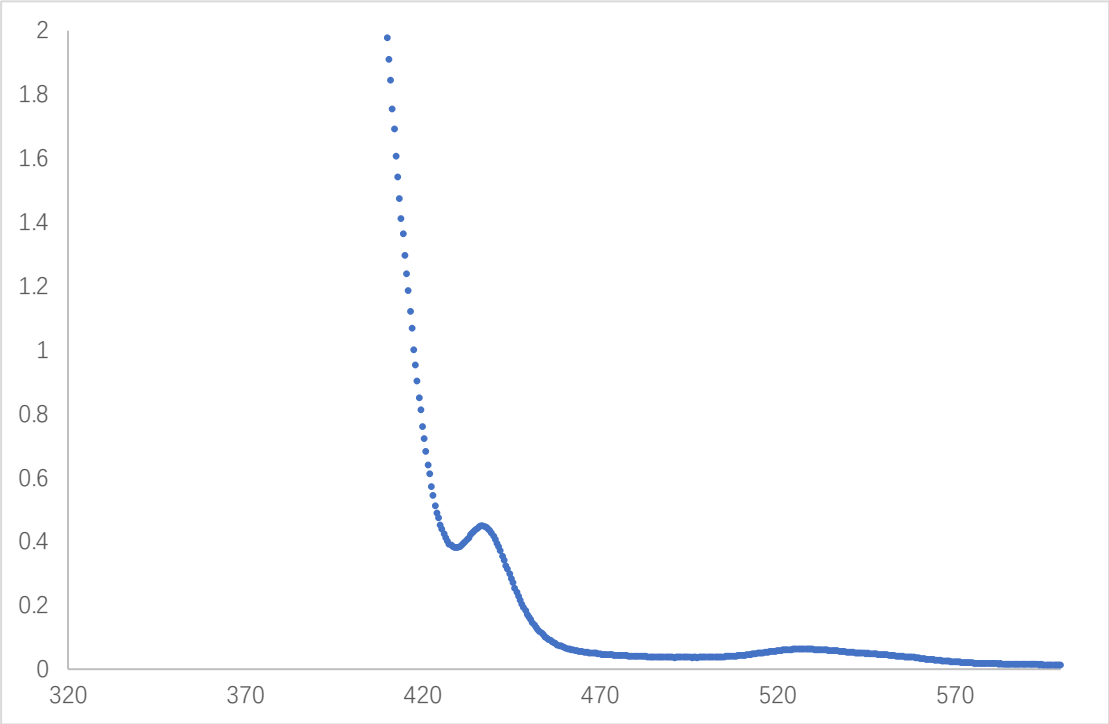

Figure 5.6 UV-Vis Absorption of reaction mixture (Concentration: **2.1** (1 mM), **2.2** (2 mM), Hantzsch ester (2.5 mM), Co(TMOTPP) (0.005 mM), 2,6-lutidine (1 mM))

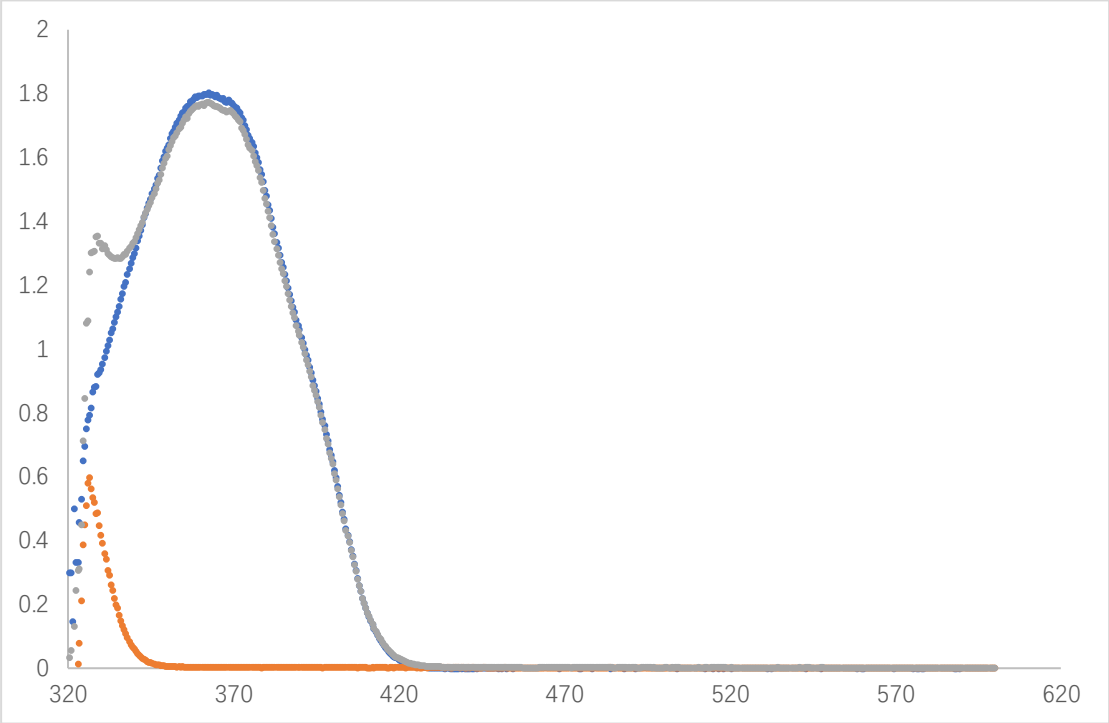

Figure 5.7 UV-Vis Absorption of Hantzsch ester (0.25 mM, blue line), **2.2** (0.2 mM, red line) and Hatzsch ester + **2.2** (0.25 mM and 0.2 mM, grey line)

Conclusion: The absorption profile of the combination of Hantzsch ester and phosphonium salt rules out the possibility of an EDA complex between the two species.

4) Fluorescence quenching

Quenching of Hantzsch ester with Co(TMOTPP)

Excitation wavelength: 365 nm.

Excitation slit: 10 nm; emission slit: 10 nm.

To standard solution of Hantzsch ester (0.1 mM in acetone) were added different amounts of a solution of Co(TMOTPP) (0.7 mM in acetone) to afford the final concentrations reported in the table below. The fluorescence of the solutions was then measured.

Entry	[Co] (mM)
1	0
2	0.005
3	0.010
4	0.015
5	0.02
6	0.025
7	0.03

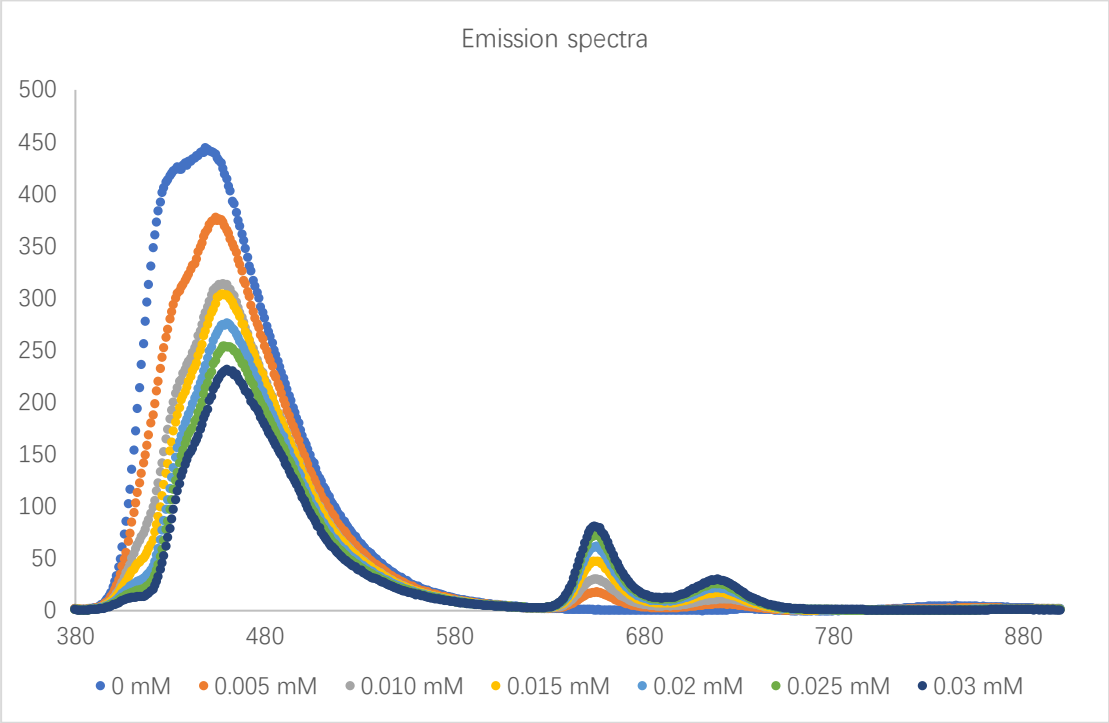

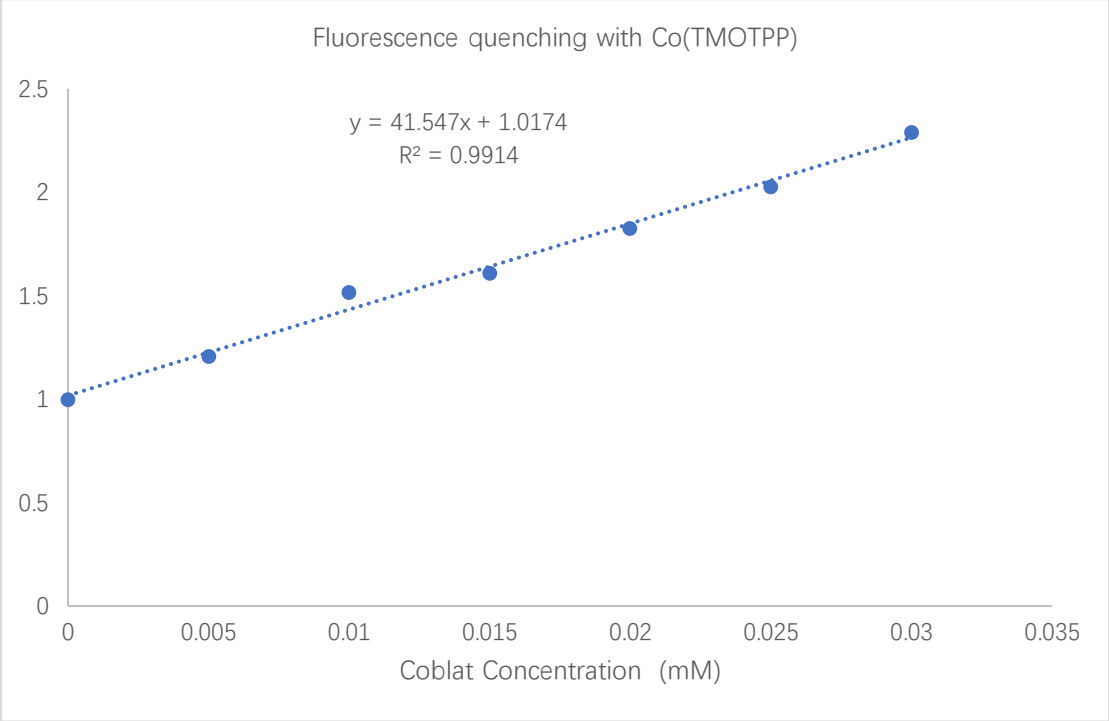

*Quenching of Hantzsch ester with **2.2**:*

Excitation wavelength: 365 nm.

Excitation slit: 10 nm; emission slit: 10 nm.

To standard solution of Hantzsch ester (0.1 mM in acetone) were added different amounts of **2.2** to afford the final concentrations reported in the table below. The fluorescence of the solutions was then measured.

Entry	[Co] (mM)
1	0

2	0.05
3	0.15
4	0.35
5	0.76
6	1.16
7	2.3
8	3.49

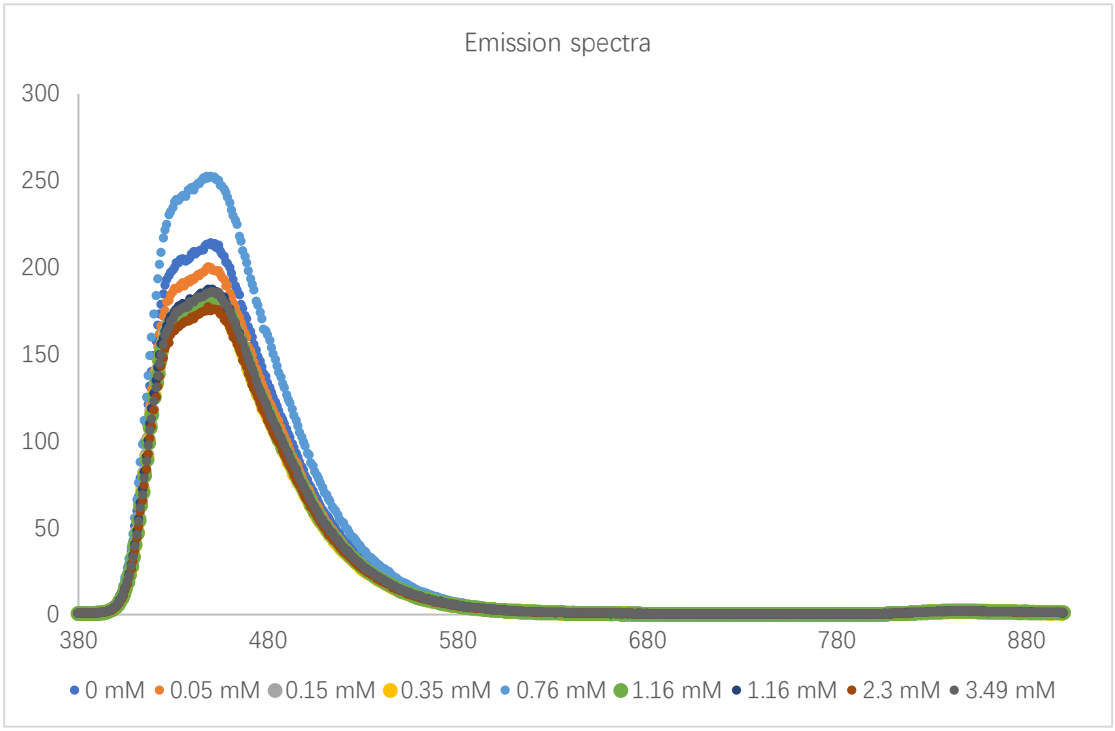

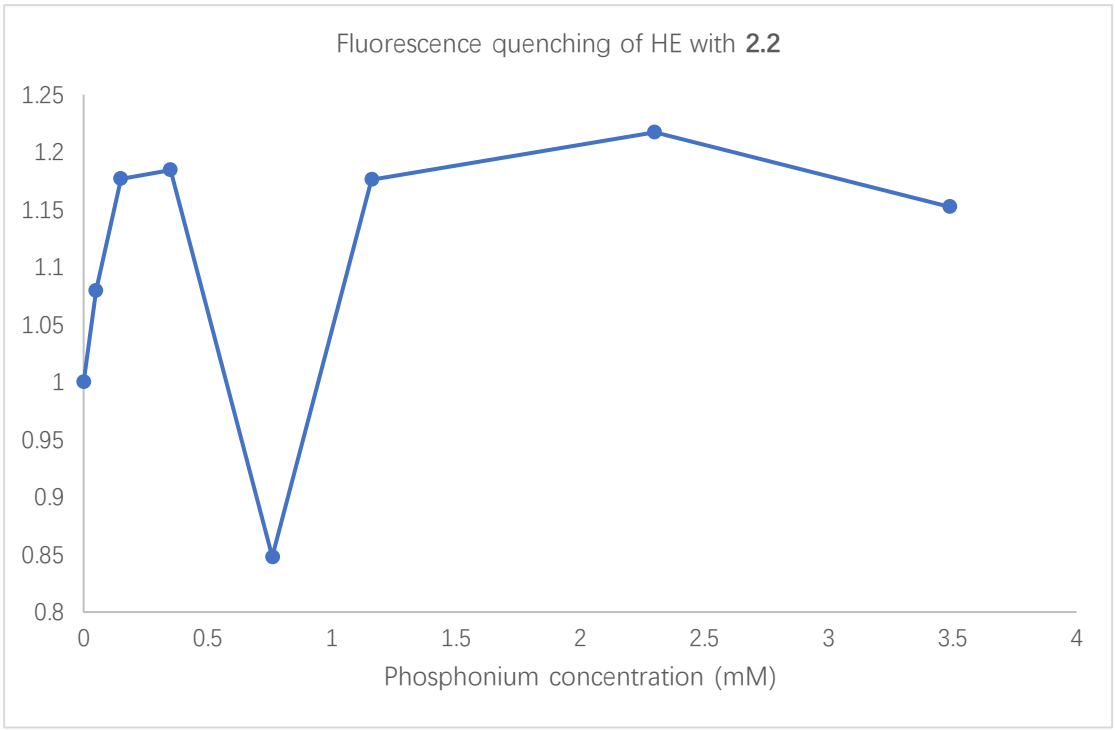

*Quenching of Co(TMOTPP) with **2.2***

Excitation wavelength: 450 nm.

Excitation slit: 20 nm; emission slit: 20 nm.

To standard solution of Co(TMOTPP) (0.1 mM in acetone) were added different amounts of a solution of **2.2** (1 mM in acetone) to afford the final concentrations reported in the table below. The fluorescence of the solutions was then measured.

Entry	[Co] (mM)
1	0
2	0.05
3	0.1
4	0.15
5	0.2
6	0.25
7	0.3

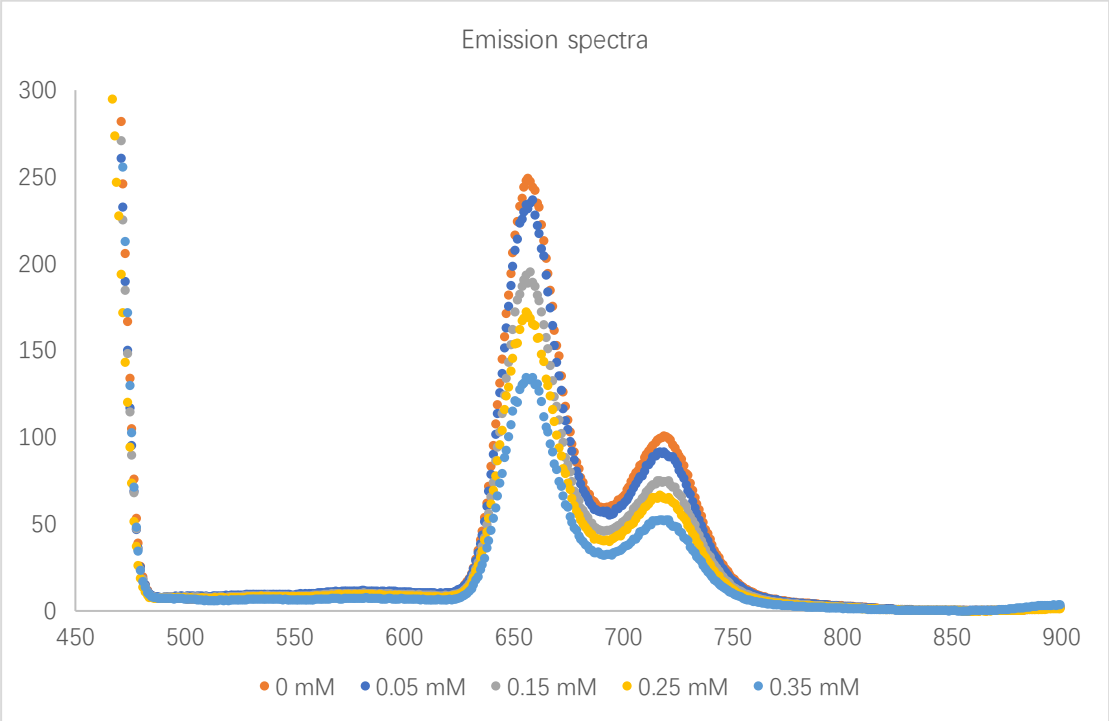

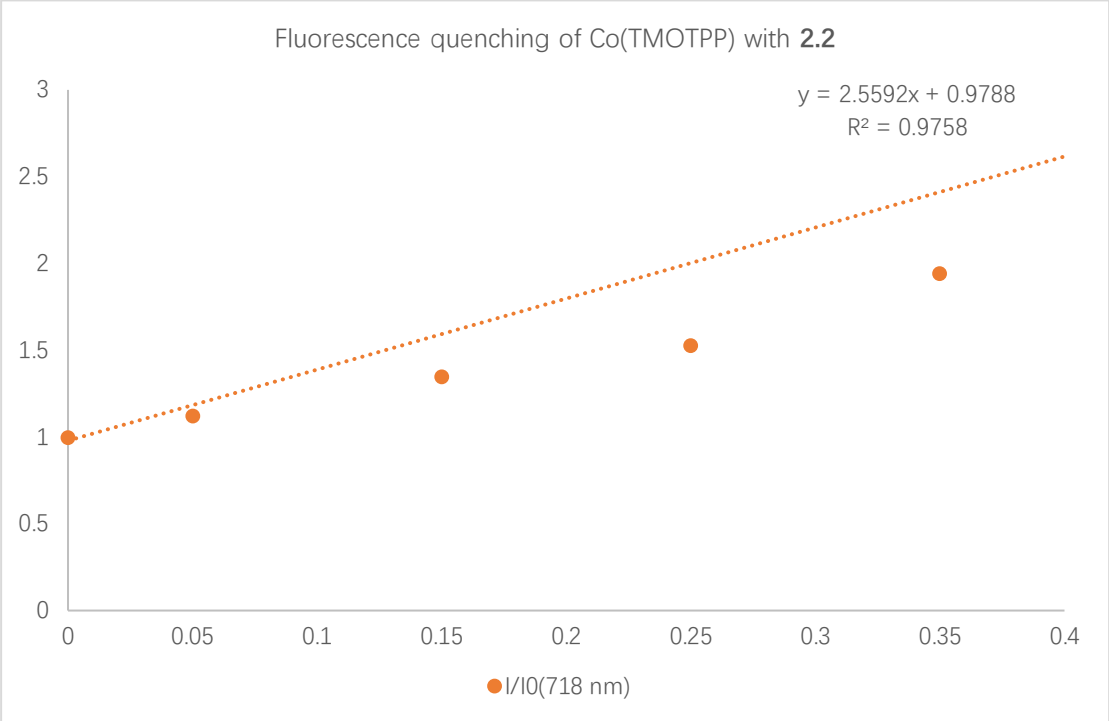

Quenching of Co(TMOTPP) with Hantzsch ester

Excitation wavelength: 450 nm.

Excitation slit: 20 nm; emission slit: 20 nm.

To standard solution of Co(TMOTPP) (0.1 mM in acetone) were added different amounts of a solution of Hantzsch ester (1 mM in acetone) to afford the final concentrations reported in the table below. The fluorescence of the solutions was then measured.

Entry	[Co] (mM)
1	0
2	0.05
3	0.06
4	0.07
5	0.08
6	0.09
7	0.1

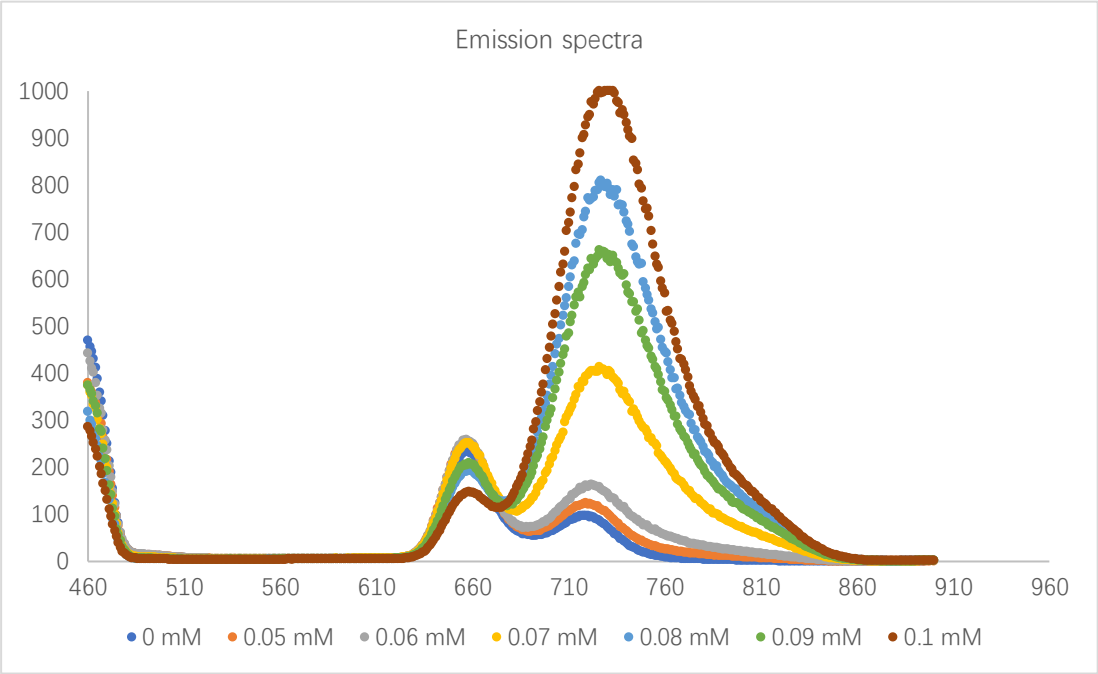

5) Additional reactions

Song Lin's conditions[124]*:*

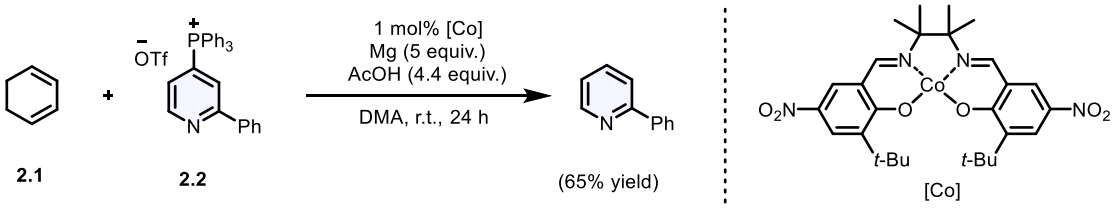

A 2 mL vial was charged with [Co] (1.2 mg, 0.002 mmol, 0.01 equiv.), magnesium (24.0 mg, 1.0 mmol, 5 equiv.) and **2.2** (169.5 mg, 0.3 mmol, 1.5 equiv.). The vial was flushed with argon for 15 minutes, then, DMA (2 mL), acetic acid (50.3 µL, 0.9 mmol, 4.4 equiv.) and **2.1** (19.0 µL, 0.2 mmol, 1.0 equiv.) were added. Argon was bubbled through the solution for 3 minutes and the vial was capped, and the mixture stirred for 24 h. The reaction was quenched with a saturated solution of $NaHCO_3$ (5 mL). The aqueous layer was extracted with EtOAc (3 x 5mL). The gathered organic layers were washed with brine, dried over $MgSO_4$, filtered and evaporated. Purification by flash column chromatography (pentane/EtOAc: 19/1) afforded 2-phenyl pyridine (29.9 mg, 65% yield).

Herzon's conditions[115]*:*

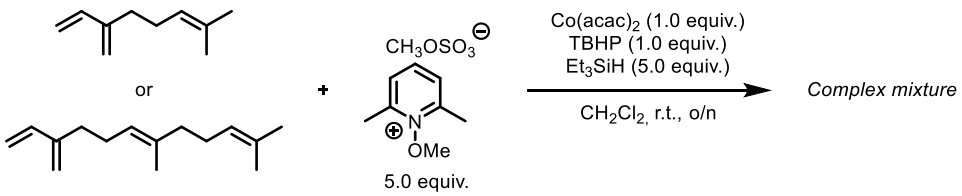

A dry 10 mL round-bottom flask under argon was charged with *N*-methoxy 2,6-lutidine methylsulfate (0.1 g, 0.5 mmol, 5 equiv.) and cobalt *bis*(acetylacetonate) (26.0 mg, 0.1 mmol, 1.0 equiv.). The flask was evacuated and backfilled with argon 3 times. Then, 1,3-diene (0.1 mmol, 1.0

equiv.) in anhydrous DCM (0.5 mL) was added, followed by triethylsilane (80.0 μL, 0.5 mmol, 5.0 equiv.) and *tert*-butyl hydroperoxide in nonane (5 M, 20.0 μL, 0.1 mmol, 1.0 equiv.). The mixture was stirred overnight at room temperature protected from light. Then, the mixture was diluted with EtOAc (50 mL) and transferred into a separating funnel. The organic layer was washed with a 3M solution of ammonium hydroxide (3 x 25 mL). The organic layer was dried over $MgSO_4$, filtered and evaporated. A complex mixture of products was observed in the crude mixture.

5.2.4. Computational details

All Density Functional Theory calculations were carried out using Gaussian 16 program package.[192] All the structures were optimized using PBE0 functional[193] combined with the Def2SVP basis set.[194] In addition, a single point calculation using the same functional and Def2TZVPP basis set were performed to further refine the potential energies. The stationary points were verified as minima (no imaginary frequencies) or transition states (one imaginary frequency) through standard frequency calculations at 298.15 K and 1 atm. Parameters for thermal correction were obtained from frequency calculation and 1M standard state correction was considered by adding 1.89 kcal/mol to all the species. Solvation using was included in both optimizations and single point calculation using SMD implicit solvent (Acetone) model.[195] Stability of the wavefunction in broken-symmetry species was corroborated using stable=opt keywork in G16. 3D structures were illustrated using CYLview 1.0 program.[196]

1) Free Energy Profile of the Catalytic Cycle

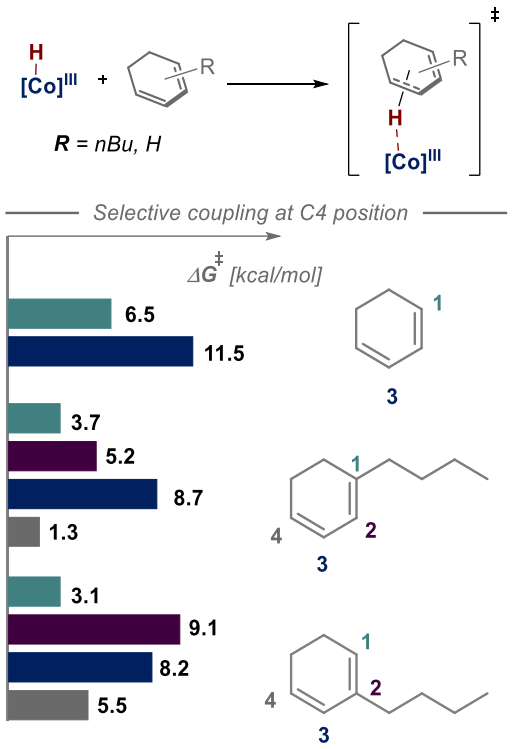

Figure 5.8: Free energy values for HAT transition state barrier of the three distinct dienes selected: cyclohexa-1,3-diene (top), 1-butylcyclohexa-1,3-diene (middle) and 2-butylcyclohexa-1,3-diene (bottom). Energy values provided from (SMD, acetone) PBE1PBE/Def2SVP// PBE1PBE/Def2TZVP are presented in kcal/mol.

2) Benchmarking

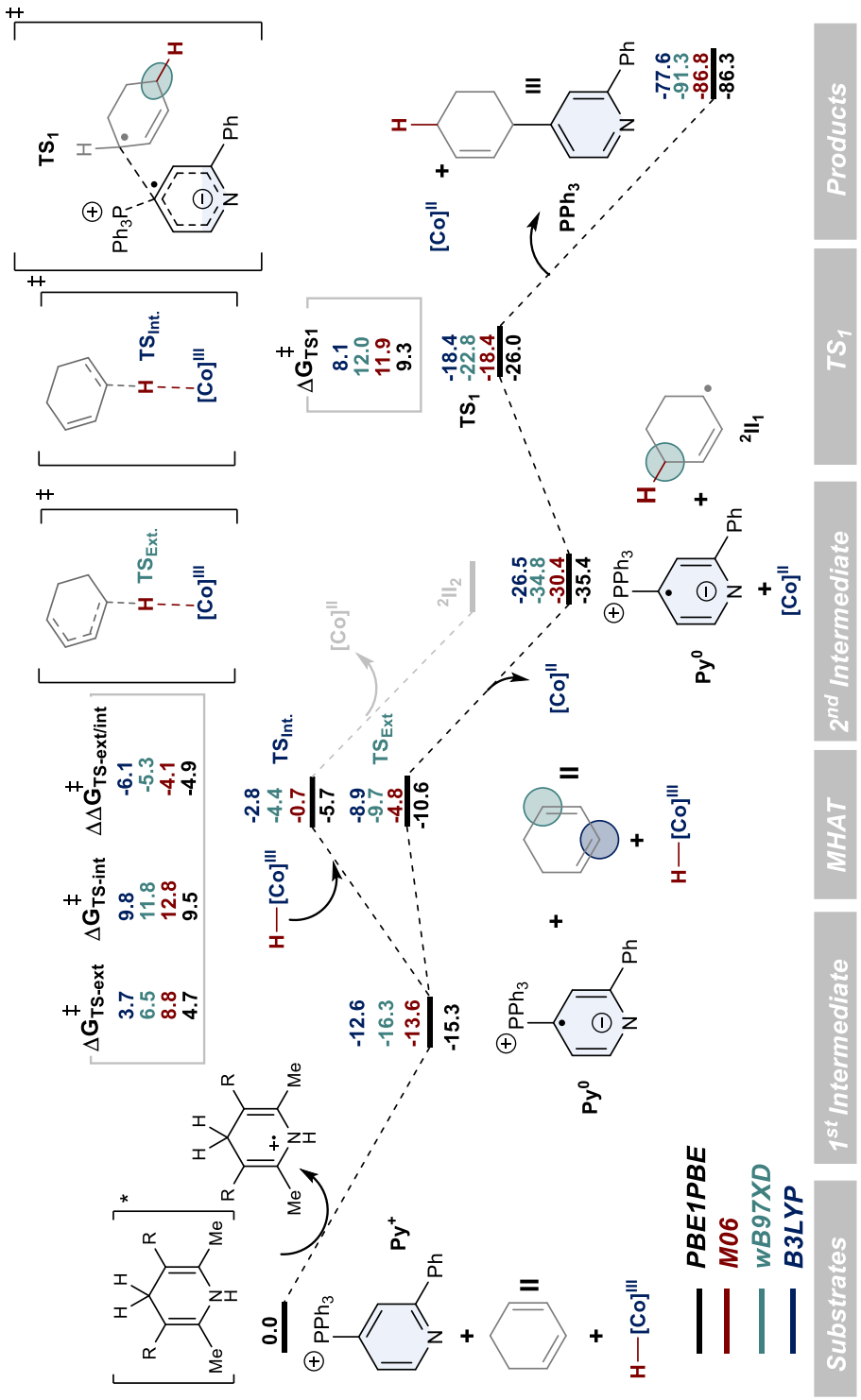

Figure 5.9: Benchmarking study using PBE1PBE, M06, wB97XD and B3LYP levels of theory and Def2TZVP as a basis set (SMD, acetone). Values in kcal/mol.

3) Cyclohexene reduction

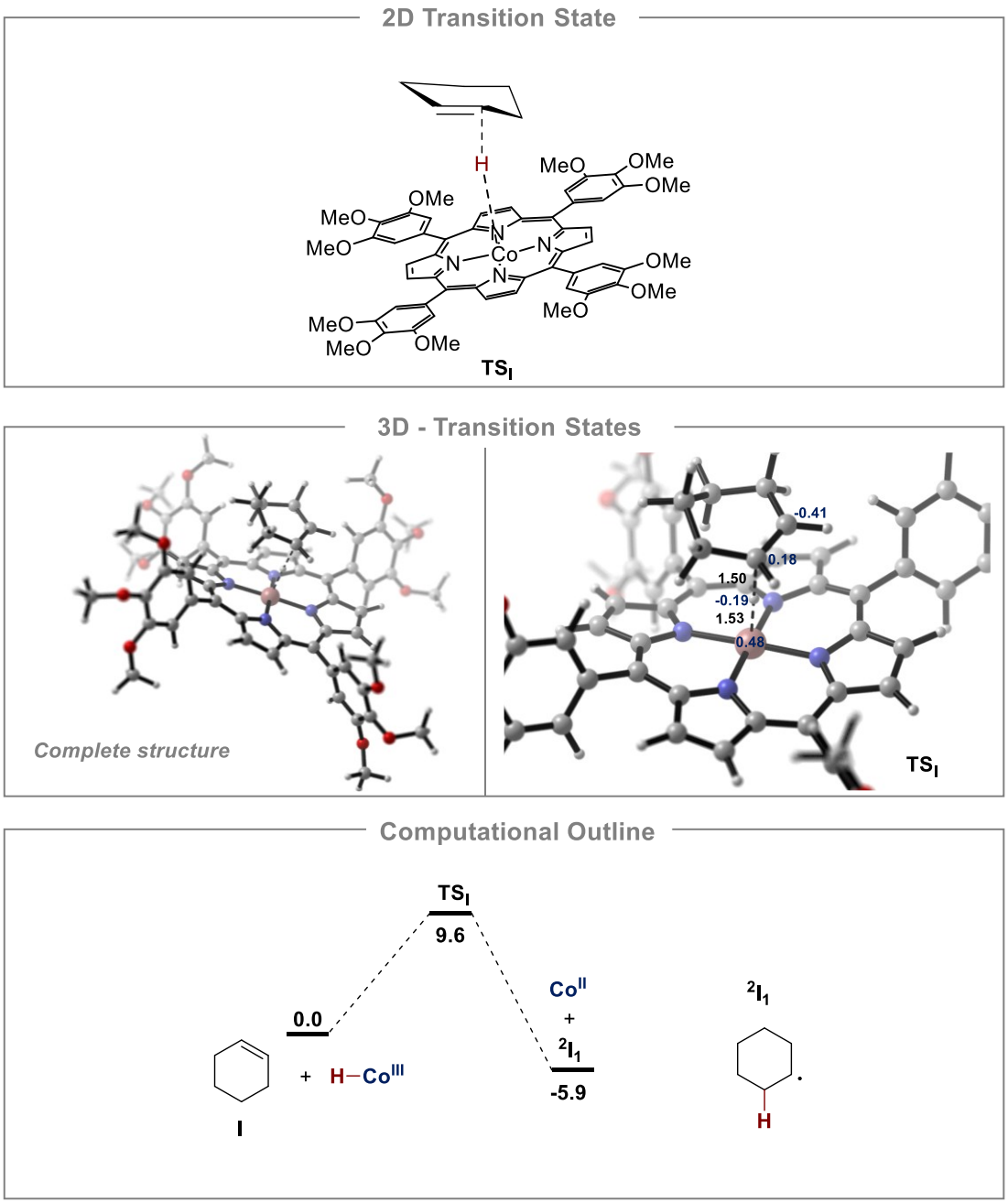

Figure 5.10: Reduction of cycloalkene affording radical $^2I_1$. Energy values provided from (SMD, acetone) PBE1PBE/Def2SVP// PBE1PBE/Def2TZVP are presented in kcal/mol. Blue values shows Spin Density and bond distances (black) are in Angstroms.

4) Cyclohexadiene reduction

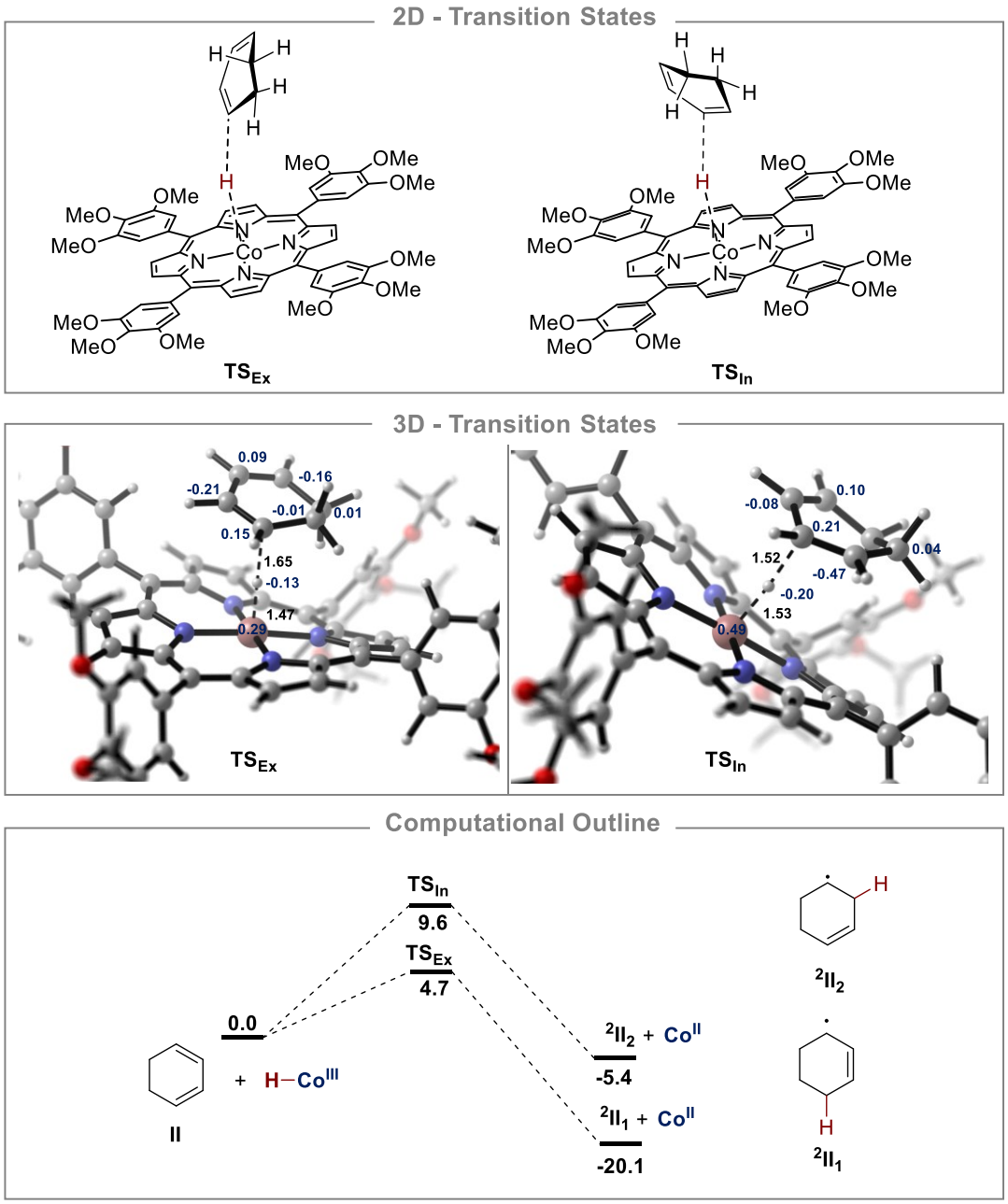

Figure 5.11: Reduction of diene affording radicals ^{2}II$_1$ and ^{2}II$_2$. Energy values provided from (SMD, acetone) PBE1PBE/Def2SVP// PBE1PBE/Def2TZVP are presented in kcal/mol. Blue values shows Spin Density and bond distances (black) are in Angstroms.

5) C-C bond formation depending on Py-PPh$_3$ structure

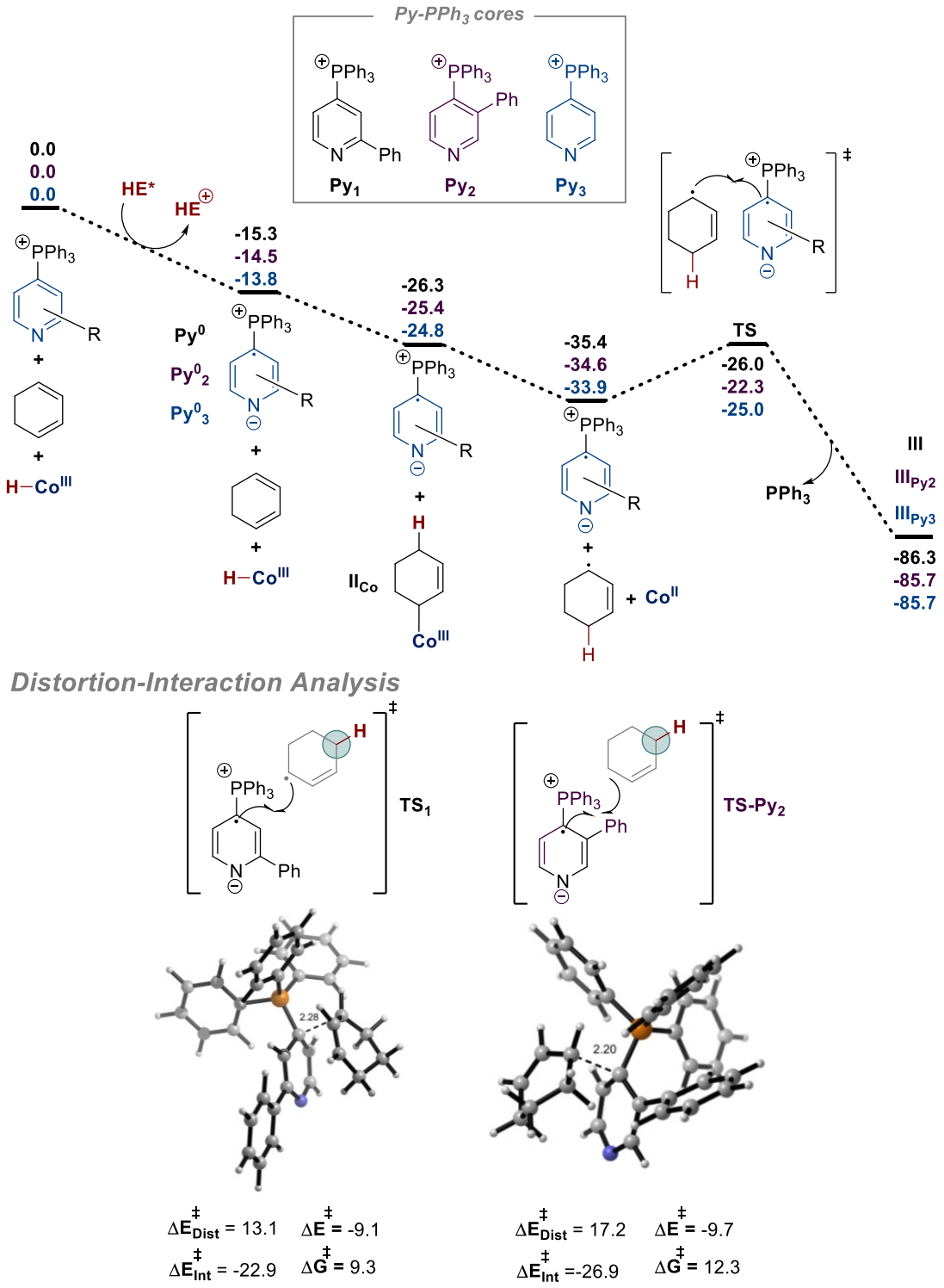

Figure 5.12: A body of three different pyridines (Py$_1$, Py$_2$, Py$_3$) were employed in this computational study. Energy values provided from (SMD, acetone) PBE1PBE/Def2SVP// PBE1PBE/Def2TZVP are presented in kcal/mol. Bond distances (black) are in Angstroms.

5.3 Supporting information for chapter 3

5.3.1 Selected optimization reactions

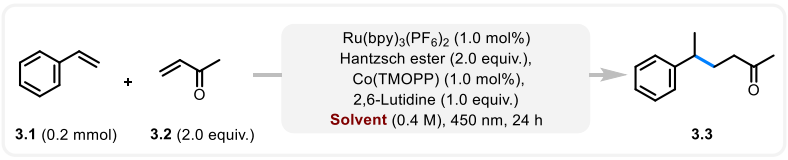

Entry	Variations	Product (%)[a]
1	DCM	81 (77)
2	Acetone	72
3	$CHCl_3$	54
4	DME	9
5	DMSO	<5
6	Benzene	<5
7	EtOAc	36
8	DCM (0.2 M)	74

Table 5.1 Solvent screening. Optimization reactions conducted with 0.2 mmol of **3.1** and 0.4 mmol of **3.2**. [a] Yields in **3.3** determined by ^{1}H-NMR analysis of crude reaction mixture with dibromomethane as an internal standard. Isolated yield in parentheses.

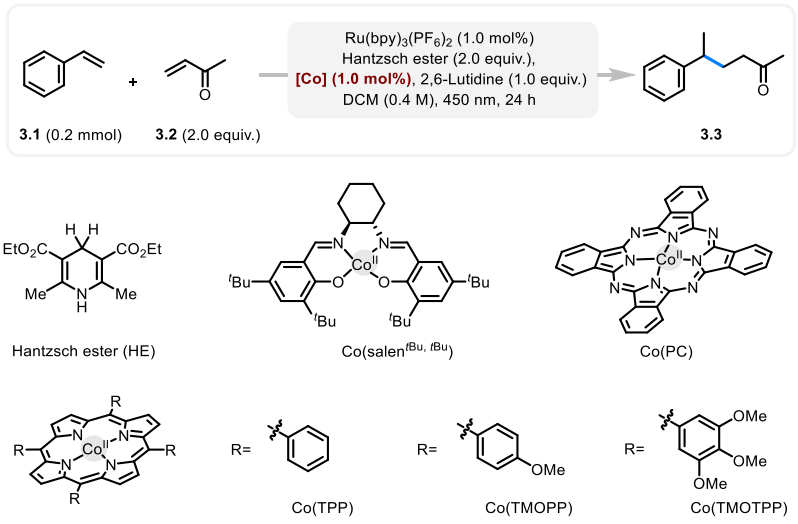

Entry	Variations	Product (%)[a]
1	Co(salen$^{t\text{Bu}, t\text{Bu}}$)	18
2	Co(PC)	15
3	Co(TPP)	70
4	Co(TMOPP)	81 (77)
5	Co(TMOTPP)	55
6	Co(TMOTPP) (0.5 mol%)	68
7	Co(TMOTPP) (2.0 mol%)	55

Table 5.2 Cobalt catalyst screening. Optimization reactions conducted with 0.2 mmol of **3.1**

and 0.4 mmol of **3.2**. [a] Yields in **3.3** determined by ^{1}H-NMR analysis of crude reaction mixture with dibromomethane as an internal standard. Isolated yield in parentheses.

Entry	Variations	Product (%)[a]
1	$Ru(bpz)_3(PF_6)_2$	12
2	$Ru(phen)_3(PF_6)_2$	71
3	$Ru(bpy)_3(PF_6)_2$	81 (77)
4	$Ru(bpy)_3(PF_6)_2$ (0.5 mol%)	74
5	$Ru(bpy)_3(PF_6)_2$ (2.0 mol%)	70
6	$Ru(bpy)_3(PF_6)_2$ (30 W LEDs)	64

Table 5.3 Photocatalyst screening. Optimization reactions conducted with 0.2 mmol of **3.1** and 0.4 mmol of **3.2**. [a] Yields in **3.3** determined by ^{1}H-NMR analysis of crude reaction mixture with dibromomethane as an internal standard. Isolated yield in parentheses.

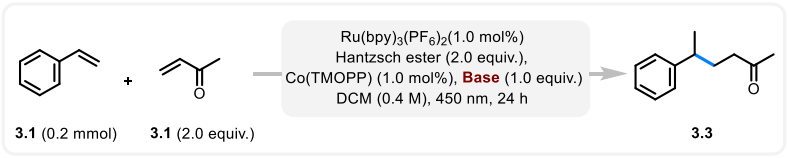

Entry	Variations	Product (%)[a]
1	Pyridine	31
2	Et_3N	<5
3	DBU	9
4	2,6-Lutidine	81 (77)
5	2,6-Lutidine (0.5 equiv.)	77
6	2,6-Lutidine (2.0 equiv.)	71

Table 5.4 Base screening. Optimization reactions conducted with 0.2 mmol of **3.1** and 0.4 mmol of **3.2**. [a] Yields in **3.3** determined by ^{1}H-NMR analysis of crude reaction mixture with dibromomethane as an internal standard. Isolated yield in parentheses.

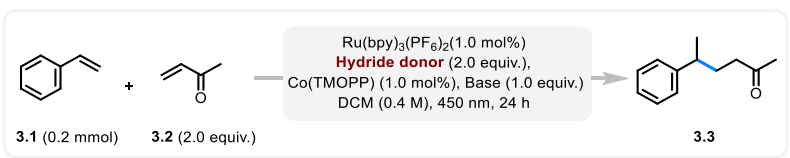

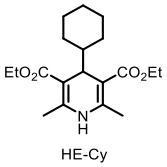

HE-Cy

Entry	Variations	Product (%)[a]
1	$PhSiH_3$	6
2	HE-Cy	16
3	HE	81 (77)

4	HE (1.0 equiv.)	47
5	HE (3.0 equiv.)	72

Table 5.5 Hydride donor screening. Optimization reactions conducted with 0.2 mmol of **3.1** and 0.4 mmol of **3.2**. [a] Yields in **3.3** determined by ^{1}H-NMR analysis of crude reaction mixture with dibromomethane as an internal standard. Isolated yield in parentheses.

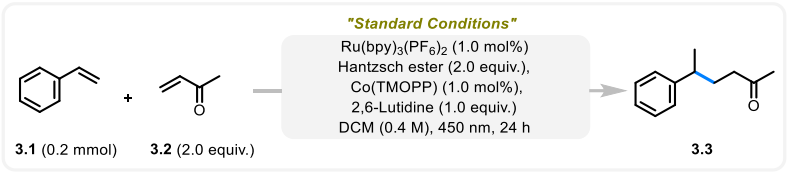

Entry	Variations	Product (%)[a]
1	None	81 (77)
2	No photocatalyst	Trace
3	No HE	0
4	No cobalt catalyst	0
5	No base	32
6	H_2O (1.0 equiv.) as additive	75

Table 5.6 Control reactions. Optimization reactions conducted with 0.2 mmol of **3.1** and 0.4 mmol of **3.2**. [a] Yields in **3.3** determined by ^{1}H-NMR analysis of crude reaction mixture with dibromomethane as an internal standard. Isolated yield in parentheses.

5.3.2 Synthesis of starting materials

1) Synthesis of (vinyloxy)benzene

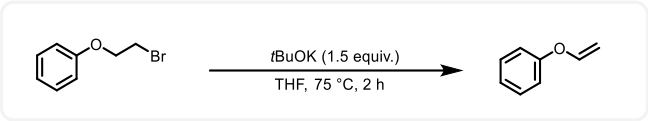

To a dry Schlenk tube with a magnetic stirring bar, β-bromophenetole (10 mmol, 2.01 g), *t*BuOK (1mol/L in THF, 15 mmol, 15 mL) were added. The reaction mixture was stirred for 2 h at 75 °C under inert atmosphere. Upon the completion of the reaction (as indicated by TLC), the reaction mixture was cooled to room temperature, diluted with DCM and washed with water for 3 times. The organic layer was dried over $MgSO_4$, filtered and concentrated in vacuo. After that, the residue was purified by flash chromatograph on silica gel eluted with pentane to afford the desired product as colorless oil. (733 mg, 61% yield)

2) Synthesis of 2-(vinylthio)benzo[d]thiazole

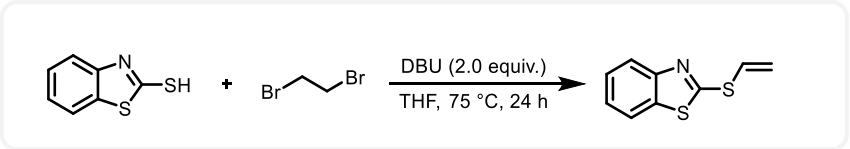

In an oven-dried Schlenk tube equipped with a magnetic stirring bar was added 2-

mercaptobenzothiazole (10 mmol, 1.67 g), 1,2-dibromoethane (20 mmol, 2.0 equiv., 1.7 ml) and THF (15 ml) under an argon atmosphere. The reaction was cooled to 0 °C and DBU (20 mmol, 2.0 equiv., 3.0 ml) was then added dropwise via syringe. After that, the reaction mixture was heated to 75 °C and stirred for 24 h. Upon the completion of the reaction (as indicated by TLC), the reaction mixture was cooled to room temperature, diluted with DCM and washed with water for 3 times. The organic layer was dried over $MgSO_4$, filtered and concentrated in vacuo. After that, the residue was purified by flash chromatograph on silica gel eluted with pentane: EtOAc =100: 1 to 50: 1 to afford the desired product as yellowish oil. (711 mg, 61% yield).

5.3.3 General procedure and characterization data of products

1) General procedures for the reductive coupling reactions

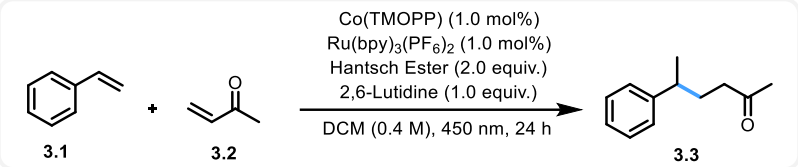

In a brand-new 4ml vial equipped with a magnetic stirring bar were added the $Ru(bpy)_3(PF_6)_2$ (0.002 mmol, 1.0 mol%, 1.72 mg), Co(TMOPP) (0.002 mmol, 1.0 mol%, 1.58 mg) and Hantzsch ester (0.4 mmol, 2.0 equiv., 101.33 mg). A plastic cap with rubber septum was used to close the vial and the system was degassed with stream of argon for 15 minutes. DCM (0.5 ml) was added followed by the styrene (0.2 mmol, 22.9 µl), methyl vinyl ketone (0.4 mmol, 2.0 equiv., 32.6 µl) and 2,6-lutidine (0.2 mmol, 1.0 equiv., 23.3 µl). The vial was then placed in the PhotoRedOx Box (see Materials and Methods for more details about the photochemical setup) and irradiated at 450 nm for 24 hours. The crude was then filtered on a plug of silica (EtOAc or DCM as eluent) and concentrated under reduced pressure.

Note: methyl vinyl ketone 3.2 was repurified by distillation for immediate use.

2) Characterization data of products

5-Phenylhexan-2-one (3.4)

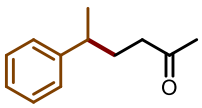

Prepared following the general procedure, **3.4** was obtained after purification by column chromatography (pentane/EtOAc: 100/1 to 50/1) as a colorless oil (27.1 mg, 77% yield). R_f = 0.43 (pentane: EtOAc= 10:1). **^{1}H NMR (600 MHz, $CDCl_3$)** δ 7.30 (t, *J* = 7.5 Hz, 2H), 7.22 – 7.18 (m, 1H), 7.17 (d, *J* = 7.6 Hz, 2H), 2.70 – 2.66 (m, 1H), 2.38 – 2.23 (m, 2H), 2.05 (s, 3H), 1.95 – 1.77 (m, 2H), 1.27 (d, *J* = 5.9 Hz, 3H). **^{13}C NMR (151 MHz, $CDCl_3$)** δ 209.0, 146.6, 128.6, 127.1, 126.3, 42.0, 39.5, 32.0, 30.03, 22.6. **HRMS (ESI)** calculated for $C_{12}H_{16}ONa$ $[M+Na]^+$: 199.1093, found:199.1094.

5-Methyl-5-phenylhexan-2-one (3.5)

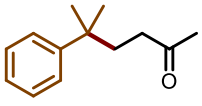

Prepared following the general procedure, **3.5** was obtained after purification by column chromatography (pentane/EtOAc: 100/1 to 50/1) as a colorless oil (19.2 mg, 50% yield). R_f = 0.43 (pentane: EtOAc= 10:1). **^{1}H NMR (600 MHz, $CDCl_3$)** δ 7.34 – 7.29 (m, 4H), 7.19 – 7.18 (m, 1H), 2.17 (t, *J* = 8.1 Hz, 2H), 2.02 (s, 3H), 1.92 (t, *J* = 8.1

Hz 2H), 1.32 (s, 3H).**^{13}C NMR (151 MHz, $CDCl_3$)** δ 209.2, 148.4, 128.4, 125.9, 125.9, 39.7, 37.7, 37.3, 30.0, 29.0. **HRMS (ESI)** calculated for $C_{13}H_{18}ONa$ $[M+Na]^+$: 213.1250, found:213.1242.

5-(4-(*tert*-Butyl)phenyl)hexan-2-one (3.6)

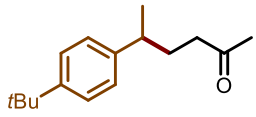

Prepared following the general procedure, **3.6** was obtained after purification by column chromatography (pentane/EtOAc: 100/1 to 50/1) as a colorless oil (38.6 mg, 83% yield). R_f = 0.58 (pentane: EtOAc= 8:1). **^{1}H NMR (600 MHz, $CDCl_3$)** δ 7.32 – 7.28 (m, 2H), 7.12 – 7.07 (m, 2H), 2.68 – 2.64 (m, 1H), 2.37 – 2.25 (m, 2H), 2.06 (s, 3H), 1.92 – 1.78 (m, 2H), 1.31 (s, 9H), 1.25 (d, *J* = 7.0 Hz, 3H).**^{13}C NMR (151 MHz, $CDCl_3$)** δ 209.2, 149.0, 143.4, 126.7, 125.4, 42.1, 38.9, 34.5, 32.1, 31.5, 30.1, 22.5. **HRMS (ESI)** calculated for $C_{16}H_{24}ONa$ $[M+Na]^+$: 255.1719, found:255.1716.

5-(4-(Chloromethyl)phenyl)hexan-2-one (3.7)

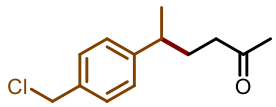

Prepared following the general procedure, **3.7** was obtained after purification by column chromatography (pentane/EtOAc: 100/1 to 50/1) as a colorless oil (18.9 mg, 42% yield). R_f = 0.42 (pentane: EtOAc= 10:1). **^{1}H NMR (600 MHz, $CDCl_3$)** δ 7.33 – 7.30 (m, 2H), 7.16 (d, *J* = 8.1 Hz, 2H), 4.57 (s, 2H), 2.72 – 2.66 (m, 1H), 2.35 – 2.23 (m, 2H), 2.06 (s, 3H), 1.94 – 1.77 (m, 2H), 1.25 (d, *J* = 6.9 Hz, 3H).**^{13}C NMR (151 MHz, $CDCl_3$)** δ 208.9, 147.0, 135.5, 128.9, 127.5, 46.3, 41.9, 39.2, 31.9, 30.1, 22.5. **HRMS (ESI)** calculated for $C_{13}H_{17}ClONa$ $[M+Na]^+$: 247.0860, found:247.0854.

5-([1,1'-Biphenyl]-4-yl)hexan-2-one (3.8)

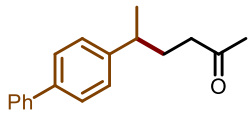

Prepared following the general procedure, **3.8** was obtained after purification by column chromatography (pentane/EtOAc: 100/1 to 50/1) as a colorless oil (31.6 mg, 63% yield). R_f = 0.45 (pentane: EtOAc= 10:1). **^{1}H NMR (600 MHz, $CDCl_3$)** δ7.52 – 7.49 (m, 2H), 7.47 – 7.43 (m, 2H), 7.35 (t, *J* = 7.8 Hz, 2H), 7.27 – 7.22 (m, 1H), 7.16 (dd, *J* = 8.7, 2.2 Hz, 2H), 2.71 – 2.60 (m, 1H), 2.31 – 2.20 (m, 2H), 1.99 (s, 3H), 1.90 – 1.73 (m, 2H), 1.22 (d, *J* = 7.0 Hz, 3H). **^{13}C NMR (151 MHz, $CDCl_3$)** δ 209.1,145.7, 141.1, 139.2, 128.9, 127.6, 127.4, 127.3, 127.2, 127.1, 42.0, 39.1, 32.0, 30.1, 22.6. **HRMS (ESI)** calculated for $C_{18}H_{20}ONa$ $[M+Na]^+$: 275.1406, found:275.1409.

5-(4-Methoxyphenyl)hexan-2-one (3.9)

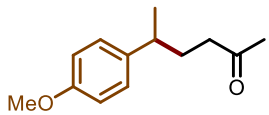

Prepared following the general procedure, **3.9** was obtained after purification by column chromatography (pentane/EtOAc: 100/1 to 50/1) as a colorless oil (33.1 mg, 80% yield). R_f = 0.50 (pentane: EtOAc= 10:1). **^{1}H NMR (600 MHz, $CDCl_3$)** δ 7.09 – 7.04 (m, 2H), 6.86 – 6.80 (m, 2H), 3.79 (s, 3H), 2.68 – 2.59 (m, 1H), 2.34 – 2.23 (m, 2H), 2.05 (s, 3H), 1.91 – 1.73 (m, 2H), 1.23 (d, *J* = 6.9 Hz, 3H).**^{13}C NMR (151 MHz, $CDCl_3$)** δ 209.2, 158.1, 138.6, 128.0, 114.0, 55.3, 42.0, 38.6, 32.2, 30.0, 22.76. **HRMS (ESI)** calculated for $C_{13}H_{18}O_2Na$ $[M+Na]^+$: 229.1199, found:229.1200.

5-(4-Chlorophenyl)hexan-2-one (3.10)

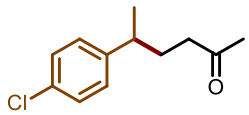

Prepared following the general procedure, **3.10** was obtained after purification by column chromatography (pentane/EtOAc: 100/1 to 50/1) as a colorless oil (23.6 mg, 56% yield). R_f = 0.56 (pentane: EtOAc= 8:1). **^{1}H**

NMR (600 MHz, $CDCl_3$) δ 7.30 – 7.26 (m, 2H), 7.13 – 7.09 (m, 2H), 2.71 – 2.68 (m, 1H), 2.36 – 2.25 (m, 2H), 2.08 (s, 3H), 1.95 – 1.75 (m, 2H), 1.25 (d, *J* = 6.9 Hz, 3H).**^{13}C NMR (151 MHz, $CDCl_3$)** δ 208.7, 145.1, 131.9, 128.7, 128.5, 41.8, 38.9, 31.9, 30.1, 22.5. **HRMS (ESI)** calculated for $C_{12}H_{15}ClONa$ $[M+Na]^+$: 233.0704, found:233.0708.

5-(4-Bromophenyl)hexan-2-one (3.11)

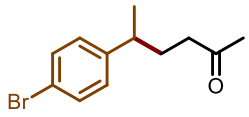

Prepared following the general procedure, **3.11** was obtained after purification by column chromatography (pentane/EtOAc: 50/1 to 20/1) as a colorless oil (25.5 mg, 50% yield). R_f = 0.44 (pentane: EtOAc= 10:1). **^{1}H NMR (400 MHz, $CDCl_3$)** δ 7.44 – 7.38 (m, 2H), 7.06 – 7.01 (m, 2H), 2.72 – 2.59 (m, 1H), 2.37 – 2.20 (m, 2H), 2.06 (s, 3H), 1.97 – 1.70 (m, 2H), 1.23 (d, *J* = 7.0 Hz, 3H). **^{13}C NMR (101 MHz, $CDCl_3$)** δ 208.7, 145.6, 131.7, 128.9, 119.9, 41.8, 39.0, 31.8, 30.1, 22.5. **HRMS (ESI)** calculated for $C_{12}H_{15}BrONa$ $[M+Na]^+$: 277.0198, found:277.0192.

Methyl-4-(5-oxohexan-2-yl)benzoate (3.12)

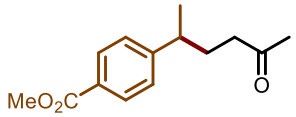

Prepared following the general procedure, **3.12** was obtained after purification by column chromatography (pentane/EtOAc: 10/1) as a colorless oil (15.5 mg, 33% yield). R_f = 0.46 (pentane: EtOAc= 5:1). **^{1}H NMR (600 MHz, $CDCl_3$)** δ 8.00 – 7.93 (m, 2H), 7.25 – 7.18 (m, 2H), 3.90 (s, 3H), 2.80 – 2.71 (m, 1H), 2.36 – 2.21 (m, 2H), 1.97 – 1.78 (m, 2H), 1.27 (d, *J* = 7.0 Hz, 3H). **^{13}C NMR (151 MHz, $CDCl_3$)** δ 208.7, 167.2, 152.1, 130.0, 128.4, 127.2, 52.1, 41.7, 39.5, 31.7, 30.1, 22.3. **HRMS (ESI)** $C_{14}H_{18}O_3Na$ $[M+Na]^+$: 257.1148, found:257.1149.

5-(4-(Trifluoromethyl)phenyl)hexan-2-one (3.13)

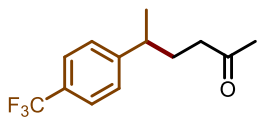

Prepared following the general procedure, **3.13** was obtained after purification by column chromatography (pentane/EtOAc: 50/1) as a colorless oil (24.9 mg, 51% yield). R_f = 0.46 (pentane: EtOAc= 10:1). **^{1}H NMR (600 MHz, $CDCl_3$)** δ 7.55 (d, *J* = 8.0 Hz, 2H), 7.28 (d, *J* = 8.0 Hz, 2H), 2.79 – 2.76 (m, 1H), 2.35 – 2.24 (m, 2H), 2.07 (s, 3H), 1.98 – 1.79 (m, 2H), 1.27 (d, *J* = 7.0 Hz, 3H).**^{13}C NMR (151 MHz, $CDCl_3$)** δ 208.5, 150.8, 128.7 (q, *J* = 32.4 Hz), 127.5, 125.6 (q, *J* = 3.6 Hz), 124.4 (q, *J* = 271.9 Hz), 41.7, 39.4, 31.7, 30.1, 22.3. **^{19}F NMR (565 MHz, $CDCl_3$)** δ -62.35. **HRMS (ESI)** calculated for $C_{13}H_{15}F_3ONa$ $[M+Na]^+$: 267.0967, found:267.0968.

5-(2-Bromophenyl)hexan-2-one (3.14)

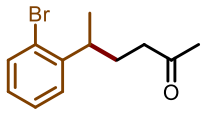

Prepared following the general procedure, **3.14** was obtained after purification by column chromatography (pentane/EtOAc: 100/1 to 50/1) as a colorless oil (32.2 mg, 65% yield). R_f = 0.50 (pentane: EtOAc= 8:1). **^{1}H NMR (600 MHz, $CDCl_3$)** δ 7.56 (dd, *J* = 8.0, 1.3 Hz, 1H), 7.32 – 7.27 (m, 1H), 7.24 (dd, *J* = 7.8, 1.8 Hz, 1H), 7.08 – 7.06 (m, 1H), 3.32 – 3.26 (m, 1H), 2.50 – 2.26 (m, 2H), 2.11 (s, 3H), 1.97 – 1.85 (m, 2H), 1.25 (d, *J* = 6.9 Hz, 3H).**^{13}C NMR (151 MHz, $CDCl_3$)** δ 208.8, 145.4, 133.0, 127.9, 127.7, 127.4, 124.9, 41.7, 37.5, 31.2, 30.1, 21.6. **HRMS (ESI)** calculated for $C_{12}H_{15}BrONa$ $[M+Na]^+$: 277.0198, found:277.0195.

5-Mesitylhexan-2-one (3.15)

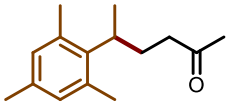

Prepared following the general procedure, **3.15** was obtained after purification by column chromatography (pentane/EtOAc: 20/1) as a colorless oil (14.5 mg, 33% yield). R_f = 0.40 (pentane: EtOAc= 10:1). **^{1}H NMR (400 MHz, $CDCl_3$)** δ 6.80 (s, 2H), 3.27 – 3.17 (m, 1H), 2.41 – 2.26 (m, 2H), 2.24 (s, 9H), 2.15 – 2.04 (m, 1H), 2.05 (s, 3H), 2.00 – 1.89 (m, 1H), 1.30 (d, *J* = 7.2 Hz, 3H). **^{13}C NMR (101 MHz, $CDCl_3$)** δ 209.2, 138.8, 136.4, 135.2, 131.4, 129.4, 42.5, 34.1, 30.1, 29.2, 21.6, 20.7, 19.3. **HRMS (ESI)** calculated for $C_{15}H_{22}ONa$ $[M+Na]^+$: 241.1563, found:241.1564.

5-(Naphthalen-2-yl)hexan-2-one (3.16)

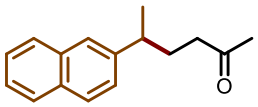

Prepared following the general procedure, **3.16** was obtained after purification by column chromatography (pentane/EtOAc: 100/1 to 50/1) as a colorless oil (26.7 mg, 59% yield). R_f = 0.51 (pentane: EtOAc= 10:1). **^{1}H NMR (600 MHz, $CDCl_3$)**. δ 7.83 – 7.78 (m, 3H), 7.61 – 7.58 (m, 1H), 7.49 – 7.42 (m, 2H), 7.34 (dd, *J* = 8.5, 1.8 Hz, 1H), 2.90 – 2.84 (m, 1H), 2.40 – 2.25 (m, 2H), 2.04 (s, 3H), 2.03 – 1.87 (m, 2H), 1.36 (d, *J* = 7.0 Hz, 3H).**^{13}C NMR (151 MHz, $CDCl_3$)** δ 209.0, 144.0, 133.7, 132.4, 128.3, 127.7, 127.7, 126.1, 125.6, 125.5, 125.4, 42.0, 39.6, 31.8, 30.1, 22.6. **HRMS (ESI)** calculated for $C_{16}H_{18}ONa$ $[M+Na]^+$: 249.1250, found:249.1246.

5-(thiophen-2-yl)hexan-2-one (3.17)

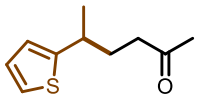

Prepared following the general procedure, **3.17** was obtained after purification by column chromatography (pentane/EtOAc: 50/1) as a colorless oil (10.6 mg, 29% yield). R_f = 0.52 (pentane: EtOAc= 10:1). **^{1}H NMR (600 MHz, $CDCl_3$)** δ 7.13 (dd, *J* = 5.1, 1.2 Hz, 1H), 6.92 (dd, *J* = 5.1, 3.4 Hz, 1H), 6.80 – 6.75 (m, 1H), 3.09 – 2.99 (m, 1H), 2.39 (t, *J* = 7.5 Hz, 2H), 2.09 (s, 3H), 2.02 – 1.73 (m, 2H), 1.33 (d, *J* = 6.9 Hz, 3H).**^{13}C NMR (151 MHz, $CDCl_3$)** δ 208.8, 150.8, 126.7, 123.1, 122.9, 41.6, 34.9, 33.0, 30.1, 23.5. **HRMS (ESI)** calculated for $C_{10}H_{14}OSNa$ $[M+Na]^+$: 205.0658, found:205.0658.

5-Phenoxyhexan-2-one (3.18)

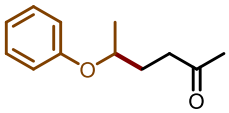

Prepared following the general procedure, **3** was obtained after purification by column chromatography (pentane/EtOAc: 50/1 as a colorless oil (9.3 mg, 24% yield). R_f = 0.48 (pentane: EtOAc= 10:1). **^{1}H NMR (400 MHz, $CDCl_3$)**. δ 7.39 – 7.19 (m, 5H), 3.21 (h, J = 6.8 Hz, 1H), 2.69 – 2.57 (m, 2H), 2.11 (s, 3H), 1.92 – 1.72 (m, 2H), 1.27 (d, J = 6.7 Hz, 3H). **^{13}C NMR (101 MHz, $CDCl_3$)** δ 208.4, 134.9, 132.3, 129.0, 127.1, 43.1, 40.9, 30.4, 30.2, 21.6. **HRMS (ESI)** calculated for $C_{12}H_{16}O_2Na$ $[M+H]^+$: 215.1043, Despite multiple attempts, a compliant HRMS analysis could not be obtained for this compound.

5-(Benzo[d]thiazol-2-ylthio)hexan-2-one (3.19)

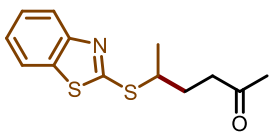

Prepared following the general procedure, **3** was obtained after purification by column chromatography (pentane/EtOAc: 50/1 to 20/1 to 10/1) as a colorless oil (21.2 mg, 40% yield). R_f = 0.21 (pentane: EtOAc= 10:1). **^{1}H NMR (400 MHz, $CDCl_3$)** δ 7.86 (ddd, *J* = 8.2, 1.2, 0.6 Hz, 1H), 7.75 (ddd, *J* = 7.9, 1.3, 0.6 Hz, 1H), 7.45 – 7.38 (m, 1H), 7.32 – 7.27 (m, 1H), 4.03 (dqd, *J* = 8.3, 6.9, 5.4 Hz, 1H), 2.76 – 2.60 (m, 2H), 2.15 (s, 3H), 2.13 – 1.92 (m, 2H), 1.52 (d, *J* = 6.9 Hz, 3H). **^{13}C**

NMR (101 MHz, $CDCl_3$) δ 207.9, 166.1, 153.5, 135.5, 126.2, 124.5, 121.8, 121.1, 44.1, 41.0, 30.7, 30.2, 22.0. **HRMS (ESI)** calculated for $C_{13}H_{16}NOS_2$ $[M+Na]^+$: 288.0487, found:288.0489.

Methyl 4-phenylpentanoate (3.20)

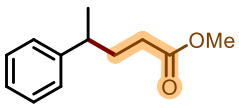

Prepared following the general procedure, **3.20** was obtained after purification by column chromatography (pentane/EtOAc: 20/1) as a colorless oil (16.9 mg, 44% yield). R_f = 0.77 (pentane: EtOAc= 5:1). **^{1}H NMR (500 MHz, $CDCl_3$)** δ 7.33 – 7.27 (m, 2H), 7.22 – 7.15 (m, 2H), 3.63 (s, 3H), 2.72 – 2.68 (m, 1H), 2.28 – 2.13 (m, 2H), 2.01 – 1.82 (m, 2H), 1.28 (d, *J* = 7.0 Hz, 3H). **^{13}C NMR (126 MHz, $CDCl_3$)** δ 174.2, 146.4, 128.6, 127.2, 126.3, 51.6, 39.6, 33.3, 32.5, 22.3. **HRMS (ESI)** calculated for $C_{12}H_{16}O_2Na$ $[M+Na]^+$: 215.1043, found:215.1043.

Phenyl-4-phenylpentanoate (3.21)

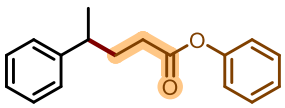

Prepared following the general procedure, **3.21** was obtained after purification by column chromatography (pentane/EtOAc: 20/1) as a colorless oil (34.6 mg, 68% yield). R_f = 0.54 (pentane: EtOAc= 5:1). **^{1}H NMR (400 MHz, $CDCl_3$)** δ 7.41 – 7.30 (m, 4H), 7.25 – 7.18 (m, 4H), 7.07 – 7.01 (m, 2H), 2.87 – 2.78 (m, 1H), 2.46 – 2.43 (m, 2H), 2.14 – 1.96 (m, 2H), 1.34 (d, *J* = 6.9 Hz, 3H). **^{13}C NMR (101 MHz, $CDCl_3$)** δ 172.3, 150.9, 146.2, 129.5, 128.7, 127.2, 126.5, 125.9, 121.7, 39.6, 33.3, 32.8, 22.3. **HRMS (ESI)** calculated for $C_{17}H_{18}O_2Na$ $[M+Na]^+$: 277.1199, found:277.1199.

((3-Phenylbutyl)sulfonyl)benzene (3.22)

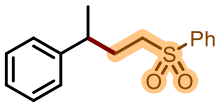

Prepared following the general procedure, **3.22** was obtained after purification by column chromatography (pentane/EtOAc: 10/1 to 5/1) as a colorless oil (28.1 mg, 51% yield). R_f = 0.33 (pentane: EtOAc= 10:1). **^{1}H NMR (400 MHz, $CDCl_3$)** δ 7.85 – 7.80 (m, 2H), 7.66 – 7.59 (m, 1H), 7.53 (ddd, *J* = 8.3, 6.7, 1.3 Hz, 2H), 7.29 – 7.22 (m, 2H), 7.21 – 7.15 (m, 1H), 7.09 – 7.02 (m, 2H), 3.02 – 2.80 (m, 2H), 2.79 – 2.66 (m, 1H), 2.10 – 1.87 (m, 2H), 1.23 (d, *J* = 6.8 Hz, 3H).**^{13}C NMR (101 MHz, $CDCl_3$)** δ 144.9, 139.23, 133.8, 129.4, 128.9, 128.1, 127.0, 126.8, 54.8, 39.0, 30.6, 22.5. **HRMS (ESI)** calculated for $C_{16}H_{18}O_2SNa$ $[M+Na]^+$: 297.0920, found:297.0920.

4-Phenylpentanenitrile (3.23)

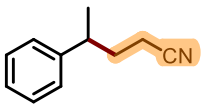

Prepared following the general procedure, **3.23** was obtained after purification by column chromatography (pentane/EtOAc: 20/1) as a colorless oil (23.9 mg, 75% yield). R_f = 0.51 (pentane: EtOAc= 10:1). **^{1}H NMR (600 MHz, $CDCl_3$)** δ 7.25 (t, J = 7.6 Hz, 2H), 7.18 – 7.14 (m, 1H), 7.11 (d, J = 6.8 Hz, 2H), 2.81 – 2.75 (m, 1H), 2.17 – 2.01 (m, 2H), 1.93 – 1.78 (m, 2H), 1.24 (d, J = 6.9 Hz, 3H). **^{13}C NMR (151 MHz, $CDCl_3$)** δ 144.7, 128.9, 127.0, 126.9, 119.8, 39.1, 33.7, 22.1, 15.6. **HRMS (ESI)** calculated for $C_{11}H_{13}NNa$ $[M+Na]^+$: 182.0940, found:182.0937.

6

Literature

6. Literature

1. Feder, H. M.; Halpern, J. Mechanism of the Cobalt Carbonyl-Catalyzed Homogeneous Hydrogenation of Aromatic Hydrocarbons. *J. Am. Chem. Soc.* **1975,** *97*, 7186–7188.

2. Sweany, R. L.; Halpern, J. Hydrogenation of .Alpha.-Methylstyrene by Hydridopentacarbonylmanganese (I). Evidence for a Free-Radical Mechanism. *J. Am. Chem. Soc.* **1977**, *99*, 8335–8337.

3. Crossley, S. W. M.; Obradors, C.; Martinez, R. M.; Shenvi, R. A. Mn-, Fe-, and Co-Catalyzed Radical Hydrofunctionalizations of Olefins. *Chem. Rev.* **2016**, *116*, 8912–9000.

4. Jana, S.; Mayerhofer, V. J.; Teskey, C. J. Photo- and Electrochemical Cobalt Catalysed Hydrogen Atom Transfer for the Hydrofunctionalisation of Alkenes. *Angew. Chem. Int. Ed.* **2023**, *62*, e202304882.

5. McGrady, G. S.; Guilera, G. The multifarious world of transition metal hydrides. *Chem. Soc. Rev.* **2003**, *32*, 383–392.

6. Wiedner, E. S.; Chambers, M. B.; Pitman, C. L.; Bullock, R. M.; Miller, A. J. M.; Appel, A. M. Thermodynamic Hydricity of Transition Metal Hydrides. *Chem. Rev.* **2016**, *116*, 8655–8692.

7. Yu, H.; Li, X.; Zheng, J. Beyond Hydrogen Storage: Metal Hydrides for Catalysis. *ACS Catal.* **2024**, 14, 3139–3157.

8. Lyons, T. W.; Sanford, M. S. Palladium-Catalyzed Ligand-Directed C–H Functionalization Reactions. *Chem. Rev.* **2010**, *110*, 1147–1169.

9. Rakowski DuBois, M.; DuBois, D. L. Development of Molecular Electrocatalysts for CO_2 Reduction and H_2 Production/Oxidation *Acc. Chem. Res.* **2009**, *42*, 1974–1982.

10. Fukuzumi, S.; Suenobu, T. Hydrogen Storage and Evolution Catalysed by Metal Hydride Complexes *Dalton Trans.* **2013**, *42*, 18–28.

11. Pearson, R. G.; Ford, P. C. The Brønsted acidity of Transition Metal Hydrides. *Comments Inorg. Chem.* **1982**, *1*, 279–291.

12. Pearson, R. G. The Transition-Metal-Hydrogen Bond. *Chem. Rev.* **1985**, *85*, 41–49.

13. Warren, J. J.; Tronic, T. A.; Mayer, J. M. Thermochemistry of Proton-Coupled Electron Transfer Reagents and its Implications. *Chem. Rev.* **2010**, *110*, 6961–7001.

14. Bullock, R. M. Metal-Hydrogen Bond Cleavage Reactions of Transition Metal Hydrides: Hydrogen Atom, Hydride, and Proton Transfer Reactions. *Comments Inorg. Chem.* **1991**, *12*, 1–33.

15. Shevick, S. L.; Wilson, C. V.; Kotesova, S.; Kim, D.; Holland, P. L.; Shenvi, R. A. Catalytic hydrogen atom transfer to alkenes: a roadmap for metal hydrides and radicals. *Chem. Sci.* **2020**,*11*, 12401-12422.

16. Kuo, J. L.; Gunasekara, T.; Hansen, A.; Vibbert, H. B.; Bohle, F.; Norton, J. R.; Grimme, S.; Quinlivan, P. J. Thermodynamics of $H^+/H^\bullet/H^-/e^-$ Transfer from $[CpV(CO)_3H]^-$: Comparisons to the

Isoelectronic $CpCr(CO)_3H$. *Organometallics* **2019**, *38*, 4319–4328.

17. Kim, D.; Rahaman, S. M. W.; Mercado, B. Q.; Poli, R.; Holland, P. L. Roles of Iron Complexes in Catalytic Radical Alkene Cross-Coupling: A Computational and Mechanistic Study. *J. Am. Chem. Soc.* **2019**, *141*, 7473–7485.

18. Franck, J.; Rabinowitch, E. Some remarks about free radicals and the photochemistry of solutions. *Trans. Faraday Soc.* **1934**, *30*, 120–130.

19. Shigehisa, H.; Aoki, T.; Yamaguchi, S.; Shimizu, N.; Hiroya, K. Hydroalkoxylation of Unactivated Olefins with Carbon Radicals and Carbocation Species as Key Intermediates. *J. Am. Chem. Soc.* **2013**, *135*, 10306–10309.

20. Wilson, C. V.; Kim, D.; Sharma, A.; Hooper, R. X.; Poli, R.; Hoffman, B. M.; Holland, P. L. Cobalt – Carbon Bonding in a Salen-Supported Cobalt(IV) Alkyl Complex Postulated in Oxidative MHAT Catalysis. *J. Am. Chem. Soc.* **2022**, *144*, 10361–10367.

21. Puyl, V.; Shenvi, R. A. Manganese-, Iron-, and Cobalt-Catalyzed Radical Alkene Hydrofunctionalization. In *Science of Synthesis: Base-Metal Catalysis* 2, **2023**, *3*, DOI: 10.1055/sos-SD-239-00183

22. Matos, J. L. M.; Green, S. A.; Chun, Y.; Dang, V. Q.; Dushin, R. G.; Richardson, P.; Chen, J. S.; Piotrowski, D. W.; Paegel, B. M.; Shenvi, R. A. Cycloisomerization of olefins in water, *Angew. Chem. Int. Ed.* **2020**, *59*, 12998–13003.

23. Fleming, I. Molecular Orbitals and Organic Chemical Reactions: Student Edition, *John Wiley & Sons Ltd, United Kingdom*, **2009**.

24. Reed, C. A. Carborane Acids. New ''Strong Yet Gentle'' Acids for Organic and Inorganic Chemistry. *Chem. Commun.* **2005**, 1669– 1677.

25. Parsaee, F.; Senarathna, M. C.; Kannangara, P. B.; Alexander, S. N.; Arche, P. D. E.; Welin, E. R. Radical philicity and its role in selective organic transformations. *Nature Reviews Chemistry* **2021**, *5*, 486–499.

26. Shenvi, R. A.; Matos, J. L. M.; Green, S. A. Hydrofunctionalization of Alkenes by Hydrogen-Atom Transfer. In *Organic Reactions*; John Wiley & Sons, Inc.: Hoboken, NJ, **2019**; pp 383–470.

27. Green, S. A.; Crossley, S. W. M.; Matos, J. L. M.; Vasquez-Cespedes, S.; Shevick, S.; Shenvi, R. A. The High Chemofidelity of Metal-Catalyzed Hydrogen Atom Transfer. *Acc. Chem. Res.* **2018**, *51*, 2628–2640.

28. Hoveyda, A. H.; Evans, D. A.; Fu, G. C. Substrate-directable chemical reactions. *Chem. Rev.* **1993**, *93*, 1307–1370.

29. Saha, S. N.; Ballav, N.; Baidya, M. Palladium(II)-Catalyzed Regioselective Hydroamination ofAllylamines to N-Alkyl Sulfoximines. *Org. Lett.* **2025**, *27*, 1999–2004.

30. Wu, J.; Ma, Z. Metal-hydride hydrogen atom transfer (MHAT) reactions in natural product synthesis. *Org. Chem. Front.* **2021**,*8* ,7050–7076.

31. Zhang, G.; Zhang, Q. Cobalt-catalyzed HAT reaction for asymmetric hydrofunctionalization of

alkenes and nucleophiles. *Chem Catal.* **2023**, *3*, 100526–200540.

32. Klingenberg, M. Pigments of rat liver microsomes. *Arch. Biochem. Biophys.* **1958**, *75*, 376–386.

33. Omura, T.; Sato, R. The carbon monoxide-binding pigment of liver microsomes: I evidence for its hemoprotein nature. *J. Biol. Chem.* **1964**, *239*, 2370–2378.

34. Okamoto, T.; Oka, S. Cobalt-Catalyzed Regiospecific Conversion of Aryl-Substituted Olefins into Alcohols using Molecular Oxygen and Tetrahydroborate. the Reaction of Oxygen with Activated Substrates. *Tetrahedron Lett.* **1981**, *22*, 2191–2194.

35. Okamoto, T.; Oka, S. Cobalt-Catalyzed Selective Conversion of Aromatic Olefins to Benzylic Alcohols by Molecular Oxygen and Tetrahydroborate. *J. Org. Chem.* **1984**, *49*, 1589–1594.

36. Mukaiyama, T.; Isayama, S.; Inoki, S.; Kato, K.; Yamada, T.; Takai, T. Oxidation-reduction hydration of olefins with molecular oxygen and 2-propanol catalyzed by bis (acetylacetonato) cobalt(II). *Chem. Lett.* **1989**, *18*, 449–452.

37. Waser, J.; Carreira, E. M. Catalytic Hydrohydrazination of a Wide Range of Alkenes with a Simple Mn Complex. *Angew. Chem. Int. Ed.* **2004**, *43*, 4099–4102.

38. Gaspar, B.; Carreira, E. M. Mild Cobalt-Catalyzed Hydrocyanation of Olefins with Tosyl Cyanide. *Angew. Chem. Int. Ed.* **2007**, *46*, 4519–4522.

39. Lo, J.; Yabe, Y.; Baran, P. S. A Practical and Catalytic Reductive Olefin Coupling. *J. Am. Chem. Soc.* **2014**, *136*, 1304–1307.

40. Lo, J.; Gui, J.; Yabe, Y.; Pan, C.-M.; Baran, P. S. Functionalized Olefin Cross-Coupling to Construct Carbon–Carbon Bonds. *Nature* **2014**, *516*, 343–348.

41. Green, S. A.; Matos, J. L. M.; Yagi, A.; Shenvi, R. A. Branch-Selective Hydroarylation: Iodoarene-Olefin Cross-Coupling. *J. Am. Chem. Soc.* **2016**, *138*, 12779–12782.

42. Shevick, S. L; Obradors, C.; Shenvi, R. A. Mechanistic Interrogation of Co/Ni-Dual Catalyzed Hydroarylation. *J. Am. Chem. Soc.* **2018**, *140*, 12056–12068.

43. Jankins, T. C.; Blank, P. M.; Brugnetti, A.; Boehm, P.; Aouane, F. A.; Morandi, B. Shuttle HAT for mild alkene transfer hydrofunctionalization. *Nat. Commun.* **2024**, *15*, 9397–9406.

44. Yang, F.; Nie, Y.-C.; Liu, H.-Y.; Mo, F.; Zhu, R. Electrocatalytic Oxidative Hydrofunctionalization Reactions of Alkenes via Co(II/III/IV) Cycle. *ACS Catal.* **2022**, *12*, 2132–2137.

45. Hartung, J.; Pulling, M. E.; Smith, D. M.; Yang, D. X.; Norton, J. R. Initiating radical cyclizations by H• transfer from transition metals. *Tetrahedron* **2008**, *64*, 11822–11830.

46. Kuo, J. L.; Hartung, J.; Han, A.; Norton, J. R. Direct generation of oxygen-stabilized radicals by H• transfer from transition metal hydrides. *J. Am. Chem. Soc.* **2015**, *137*, 1036–1039.

47. Kuo, J.; Lorenc, C.; Abuyuan, J. M.; Norton, J. R. Catalysis of Radical Cyclizations from Alkyl Iodides under H_2: Evidence for Electron Transfer from $[CpV(CO)_3H]^-$. *J. Am. Chem. Soc.* **2018**, *140*, 4512–4516.

48. Mondal, P.; Pirovano, P.; Das, A.; Farquhar, E. R.; McDonald, A. R. Hydrogen Atom Transfer by a

High Valent Nickel-Chloride Complex. *J. Am. Chem. Soc.* **2018**, *140*, 1834–1841.

49. Yao, C.; Wang, S.; Norton, J.; Hammond, M. Catalyzing the Hydrodefluorination of CF_3-Substituted Alkenes by $PhSiH_3$. H• Transfer from a Nickel Hydride. *J. Am. Chem. Soc.* **2020**, *142*, 4793–4799.

50. Song, P.; Zhu, S. Nickel-Catalyzed Hydrofluorination of Unactivated Alkenes through a HAT Pathway. *ACS Catal.* **2020**, *10*, 13165–13170.

51. Wang, J.-J.; Huang, H.; Sun, H.-L.; Yang, F.; Wen, J.; Zhu, R. Mimicking hydrogen-atom-transfer-like reactivity in copper-catalysed olefin hydrofunctionalization. *Nat. Catal.* **2024**, *7*, 838–846.

52. Shigehisa, H.; Hayashi, M.; Ohkawa, H.; Suzuki, T.; Okayasu, H.; Mukai, M.; Yamazaki, A.; Kawai, R.; Kikuchi, H.; Satoh, Y.; Fukuyama, A.; Hiroya, K. Catalytic Synthesis of Saturated Oxygen Heterocycles by Hydrofunctionalization of Unactivated Olefins: Unprotected and Protected Strategies. *J. Am. Chem. Soc.* **2016**, *138*, 10597–10604.

53. Discolo, C. A.; Touney, E. E.; Pronin, S. V. Catalytic Asymmetric Radical–Polar Crossover Hydroalkoxylation. *J. Am. Chem. Soc.* **2019**, *141*, 17527–17532.

54. Song, L.; Fu, N.; Ernst, B. G.; Lee, W. H.; Frederick, M. O.; DiStasio, R. A.; Lin, S. Dual electrocatalysis enables enantioselective hydrocyanation of conjugated alkenes. *Nat. Chem.* **2020**, *12*, 747–754.

55. Matsushita, Y.; Furusawa, H.; Matsui, T.; Nakayama, M. Total Synthesis of (−)-Pyrenophorin via Cobalt(II) Porphyrin- Catalyzed Oxygenation of Ethyl (2E,4E,7R)-7-Acetoxy-2,4-octadienoate. *Chem. Lett.* **1994**, *23*, 1083–1084.

56. Tanaka, M.; Mitsuhashi, H.; Maruno, M.; Wakamatsu, T. First Total Synthesis of Optically Pure Metabolites of Gomisin A. *Synlett* **1994**, *1994*, 604–606.

57. Xu, G.; Wu, J.; Li, L.; Lu, Y.; Li, C. Total Synthesis of (−)-Daphnezomines A and B. *J. Am. Chem. Soc.* **2020**, *142*, 15240–15245.

58. Xin, Z.; Wang, H.; He, H.; Zhao, X.; Gao, S. Asymmetric Total Synthesis of Norzoanthamine. *Angew. Chem. Int. Ed.* **2021**, *60*, 12807–12812.

59. Zeitler, K. Photoredox Catalysis with Visible Light. *Angew. Chem. Int. Ed.* **2009**, *48*, 9785–9789.

60. Narayanam, J. M. R.; Stephenson, C. R. J. Visible Light Photoredox Catalysis: Applications in Organic Synthesis. *Chem. Soc. Rev.* **2011**, *40*, 102–113.

61. Holmberg-Douglas, N.; Nicewicz, D. A. Photoredox-Catalyzed C–H Functionalization Reactions. *Chem. Rev.* **2022**, *122*, 1925–2016.

62. Prier, C. K.; Rankic, D. A.; MacMillan, D. W. C. Visible Light Photoredox Catalysis with Transition Metal Complexes: Applications in Organic Synthesis. *Chem. Rev.* **2013**, *113*, 5322–5363.

63. Kojima, M.; Matsunaga, S. The Merger of Photoredox and Cobalt Catalysis. *Trends in Chemistry* **2020**, *2*, 410–426.

64. Chan, A. Y.; Perry, I. B.; Bissonnette, N. B.; Buksh, B. F.; Edwards, G. A.; Frye, L. I.; Garry, O. L.;

Lavagnino, M. N.; Li, B. X.; Liang, Y.; Mao, E.; Millet, A.; Oakley, J. V.; Reed, N. L.; Sakai, H. A.; Seath, C. P.; MacMillan, D. W. C. Metallaphotoredox: The Merger of Photoredox and Transition Metal Catalysis. *Chem. Rev.* **2022**, *122*, 1485–1542.

65. Sun, H.-L.; Yang, F.; Ye, W.-T.; Wang, J.-J.; Zhu, R. Dual Cobalt and Photoredox Catalysis Enabled Intermolecular Oxidative Hydrofunctionalization. *ACS Catal.* **2020**, *10*, 4983–4989.

66. Fang, X.; Zhang, N.; Chen, S.-C.; Luo, T. Scalable Total Synthesis of (−)-Triptonide:Serendipitous Discoveryof a Visible-Light-Promoted Olefin Coupling Initiated by Metal-Catalyzed Hydrogen Atom Transfer (MHAT). *J. Am. Chem. Soc.* **2022**, *144*, 2292–2300.

67. Kamei, Y.; Seino, Y.; Yamaguchi, Y.; Yoshino, T.; Maeda, S.; Kojima, M.; Matsunaga, S. Silane- and peroxide-free hydrogen atom transfer hydrogenation using ascorbic acid and cobalt-photoredox dual catalysis. *Nat. Commun.* **2021**, *12*, 966–974.

68. Bergamaschi, E.; Mayerhofer, V. J.; Teskey, C. J. Light-Driven Cobalt Hydride Catalyzed Hydroarylation of Styrenes. *ACS Catal.* **2022**, *12*, 14806–14811.

69. Takekawa, Y.; Nakagawa, M.; Nagao, K.; Ohmiya, H. A Quadruple Catalysis Enabling Intermolecular Branch-Selective Hydroacylation of Styrenes. *Chem. Eur. J.* **2023**, *29*, e202301484.

70. Schreier, M. R.; Pfund, B.; Guo, X.; Wenger, O. S. Photo-triggered hydrogen atom transfer from an iridium hydride complex to unactivated alkenes. *Chem. Sci.* **2020**,*11*, 8582–8594.

71. Yan, H.; Liao, Q.; Chen, Y.; Gurzadyan, G. G.; Lu, B.; Wu, C.; Shi, L. Photocatalytic Metal Hydride Hydrogen Atom Transfer Mediated Allene Functionalization by Cobalt and Titanium Dual Catalysis. *Angew. Chem. Int. Ed.* **2023**, *62*, e202302483.

72. Yan, H.; Shan, J.-R.; Zhang, F.; Chen, Y.; Zhang, X.; Liao, Q.; Hao, E.; Shi, L. Radical Crotylation of Aldehydes with 1,3-Butadiene by Photoredox Cobalt and Titanium Dual Catalysis. *Org. Lett.* **2023**, *25*, 7694–7699.

73. Matolscy, G. *Pesticide Chemistry*; Elseiver Scientific: Amsterdam, 1988.

74. Zakharychev, V. V.; Martsynkevich, A. M. Development of novel pyridine-based agrochemicals: A review. *Advanced Agrochem* **2025**, *4*, 30–48.

75. Ruiter, G.; Lahav, M.; Boom, M. E. Pyridine Coordination Chemistry for Molecular Assemblies on Surfaces. *Acc. Chem. Res.* **2014**, *47*, 3407–3416.

76. Kwong, H.-L.; Yeung, H.-L.; Yeung, C.-T.; Lee, W.-S.; Lee, C.-S.; Wong, W.-L. Chiral pyridine-containing ligands in asymmetric catalysis. *Coord. Chem. Rev.* **2007**, *251*, 2188–2222.

77. Vitaku, E.; Smith, D. T.; Njardarson, J. T. Analysis of the Structural Diversity, Substitution Patterns, and Frequency of Nitrogen Heterocycles among U.S. FDA Approved Pharmaceuticals. *J. Med. Chem.* **2014**, *57*, 10257–10274.

78. Golunski, S. E.; Jackson, D. Heterogeneous conversion of acyclic compounds to pyridine bases - a review. *Appl. Catal.* **1986**, *23*, 1–14.

79. Varela, J. A.; Saá, C. Recent Advances in the Synthesis of Pyridines by Transition-Metal-Catalyzed [2+2+2] Cycloaddition. *Synlett* **2008**, *17*, 2571–2578.

80. Guillemard, L.; Kaplaneris, N.; Ackermann, L.; Johansson, M. J. Late-stage C–H functionalization offers new opportunities in drug discovery. *Nat. Rev. Chem.* **2021**, *5*, 522–545.

81. Maity, S.; Bera, A.; Bhattacharjya, A.; Maity, P. C–H functionalization of pyridines. *Org. Biomol.*

Chem. **2023**, *21*, 5671–5690.

82. Zhou, F.-Y.; Jiao, L. Recent Developments in Transition-Metal-Free Functionalization and Derivatization Reactions of Pyridines. *Synlett* **2021**, *32*, 159–178.

83. Bacos, P. D.; Lahdenpera, A. S. K.; Phipps, R. J. Discovery and Development of the Enantioselective Minisci Reaction. *Acc. Chem. Res.* **2023**, *56*, 2037–2049.

84. Cao, H.; Cheng, Q.; Studer, A. meta-Selective C–H Functionalization of Pyridines. *Angew. Chem. Int. Ed.* **2023**, *62*, e202302941.

85. Bull, J. A.; Mousseau, J. J.; Pelletier, G.; Charette, A. B. Synthesis of Pyridine and Dihydropyridine Derivatives by Regio- and Stereoselective Addition to N-Activated Pyridines. *Chem. Rev.* **2012**, *112*, 2642–2713.

86. Nakao, Y. Transition-Metal-Catalyzed C-H Functionalization for the Synthesis of Substituted Pyridines. *Synthesis* **2011**, *20*, 3209–3219.

87. Tang, S.; Liu, Z.; Zhang, J.; Li, B.; Wang, B. Copper-Catalyzed C4-selective Carboxylation of Pyridines with CO_2 via Pyridylphosphonium Salts. *Angew. Chem. Int. Ed.* **2024**, *63*, e202318572.

88. Wang, Z.-J.; Chen, J.-J.; Huang, H.-M. Site-Selective Pyridine Carbamoylation Enabled by Consecutive Photoinduced Electron Transfer. *ACS Catal.* **2024**, *14*, 15521–15527.

89. Dolewski, R. D.; Hilton, M. C.; McNally, A. 4-Selective Pyridine Functionalization Reactions via Heterocyclic Phosphonium Salts. *Synlett* **2018**, *29*, 8–14.

90. Anders, E.; Markus, F. Neue methode zur regiospezifischen substitution einiger reaktionsträcer N-heteroaromatischer ringsysteme. *Tetrahedron Lett.* **1987**, *28*, 2675–2676.

91. Sugimoto, O.; Tanji, K.-I.; Sato, A. Chemistry of heteroaryltriphenylphosphonium iodides: preparation from iodoheteroaromatics and elimination of the phosphonium iodide group using basic solvents. *Heterocycles* **2009**, *78*, 2735–2739.

92. Sugimoto, O.; Shimada, M.; Sato, A.; Tanji, K.-I. Preparation and Reaction of Quinolinyl (or Pyridinyl)-phosphonium Salts with Base and Pivalaldehyde. *Heterocycles* **2011**, *83*, 837–847.

93. Hilton, M. C.; Dolewski, R. D.; McNally, A. Selective Functionalization of Pyridines via Heterocyclic Phosphonium Salts. *J. Am. Chem. Soc.* **2016**, *138*, 13806–13809.

94. Koniarczyk, J. L.; Greenwood, J. W.; Alegre-Requena, J.; Paton, R. S.; McNally, A. A Pyridine–Pyridine Cross-Coupling Reaction via Dearomatized Radical Intermediates. *Angew. Chem. Int. Ed.* **2019**, *58*, 14882–14886.

95. Greenwood, J. W.; Boyle, B. T.; McNally, A. Pyridylphosphonium salts as alternatives to cyanopyridines in radical–radical coupling reactions. *Chem. Sci.* **2021**, *12*, 10538–10543.

96. Huang, W.; Ding, X.; Zi, Y. Research Progress of Vinyl/Aryl Phosphonium Salts in Organic Synthesis. *Chin. J. Org. Chem.* **2022**, *42*, 471–486.

97. Zhang, X.; Nottinghan, K. G.; Patel, C.; Alegre-Requena, J. V.; Levy, J. N.; Paton, R. S.; McNally, A. Phosphorus-mediated sp^2–sp^3 couplings for C–H fluoroalkylation of azines. *Nature* **2021**, *594*, 217–222.

98. Josephitis, C. M.; Nguyen, H. M. H.; McNally, A. Late-Stage C–H Functionalization of Azines. *Chem. Rev.* **2023**, *123*, 7655–7691.

99. Qin, J.; Barday, M.; Jana, S.; Sanosa, N.; Funes-Ardoiz, I.; Teskey, C. J. Photoinduced Cobalt Catalysis for the Reductive Coupling of Pyridines and Dienes Enabled by Paired Single-Electron Transfer. *Angew. Chem. Int. Ed.* **2023**, *62*, e202310639.

100. Herrmann, N.; Vogelsang, D.; Behr, A.; Seidensticker, T. Homogeneously catalyzed 1, 3-diene functionalization–A success story from laboratory to miniplant scale. *ChemCatChem* **2018**, *10*, 5342–5365.

101. Holmes, M.; Schwartz, L. A.; Krische, M. J. Intermolecular Metal-Catalyzed Reductive Coupling

of Dienes, Allenes, and Enynes with Carbonyl Compounds and Imines. *Chem. Rev.* **2018**, *118*, 6026–6052.

102. Doerksen, R. S.; Meyer, C. C.; Krische, M. J. Feedstock Reagents in Metal-Catalyzed Carbonyl Reductive Coupling: Minimizing Preactivation for Efficiency in Target-Oriented Synthesis. *Angew. Chem. Int. Ed.* **2019**, *58*, 14055–14064.

103. Perry, G. J. P.; Jia, T.; Procter, D. J. Copper-Catalyzed Functionalization of 1,3-Dienes: Hydrofunctionalization, Borofunctionalization, and Difunctionalization. *ACS Catal.* **2020**, *10*, 1485–1499.

104. Adamson, N. J.; Malcolmson, S. J. Catalytic Enantio- and Regioselective Addition of Nucleophiles in the Intermolecular Hydrofunctionalization of 1,3-Dienes. *ACS Catal.* **2020**, *10*, 1060–1076.

105. Liao, L.; Sigman, M. S. Palladium-Catalyzed Hydroarylation of 1,3-Dienes with Boronic Esters via Reductive Formation of π-Allyl Palladium Intermediates under Oxidative Conditions. *J. Am. Chem. Soc.* **2010**, *132*, 10209–10211.

106. Marcum, J. S.; Taylor, T. R.; Meek, S. J. Enantioselective Synthesis of Functionalized Arenes by Nickel-Catalyzed Site-Selective Hydroarylation of 1,3-Dienes with ArylBoronates. *Angew. Chem. Int. Ed.* **2020**, *59*, 14070–14075.

107. Roberts, C. C.; Matías, D. M.; Goldfogel, M. J.; Meek, S. J. Lewis Acid Activation of Carbodicarbene Catalysts for Rh-Catalyzed Hydroarylation of Dienes. *J. Am. Chem. Soc.* **2015**, *137*, 6488–6491.

108. Kumar, G.; Qu, Z.-W.; Grimme, S.; Chatterjee, I. Boron-Catalyzed Hydroarylation of 1,3-Dienes with Arylamines. *Org. Lett.* **2021**, *23*, 8952–8957.

109. Mohite, S. B.; Mirza, Y. K.; Bera, P. S.; Nadigar, S.; Yugendhar, S.; Karpoormath, R.; Bera, M. Advances in Pyridine C–H Functionalizations: Beyond C2 Selectivity. *Chem. Eur. J.* **2025**, *31*, e202403032.

110. Tan, C.-Y.; Kim, M.; Park, I.; Kim, Y.; Hong, S. Site-Selective Pyridine C−H Alkylation with Alcohols and Thiols via Single-Electron Transfer of Frustrated Lewis Pairs. *Angew. Chem. Int. Ed.* **2022**, *61*, e202213857.

111. Nakao, Y.; Yamada, Y.; Kashihara, N.; Hiyama, T. Selective C-4 Alkylation of Pyridine by Nickel/Lewis Acid Catalysis. *J. Am. Chem. Soc.* **2010**, *132*, 13666–13668.

112. Hsu, H.-H.; Kang, S.; Chen, C.-C.; Sk, M. R.; Thomas, A. A. Functionalization of Pyridines at the C4 Position via Metalation and Capture. *Angew. Chem. Int. Ed.* **2025**, e202424172, in press. https://doi.org/10.1002/anie.202424172

113. Saux, E. L.; Georgiou, E.; Dmitriev, I. A.; Hartley, W. C.; Melchiorre, P. Photochemical Organocatalytic Functionalization of Pyridines via Pyridinyl Radicals. *J. Am. Chem. Soc.* **2023**, *145*, 47–52.

114. Leifert, D.; Studer, A. The Persistent Radical Effect in Organic Synthesis. *Angew. Chem. Int. Ed.* **2020**, *59*, 74–108.

115. Ma, X.; Herzon, S. B. Intermolecular Hydropyridylation of Unactivated Alkenes. *J. Am. Chem. Soc.* **2016**, *138*, 8718–8721.

116. Ma, X.; Dang, H.; Rose, J. A.; Rablen, P.; Herzon, S. B. Hydroheteroarylation of Unactivated Alkenes Using N-Methoxyheteroarenium Salts. *J. Am. Chem. Soc.* **2017**, *139*, 5998–6007.

117. Lo, J. C.; Kim, D.; Pan, C.-M.; Edwards, J. T.; Yabe, Y.; Gui, J.; Qin, T.; Gutiérrez, S.; Giacoboni, J.; Smith, M. W.; Holland, P. L.; Baran, P. S. Fe-Catalyzed C–C Bond Construction from Olefins via Radicals. *J. Am. Chem. Soc.* **2017**, *139*, 2484–2503.

118. Iwasaki, K.; Wan, K. K.; Oppedisano, A.; Crossley, S. W. M.; Shenvi, R. A. Simple, Chemoselective Hydrogenation with Thermodynamic Stereocontrol. *J. Am. Chem. Soc.* **2014**, *136*, 1300–1303.

119. King, S. M.; Ma, X.; Herzon, S. B. A Method for the Selective Hydrogenation of Alkenyl Halides

to Alkyl Halides. *J. Am. Chem. Soc.* **2014**, *136*, 6884–6887.

120. Ma, X.; Herzon, S. B. Non-classical selectivities in the reduction of alkenes by cobalt-mediated hydrogen atom transfer**.** *Chem. Sci.* **2015**, *6*, 6250–6255.

121. Dalle, K. E.; Warnan, J.; Leung, J. J.; Reuillard, B.; Karmel, I. S.; Reisner, E. Electro- and Solar-Driven Fuel Synthesis with First Row Transition Metal Complexes. *Chem. Rev.* **2019**, *119*, 2752–2875.

122. Goswami, M.; Lyaskovskyy, V.; Domingos, S. R.; Buma, W. J.; Woutersen, S.; Troeppner, O.; Ivanović Burmazović, I.; Lu, H.; Cui, X.; Zhang, X. P.; Reijerse, E. J.; DeBeer, S.; Schooneveld, M. M.; Pfaff, F. F.; Ray, K.; Bruin, B. Characterization of Porphyrin-Co(III)-'Nitrene Radical' Species Relevant in Catalytic Nitrene Transfer Reactions. *J. Am. Chem. Soc.* **2015**, *137*, 5468–5479.

123. Pamin, K.; Tabor, E.; Górecka, S.; Kubiak, W. W.; Rutkowska-Zbik, D.; Połtowicz, J. Three Generations of Cobalt Porphyrins as Catalysts in the Oxidation of Cycloalkanes. *ChemSusChem* **2019**, *12*, 684–691.

124. Wu, X.; Gannett, C. N.; Liu, J.; Zeng, R.; Novaes, L. F. T.; Wang, H.; Abruña, H. D.; Lin, S. Intercepting Hydrogen Evolution with Hydrogen-Atom Transfer: Electron-Initiated Hydrofunctionalization of Alkenes. *J. Am. Chem. Soc.* **2022**, *144*, 17783–17791.

125. Jung, J.; Kim, J.; Park, G.; You, Y.; Cho, E. J. Selective Debromination and α-Hydroxylation of α-Bromo Ketones Using Hantzsch Esters as Photoreductants. *Adv. Synth. Catal.* **2016**, *358*, 74–80.

126. Limburg, B.; Cristòfol, À.; Kleij, A. W. Decoding Key Transient Inter-Catalyst Interactions in a Reductive Metallaphotoredox-Catalyzed Allylation Reaction. *J. Am. Chem. Soc.* **2022**, *144*, 10912–10920.

127. Ravelli, D.; Protti, S.; Fagnoni, M. Carbon–Carbon Bond Forming Reactions via Photogenerated Intermediates Photocatalysis for the Formation of the C–C Bond. *Chem. Rev.* **2016**, *116*, 9850–9913.

128. Smith, J. M.; Harwood, S. J.; Baran, P. S. Radical Retrosynthesis. *Acc. Chem. Res.* **2018**, *51*, 1807–1817.

129. Ni, S.; Padial, N. M.; Kingston, C.; Vantourout, J. C.; Schmitt, D. C.; Edwards, J. T.; Kruszyk, M. M.; Merchant, R. R.; Mykhailiuk, P. K.; Sanchez, B. B.; Yang, S.; Perry, M. A.; Gallego, G. M.; Mousseau, J. J.; Collins, M. R.; Cherney, R. J.; Lebed, P. S.; Chen, J. S.; Qin, T.; Baran, P. S. A Radical Approach to Anionic Chemistry: Synthesis of Ketones, Alcohols, and Amines. *J. Am. Chem. Soc.* **2019**, *141*, 6726–6739.

130. Giese, B.; Lachhein, S. Steric Effects in the Addition of Alkyl Radicals to Alkenes. *Angew. Chem. Int. Ed. Engl.* **1981**, *20*, 967–967.

131. Giese, B.; Dupuis, J. Diastereoselective Syntheses of C-Glycopyranosides. *Angew. Chem. Int. Ed. Engl.* **1983**, *22*, 622–623.

132. Giese, B.; Gonzalez-Gomez, J. A.; Witzel, T. The Scope of Radical CC-Coupling by the "Tin Method". *Angew. Chem. Int. Ed. Engl.* **1984**, *23*, 69–70.

133. Shu, C.; Mega, R. S.; Andreassen, B. J.; Noble, A.; Aggarwal, V. K. Synthesis of Functionalized Cyclopropanes from Carboxylic Acids by a Radical Addition–Polar Cyclization Cascade. *Angew. Chem., Int. Ed.* **2018**, *57*, 15430–15434.

134. Cheng, Y.-Y.; Yu, J.-X.; Lei, T.; Hou, H.-Y.; Chen, B.; Tung, C.-H.; Wu, L.-Z. Direct 1,2-Dicarbonylation of Alkenes towards 1,4-Diketones via Photocatalysis. *Angew. Chem., Int. Ed.* **2021**, *60*, 26822–26828.

135. Kanegusuku, A. L. G.; Roizen, J. L. Recent Advances in Photoredox-Mediated Radical Conjugate Addition Reactions: An Expanding Toolkit for the Giese Reaction. *Angew. Chem. Int. Ed.* **2021**, *60*,

21116–21149.

136. Jamison, C. R.; Overman, L. E. Fragment Coupling with Tertiary Radicals Generated by Visible-Light Photocatalysis. *Acc. Chem. Res.* **2016**, *49*, 1578–1586.

137. Pitre, S. P.; Overman, L. E. Strategic Use of Visible-Light Photoredox Catalysis in Natural Product Synthesis. *Chem. Rev.* **2022**, *122*, 1717–1751.

138. Kim, J.; Li, B. X.; Huang, R. Y.-C.; Qiao, J. X.; Ewing, W. R.; MacMillan, D. W. C. Site-Selective Functionalization of Methionine Residues via Photoredox Catalysis. *J. Am. Chem. Soc.* **2020**, *142*, 21260–21266.

139. Bloom, S.; Liu, C.; D. Kölmel, K.; Qiao, J. X.; Zhang, Y.; Poss, M. A.; Ewing, W. R.; MacMillan, D. W. C. Decarboxylative alkylation for site-selective bioconjugation of native proteins via oxidation potentials. *Nat. Chem.* **2018**, *10*, 205–211.

140. Ritts, A.; ElMarrouni, C. B.; Balsells, J. Silyl-mediated photoredox-catalyzed Giese reaction: addition of non-activated alkyl bromides. *Chem. Sci.* **2018**, *9*, 6639–6646.

141. Conradi, M. S.; Zeldes, H.; Livingston, R. Electron spin resonance determination of hindered rotation in benzyl radicals. Resonance stabilization energy. *J. Phys. Chem.* **1979**, *83*, 2160–2161.

142. Nicholas, A. M. D.; Arnold, D. R. Substituent effects on benzyl radical hydrogen hyperfine coupling constants (hfc's).: Part 5. The comparison of electron spin resonance hfc's and the stabilization energy of π-radicals due to spin delocalization. *Can. J. Chem.* **1986**, *64*, 270–276.

143. Fischer, H.; Radom, L. Factors Controlling the Addition of Carbon-Centered Radicals to Alkenes—An Experimental and Theoretical Perspective. *Angew. Chem. Int. Ed.* **2001**, *40*, 1340–1371.

144. Schweitzer-Chaput, B.; Horwitz, M.A.; Beato, E. P.; Melchiorre, P. Photochemical generation of radicals from alkyl electrophiles using a nucleophilic organic catalyst. *Nat. Chem.* **2019**, *11*, 129–135.

145. Kitcatt, D. M.; Nicolle, S.; Lee, A.-L. Direct decarboxylative Giese reactions. *Chem. Soc. Rev.* **2022**,*51*, 1415-1453.

146. Chu, L.; Ohta, C.; Zuo, Z.; MacMillan, D. W. C. Carboxylic Acids as A Traceless Activation Group for Conjugate Additions: A Three-Step Synthesis of (±)-Pregabalin. *J. Am. Chem. Soc.* **2014**, *136*, 10886–10889.

147. Wang, J. Z.; Sakai, H. A.; MacMillan, D. W. C. Alcohols as Alkylating Agents: Photoredox-Catalyzed Conjugate Alkylation via In Situ Deoxygenation. *Angew. Chem. Int. Ed.* **2022**, e202207150.

148. Wu, J.; Grant, P. S.; Li, X.; Noble, A.; Aggarwal, V. K. Catalyst-Free Deaminative Functionalizations of Primary Amines by Photoinduced Single-Electron Transfer. *Angew. Chem. Int. Ed.* **2019**, *58*, 5697–5701.

149. Chinzei, T.; Miyazawa, K.; Yasu, Y.; Kioke, T.; Akita, M. Redox-economical radical generation from organoborates and carboxylic acids by organic photoredox catalysis. *RSC Adv.* **2015**, *5*, 21297–21300.

150. Silvi, M.; Varrier, C.; P. Rey, Y.; Buzzetti, L.; Melchiorre, P. Visible-light excitation of iminium ions enables the enantioselective catalytic β-alkylation of enals. *Nat. Chem.* **2017**, *9*, 868–873.

151. Gualandi, A.; Mazzarella, D.; Ortega-Martinez, A.; Mengozzi, L.; Calcinelli, F.; Matteucci, E.; Monti, F.; Armaroli, N.; Sambri, L.; Cozzi, P. G. Photocatalytic Radical Alkylation of Electrophilic Olefins by Benzylic and Alkylic Zinc-Sulfinates. *ACS Catal.* **2017**, *7*, 5357–5362.

152. Aycock, R. A.; Pratt, C. J.; Jui, N. T. Aminoalkyl Radicals as Powerful Intermediates for the Synthesis of Unnatural Amino Acids and Peptides. *ACS Catal.* **2018**, *8*, 9115–9119.

153. An, Q.; Wang, Z.; Chen, Y.; Wang, X.; Zhang, K.; Pan, H.; Liu, W.; Zuo, Z. Cerium-Catalyzed C–H Functionalizations of Alkanes Utilizing Alcohols as Hydrogen Atom Transfer Agents. *J. Am. Chem. Soc.* **2020**, *142*, 6216–6226.

154. Zhang, J.; Li, Y.; Zhang, F.; Hu, C.; Chen, Y. Generation of Alkoxyl Radicals by Photoredox Catalysis Enables Selective C(sp^3)–H Functionalization under Mild Reaction Conditions. *Angew. Chem. Int. Ed.* **2016**, *55*, 1872–1875.

155. Jiang, H.; Studer, A. Iminyl-Radicals by Oxidation of α-Imino-oxy Acids: Photoredox-Neutral Alkene Carboimination for the Synthesis of Pyrrolines. *Angew. Chem. Int. Ed.* **2017**, *56*, 12273–12276.

156. Jiang, H.; Seidler, G.; Studer, A. Carboamination of Unactivated Alkenes through Three-Component Radical Conjugate Addition. *Angew. Chem. Int. Ed.* **2019**, *58*, 16528–16532.

157. Mega, R. S.; Duong, V.K.; Noble, A.; Aggarwal, V. K. Decarboxylative Conjunctive Cross-coupling of Vinyl Boronic Esters using Metallaphotoredox Catalysis. *Angew. Chem. Int. Ed.* **2020**, *59*, 4375–4379.

158. Snape. T. J. A truce on the Smiles rearrangement: revisiting an old reaction—the Truce–Smiles rearrangement. *Chem. Soc. Rev.* **2008**,*37*, 2452-2458.

159. Chen, Y.; Chang, L.; Zuo, Z. Visible Light Photoredox-Induced Smiles Rearrangement. *Acta Chimica Sinica* **2019**, *77*, 794-802.

160. Chen, Z.-M.; Zhang, X.-M.; Tu, Y.-Q. Radical aryl migration reactions and synthetic applications *Chem. Soc. Rev.* **2015**,*44*, 5220-5245.

161. Zhang, J.-H.; Miao, H.-J.; Xin, H.; Wang, G.; Yang, X.; Wang, X.; Gao, P.; Duan, X.-H.; Guo, L.-N. Photoredox-catalyzed alkylarylation of activated alkenes via a ring-opening/Truce – Smiles rearrangement cascade. *Chem. Commun.* **2024**,*60*, 5334-5337.

162. Kong, W.; Casimiro, M.; Merino, E.; Nevado, C. Copper-Catalyzed One-Pot Trifluoromethylation/Aryl Migration/Desulfonylation and C(sp^2)–N Bond Formation of Conjugated Tosyl Amides. *J. Am. Chem. Soc.* **2013**, *135*, 14480–14483.

163. Shu, W.; Genoux, A.; Li, Z.; Nevado, C. γ-Functionalizations of Amines through Visible-Light-Mediated, Redox-Neutral C–C Bond Cleavage. *Angew. Chem. Int. Ed.* **2017**, *56*, 10521–10524.

164. Hervieu, C.; Kirillova, M. S.; Suárez, T.; Müller, M.; Merino, E.; Nevado, C. Asymmetric, visible light-mediated radical sulfinyl-Smiles rearrangement to access all-carbon quaternary

stereocentres. *Nat. Chem.* **2021**, *13*, 327–334.

165. Radhoff, N.; Studer, A. Functionalization of α-C(sp^3)–H Bonds in Amides Using Radical Translocating Arylating Groups. *Angew. Chem. Int. Ed.* **2021**, *60*, 3561-3565.

166. Ma, W.-Y.; Leone, M.; Derat, E.; Retailleau, P.; Reddy, C. R.; Neuville, L.; Masson, G. Photocatalytic Asymmetric Acyl Radical Truce–Smiles Rearrangement for the Synthesis of Enantioenriched α-Aryl Amides. *Angew. Chem. Int. Ed.* **2024**, *63*, e20240815.

167. Zhou, H.; Lunic, D.; Sanosa, N.; Sampedro, D.; Ardoiz, I. F.; Teskey, C. J. Merging Hydrogen-Atom-Transfer and the Truce-Smiles Rearrangement for Synthesis of beta-Arylethylamines from Unactivated Allylsulfonamides. *Angew. Chem. Int. Ed.* **2025**, *64*, e202418869.

168. Lunic, D.; Vystavkin, N.; Qin, J.; Teskey, C. J. Dual-Catalytic Structural Isomerisation as a Route to α-Arylated Ketones. *Angew. Chem. Int. Ed.* **2024**, *63*, e202409388.

169. Johansson, C. C. C.; Colacot, T. J. Metal-Catalyzed α-Arylation of Carbonyl and Related Molecules: Novel Trends in C–C Bond Formation by C–H Bond Functionalization. *Angew. Chem. Int. Ed.* **2010**, *49*, 676–707.

170. Mbela, T. K. N.; Poupaert, J. H.; Cumps, J.; Moussebois, C.; Haemers, A.; Borloo, M.; Dumont, P. Phenyl-substituted Normethadones: Synthesis and Pharmacology. *J. Pharm. Pharmacol.* **1995**, *47*, 237–242.

171. Culkin, D. C.; Hartwig, J. F. Palladium-Catalyzed α-Arylation of Carbonyl Compounds and Nitriles. *Acc. Chem. Res.* **2003**, *36*, 234–245.

172. Alsabeh, P. G.; Stradiotto, M. Addressing Challenges in Palladium-Catalyzed Cross-Couplings of Aryl Mesylates: Monoarylation of Ketones and Primary Alkyl Amines. *Angew. Chem. Int. Ed.* **2013**, *52*, 7242–7246.

173. Jurczyk, J.; Woo, J.; Kim, S. F.; Dherange, B. D.; Sarping, R.; Levin, M. D. Single-atom logic for heterocycle editing. *Nat. Synth.* **2022**, *1*, 352–364.

174. Cheng, Q.; Bhattacharya, D.; Haring, M.; Cao, H.; Mück-Lichtenfeld, C.; Studer, A. Skeletal editing of pyridines through atom-pair swap from CN to CC. *Nat. Chem.* 2024, 16, 741–748.

175. Ma, C.; Lindsley, C. W.; Chang, J.; Yu, B. Rational Molecular Editing: A New Paradigm in Drug Discovery. *J. Med. Chem.* 2024, 67, 14, 11459–11466.

176. Foster, J. C.; Damron, J. T.; Zheng, J.; Guan, C.; Popovs, I.; Rahman, M. A.; Galan, N. J.; Dishner, I. T.; Saito, T.; Polyalkenamers as Drop-In Additives for Ring-Opening Metathesis Polymerization: A Promising Upcycling Paradigm. *J. Am. Chem. Soc.* **2024**, *146*, 33084–33092.

177. Candeias, N. R.; Paterna, R.; Gois, P. M. P. Homologation Reaction of Ketones with Diazo Compounds. *Chem. Rev.* **2016**, *116*, 2937–2981.

178. Schönherr, H.; Cernak, T. Profound Methyl Effects in Drug Discovery and a Call for New C–H Methylation Reactions. *Angew. Chem. Int. Ed.* **2013**, *52*, 12256–12267.

179. Pritha, S; Bhirisha, S; Jagruti, S. Magic Methyl Effects in Drug Design. *Glob J Pharmaceu Sci.* **2021**, *9*, 555761–555767.

180. Cui, Y.-Y.; Na, J.-H.; Guo, M.-M.; Huang, J.-Y.; Chu, X.-Q.; Rao, W.; Shen. Z. Cobalt-catalyzed cross-coupling of nitrogen-containing heterocyclic phosphonium salts with arylmagnesium reagents. *Tetrahedron Lett.* **2022**, *92*, 153662–153665.

181. Zhang, X.; McNally, A. Phosphonium Salts as Pseudohalides: Regioselective Nickel-Catalyzed Cross-Coupling of Complex Pyridines and Diazines. *Angew. Chem. Int. Ed.* **2017**, *56*, 9833 –9836.

182. Koniarczyk, J. L.; Hesk, D.; Overgard, A.; Davies, I. W.; McNally, A. A General Strategy for Site-Selective Incorporation of Deuterium and Tritium into Pyridines, Diazines, and Pharmaceuticals. *J. Am. Chem. Soc.* **2018**, *140*, 1990–1993.

183. Nilsson, A.-M.; Bergstörm, M. A.; Luthman, K.; Nilsson, J. L. G.; Karlberg, A.-T. A Conjugated Diene Identified as a Prohapten: Contact Allergenic Activity and Chemical Reactivity of Proposed Epoxide Metabolites. *Chem. Res. Toxicol.* **2005**, *18*, 308–316.

184. Sellén, M.; Backvall, J.-E.; Helquist, P. Synthesis of substituted cyclic 1, 3-dienes via selective 1, 4-elimination of benzenesulfinic acid from allylic phenyl sulfones. *J. Org. Chem.* **1991**, *56*, 835–839.

185. Thesmar, P.; Coomar, S.; Prescimone, A.; Häussinger, D.; Gillingham, D.; Baudoin, O. Divergent Synthesis of Bioactive Dithiodiketopiperazine Natural Products Based on a Double C(sp3)–H Activation Strategy. *Chem. Eur. J.* **2020**, *26*, 15298–15312.

186. Karlström, A. S. E.; Rönn, M.; Thorarensen, A.; Bäckvall, J.-E. A Versatile Route to 2-Substituted Cyclic 1,3-Dienes via a Copper(I)-Catalyzed Cross-Coupling Reaction of Dienyl Triflates with Grignard Reagents. *J. Org. Chem.* **1998**, *63*, 2517–2522.

187. Verboom, R. C.; Persson, B. A.; Bäckvall, J.-E. Palladium(II)-Catalyzed Intramolecular 1,4-Oxyacyloxylation of Conjugated Dienes. A Stereocontrolled Route to Fused Six-Membered Lactones and Pyrans. *J. Org. Chem.* **2004**, *69*, 3102–3111.

188. Yuan, C.; Tu, G.; Zhao, Y. Rhodium(III)-Catalyzed Selective Monoarylation of β or γ C(sp3)–H Bonds Assisted by a Trimethylpyrazole Group. *Org. Lett.* **2017**, *19*, 356–359.

189. J. Lee, T. Ha, C. Park, H. Lee, G. Lee, Y. Chang, WO03/057684A1.

190. Boi, T.; Deagostino, A.; Prandi, C.; Tabasso, S.; Toppino, A.; Venturello, P. Heck reaction on protected 3-alkyl-1,2-dien-1-ols: an approach to substituted 3-alkenylindoles, 2-alkoxy-3-alkylidene-2,3-dihydrobenzofuranes and -indolidines. *Org. Biomol. Chem.* **2010**, *8*, 2020-2027.

191. Li, H.; Liu, Y.; Chiba, S. Anti-Markovnikov hydroarylation of alkenes via polysulfide anion photocatalysis. *Chem. Commun.* **2021**, *57*, 6264–6267.

192. Gaussian 16, Revision C.01, Frisch, M. J., Trucks, G. W., Schlegel, H. B., Scuseria, G. E., Robb, M. A., Cheeseman, J. R., Scalmani, G., Barone, V., Petersson, G. A., Nakatsuji, H., Li, X., Caricato, M., Marenich, A. V., Bloino, J., Janesko, B. G., Gomperts, R., Mennucci, B., Hratchian, H. P., Ortiz, J. V., Izmaylov, A. F., Sonnenberg, J. L., Williams-Young, D., Ding, F., Lipparini, F., Egidi, F., Goings, J., Peng, B., Petrone, A., Henderson, T., Ranasinghe, D., Zakrzewski, V. G., Gao, J., Rega, N., Zheng, G., Liang, W., Hada, M., Ehara, M., Toyota, K., Fukuda, R., Hasegawa, J., Ishida, M., Nakajima, T., Honda, Y., Kitao, O., Nakai, H., Vreven, T., Throssell, K., Montgomery, J. A., Jr., Peralta, J. E., Ogliaro, F., Bearpark, M. J., Heyd, J. J., Brothers, E. N., Kudin, K. N., Staroverov, V. N., Keith, T. A., Kobayashi, R., Normand, J.,

Raghavachari, K., Rendell, A. P., Burant, J. C., Iyengar, S. S., Tomasi, J., Cossi, M., Millam, J. M., Klene, M., Adamo, C., Cammi, R., Ochterski, J. W., Martin, R. L., Morokuma, K., Farkas, O., Foresman, J. B., Fox, D. J. Gaussian, Inc., Wallingford CT, 2016.

193. Adamo, C., Barone, V. Toward reliable density functional methods without adjustable parameters: The PBE0 model. *J. Chem. Phys*. **1999**, *110*, 6158-6169.

194. Weigend, F., Ahlrichs, R. Balanced basis sets of split valence, triple zeta valence and quadruple zeta valence quality for H to Rn: Design and assessment of accuracy. *Phys. Chem. Chem. Phys.* **2005**, *7*, 3297-3305.

195. A. V. Marenich, A.V., Cramer, C. J., Truhlar, D. G. Universal Solvation Model Based on Solute Electron Density and on a Continuum Model of the Solvent Defined by the Bulk Dielectric Constant and Atomic Surface Tensions. *J. Phys. Chem. B*, **2009**, *113*, 6378-6396.

196. CYLview1.0; Legault, C. Y., Université de Sherbrooke, 2020 (http://www.cylview.org).